

Università degli Studi di Napoli Federico II  
Facoltà di Ingegneria



Comunità Europea  
Fondo Sociale Europeo

Dottorato di Ricerca  
in Ingegneria delle Costruzioni

XVIII ciclo

**Doctoral Thesis**

**Modelling, Analysis and Testing  
of Masonry Structures**

*Alessandra Romano*

*November 2005*



*“Ars sine scientia nihil est -  
practice is nothing without theory,  
but theory without practice is simply dangerous.”*

[S. Huerta, 2001]

## *Acknowledgements*

Many things have changed in me and in my life during this course of study. Naturally I am three years older than before, but I have also acquired an internal richness I did not believe could happen to me.

Thank you to my professors Antonello De Luca and Elena Mele for contributing to my growth; they have made me aware of the charm and rigour of scientific research and have given me the chance to spend a period of my PhD abroad.

I am deeply grateful to my “acquired” professor John Ochsendorf for having welcomed me in his research group and having trusted me. I really had a marvellous time at MIT in Boston.

I feel sincerely in debt to all the people that have been close to me throughout these years: among them Aldo, who, though our difficulties, has always helped and encouraged me with his calm and joy.

I will never forget my friendship with Ernesto: we have spent nice moments together and I really hope this work can be helpful to him for his new studies in masonry structures.

Last but not least, thank you to my parents for believing in me every single day of my life.

## CONTENTS

### INTRODUCTION

1. Seismic behaviour of masonry churches.....	1
2. Damages in masonry churches.....	3
3. Principal aim and content of the thesis.....	5

### CHAPTER 1

#### *MASONRY STRUCTURES: MODELLING AND ANALYSIS*

1. Introduction.....	9
2. Material modelling.....	10
3. Structural modelling.....	12
4. Horizontal Actions.....	15
4.1. Equivalent seismic forces.....	15
4.2. Elastic spectra.....	16

4.3. Design spectra.....	18
5. Analyses types.....	22
5.1. Linear analyses.....	22
5.1.1. Linear static analyses.....	23
5.1.2. Modal dynamic analyses.....	23
5.2. Non Linear analyses.....	24
5.2.1. Non linear static analyses.....	24
5.3. Limit analyses.....	25
5.3.1. Limit analysis applied to masonry structures.....	26
6. Methodology in Literature.....	28
7. The Applied Methodology.....	32

## CHAPTER 2

### STUDY CASES

1. Introduction.....	33
2. S. Giovanni a Mare.....	34
2.1. Geometry.....	35
2.2. Macroelements.....	35
2.3. Load condition.....	39
3. S. Ippolisto.....	41
3.1. Geometry.....	41
3.2. Macroelements.....	42
3.3. Load condition.....	45
4. S. Giovanni Maggiore.....	46
4.1. Geometry.....	46
4.2. Macroelements.....	47
4.3. Load condition.....	50
5. S. Paolo Maggiore.....	52

---

5.1. Geometry.....	52
5.2. Macroelements.....	53
5.3. Load condition.....	56
6. Geometrical and typological features.....	57
7. Classes Comparison.....	60
8. Conclusions.....	63

### CHAPTER 3

#### *LINEAR ANALYSES*

1. Introduction.....	65
2. Structure, material and seismic action.....	66
3. Dynamic behaviour of churches.....	68
3.1. “as is” models.....	68
3.2. rigid diaphragms models.....	71
4. Seismic actions distribution.....	74
4.1. Structures without rigid diaphragms.....	77
4.2. Structures with rigid diaphragms.....	78
4.3. Out of plane contribution.....	79
5. Strength demand.....	79
6. Conclusions.....	81

### CHAPTER 4

#### *FEM NON LINEAR ANALYSES*

1. Introduction.....	83
2. Modelling through ABAQUS.....	84
3. Model calibration.....	88
4. Bearing capacity in the four study cases.....	89
4.1. S. Giovanni a Mare.....	89

4.1.1. Summary of the results in SGMR.....	98
4.1.2. Strength vs capacity in SGMR.....	99
4.2. S. Ippolisto.....	101
4.2.1. Summary of the results in SI.....	106
4.2.2. Strength vs capacity in SI.....	107
4.3. S. Giovanni Maggiore.....	109
4.3.1. Summary of the results in SGMG.....	114
4.3.2. Strength vs capacity in SGMG.....	116
4.4. S. Paolo Maggiore.....	117
4.4.1. Summary of the results in SP.....	124
4.4.2. Strength vs capacity in SP.....	125
5. Conclusions.....	125

## CHAPTER 5

### *THE MASONRY PORTAL FRAME*

1. Introduction.....	129
2. A Limit Analysis application.....	130
3. Expressions for kinematic multipliers.....	132
3.1. Mechanism I (Frame mechanism).....	132
3.2. Mechanism II (Mixed mechanism).....	133
3.3. Mechanism III (Mixed mechanism).....	134
3.4. Mechanism IV (Storey mechanism).....	135
4. Normalization.....	136
5. Parametric Analyses.....	138
6. An abacus for evaluating the collapse multiplier.....	143
7. Advances with respect to previous formulations.....	145
8. Proposal for a simple approximate expression.....	149
9. Conclusions.....	152



**CHAPTER 6*****SIMPLIFIED ANALYSES OF CHURCHES MACROELEMENTS***

1. Introduction.....	155
2. Extension of the single portal frame to the multy-bay frame.....	156
3. FEM - Limit analysis: comparison.....	157
3.1. S. Giovanni a Mare.....	159
3.1.1. Summary of the SGMR results.....	167
3.2. S. Ippolisto.....	169
3.2.1. Summary of the SI results.....	177
3.3. S. Giovanni Maggiore.....	179
3.3.1. Summary of the SGMG results.....	185
3.4. S. Paolo Maggiore.....	187
3.4.1. Summary of the SP results.....	194
3.5. Collection of the results.....	196
4. Conclusions.....	198

**CHAPTER 7*****THE MASONRY POINTED ARCH***

1. Introduction.....	201
1.1. The origin of the pointed arch.....	202
1.2. Analitical studies on masonry arches.....	203
2. Problem statement.....	207
3. Methodology.....	208
3.1. Numerical Algorithm.....	208
3.2. Graphical Statics.....	209
4. Minimum thickness.....	211
4.1. Theory.....	211

4.2. Numerical and graphical analyses.....	212
5. Thrust values.....	214
5.1. Theory.....	214
5.2. Numerical and graphical analyses.....	215
6. Horizontal support displacement.....	219
6.1. Theory.....	219
6.2. Numerical and graphical analyses.....	221
7. Domains of possible displacements.....	223
8. The half arch.....	225
8.1. Thrust values.....	225
8.2. Maximum displacements.....	226
9. Arches with the same span.....	227
9.1. Same span and thickness.....	228
9.2. Same span and weight.....	230
9.3. Half and whole arches with same span and thickness.....	231
10. Conclusions.....	233

## CHAPTER 8

### *EXPERIMENTS ON POINTED ARCHES*

1. Introduction.....	237
2. The experimental campaign.....	239
3. Friction test.....	242
4. Moving the supports apart.....	245
5. Moving the supports together.....	249
6. Moving the support vertically.....	255
7. Experiments vs Modelling.....	261
8. Conclusions.....	264

---

<b>CONCLUSIONS.....</b>	<b>267</b>
<b>REFERENCES.....</b>	<b>273</b>
<b>APPENDIX: COMPUTER PROGRAMS.....</b>	<b>281</b>



## **INTRODUCTION**

Masonry churches are particularly prone to damages and partial or global collapses when subjected to horizontal actions. High seismic vulnerability of these ancient buildings can be associated both to the particular configuration of this type of constructions and to the mechanical properties of the masonry “material”.

Basilica churches have been selected in this study because of this typology is widely spread all over the national territory and is characterized by the presence of typical constituting elements so that a generalization of results obtained from a small group of study cases to a larger sample of religious buildings is possible.

### **1. SEISMIC BEHAVIOUR OF MASONRY CHURCHES**

Basilica structures are usually constituted by a façade, a hall (with one or more naves), a presbytery and an apse; besides, a transept, a dome, the lateral chapels can be added; often, a bell tower or a sail is present.

More in general, churches are characterized by the presence of large wall panels of (both in length and in height) without internal thorn walls, slenderness of some vaulted structures (folded vaults), presence of thrusting elements of large span (arches, vaults and domes), lack of intermediate connection, degradation due to the scarce use and maintenance of some parts (bell towers).

Furthermore, ancient constructions generally show several sources of seismic vulnerability. More specifically, the horizontal inertial forces can provoke the lost of equilibrium, especially in the slender and not connected elements (spires, sails, bad connected parts). Besides, the lack of rigid horizontal elements allows an autonomous dynamic vibration of the different parts of the structure. Churches, more than other typologies, show the absence of box behaviour with the consequent partial collapse possibility.

Moreover, almost all the churches have undergone deep transformations during their life, which eventually turn out in:

- *uncertain characterization of the mechanical properties* (large variability of the mechanical properties due to the making and working process, and use of natural elements);
- *lacking of the knowledge of the original construction*;
- *construction steps* like plan increasing, raisings, masonry wall insertion in the hall, realization of new buildings leaning on the old structure;
- *damaging* (soil movements, damaging of the materials);
- *permanent or progressive strains, cracking, physical or chemical degradation of the materials* (mainly due to traffic jam, wind and thermal loads);
- *induced damages from previous interventions* (earthquakes, fires, thunderbolts) that have induced cracking in the walls (cracking states) through which tension stresses can not be transmitted anymore;
- *recent retrofit interventions* (a part from their efficacy, have generally transformed the original structural working);

- *non applicability of the code provisions;*

Therefore, ancient buildings undergoing exceptional events are also affected by interaction with phenomena that can seriously compromise the whole structure [Roca P. & Gonzalez J.L., 1996].

## **2. DAMAGES IN MASONRY CHURCHES**

Generally, the seismic collapse of masonry constructions occurs for the equilibrium loss of some structural parts, rather than the overcoming of a limit stress state of strength.

Masonry walls are subjected to compression vertical stresses, to which bi-dimensional stress in the plane of the wall, close to the openings or pointed loads, and flexural stresses, if horizontal loads due to the presence of arches and vaults are present, are superimposed.

The collapse mechanisms related to the action induced by vertical loads are:

- *local crushing of constituting elements:* it occurs in the mortar when it is particularly poor and the thickness of the joints is high; or in the units if poor or very degraded. Furthermore an irregular composition of the stone elements can determine stresses concentration so that local crushing phenomena can occur.

- *instability of the walls:* it is dependent on: 1) insufficient thickness of the walls compared to the internal core; 2) lack of diatoms or other type of tothing able to guarantee the monolithicity of the wall; 3) strongly eccentric load condition.

In the wall loaded out of the plane, Rondelet (1802) individuated three collapse modes as a function of the geometry and constraint conditions. In all three mechanisms, a loss of equilibrium of the collapsing portion occurs: the static vertical loads have a stabilizing effect, whilst the horizontal action implies a bending moment with respect to the rotation axes. If the horizontal action acts in the plane of the wall, two types of mechanisms dependent on the geometry, constraint conditions, the compression state, the wall composition are individuated. In stocky walls the sliding

of the superior parts on the inferior ones is ruled by the friction coefficient. In slender walls the overturning of a part of wall around a hinge point will occur.

Referring to churches, some particular collapse mechanisms have been individuated after seismic events [Doglioni F., Moretti A. & Petrini V., 1994]; in the following they will be summarized as a function of the constituting elements of the structure.

1. **façade**: typical collapse mechanisms of this macroelement, studied in detail also in [Casolo S. et Al., 2000], are generally due to the interaction with the orthogonal elements, the presence of openings or thrusting roof structures, the shear failure in stocky elements.

More in detail, when the tympanum on the top, lacking a good connection with the roof, undergoes the maximum oscillations, its overturning out of the plane around a horizontal or a diagonal axis could occur. Furthermore since the presence of openings is a weakening factor of the wall texture, the overturning of the element at the height of the openings can develop. The horizontal thrust of vaults and arches on the lateral walls with tension stresses in the panel could imply the formation of vertical cracks in the middle of the panel as well as the shear effect can be detected with diagonal crossed cracks. Finally, the rotation out of plane of the corner is due to the interaction of the forces acting on orthogonal walls.

2. **triumphal arch**: vertical loads involve symmetrical mechanisms in the element like sliding in the abutments (which implies some cracks in the arch) or five hinges kinematics. These mechanisms could cause the collapse as a function of the material, the constructive way, the presence of niches or dimensions of the blocks. The horizontal action represents, on the contrary, an asymmetric system so that the collapse occurs for the overturning of one or both the abutments if slender piers are present. Non symmetrical cracks can happen because of the presence of some rotational restraints. Another mechanism with discordant rotation of the piers has been noticed when a chain is present on the top of the arch.



3. *lateral walls*: the collapse mechanisms of perimetrical walls in churches are function of the trusses constraint to the piers and the presence of openings. In lacking or small openings walls the formation of horizontal cracks at a low level (close to the foundation) could occur. When some openings are present, a more complex distribution of the damages will be detected. A frequent mechanism is the formation of horizontal cracks at the base of the holes and vertical in correspondence of the architrave determining the formations of rotating blocks outside. Due to the interaction of the roof, this mechanism can also occur in association with the expulsion of the truss beam support and the rotation out of the plane of the façade.

4. *apse*: its failure depends mainly on the shape, presence of openings and truss constraints. In case of circular apses or chapels, the localization of the crack lines starting from the top at the intersection with the hall until low quotes in the middle is the most recurrent mechanism. Cracks are characterized by a V opening, bigger on the top and decreasing toward the bottom. The presence of vaults or struts which thrusts are not absorbed by beams or steel hoopings or openings in the panels can determine preferential crack patterns. In case these forces are absorbed, the mechanisms transforms in diagonal cracks with the typical shear behaviour.

### **3. PRINCIPAL AIM AND CONTENT OF THE THESIS**

This thesis intends to study the structural behaviour of basilica churches under horizontal actions. Hard topics for masonry structures like material and elements modelling and analysis methodology are taken into account. Surprisingly, also the seismic action indicated by Code Provisions shows some troubles. In order to apply the issues above cited, some study cases have been selected and deeply analyzed in their features. After carrying out a geometrical assessment of the churches some different analysis types are conducted: linear analysis on three-dimensional complexes and non linear analysis on bi-dimensional elements. Results in terms of

dynamic behaviour, seismic action distribution, strength demand, horizontal stiffness and bearing capacity are evaluated in the study cases.

Successively, the need of a simplified analysis with the aim of obtaining an approximate evaluation of the bearing capacity of single elements, with few calculations and without time consuming and complex analyses, is considered. In order to seek this procedure on churches macroelements, a basic structural element in historical buildings, such as the portal frame, is studied in detail. Collapse mechanisms and maximum load multiplier and simplified formulas are obtained for the portal frame. The extension of the single portal frame to the multi-bay frame is applied in order to perform the comparison between non linear analyses and simplified analyses.

Finally, another typical masonry element is analyzed through the application of limit analysis: the masonry arch. The theoretical formulation for determining the range of horizontal thrust and maximum displacements in the plane is verified through an experimental campaign.

In the following a brief summary of the content of this thesis is reported:

In **Chapter 1**, the state of the art in modelling and analysis of masonry structures is illustrated; in particular, the material and the structural approach, the horizontal actions (in terms of equivalent seismic forces and spectra), the analyses types (linear, non linear and limit ones) are analyzed. Finally, the applied methodology chosen in a range of possibilities illustrated in literature is exposed.

In order to assess the seismic behaviour of basilica structures, four study cases have been selected. These churches are illustrated in **Chapter 2**, characterizing the geometry (global and of the single elements) and the load conditions. In the light of this study, the geometrical and typological features are analyzed and a comparison in geometrical terms of the churches is made.

In **Chapter 3**, linear analyses of three-dimensional models of the study cases are conducted. The dynamic behaviour of the churches, the seismic action distribution,

and the strength demands are analyzed in the hypothesis of presence or lack of a rigid diaphragm at the roof level.

The second part of the methodology is based on non linear analyses which are carried out in **Chapter 4**. After having exposed the model calibration, bi-dimensional analyses are illustrated. The bearing capacity and the horizontal stiffness of the churches elements are calculated. Summary plot for each church and the comparison between strength demand and bearing capacity are furnished and the reliability of the used computer code is commented.

In the following two Chapters, a simplified procedure for the seismic assessment of basilica macroelements is provided. Through the application of the kinematic theorem of Limit analysis, in **Chapter 5** the behaviour of masonry portal frame is analyzed. Expressions of kinematic multipliers in closed form are given and a parametric analysis is performed varying the geometrical proportions so that a simplified formula is proposed. Later, in **Chapter 6** the application of this simplified methodology to the churches macroelements is made. The comparison of FEM – limit analysis is discussed with reference to the analyzed study cases and some conclusive remarks for each church are made.

In the last two chapters, the behaviour of masonry pointed arch is studied in detail. The theoretical approach is exposed in **Chapter 7** through the application of the static theorem of Limit Analysis. The proposed methodology consists into the evaluation of the thrust values ranges, the minimum thickness, the maximum displacements of one support of the arch through numerical algorithm and graphical statics. Furthermore, the behaviour of the half arch and a comparison of arches with same span and weight or same span and thickness are made. In the following **Chapter 8** the validation of the theory on pointed arches is made through a vast experimental campaign on small scale structures. The test procedure has been illustrated and the test types as well. The comparison between theory and practice is enlightened.



## **CHAPTER 1:**

### ***MASONRY STRUCTURES: MODELLING AND ANALYSES***

#### **1. INTRODUCTION**

Seismic behaviour analysis of masonry historical structures is a hard topic due to the difficulties in the numerical modelling of material non linear behaviour, to the incomplete experimental characterization of the mechanical properties and to the complexity of the geometrical configuration.

A panoramic view of the different approaches adopted in the research field to the study of masonry structures is illustrated in this chapter, dealing with the modelling of the material and the structure, the action applied and the analysis types.

## 2. MATERIAL MODELLING

With the term masonry we intend a structural material made by the assemblage of natural (stones) or artificial (bricks) elements with or without mortar, suitable for the realization of the bearing elements of a construction.

The difficulty of modelling the masonry depends on the following factors:

- masonry is a discrete material (blocks and mortar) in which the dimension of the single constituting element is large compared to the dimensions of the structural element;
- the geometry, origin and blocks placing can vary considerably;
- blocks are stiffer than mortar;
- the mortar thickness is limited (if compared to the block dimensions);
- stiffness of the vertical joints is remarkably smaller than the one of the horizontal joints.

More in detail, the physic-chemical and mechanical parameters in the interaction between the stone units and the mortar joints are referable to the following factors:

*Properties of the stone elements* such as: compression and tension strength with monoaxial and pluriaxial stresses; elasticity module, Poisson coefficient, ductility and creep; water proof and superficial (roughness) characteristics; chemical agent resistance; volume variation for humidity, temperature and chemical reaction; weight, shape and holes dimensions.

*Properties of the mortar* such as: compression strength and behaviour under pluri-axial stresses; elasticity module, Poisson coefficient, ductility and creep; adhesive force; workmanship, plasticity and capacity of detaining water.

*Construction formality* such as: geometry and placing of the stone elements; filling of the joints at the head; ratio of the joint thickness and dimensions of the stone elements; placing hand crafty; dis-uniformity of the layers.

Actually, if some mono-axial tests are carried out separately on the constituting masonry elements (mortar and blocks), the typical qualitative behaviour shows good

compression strength and very poor tensile strength. But, whilst the stone has a nearly linear behaviour, larger elastic module and almost brittle failure, the mortar shows a non linear behaviour, larger elastic module and certain ductility.

The need of characterizing with a suitable constitutive model the masonry material has lead to a series of modelling strategies [Sacchi Landriani G. & Riccioni R., 1982; Molins Borrel C., 1995].

Depending on the desired level of accuracy and simplicity, the following methods have been individuated:

1. detailed micro-modeling: the block and the mortar in the joints are represented by continuum models, whilst the interface unit-mortar is represented by discontinuous elements. The Young model, the Poisson coefficient and the inelastic properties of the units and the mortar are taken into account.
2. simplified micro-modelling: the units are extended through the joints and are represented by continuous elements, whilst the interface unit-mortar is represented by discontinuous models. In other words, masonry is considered as a whole of elastic blocks surrounded by fracture lines in the joints. Poisson coefficient and the inelastic properties of the unit and the mortar are neglected.
3. macro-modelling: units, mortar and interface unit-mortar are spread in a continuum. The difference between the units and the joints does not occur anymore but it is considered as an isotropic or anisotropic homogeneous continuum.

Some homogenization theories for periodic media have been developed in literature in order to derive the global behaviour of masonry from the behaviour of the constitutive materials (brick and mortar). The procedure has been performed in several steps (head joints and bed joints being introduced successively) [Lee J.S., Pande G.N. & Al., 1996] or in one step on the real geometry of masonry [Anthoine A., 1995; Luciano R. & Sacco E., 1997; Zucchini A. & Lourenco P.B., 2002]. Later a

continuum damage modelling for the brick and the mortar has been added [P. Pegon, A. Anthoine, 1997; Luciano R. & Sacco E., 1998; Zucchini A. & Lourenco P.B., 2004].

This physic-mathematic abstraction, i.e. transforming the reality into a scheme governed by mathematically treatable laws, can appear arbitrary for masonry. In reality, each material is provided with a micro-structure and the assimilation to a continuum implies an operation of stress average on a suitable reference volume. The masonry material, realized through the assemblage of two components, shows a constitutive bond characterized by a non linear law and intermediate compression strength to both the single components. The limit of the linear behaviour coincides with the beginning of the partialization of the section; it has to be pointed out that this phenomenon, in a material provided of reduced tension strength, occurs for smaller load levels compared to the bearable ones.

Therefore, micro-modelling is necessary to better understand the local behaviour of masonry structures; macro-modelling is applicable when the structure is composed of walls of sufficient dimensions so that the stresses along the length of the element are uniform. This type of modelling is preferable when a compromise between accuracy and efficiency is required.

In this study only the macro-modelling approach has been considered in the application to the study cases.

Other two important aspects related to the material in the analysis and behaviour of masonry are the size effect (unit size vs. structural size) and the influence of the material parameters on the numerical analysis [Lourenço P.B., 1997].

### **3. STRUCTURAL MODELLING**

Another complex topic in masonry is the choice of a suitable model representing the structure. Inside the hypothesis of homogeneous material, two model types can be distinguished:



1. models with structural components among which different approaches are distinguishable:
  - *With lumped masses*: it's a rough approximation of the geometry of the structure but it can be sufficient in order to determinate the structural dynamic response (if the non linearity of the material and the resultants effects of the real geometry of the structure are included). Quite obviously, this type of model can't be used to predict the local or global collapse mechanisms or the damage levels of the single structural components.
  - *With beams and columns*: it defines in greater detail the behaviour of the system than the former one. It's possible to determine the sequential formation of the collapse mechanisms both statically and dynamically.
  - *Macroelements*: introduced by [Doglioni F., 1994] for the first time, it considers the structure as a whole of wall panels each of them is a recognizable and complete part of the building. It can also coincide with an identifiable part of it under the architectural and functional aspect (for example: the façade, the apse, the chapels); usually it is formed by more panels and horizontal elements connected each other so that they represent a unitary constructive part even if it is joined and not independent from the whole of the construction.
2. Finite Element Method that can be bi and three-dimensional models with mono-dimensional (frame), bi-dimensional (shell) or three-dimensional (brick) elements. Shell elements produce faster and more controllable models because of the presence of a smaller number of joints if compared to the brick elements. The model with the three-dimensional elements allows, on the contrary, the visualization of the stresses evolution inside the structure. Notwithstanding this, the results gained in the two analysis types are similar, both in terms of structural strains and stress distribution, even if with a factor scale (for the bigger stiffness of the brick elements). It seems preferable, therefore, avoiding the shell elements in important areas for the global behaviour of the structure. In the Finite Element Model there is also the meshing

problem: to its increasing, the results reliability is strongly influenced by convergence problem solution; therefore, using a dense mesh could not be the better option.

Another hard topic in the study of masonry structures is the use of bi-dimensional models (parts of the structure) or three-dimensional models (structures in their whole). It has to be said that the last ones are time consuming in the preparation of the model and in the analysis of the results and that because of the big dimension of the model, some important aspects could be lost in sight. From one point of view, it's preferable modelling some structural parts and details instead of modelling great and complex structures.

More in general, a global model is worth because it is able to implicitly catch the interactions between the different parts of the building, but usually it is too complex from the conceptual and operative point of view in an historical construction.

The study of the dynamic response through a modal global analysis could not have a lot of meaning because it founds on the superimposition of independent vibration modes, each of them involves the whole construction. If some disconnectedness is present in the structure, each element will tend to vibrate autonomously, with a self vibration frequency. The other prerogative of the modal analysis is the linearity of the material behaviour, necessary to carry out the superimposition of the effects in the different modes: also this qualification could not be satisfied in an historical building. On the other point of view local models tend to simplify sometimes the analysis through rough hypothesis; nevertheless they have the value of using intuitive calculus schemes and easy interpretability of the results.

Herein, the study cases are analyzed through both the approaches above illustrated. Models with structural components (macroelements) are used in the application of the Limit Analysis; Finite Element Method is applied in linear and non linear analyses. More in particular, the commercial computer code SAP2000 (CSI,

2000) has been used for the analysis of three-dimensional structures in the linear field; the code ABAQUS (HKS, 2004) has been used for non linear analyses of bi-dimensional structures.

#### 4. HORIZONTAL ACTIONS

In seismic areas, in addition to vertical loads, horizontal actions have to be applied onto the structure. DM96 (M.LL.PP., 1996), EC8 (CEN, 2002), ORDINANZA 3274 (O.P.C.M. 2003) and the following ORDINANZA 3431 (O.P.C.M. 2005) codes have been taken into account. Being the ground acceleration function of the seismic code, the difficulty into considering a suitable horizontal action applicable onto masonry structures is here enlightened.

Notwithstanding it in [Meli R. & Sanchez-Ramirez R., 1996] some comments are made about the effects of different types of ground motion on monuments and about the qualification of the seismic action for the analysis of the structure.

##### 4.1. EQUIVALENT SEISMIC FORCES

In static analyses, loads equivalent to the seismic action are applied onto the structure through the introduction of proportional weight forces.

In the DM96 code provisions, the values of these forces on buildings are:

$$F_h = c \cdot R \cdot I \cdot \varepsilon \cdot \beta \cdot \gamma \cdot W \quad (1)$$

Where:  $c$  is intensity seismic coefficient,  $R$  is the reply coefficient,  $I$  is the seismic protection coefficient,  $\varepsilon$  is the foundation coefficient,  $\beta$  is the structure coefficient,  $\gamma$  is the distribution coefficient and  $W$  is the whole weight of the masses.

In masonry structures, the value assumed by the structure coefficient  $\beta$  has a special meaning. It is the product of two other coefficients that are  $\beta_1$  and  $\beta_2$ . The first one takes into account the ductility of masonry constructions and it is equal to 2 in any case; the second one considers the collapse check modality and is assumed equal to 1 for new constructions and 2 for existing buildings.

In the EC8 (version November 2002 - draft n.6), OPCM 3274 and OPCM 3431 codes, the force is evaluated in the same way as:

$$F_h = S_d(T_1) \cdot m \cdot \lambda \quad (2)$$

Where:  $S_d(T_1)$  is the ordinate in the design spectra assumed by the building in the considered direction,  $m$  is the mass and  $\lambda$  a reductive coefficient that takes into account of the static analysis.

Compared to the previous formula, in this expression different structural systems are considered in an indirect way and are included in the definition of the first period of the structure. The approximated evaluation of this number depends on the height of the building and a coefficient considering the different typologies.

#### 4.2. ELASTIC SPECTRA

The earthquake motion in a given point of the surface is represented by an elastic ground acceleration response spectrum, called “elastic response spectrum”. The shape of the elastic response spectrum is the same for the no collapse requirement (Ultimate Limit State) and for the damage limitation requirement (Damage Limit State).

According to **EC8**, **OPCM 03** and **OPCM 05** the elastic spectrum is:

$$\begin{aligned} 0 \leq T \leq T_B & \quad S_e(T) = a_g \cdot S \cdot \left[ 1 + \frac{T}{T_B} \cdot (\eta \cdot 2.5 - 1) \right] \\ T_B \leq T \leq T_C & \quad S_e(T) = a_g \cdot S \cdot \eta \cdot 2.5 \\ T_C \leq T \leq T_D & \quad S_e(T) = a_g \cdot S \cdot \eta \cdot 2.5 \cdot \left( \frac{T_C}{T} \right) \\ T_D \leq T \leq 4s & \quad S_e(T) = a_g \cdot S \cdot \eta \cdot 2.5 \cdot \left( \frac{T_C \cdot T_D}{T^2} \right) \end{aligned} \quad (3)$$

Where:  $a_g$  is the design ground acceleration,  $S$  is the soil factor,  $T$  is the vibration period of a linear single-degree-of freedom system,  $\eta$  is the damping correction factor with reference value of 1 for 5% viscous damping,  $T_B$ - $T_C$  are the limits of the constant spectral acceleration

branch,  $T_D$  is the value defining the beginning of the constant displacement response range of spectrum.

The value of  $a_g$  varies in function of the seismic zones and the values of  $S$ ,  $T_B$ ,  $T_C$  and  $T_D$  are function of the soil type. In case of soil B, they are reported in Tab.1.

Soil B	S	$T_B$ [s]	$T_C$ [s]	$T_D$ [s]
EC8	1.2	0.15	0.50	2
OPCM03-05	1.25	0.15	0.50	2

Table 1. Coefficients for Soil Type B.

In elastic spectra another quantity is also present, namely  $\eta$ , which is considered equal to 1 if the viscous damping ratio of the structure  $\xi$  is 5%.

In the following plot (Fig. 1), the shape of EC8, OPCM 03 and OPCM 05 spectra are reported for class of soil B, in zone 1 ( $a_g=0.35$  g) and  $\eta=1$ .

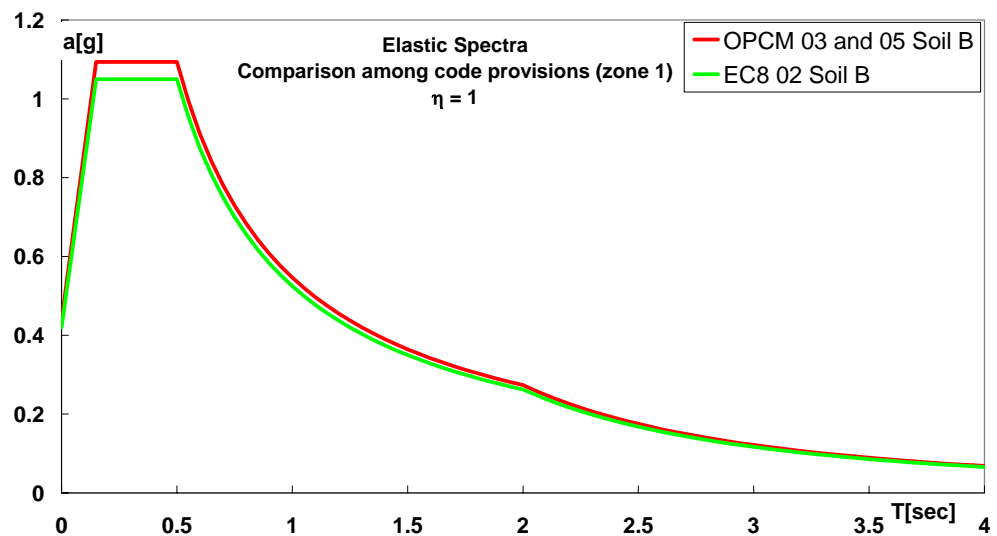


Figure 1. Elastic spectra in EC8, OPCM 03 and OPCM05 codes.

They are fairly similar except the fact that OPCM 03 and 05 consider a Soil factor  $S$  equal to 1.25 instead of 1.2 by EC8.

It has to be pointed out, furthermore, that the material and the type construction do not play any role in the elastic spectra, so that they are valid for any structure.

### 4.3. DESIGN SPECTRA

The capacity of structural systems to resist to seismic actions in the non linear range generally permits their design for smaller forces than those corresponding to a linear elastic response. To avoid explicit inelastic structural analysis in design, the capacity of the structure to dissipate energy, mainly through ductile behaviour of its elements, is taken into account by performing an elastic analysis based on a reduced response spectrum with respect to the elastic one, called “design spectrum”. This reduction is accomplished by introducing the behaviour factor  $q$ . It is the ratio of the seismic forces that the structure would experience if its response was completely elastic to the minimum seismic forces that may be used in design still ensuring a satisfactory response of the structure. The values of  $q$  are given by the code provisions for the various materials and structural systems.

Generally, for masonry structures this value is fairly low because of the small plastic re-distribution (masonry works mainly to pure compression where stresses are uniformly distributed).

According to EC8, values in masonry are depicted in table 2 where the underlined values are recommended:

Type of construction	Behaviour factor $q$
Unreinforced masonry according to EN 1996 (recommended only for low seismicity cases)	<u>1.5</u>
Unreinforced masonry according to EN 1998-1	<u>1.5</u> – 2.5
Confined masonry	<u>2.0</u> – 3.0
Reinforced masonry	<u>2.5</u> – 3.0

Table 2. Types of construction and behaviour factor according to EC8 code.

In the recent Italian code OPCM 03 this range of variability is limited only to two classes of masonry types (Table 3).

Type of construction	Behaviour factor $q$
Unreinforced masonry	1.5
Reinforced masonry	2.0 – 3.0

Table 3. Types of construction and behaviour factor according to OPCM 03.

But in its upgrading (OPCM 05) the behaviour factor  $q$  has been deeply changed according to the building technique and if the structure is new or already existing. Political reason maybe are under the decision of increasing the behaviour factor in masonry structures; values of ground acceleration so high in OPCM03 would have involved the retrofit of a too huge quantity of ancient buildings in the country non comforted by the economical aspect. At the moment for existing buildings, it is equal to the product of a number (function of the regularity in height) and a coefficient  $\alpha_u/\alpha_1$  so defined:

- $\alpha_1$  is the multiplier of the horizontal seismic action for which, keeping constant the other actions, the first masonry panel reaches the ultimate strength (for shear or compression+bending).
- $\alpha_u$  is the 90% of the seismic horizontal action for which, keeping constant the other actions, the building reaches the maximum resistant force.

The value of this ratio can be calculated through a non linear static analysis and can not be larger than 2.5, or the following values can be adopted:

Type of construction	$\alpha_u/\alpha_1$
Unreinforced masonry buildings with 1 floor	1.4
Unreinforced masonry buildings with 2 or more floors	1.8
Reinforced masonry buildings with 1 floor	1.3
Reinforced masonry buildings with 2 or more floors	1.5
Reinforced masonry designed with the strength hierarchy	1.3

Table 4. Evaluation of  $\alpha_u/\alpha_1$  according to OPCM 05.

and the behaviour factor  $q$  assumes the following values:

Regularity	$q$
Buildings regular in height	$2.0 * \alpha_u / \alpha_1$
In the other cases	$1.5 * \alpha_u / \alpha_1$

Table 5. Evaluation of  $q$  according to OPCM 05.

In the same section of masonry existing buildings it is declared that, in absence of precise evaluations, a ratio  $\alpha_u/\alpha_1$  equal to 1.5 can be assumed. This means that for masonry churches, generally 1 floor developed and not regular in height, the factor  $q$  should be equal to the product of  $1.4 * 1.5 = 2.1$  if table 4 is considered or  $1.5 * 1.5 = 2.25$  if the note in the existing section is taken into account.

The design spectrum indicated in the **EC8** assumes the shape of:

$$\begin{aligned}
 0 \leq T \leq T_B & \quad S_d(T) = a_g \cdot S \cdot \left[ \frac{2}{3} + \frac{T}{T_B} \cdot \left( \frac{2.5}{q} - \frac{2}{3} \right) \right] \\
 T_B \leq T \leq T_C & \quad S_d(T) = a_g \cdot S \cdot \frac{2.5}{q} \\
 T_C \leq T \leq T_D & \quad S_d(T) = a_g \cdot S \cdot \frac{2.5}{q} \cdot \left( \frac{T_C}{T} \right) \\
 T_D \leq T \leq 4s & \quad S_d(T) = a_g \cdot S \cdot \frac{2.5}{q} \cdot \left( \frac{T_C \cdot T_D}{T^2} \right)
 \end{aligned} \tag{4}$$

Where:  $a_g$  is the design ground acceleration,  $S$  is the soil factor,  $T$  is the vibration period of a linear single-degree-of freedom system,  $q$  is the behaviour factor,  $T_B$ - $T_C$  are the limits of the constant spectral acceleration branch,  $T_D$  is the value defining the beginning of the constant displacement response range of spectrum.

In the **OPCM 03** and **OPCM 05** the design spectrum in the ULS is:

$$\begin{aligned}
 0 \leq T \leq T_B & \quad S_d(T) = a_g \cdot S \cdot \left[ 1 + \frac{T}{T_B} \cdot \left( \frac{2.5}{q} - 1 \right) \right] \\
 T_B \leq T \leq T_C & \quad S_d(T) = a_g \cdot S \cdot \frac{2.5}{q}
 \end{aligned} \tag{5}$$



$$T_C \leq T \leq T_D \quad S_d(T) = a_g \cdot S \cdot \frac{2.5}{q} \cdot \left( \frac{T_C}{T} \right)$$

$$T_D \leq T \leq 4s \quad S_d(T) = a_g \cdot S \cdot \frac{2.5}{q} \cdot \left( \frac{T_C \cdot T_D}{T^2} \right)$$

Where:  $a_g$  is the design ground acceleration,  $S$  is the soil factor,  $T$  is the vibration period of a linear single-degree-of freedom system,  $q$  is the behaviour factor,  $T_B$ - $T_C$  are the limits of the constant spectral acceleration branch,  $T_D$  is the value defining the beginning of the constant displacement response range of spectrum.

In DM96 spectrum, instead of the  $q$  factor, there is the  $\beta$  factor whose values already explicated in the equivalent seismic forces, characterize the masonry structures.

$$\frac{a}{g} = c \cdot R \cdot I \cdot \beta \quad (6)$$

Where:  $c$  is intensity seismic coefficient,  $R$  is the reply coefficient,  $I$  is the seismic protection coefficient and  $\beta$  is the structure coefficient.

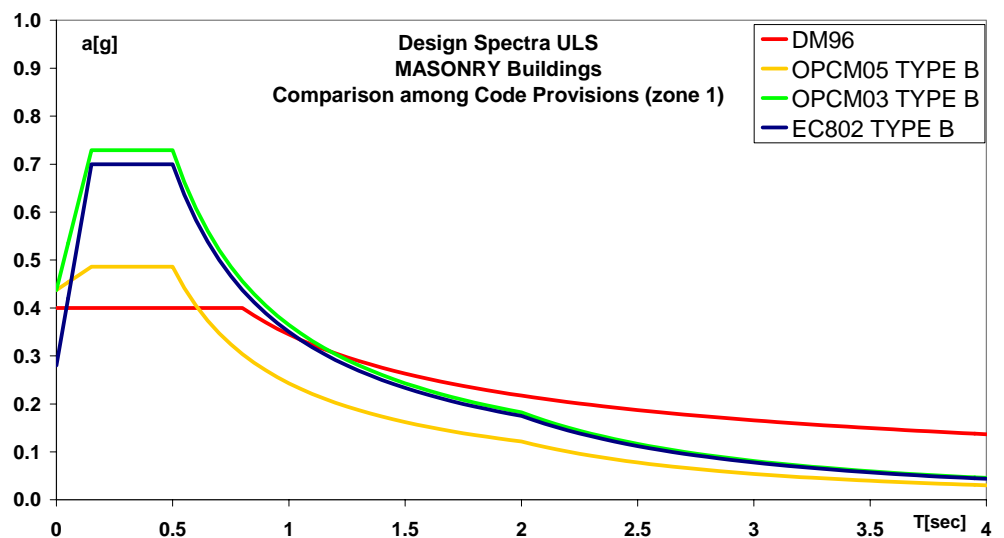


Figure 2. Elastic spectra in EC8, OPCM 03 – OPCM 05 and DM96 Codes.

In Fig. 2 the design spectra given by EC8, OPCM03-05 and DM96 are provided in the first zone ( $a_g = 0.35g$ ). It can be noticed how EC802 and OPCM03 design spectra are close except for the starting value because of the different evaluation of  $S$  (as in the elastic spectra) and a factor equal to 1 in OPCM03 and 2/3 in EC8 when period varies between 0 and  $T_B$ . On the other side, the OPCM05 is fairly close in terms of spectral ordinate to the previous evaluation made by DM96 compared to OPCM03 and EC8.

In this study, the DM96 and EC8 codes have been considered using the equivalent seismic forces in the static analyses and the design spectra in the dynamic analyses. The coefficient  $\beta$  adopted in the calculation of the forces in DM96 is equal to 4 being the study cases existing constructions. In the EC8 spectra, on the contrary, the reference soil was type A with a behaviour factor  $q = 1.5$ . As furnished by the two codes, seismic actions have been considered acting not contemporarily in the two principal directions of the buildings.

## **5. ANALYSES TYPES**

On masonry structures it is possible to carry out numerous analysis types. They are summarizable in three groups: linear analyses, non linear analyses and limit analysis.

### **5.1. LINEAR ANALYSES**

It is the simplest analysis type in which the material obeying to the Hooke's law is assumed. Therefore the elastic properties of the material and the maximum allowable stresses are necessary. The obtainable results are the deformed shapes and the stress distribution in the structure. In case of stress redistribution it is possible to assume a reduced stiffness in correspondence of the cracked areas. A linear analysis can help in the comprehension of the behaviour of a construction with regard to service loads, when the material still shows an elastic behaviour. On the other hand, it is not useful into the establishment of the collapse limits. The linear model is particular effective

into the identification of the global behaviour tendency of the building and the individuation of the points where the structure is subjected to tension stresses able to break the continuity of masonry elements.

In seismic areas, linear analyses are applicable also in the calculation of structures in presence of seismic forces. More in particular, it is possible to carry out two types of analyses: the linear static and the modal dynamic ones, as described in the following.

#### **5.1.1. LINEAR STATIC ANALYSES**

The linear static analysis consists in the application of a force system distributed along the height of the building assuming a linear distribution of the displacements. In case of buildings made of a series of floors, these forces are applied at each slab where it is assumed that forces can be concentrated. In case of masonry monumental buildings, like churches (lacking slabs if not on the roof) the problem is overcome in a different way. Whether the walls are modelled with bi-dimensional elements, the horizontal forces, proportional to the weight, can be introduced directly on the shells. In this way, every single geometric variation, like the presence of openings or different thickness in the walls, will be taken into account.

This type of analyses has been carried out on three-dimensional models of the four study cases.

#### **5.1.2. MODAL DYNAMIC ANALYSES**

The modal analysis, associated with the design response spectrum, can be performed on bi or three-dimensional structures in order to obtain the stresses values in the elements. In this analysis, all the vibration modes with a participating mass bigger than 5% should be considered summing up a number of modes so that the total participating mass is larger than 85%. In order to calculate stresses and displacements in the structure, SRSS or CQC combination rules may be used.

Also this type of analyses has been considered in the study of the four study cases.

## **5.2. NON LINEAR ANALYSES**

It is possible to study the complete response of the structure from the elastic field through the cracking, until the complete collapse. Different types of non linear behaviour exist: *mechanical* (connected to the non linearity of the material), *geometrical* (connected to the fact that the application point of the loads changes increasing the actions) and *of contact* (connected to the interaction of two corps). It is also possible to carry out non linear analyses with damage models very useful into the evaluation of the stiffness loss at global and local level. This type of analysis requests the elastic and inelastic properties and the strength of the material. The results that can be gained are the strain behaviour, the stress distribution and the collapse mechanism of the structure.

In addition to the vertical ones, in presence of horizontal actions, a non linear static analysis can be carried out.

### **5.2.1. NON LINEAR STATIC ANALYSES**

The non linear static analysis consists into the application on the structure of the vertical loads (self weight and dead loads) and a horizontal forces system monotonously increasing until the reaching of the limit conditions. The method, used also in the evaluation of the bearing capacity of existing buildings, is comprised in the last seismic codes.

This type of analysis has also been carried out in this study on bi-dimensional elements extrapolated from the whole structures of the four study cases.

### 5.3. LIMIT ANALYSES

This analysis type is aimed at the evaluation of the collapse load. The theoretical principles that allow making a seismic check through the limit analysis are conceptually simple but result of complex and delicate application for the following reasons: it is not useful to interpret the cause and the extension of the cracks, strains or other damages not directly related to the collapse generation; furthermore its use is fairly difficult in complex structures with a lot of elements.

The two theorems of the limit analysis, due to Godzev (1938) and Drucker, Prager and Greenberg (1952), are:

- static theorem: the plastic collapse load multiplier  $\gamma_p$  is the largest of all the multipliers  $\gamma_\sigma$  correspondent to the statically admissible set ( $\gamma_p \geq \gamma_\sigma$ ). For statically admissible set, a stress distribution in equilibrium with the external forces that in no point violates the plastic conditions is intended.
- kinematic theorem: the plastic collapse load multiplier  $\gamma_p$  is the smallest of all the multipliers  $\gamma_\sigma$  correspondent to possible collapse mechanisms ( $\gamma_p \leq \gamma_\sigma$ ). For kinematically admissible set, a kinematism or a distribution of velocity of plastic deformations, related to the distribution of plastic hinges, which satisfies the condition of kinematic compatibility, is intended.

These theorems generate two correspondent calculus methods of the collapse multiplier:

- static method: it consists into assuming a distribution of statically admissible stresses dependent by a certain numbers of parameters and search them so that the correspondent load multiplier is maximum.
- kinematic method: it consists into assuming a collapse mechanism dependent on some geometrical parameters and in the following minimization of the correspondent multiplier to the considered mechanism.

According to the uniqueness theorem, a multiplier that is statically and kinematically admissible coincides necessarily with the collapse multiplier.

### 5.3.1. LIMIT ANALYSIS APPLIED TO MASONRY STRUCTURES

The masonry constitutive model is of fragile type with a high value of collapse in compression compared to tension. The collapse tension stress is not only small but is characterized by a high uncertainty of evaluation because of the great scattering of the experimental results as well. This is the reason why in limit analysis a simplified diagram of linear indefinite elasticity on compression side and null collapse strength on tension is admitted. The masonry constitutive model coincides with materials called NRT (non resistant tension) and is defined by the following relationship:

$$\varepsilon = C\sigma + \varepsilon^{(f)}$$

$$\sigma \leq 0 \quad (\text{lack of tension})$$

$$\varepsilon^{(f)} \geq 0 \quad (\text{cracking strains})$$

$$\sigma \varepsilon^{(f)} = 0 \quad (\text{lack of internal dissipation})$$

The condition of convexity and the respect of the normality condition to the limit surface from the cracking strains, imply a tight connection between the theory developed by NRT materials and the classic theory of perfect plastic materials.

The study of masonry structures through limit analysis investigates the very essential aspects of the behaviour at collapse and, at the same time, seems to match modern analysis techniques with geometrical static principles raising from traditional theories.

The applicability of limit analysis to masonry structures has been firstly investigated by [Coulomb, 1773], in which a theory on the collapse behaviour of masonry elements was formulated. More recently, [Koorian, 1953] demonstrated how stone masonry can be dealt with through plasticity theorems. However, the main contribution in this regard is by [Heyman, J. 1966, 1969, 1995], who clearly stated some hypotheses on the mechanical behaviour of masonry, (already adopted, though implicitly, in the traditional pre-elastic theories). The following assumptions regarding material properties are made:

1. *Masonry has zero tensile strength.* Although this statement is conservative, it has to be considered that even if stones have a certain resistance, only very small tension forces will be transferred across joints because of the weakness or absence of the mortar;
2. *Infinite compression strength of the blocks.* In most cases, collapse of masonry structures is not governed by compression failure, but is due to cracks opening and mechanisms formation: this assumption is slightly unconservative;
3. *Sliding of a stone, or of part of the structure, upon another cannot occur.* Based on the experimental evidence that, generally, the angle between the thrust line and the sliding surface is greater than the friction angle.

With these assumptions, the only possible collapse mode is the rotation of adjacent blocks about a common point, so that masonry behaves as an assemblage of rigid bodies held up by compressive contact forces. The collapse is characterized by the formation of hinges among the single parts.

Uniqueness and safe theorems can be then respectively expressed as follows:

“If a thrust line representing an equilibrium condition for the structure under certain loads lies fully within the masonry, and allows the formation of sufficient hinges to drive the structure into a mechanism, then the structure is about to collapse. Further, in case of proportional loads, the load proportionality factor at collapse is unique.”

“If a thrust line, in equilibrium with the external loads and lying wholly within the structure, can be found, then the structure is safe.”

With these statements and under the outlined hypotheses, collapse analysis of masonry structures basically consists in seeking a thrust line, which is actually the graphical representation of equilibrium conditions, passing through a number of hinges sufficient to transform the structure into a mechanism.

Though the approach is conceptually simple and well posed from a theoretical point of view, a few points on its applicability and reliability can be arisen. First of all, infinite compression strength is assumed, while experience has shown how

structures made of materials with poor mechanical properties often do not develop mechanism-like collapse, rather large portions of masonry crush. Possibly, finite values of compression strength can be accounted for by moving the position of the hinges from the external boundary towards the inside of the masonry.

Secondly, it must be said that though limit analysis actually reveals the weakest points of the structure and provides a bound of the admissible horizontal action, it neglects, due to material assumptions, a few structural inelastic capacity issues, so that the safety assessment turns out to be fairly pessimistic.

The application of limit analysis in studying the collapse of structural elements under seismic-type lateral loadings seems to be very appealing. As a matter of fact, on account of the hypotheses assumed regarding the material properties and the mechanism formation schemes, the horizontal bearing capacity of a masonry element can be derived as a function of the geometry alone. In this regard several authors have made use of limit analysis for treating simple masonry elements, since complex buildings are often seen as assemblages of elementary structural schemes, so that the overall capacity can be somehow derived from the ones of the components. Although in complex structures it might be difficult to find the correct failure mechanism by limit analysis, it is outlined that this simplified modelling combines, on one side, sufficient insight into collapse mechanism, ultimate stress distributions and load capacity, and on the other, simplicity to be cast in a practical computational tool. Another appealing feature of limit analysis is the reduced number of necessary material parameters, given the difficulties in obtaining reliable data for historical masonry.

## **6. METHODOLOGY IN LITERATURE**

In the last forty years an enormous growth in the development of numerical tools for structural analysis has been achieved. On the same way, many possibilities of analyses have figured out to the attention of the researchers. In the following, an



overview of the procedures applied to masonry structures in order to understand their response is presented.

Limit analysis on masonry portals is applied in [Como M. & Grimaldi A., 1983]; the extension to this scheme is the full opened wall analyzed in [Como M., Lanni G., Sacco E., 1991; Abruzzese D. & Lanni G., 1994] and the presence of reinforcing chains exposed in [Abruzzese D., Como M. & Grimaldi A., 1985; Abruzzese D., Abruzzese D., Como M. & Lanni G., 1993; 1996]. Furthermore, in [Abruzzese D., Como M. & Lanni G., 1995] strength evaluation of circular and pointed arch with abutment piers with or without a reinforcing chain is evaluated as such as in [Abruzzese D., Como M. & Lanni G., 1990] the case of gothic cathedral is exposed. In [Bosco D. & Limongelli M.P., 1992], on the basis of [Como M. & Grimaldi A., 1983], a collapse analysis of a simple frame is made considering its most general, both geometric and loading features.

An application of limit analysis combined to structural dynamic is given in [Lo Bianco M. & Mazzearella C., 1985] in which the soil acceleration transforms the structure in a mechanism;

In 1994, [Pistone G., 1994] analyzes and compares different analysis methods (2D and 3D) through FEM on a case study.

Some computer programs have been developed by researches in these years with different purposes. In [Briccoli Bati S., Paradiso M. & Tempesta G., 1997] collapse loads of masonry arches subjected to vertical and horizontal loads are implemented in the commercial code AEDES 2000. In [Orduna A. & Lourenco P.B., 2001] a formulation, implemented in a computer program, accounting for a limited compressive stress in the masonry and non-associated flow rules for sliding failure is presented. In [D'Ayala D. Speranza E., 2003] analytical models developed to calculate load factors of various collapse mechanisms have been developed into a numerical procedure interfaced with an electronic form and database called FAMIVE. Also in [Valluzzi et Al., 2004] a compendium of the main mechanisms has

been implemented in the automatic procedure VULNUS able to carry global vulnerability analyses.

An overview of possible approaches for the numerical modelling of masonry structures is presented in an extensive way in [Lourenco P.B., 1998, 2001 and 2002]. Herein a review of displacement controlled experimental results and set-ups carried out in the last decade that are relevant for the purpose of sophisticated numerical modelling of masonry are also provided.

In [Roca P. et Al., 1998] the validity of several modelling techniques with a very different level of sophistication is studied through their use in the study of the Barcelona Cathedral.

Applications of limit analysis coupled to graphic static on real historical churches can be found in [Roca P. et Al., 1998] for the Barcelona cathedral and in [Huerta S., 2001] for the gothic cathedral of Palma de Mallorca.

In [Genna F., Di Pasqua M. & Veroli M., 1998], with reference to several constitutive models developed for the analysis of structures made of components weak in tension, many analysis types have been carried out on a model of a part of an old monastery placed in Brescia.

In [Lagomarsino S. et Al., 1998, 1999] the approach of macroelements combined to collapse mechanisms (overturning and shear) applied on churches is presented. Also [Augusti G. Ciampoli M. & Giovenale P., 2001; Augusti G. Ciampoli M. & Zanobi S., 2002], on the basis of the macroelement approach and of limit analysis techniques, have elaborated a procedure that allows to calculate the probability of collapse or distribution of damages of monumental buildings.

Pegon [Pegon P., Pinto A.V. & Geradin M., 2001] describes how 2D and 3D numerical modelling can be used in order to design a representative model of a built cultural heritage structure to test at the laboratory and to characterize its behaviour. Details on the models, starting from mesh generation and material description up to their non-linear results are given.

In [Roeder-Carbo G.M. and Ayala A.G., 2001] a review and evaluation of the methods of analysis currently used for the determination of stability conditions for historical buildings considering the elastic and inelastic properties of the masonry is presented.

The growing interest in the preservation of historic structures has allowed [Boothby T.E., 2001] to underline that although plasticity methods provide an intuitive approach, the usefulness in performing actual assessments has limitations. According to the author, the recent progress in the development of constitutive laws for ancient masonry structures and various formulations of 3D FEM and plasticity methods have also proven useful.

Performance-based concepts are discussed and applied in seismic assessment, rehabilitation and design of unreinforced masonry buildings in [Abrams D.P., 2001].

In [Giordano A., Mele E. & De Luca A., 2002] the applicability of different numerical techniques is investigated, comparing the computed results with the experimental test data obtained on a full scale masonry specimen (namely: ABAQUS, CASTEM 2000, UDEC).

Comparing the results of physical non linear analysis and limit analysis on a masonry arch, Lourenco [Lourenco P.B., 2002] yield the same failure mechanisms and safety factors, if a zero tensile strength is assumed.

In [Salonikios T. et Al., 2003] the results of comparative pushover analyses (through SAP2000 Non linear and CAST3M programs) of masonry plane frames are presented.

With reference to masonry panels 1 or 2 floors high, in [Decanini L.D. & Tocci C., 2004] it is recognised that limit analysis-based procedures are more conservative than strength-based ones.

As it can be noticed, generally the Authors propose two or more analysis types, enlightening the advantages and disadvantages, comparing and contrasting the results

and the reliability. Undoubtedly, the reason of this procedure has to be searched in the difficulty of really understanding the behaviour of these structures.

## **7. THE APPLIED METHODOLOGY**

The proposed analysis method is based on a two step procedure [Mele E., De Luca A. & Giordano A., 2003; De Luca A., Giordano A. & Mele E., 2004]: a) first of all, the whole structure is analyzed in the linear field through a complete 3D model, with the aim of characterizing the static and dynamic behaviour, defining of the distribution of the internal forces through the elementary parts and identifying the points of possible collapse of the structure; b) afterwards, the single structural elements are extrapolated from the 3D global contest into detailed 2D models, analyzed in linear and non linear field. These more refined analyses have the goal to define some structural properties (horizontal strength, lateral bearing capacity) that can be used for the simplified evaluation of the seismic behaviour of the whole building.

Finally, limit analysis has been used as a valid complement to the non-linear analysis of the macroelements under horizontal actions. This with the aim of comparing the results of the FEM analyses with a level that correspond to the minimum collapse multiplier among all the possible class of kinematics.

## **CHAPTER 2:**

### ***STUDY CASES***

#### **1. INTRODUCTION**

The religious buildings considered in this study are the church of “S. Giovanni a mare” (SGMR), of “S. Ippolisto” (SI), of “S. Giovanni Maggiore” (SGMG) and of “S. Paolo Maggiore” (SP) all placed in Naples with the exception of S. Ippolisto located in the area of Avellino. Some of these churches have been object of research in [Mele E., et Al. 1999] for SI and [Mele E., et Al. 2001] for SGMR.

In this chapter, a detailed analysis of these basilicas is conducted in terms of geometry, typology and load conditions. The type and the repetition of the structural elements open to the possibility of a general unique model differentiable only by a scale factor with a common seismic behaviour.

## 2. S. GIOVANNI A MARE

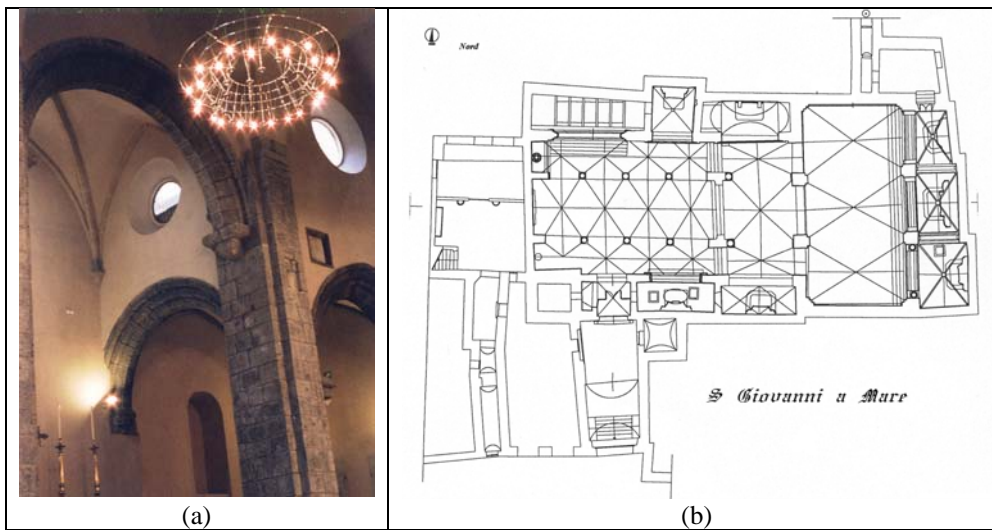


Figure 1. SGMR – a) Picture; b) Plant.

Firstly referred of in 1186, this church was annexed to a gerosolimitan hospital. It was built on a pre-existence, whose remains are still “in situ”. Since 1200, a transept with high cross vaults was leaned to the Norman building. Later to the primitive installation, recognizable for the central core with three naves scanned by columns, a second transept and lateral chapels were added. Around 1300 three apses were built. In 1336 and around 1400 the church underwent some modifications. The 1456 earthquake damaged the church and new alterations were made (the substitution of the wooden truss with cross vaults, the building of the bell tower). In 1500 the hospital disappeared. With the Risanamento works at the end of the XIX Century the church was included in new buildings. In 1949, the restoration of the church cancelled some pre-existences. After the 1980 earthquake the church was abandoned. In 1987 new restoration works began and in 2000 ended. Nowadays, the church is as shown in Fig.1.

## 2.1. GEOMETRY

The building is 38 m long and 19 m wide approximately; roof heights vary from 7 m on some chapels to 13.3 m on the transept roof. The thickness of masonry walls is around 0.8 m, the diameter of the columns between the principal nave and the lateral ones is around 0.5 m. The roof is formed by different types of vaults: sometimes barrel vaults, other times crossed vaults or “lunettate” that are the intersection of a barrel vault with a semicircular directrix with another one posed on pointed arches.

## 2.2. MACROELEMENTS

In Fig. 2 the schematic plan with the individuation of the alignments or the macroelements which form the structural system of the church are depicted.

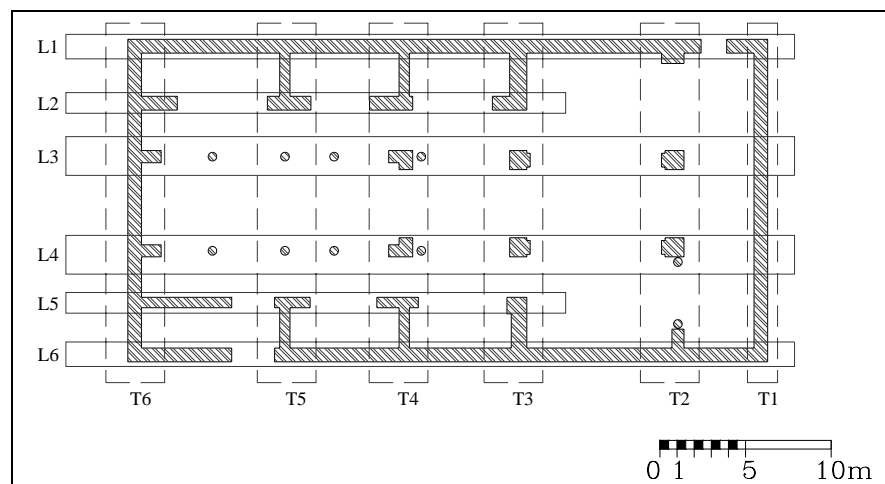


Figure 2. SGMR – individuation of the macroelements in plant.

They are identified by an alphanumeric code constituted by a letter and a number: the letter will be an L in case of longitudinal elements and a T in case of transversal ones; the number, on the contrary, identifies the single element in a crescent order from the apse to the façade for the transversal elements and from the left front to the right front for the longitudinal elements.

In the following Figures (from 3 to 13) each macroelement is described in detail. On the left side the geometry and the applied dead loads are plotted; on the right part some general data characterizing the macroelement are precised. They are the total and the opening areas with the correspondent net area, the opening ratio intended as the ratio of the voids and the total area of the element, the thickness of the wall, the self weight, the dead load and their sum, the ratio of the dead load over the total weight.

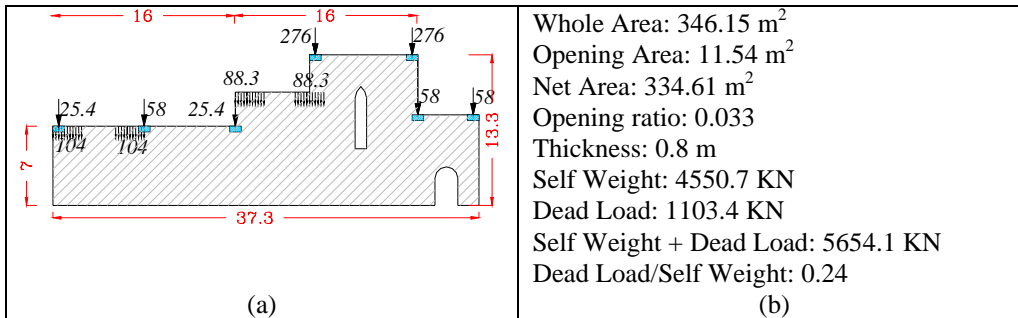


Figure 3. L1 macroelement – a) geometry and loads; b) general data.

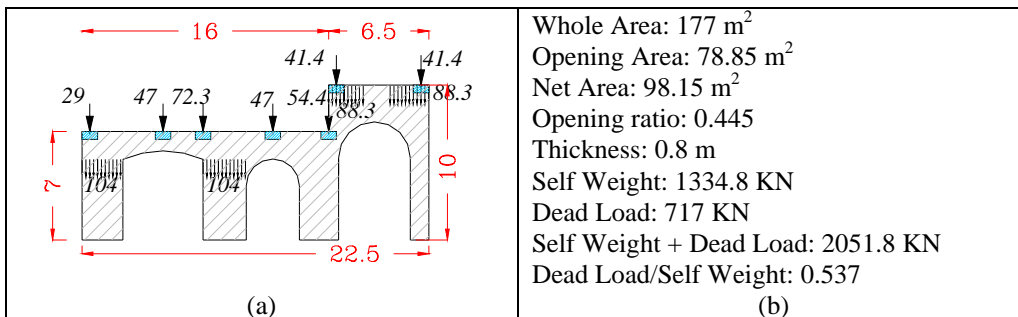


Figure 4. L2 macroelement – a) geometry and loads; b) general data.



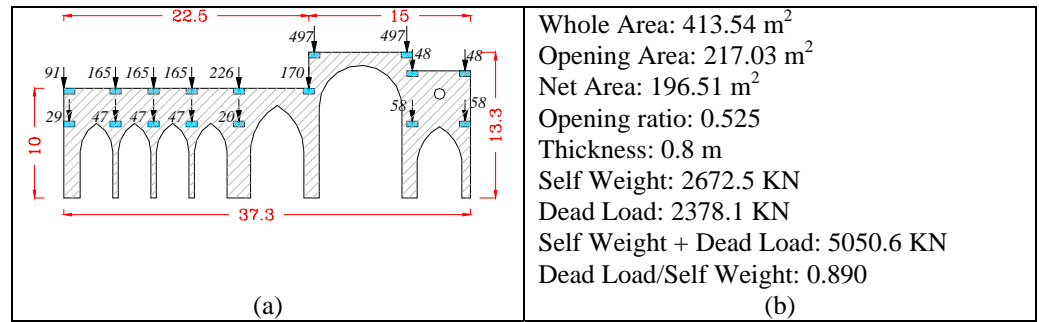


Figure 5. L3-L4 macroelement – a) geometry and loads; b) general data.

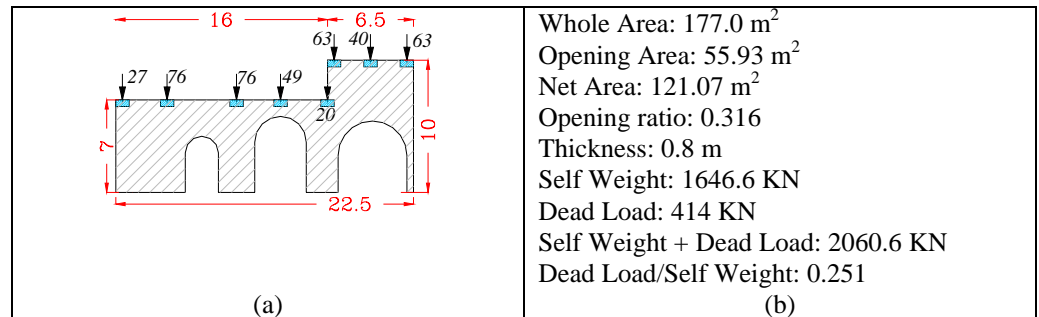


Figure 6. L5 macroelement – a) geometry and loads; b) general data.

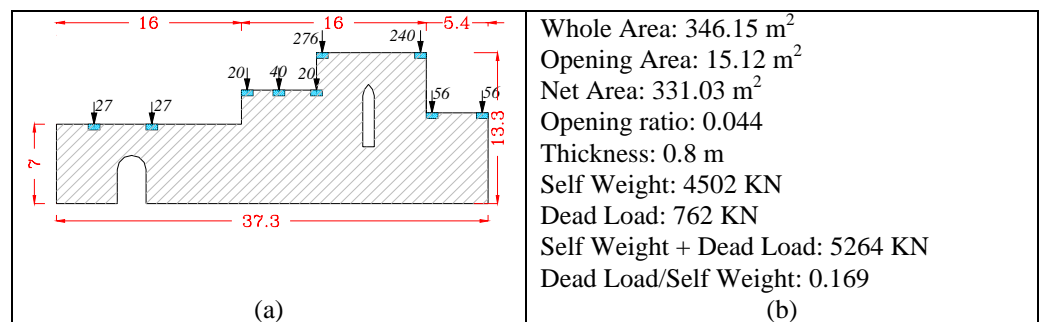


Figure 7. L6 macroelement – a) geometry and loads; b) general data.

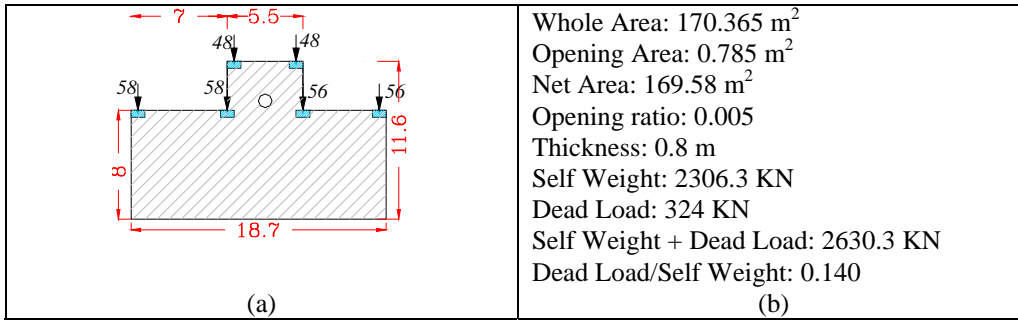


Figure 8. T1 macroelement – a) geometry and loads; b) general data.

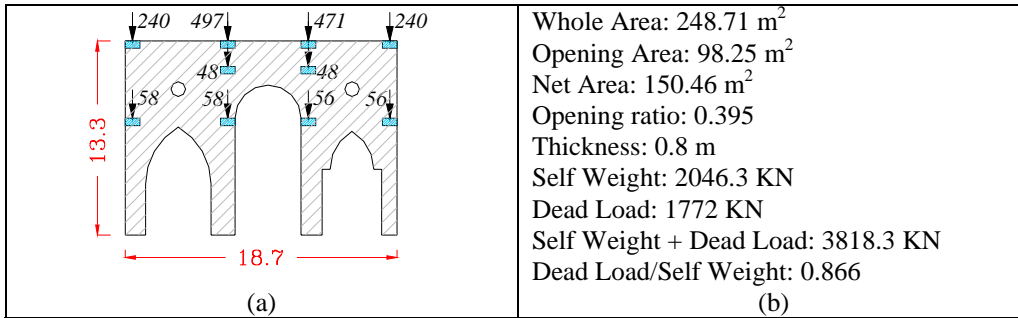


Figure 9. T2 macroelement – a) geometry and loads; b) general data.

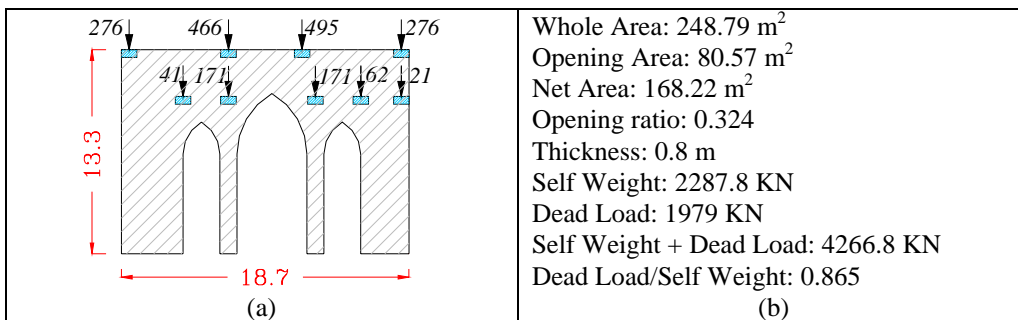


Figure 10. T3 macroelement – a) geometry and loads; b) general data.

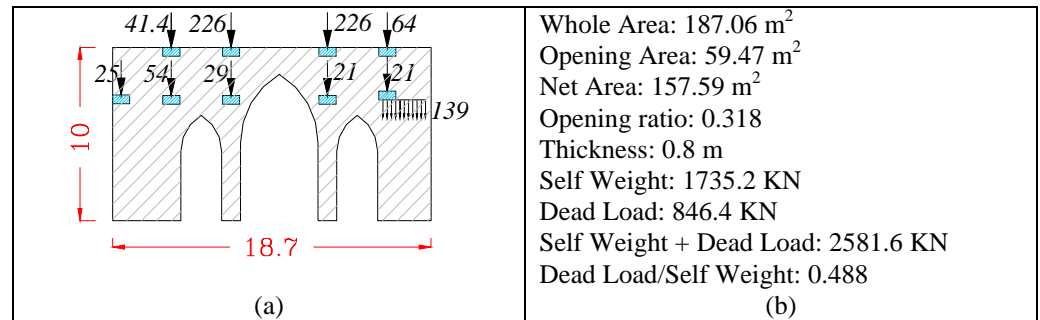


Figure 11. T4 macroelement – a) geometry and loads; b) general data.

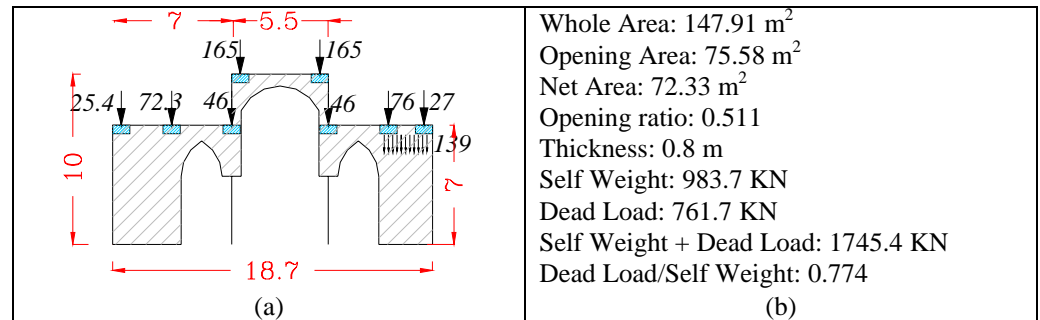


Figure 12. T5 macroelement – a) geometry and loads; b) general data.

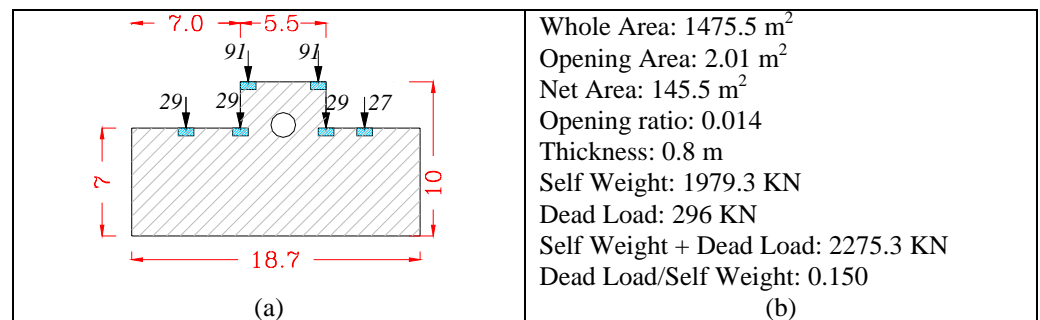


Figure 13. T6 macroelement – a) geometry and loads; b) general data.

### 2.3. LOAD CONDITION

In Fig. 14 the visualization of the dead loads is given on the three-dimensional model at the different heights. In this case, pointed loads are representative of the load path coming from cross vaults whilst distributed loads represent the barrel vaults.

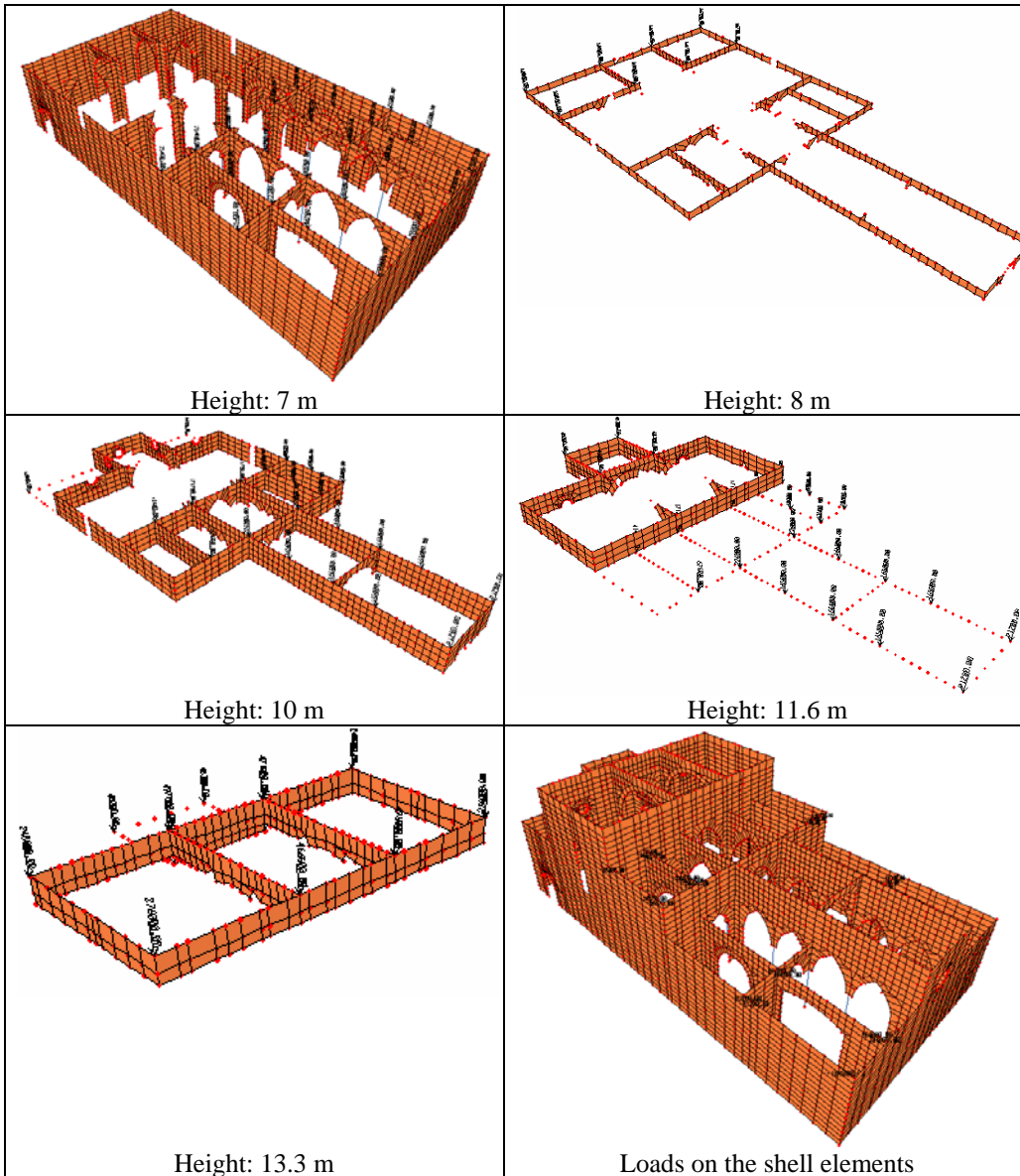


Figure 14. SGMR dead loads.

### 3. S. IPPOLISTO

The building was progressively built on a small roman catacomb starting from the V Century. Between the end of XVI Century and the beginning of XVII Century the church assumed the shape of nowadays (Fig. 15). In 1635 the church gallery caused the collapse of part of the crypt vaults. The 1980 earthquake has implied the whole collapse of the transept, the apse roof and the breaking of the lower crypt.

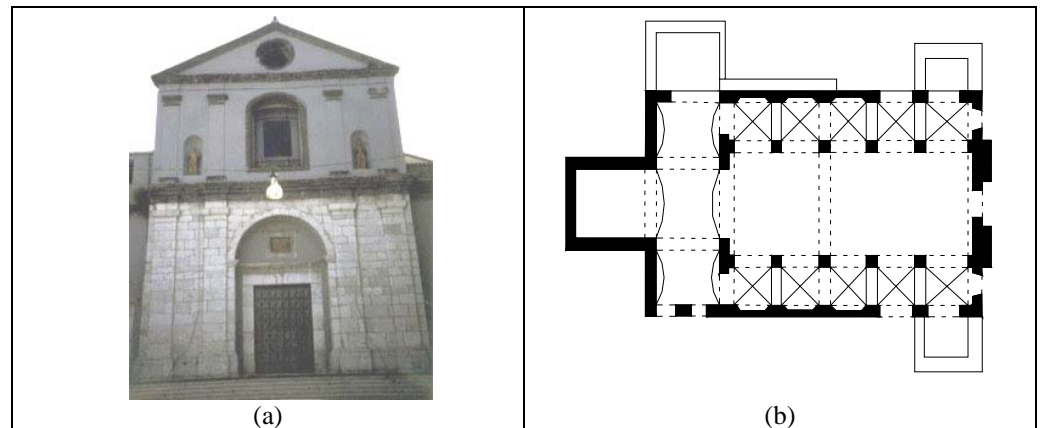


Figure 15. SI – a) Picture; b) Plant.

#### 3.1. GEOMETRY

The principal nave, 11.6 m wide, develops for 28 m with a maximum height of 16.5 m. The two side naves are 5 m wide and have a maximum height of 8.5 m. The wall thicknesses vary from 1.0 to 2.0 m; the columns of the arcades on the side of the principal nave, have a squared section of 1.2 m per side. The rectangular apse is 11.6 m wide and 8.8 m long, while the height varies between 14 and 18 m. The principal nave has a wood and bent tile roof, leaning on a wood truss placed in correspondence of columns 6 m distant. Also on the apse there is a wood truss leaning on lateral walls. Cross vaults span the lateral naves.

### 3.2. MACROELEMENTS

In Figure 16 the plant of the church is represented. Again the longitudinal and transversal macroelements are depicted and better illustrated in the following cards (from Fig. 17 to Fig. 24).

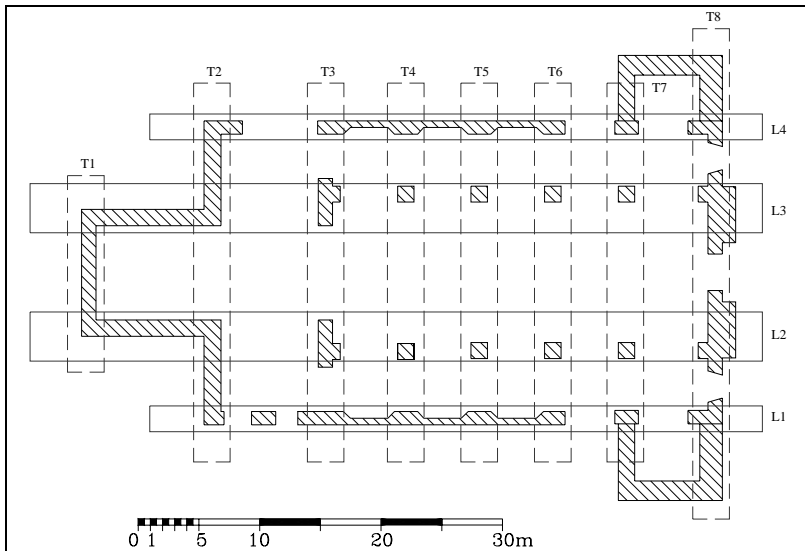


Figure 16. Individuation of the macroelements in plant.

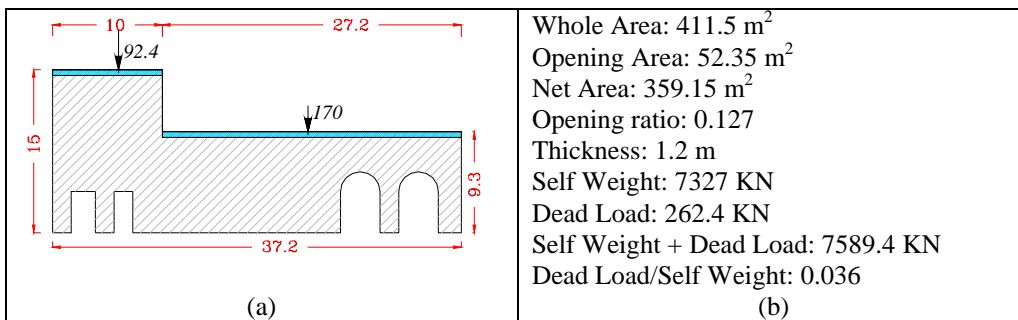


Figure 17. L1 macroelement – a) geometry and loads; b) general data.

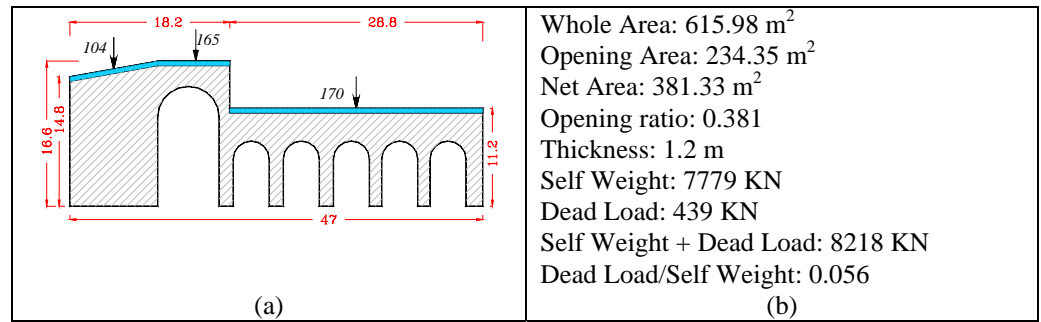


Figure 18. L2-L3 macroelement – a) geometry and loads; b) general data.

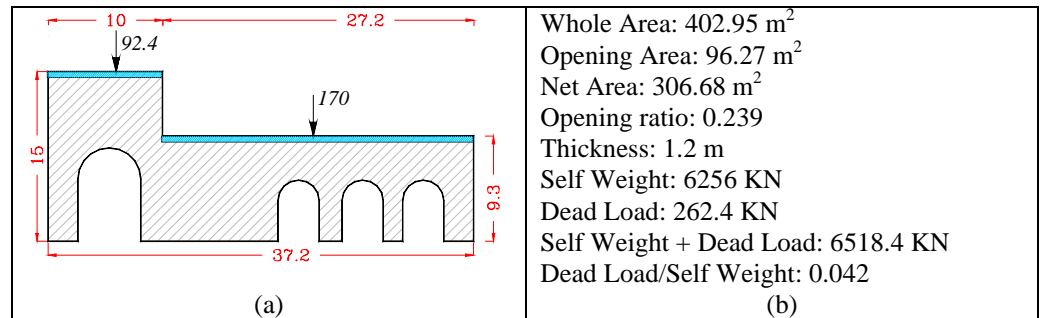


Figure 19. L4 macroelement – a) geometry and loads; b) general data.

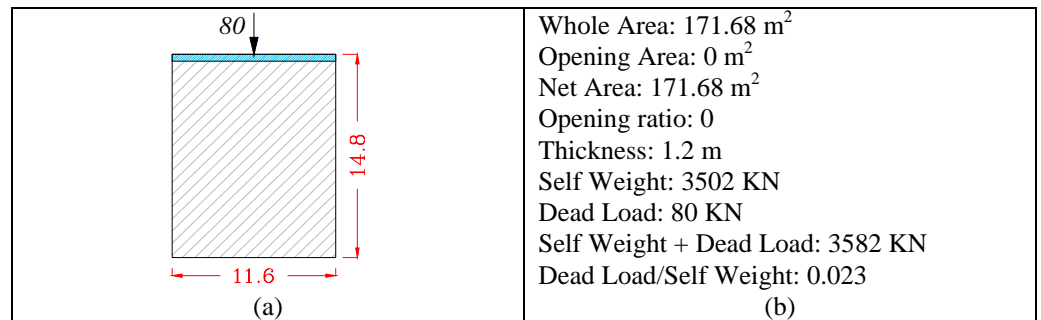


Figure 20. T1 macroelement – a) geometry and loads; b) general data.

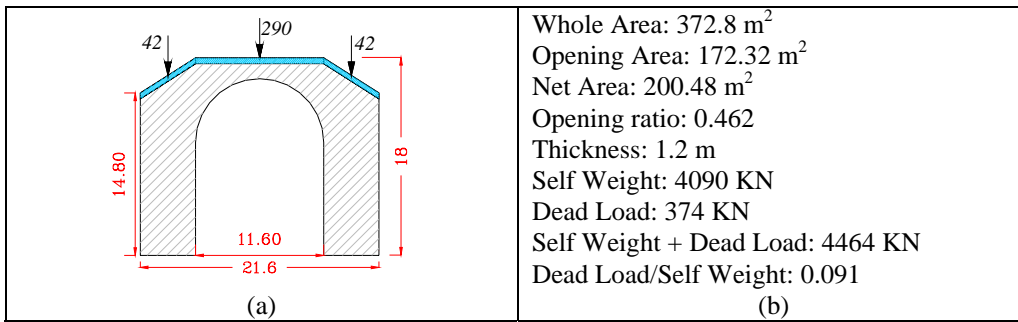


Figure 21. T2 macroelement – a) geometry and loads; b) general data.

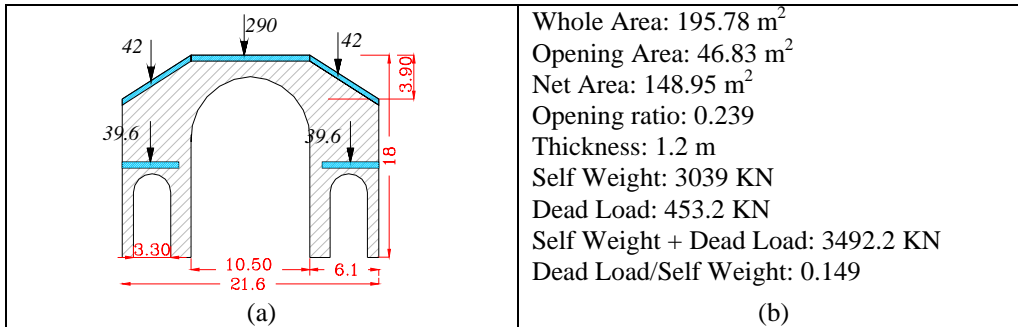


Figure 22. T3 macroelement – a) geometry and loads; b) general data.

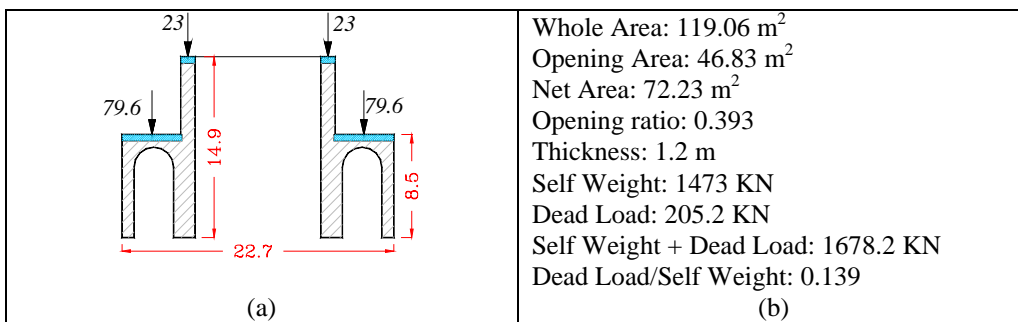


Figure 23. T4-T7 macroelement – a) geometry and loads; b) general data.



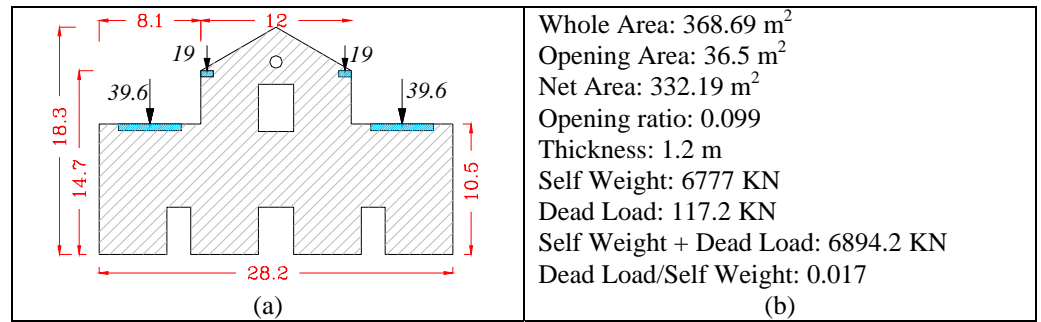


Figure 24. T8 macroelement – a) geometry and loads; b) general data.

### 3.3. LOAD CONDITION

In Fig. 25 the dead loads applied on masonry walls coming from the vaults and the wooden truss, depending on the height, are shown.

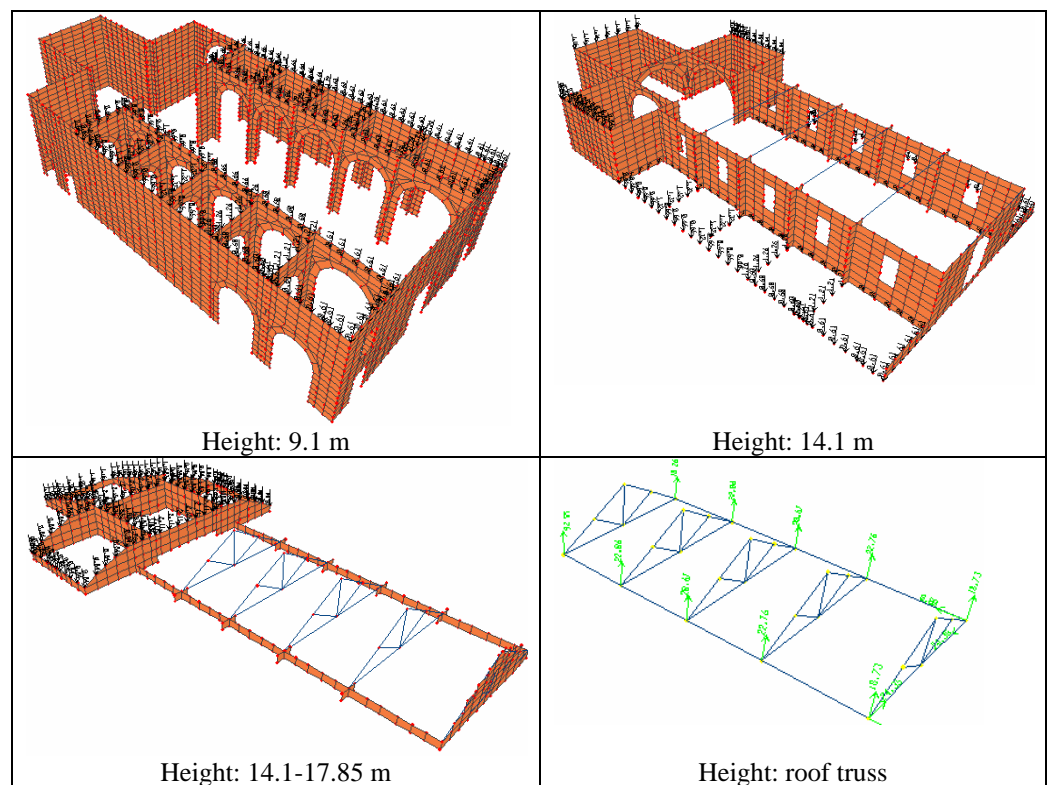


Figure 25. SI dead loads.

#### 4. S. GIOVANNI MAGGIORE

Founded around 555 on a site already occupied by a pagan sanctuary, the basilica of S. Giovanni Maggiore is one of the main buildings of Naples (Fig.26). The 1456 earthquake seriously damaged the church. In 1645 in the gallery, after the collapse of the original roof apse, the columns were reinforced and a new wall with the thickness of 2.70 m was realized. At that moment, the church was fairly big with its 24 altars. In 1656 the elliptical dome was erected on a short tambour. In 1732 another seismic event further ruined the transept and the lantern above the dome was demolished. In the 1805 earthquake, the transept is cracked again and unexpectedly in 1870 the right lateral nave collapsed. The following restoration works involved the destroyed part, the transept and the gallery. The last earthquake in 1980 has overburdened the static of the church so that retrofit works have interested the structure in the last years.

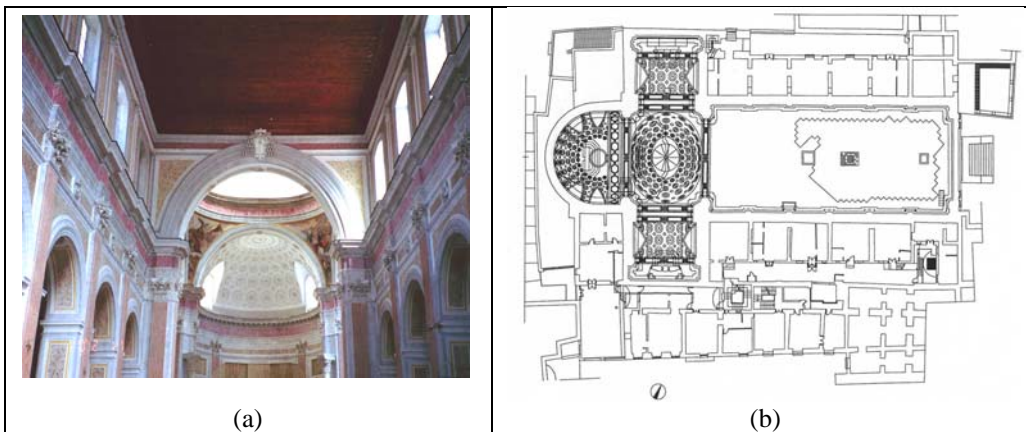


Figure 26. SGMG – a) Picture; b) Plant.

##### 4.1. GEOMETRY

The global dimensions in plant are 61 m long and 37 m wide, while the net length of the hall is 37 m. The height of the truss top on the central nave is 25.90 m, decreasing to 14.30 in the lateral naves and 9.30 in the lateral chapels. The dome is placed on a

tambour of 2 m at the height of 22 m reaching the new height of 32.7 m; the height of the apse is 19.8 m and the thickness of masonry elements varies from 0.6 to 2.4 m.

#### 4.2. MACROELEMENTS

The individuation of the macroelements in the plan of the church is plotted in Fig. 27. In the following Figures (from 28 to 35) the main data referred to each element are analyzed.

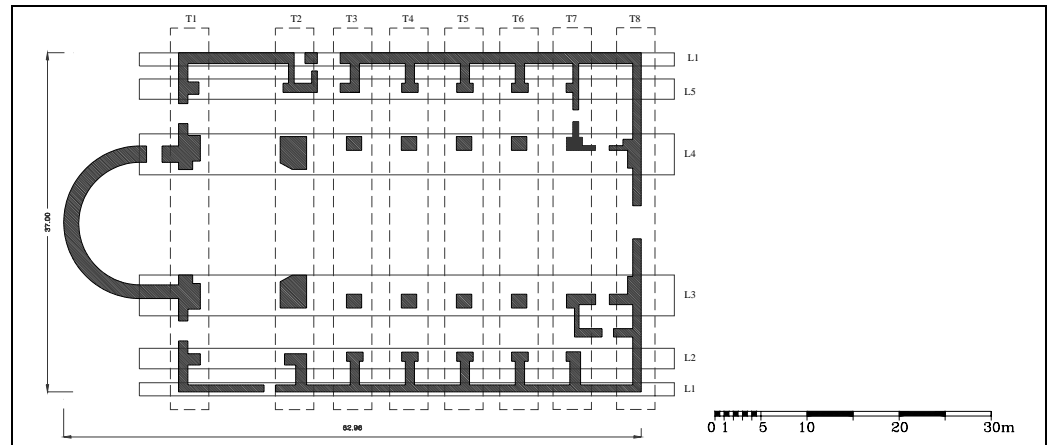


Figure 27. Individuation of the macroelements in SGMG.

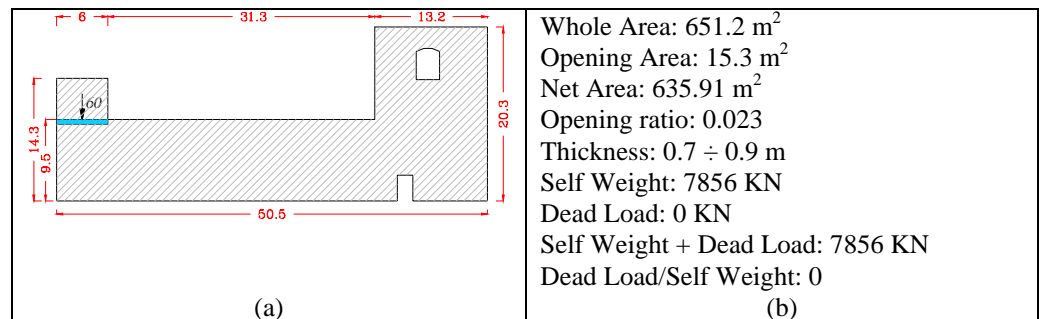


Figure 28. L1-L6 macroelement – a) geometry and loads; b) general data.

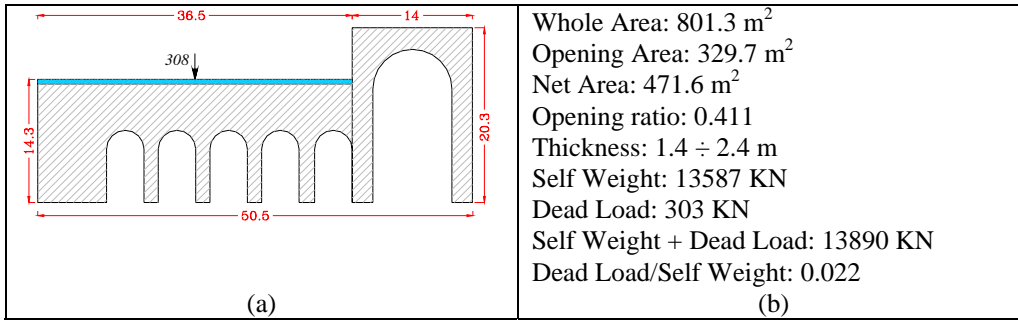


Figure 29. L2-L5 macroelement – a) geometry and loads; b) general data.

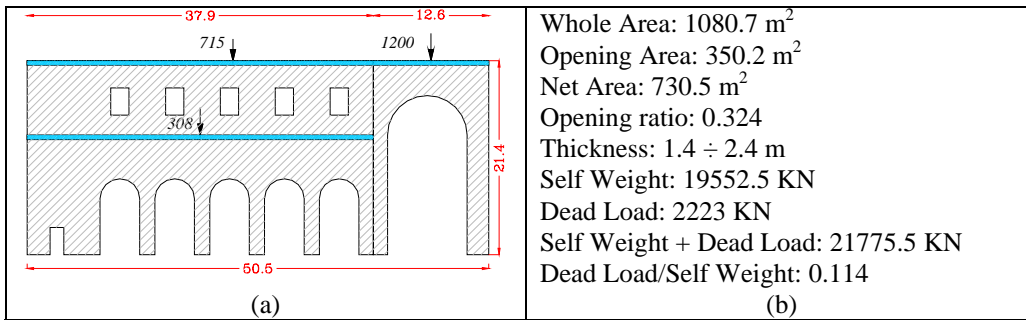


Figure 30. L3-L4 macroelement – a) geometry and loads; b) general data.

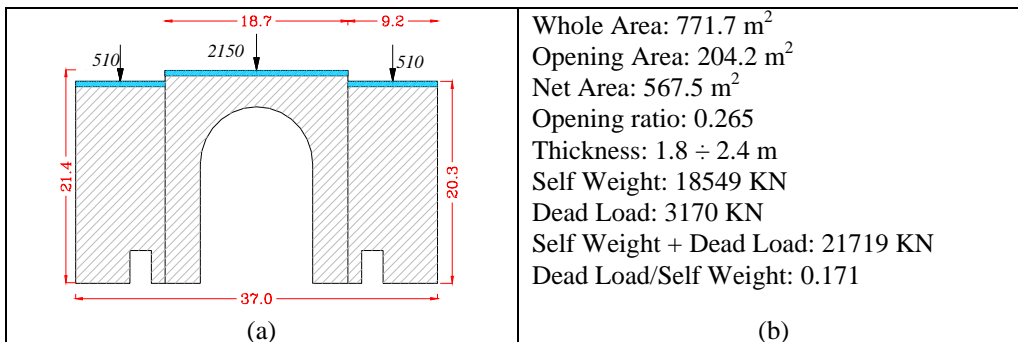


Figure 31. T1 macroelement – a) geometry and loads; b) general data.

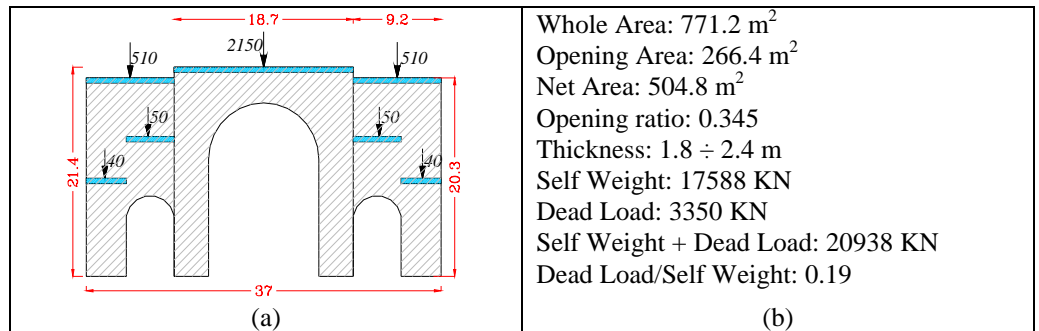


Figure 32. T2 macroelement – a) geometry and loads; b) general data.

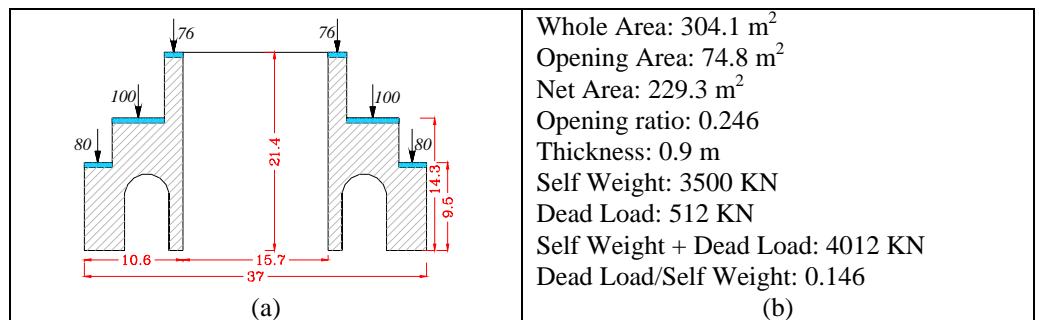


Figure 33. T3-T6 macroelement – a) geometry and loads; b) general data.

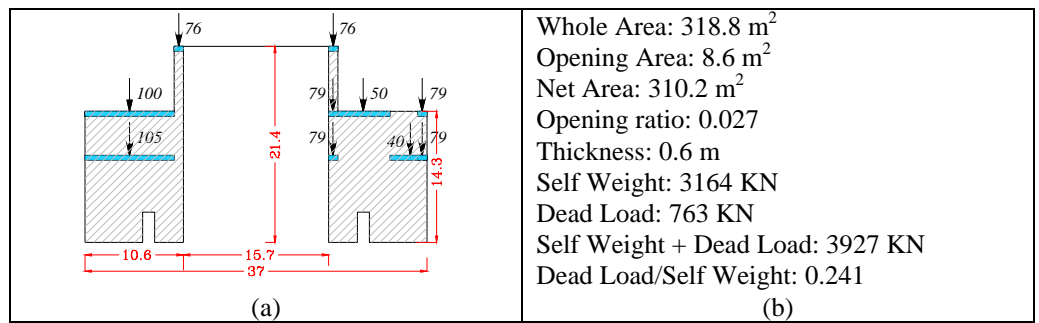


Figure 34. T7 macroelement – a) geometry and loads; b) general data.

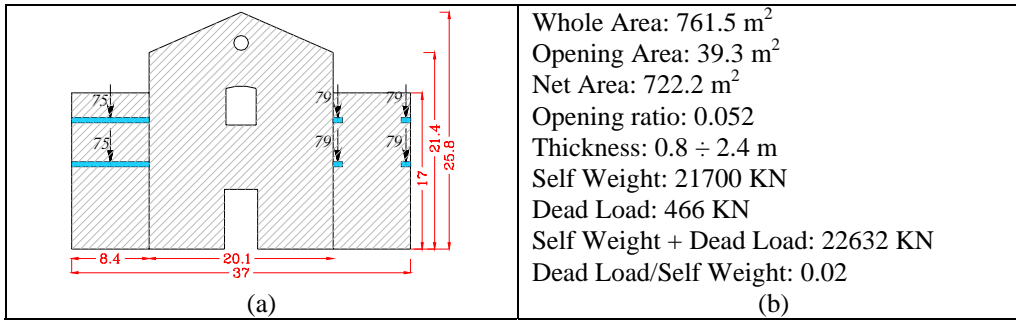
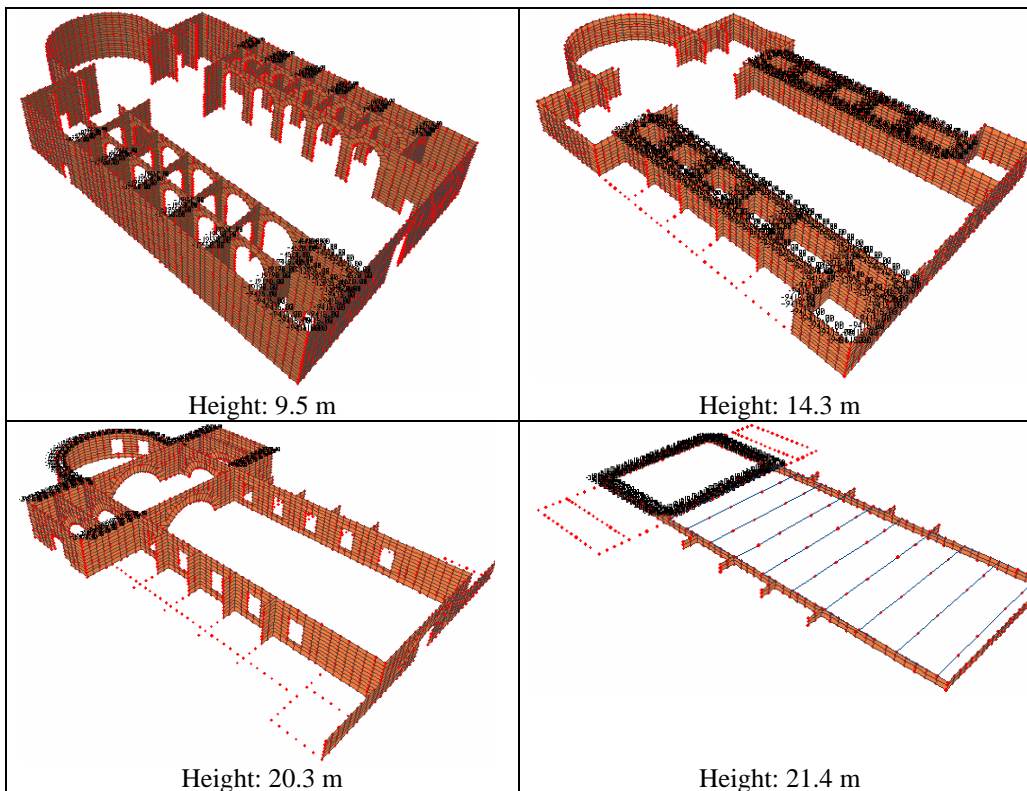


Figure 35. T8 macroelement – a) geometry and loads; b) general data.

### 4.3. LOAD CONDITION

In Fig. 36 the load conditions are illustrated in function of the height, the location and the type.



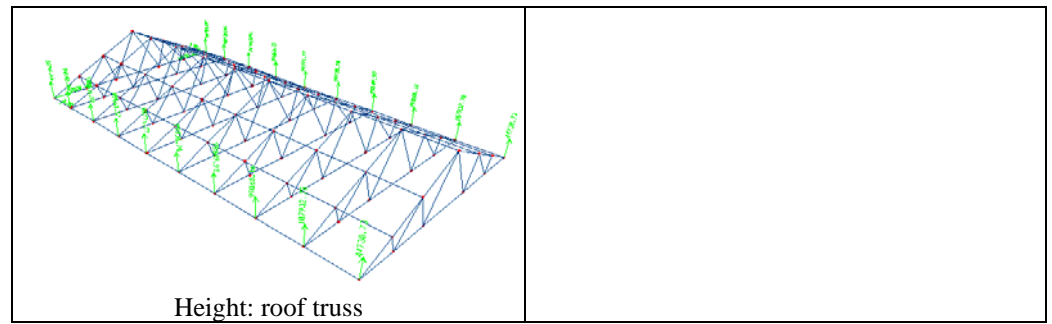


Figure 36. SGMG dead loads

Lloads on the shell elements are representative of uniform loads transferred by the barrel and pavilion vaults; the pointed loads are representative of the load path coming from the steel truss.

## 5. S. PAOLO MAGGIORE

The church was built on a hexastyle and prostyle temple 24 m long and 17.40 m wide of the I Century. The construction was transformed into a Christian church between the end of VIII Century and the beginning of IX Century (Fig. 37). The building presented three naves separated by 18 columns wide as the temple which pronaos was conserved until the earthquake in 1688. Between the end of the XVI and the beginning of the XVII Century the church was restored more times. The inner part of the basilica has undergone severe damages during the II world war. The apse roof and the transept were destroyed whilst the central nave was heavily damaged. The following works involved the rebuilding of the apse walls, the temporary restoration of the transept roof and the strengthening of some columns of the central and left nave. In 1971 an exhaustive restoration design interested the substitution of the wooden truss with steel truss and the placing of reinforced concrete beams in the upper part of the building. These strengthening works have allowed to the structure to resist to the following seismic event in 1980.

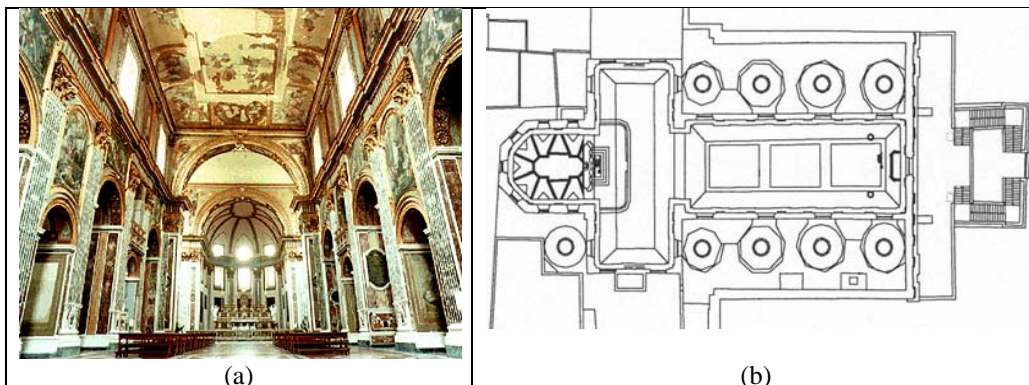


Figure 37. SP – a) Picture; b) Plant.

### 5.1. GEOMETRY

Nowadays, the basilica develops in plan on a total length of 63 m and a width of 39 m; close to the transept, the width is 56 m and the length is 35 m. The height at the



top of the truss on the central nave is 27.6 m, the domes on the lateral naves are 13.3 m high and the lateral chapels are 6.5 m high; the height of the apse is 16.3 m and the thickness of the walls varies from 0.7 to 1.9 m.

## 5.2. MACROELEMENTS

The following macroelements represented in Fig. 38 are analyzed in more detail from Fig. 39 to Fig. 48.

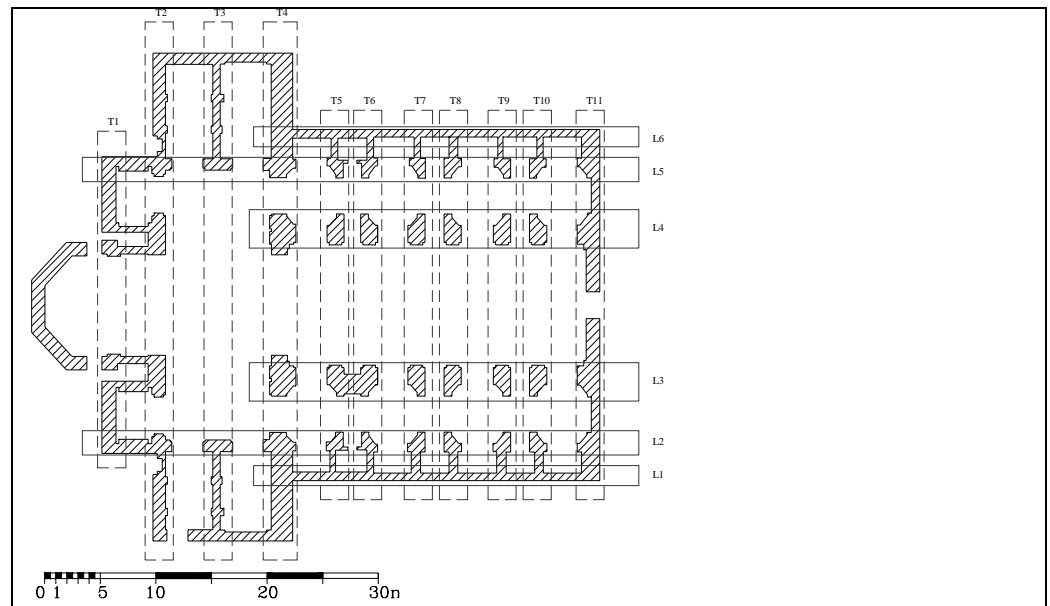


Figure 38. individuation of the macroelements in SP

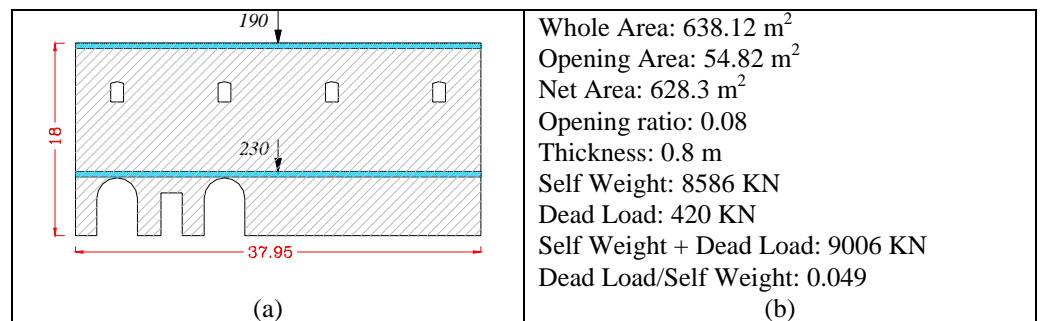


Figure 39. L1 macroelement – a) geometry and loads; b) general data.

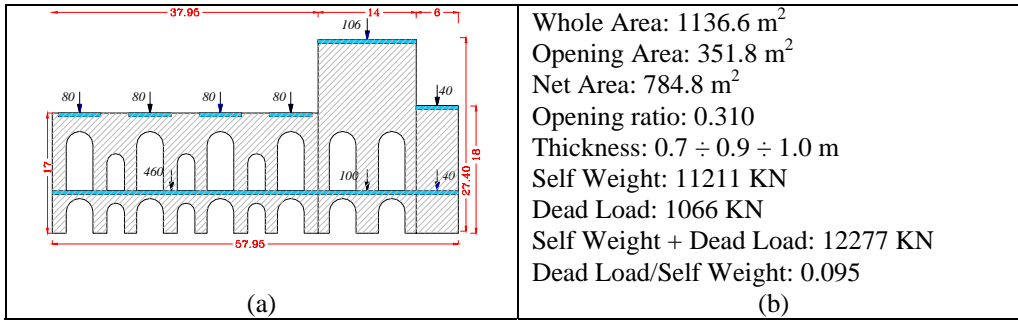


Figure 40. L2-L5 macroelement – a) geometry and loads; b) general data.

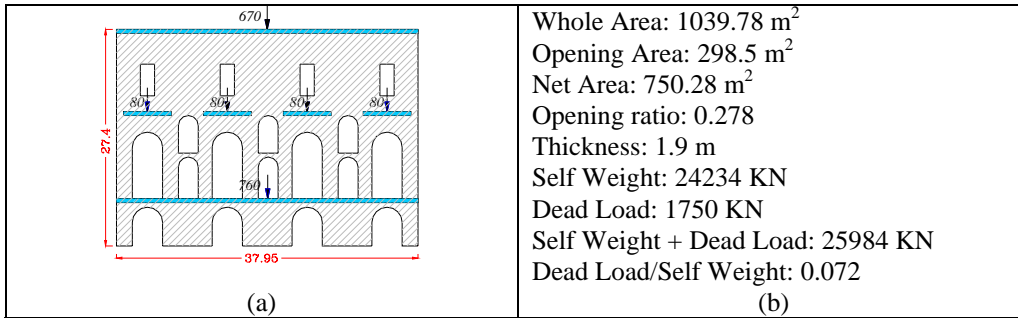


Figure 41. L3-L4 macroelement – a) geometry and loads; b) general data.

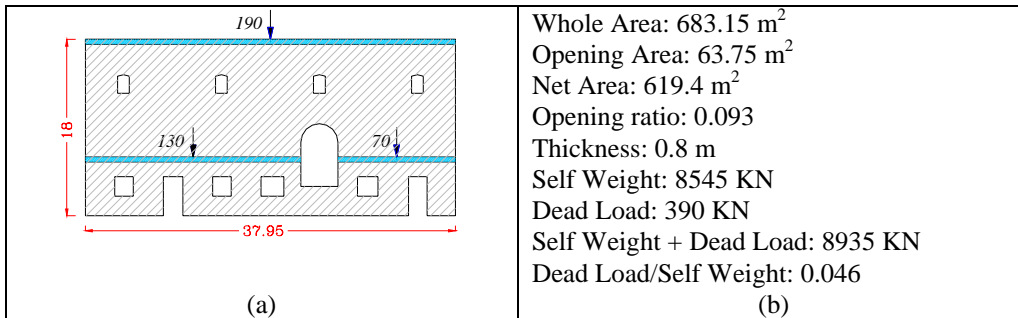


Figure 42. L6 macroelement – a) geometry and loads; b) general data.

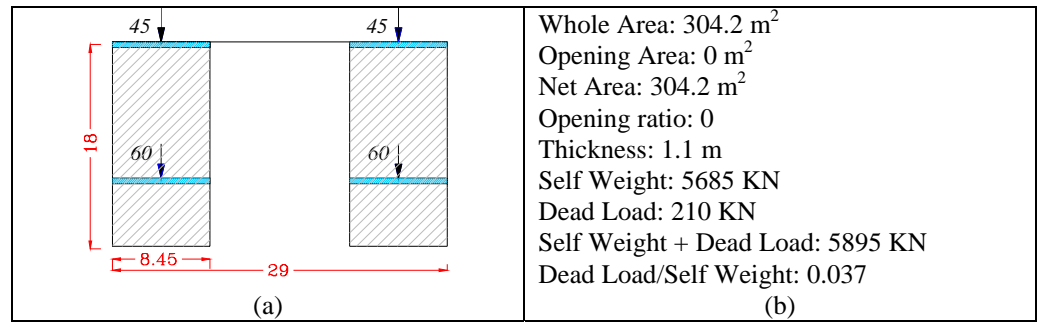


Figure 43. T1 macroelement – a) geometry and loads; b) general data.

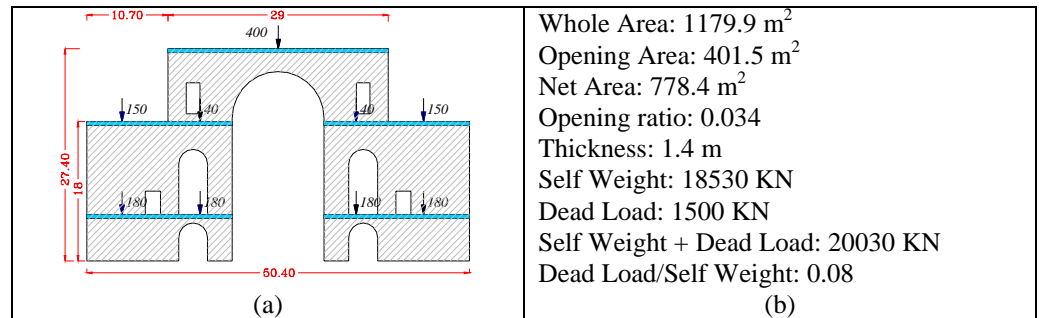


Figure 44. T2 macroelement – a) geometry and loads; b) general data.

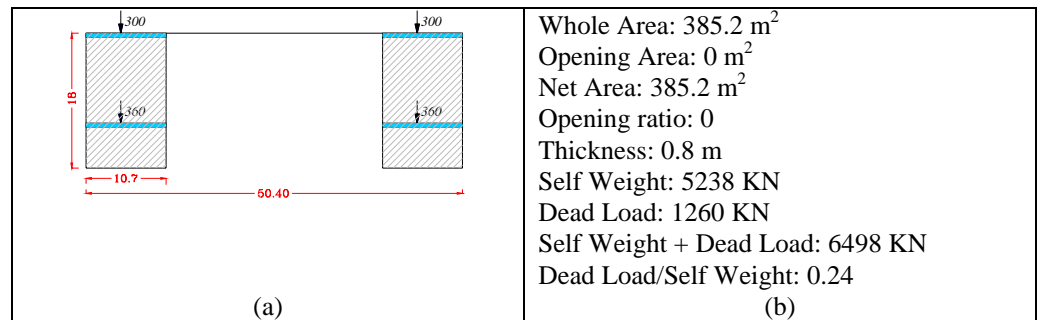


Figure 45. T3 macroelement – a) geometry and loads; b) general data.

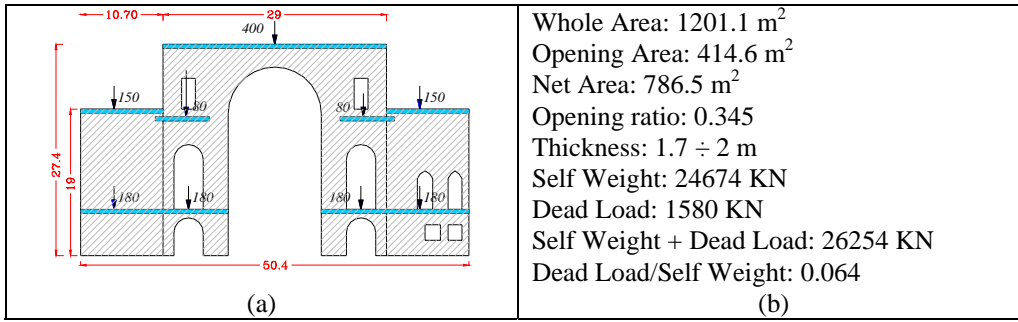


Figure 46. T4 macroelement – a) geometry and loads; b) general data.

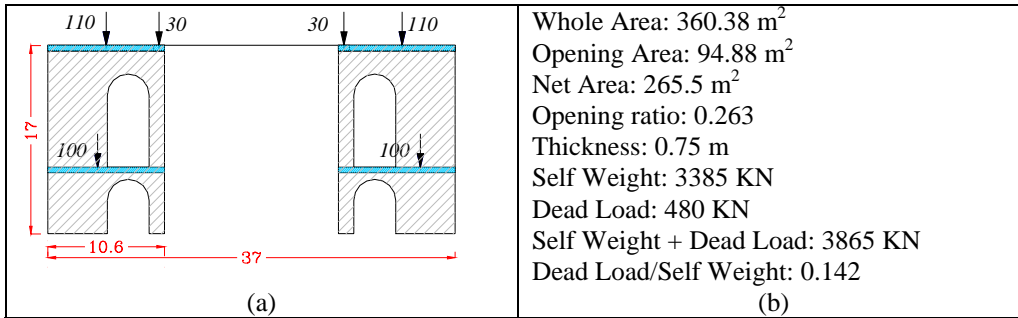


Figure 47. T5-T10 macroelement – a) geometry and loads; b) general data.

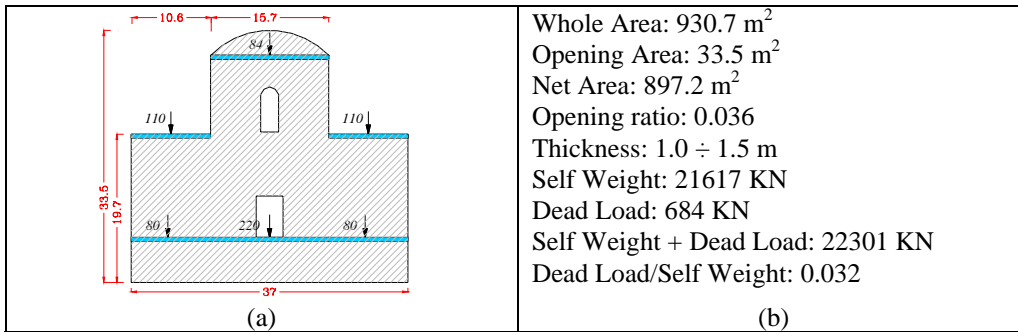


Figure 48. T11 macroelement – a) geometry and loads; b) general data.

### 5.3. LOAD CONDITION

In Fig. 49 the load placing at the different heights are shown on the three-dimensional models.

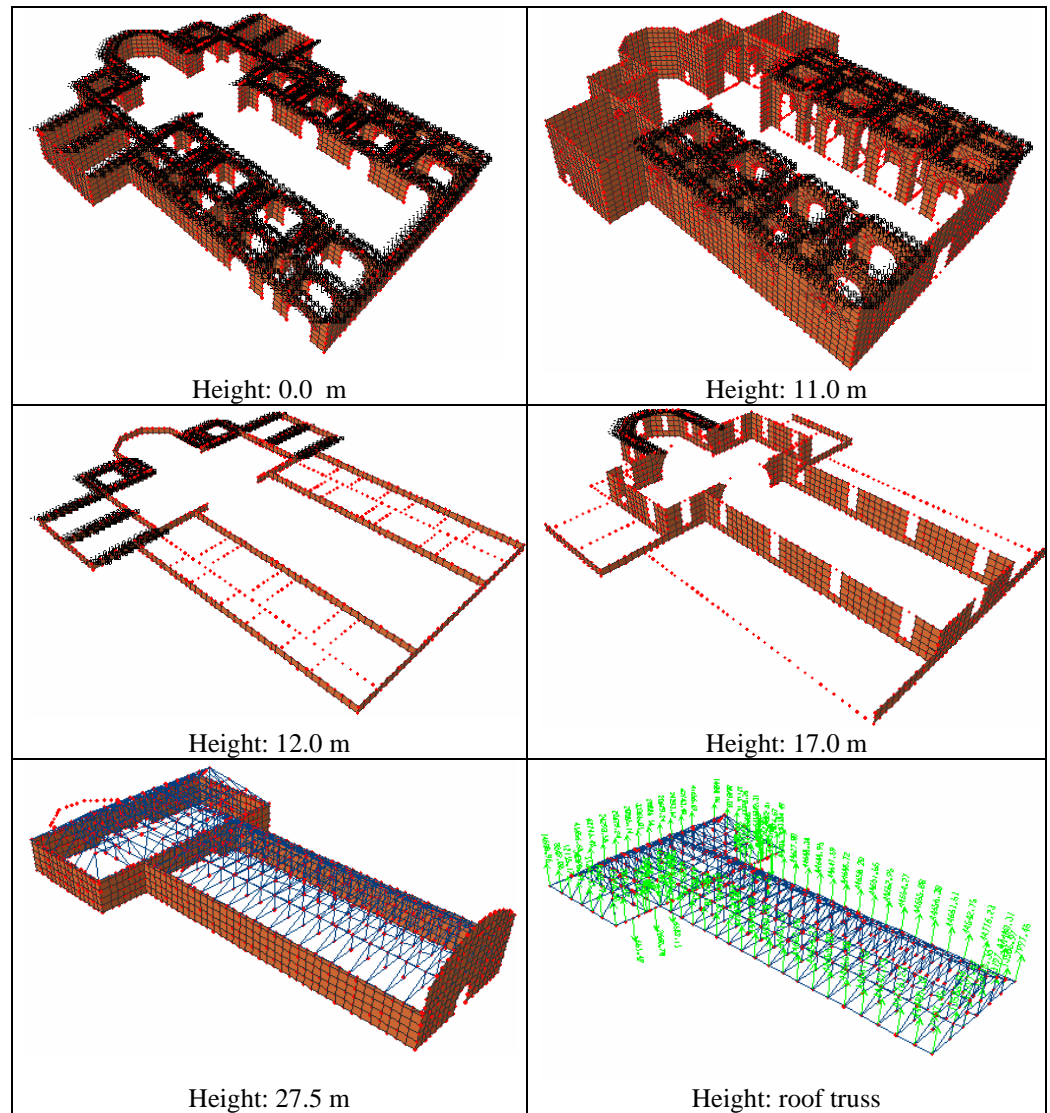


Figure 49. SP dead loads

## 6. GEOMETRICAL AND TYPOLOGICAL FEATURES

A geometrical-dimensional analysis has been conducted on the macroelements above cited. In particular, for each case and macroelement, the ratio  $A_{\text{opening}}/A_{\text{total}}$  between the area of the holes and the surface of the whole masonry panel has been valued.

The results are represented in Fig. 50 where in a bar diagram, for each church and macroelement, this ratio is reported.

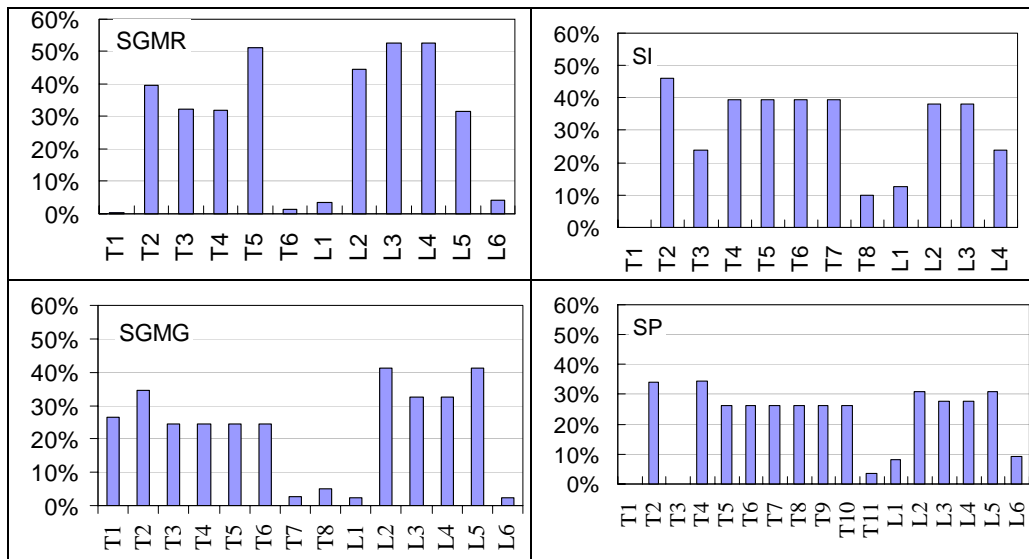


Figure 50. Opening ratio

Generally, the external elements, corresponding to the apse and the façade among the transversal elements (T) and to the two fronts among the longitudinal elements (L) lack openings. The inner panels, on the contrary, are fairly opened so that two different typologies of elements are identified.

Afterwards, the geometrical dimensions of each macroelement have been characterized; in particular, the maximum values of the height  $H$  and the length  $L$  (in terms of the ratio  $H/L$ ) have been detected and the same macroelements have been divided in parts with the same thickness ( $H_i$  and  $L_i$  of the parts) as well. The dimensional results are reported in Fig. 51.

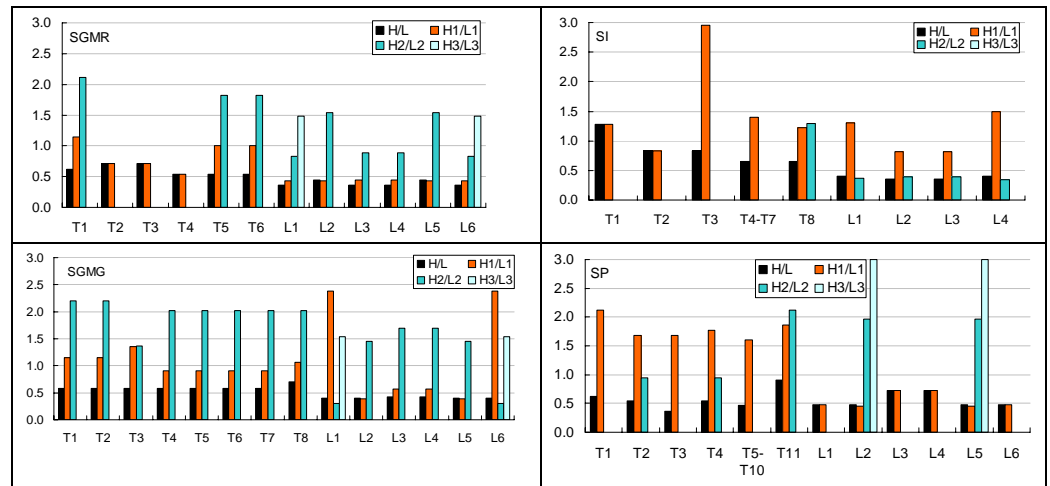


Figure 51. Dimensional Ratios.

In order to compare the geometrical parameters already defined, some classes of macroelements morphologically similar have been identified. In the specific case, eight of them have been selected:

1. the apse;
2. the first triumphal arch (element between the apse and the transept);
3. the second triumphal arch (separation between the transept and the nave);
4. the transversal elements along the nave;
5. the façade;
6. the external longitudinal front;
7. the internal longitudinal arcade;
8. the ulterior longitudinal internal arcade.

They are reported in the abacus of Fig. 52, in which the classes, the common elements in the basilicas and the correspondent alphanumeric code of the single macroelement are reported. It can be observed that, among the four churches, two subgroups can be defined. In the first one there are SGMG and SP that are more similar to the basilica type, the other two churches, SI and SGMR, although they are included in the group, are slightly atypical.

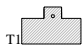



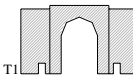
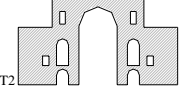



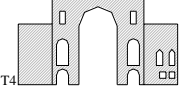
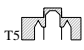



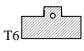
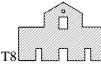
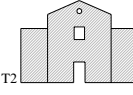
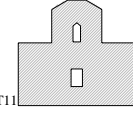
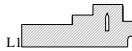
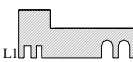
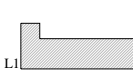
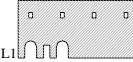


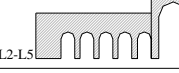
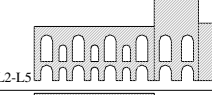
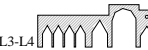
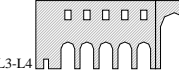
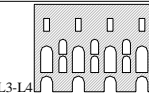
Element	SGMR	SI	SGMG	SP
1	 T1	 T1		
2	 T2	 T2	 T1	 T2
3	 T3	 T3	 T2	 T4
4	 T5	 T4-T5-T6-T7	 T3-T4-T5-T6	 T5-T6-T7-T8-T9-T10
5	 T6	 T8	 T2	 T11
6	 L1	 L1	 L1	 L1
7	 L2	 L2-L3	 L2-L5	 L2-L5
8	 L3-L4		 L3-L4	 L3-L4

Figure 52. Typological correspondence of the macroelements.

## 7. CLASSES COMPARISON

Looking at Fig. 52, the four churches, besides having the common configuration in plant, are also characterized by some uniformity in the global plano-altimetric apparatus.

A comparison in terms of global dimensions among the study cases is reported in Fig. 53.



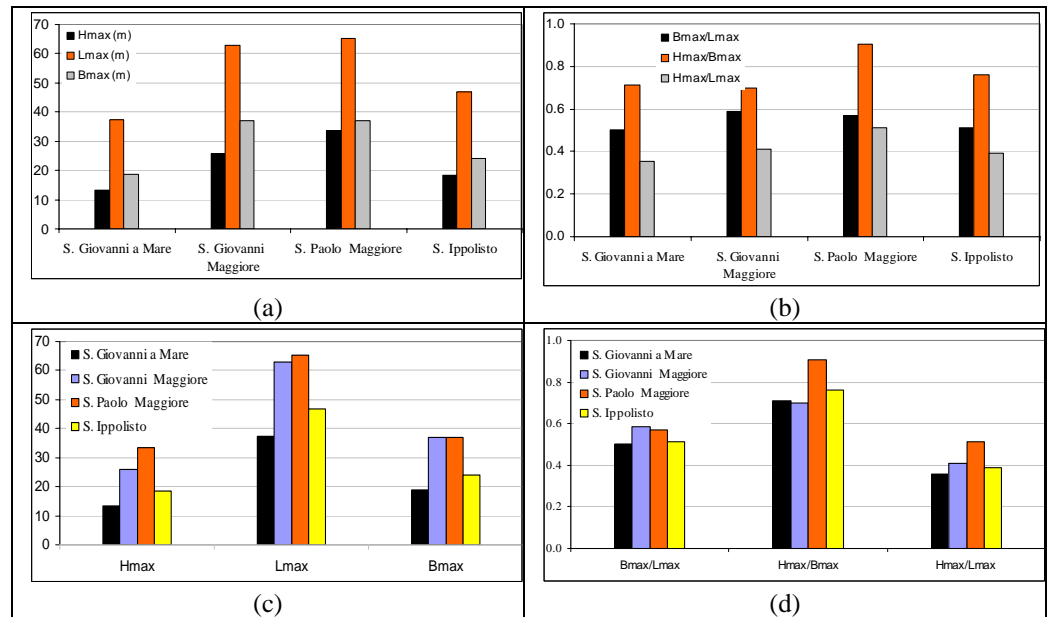


Figure 53. Dimensional comparison.

In particular, in the first two pictures, for each church, maximum dimensions in terms of  $H_{\max}$ ,  $L_{\max}$  and  $B_{\max}$  and of ratios  $B_{\max}/L_{\max}$ ,  $H_{\max}/B_{\max}$  and  $H_{\max}/L_{\max}$  are reported. In the third and the fourth picture, such values are grouped with reference to the relevant church. From the observation of the last plot, it's clear the regularity of the ratios between the global dimensions of the four churches:  $B_{\max}/L_{\max}$  varies in the range  $0.5 \div 0.59$ ;  $H_{\max}/B_{\max}$  between  $0.7 \div 0.9$ ;  $H_{\max}/L_{\max}$  in the range  $0.35 \div 0.51$ .

A comparison among the 8 classes of macroelements of the churches is depicted in Fig. 54. In particular, if the first class is neglected (bi or three-dimensional apse), a certain similarity can be observed among the elements:

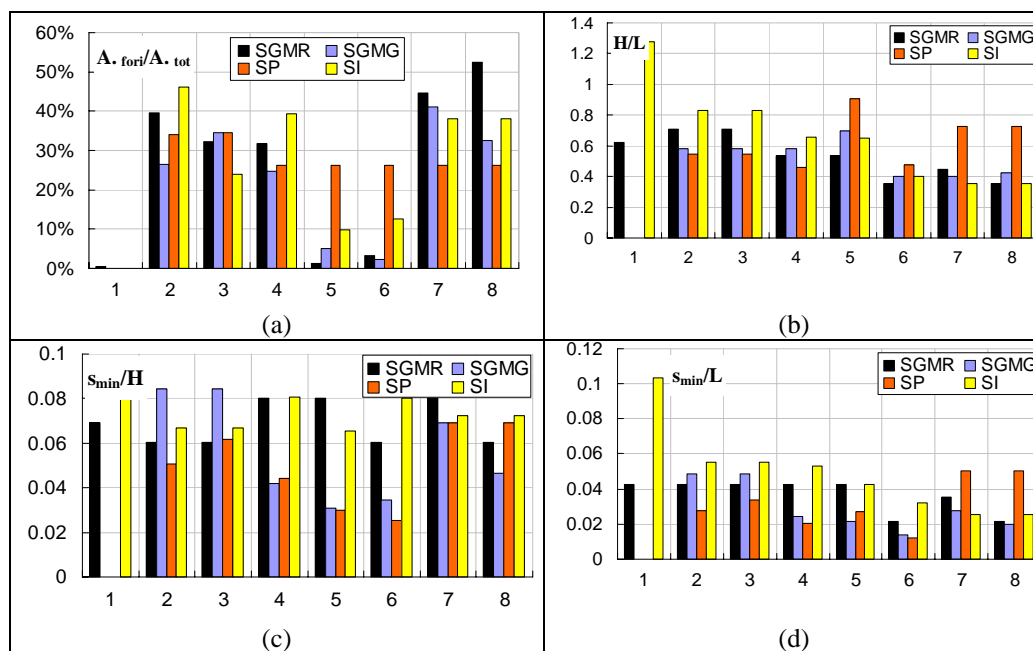


Figure 54. Dimensional comparison in classes - a)  $A_{for}/A_{tot}$ ; b)  $H/L$ ; c)  $s_{min}/H$ ; d)  $s_{min}/L$ .

1. ratio  $A_{for}/A_{tot}$  (Fig. 54.a): classes 2, 3, 7 and 8 are bounded in the range 20% ÷ 40% and classes 5 and 6 in the range 5% ÷ 15%.

2. ratio  $H/L$  (Fig 54.b): it shows a uniform trend in all the classes of macroelements with the exception of the first one (correspondent to the apse). In particular the following ranges are defined: 0.58÷0.8 for classes 2 and 3; 0.50 ÷ 0.65 for classes 4 and 5; 0.38 ÷ 0.5 for classes 6, 7 and 8. It has to be underlined that for the longitudinal macroelements, S. Paolo Maggiore church has higher values because it features a crypt at the bottom of the building which influences this ratio.

3. ratio  $s_{min}/H$  (fig. 54.c): there is a certain regularity for classes of macroelements 2, 3 and 7 (triumphal arches and longitudinal internal arcades), defined in the range 0.05 ÷ 0.085.

4. ratio  $s_{min}/L$  (fig. 54.d): there is a certain uniformity in the macroelements 2, 3, 7 and 8 defined in the range 0.01÷ 0.58.

## 8. CONCLUSIONS

From the analysis of these results, it is possible to affirm that the four study cases, besides the typical plan (defined basilica type), have certain uniformity in the global plan-altimetric apparatus. Furthermore it has been noticed that these ratios are recurrent also among the single macroelements belonging to the same class.

Generally, it can be said that, with the exception of some particularities, the four study cases derive from a sort of three-dimensional global model that changes only for a scale factor.

Considering that a large amount of the seismic action on the macroelements is due to their mass, it is allowed to expect also a similar seismic behaviour among the buildings or, in other words, a typical seismic behaviour.



## **CHAPTER 3:**

### ***LINEAR ANALYSES***

#### **1. INTRODUCTION**

The evaluation of the behaviour of religious masonry buildings under seismic actions shows objective difficulties because of the geometrical - morphological characteristics and the non linear behaviour of the material.

In this chapter, the first part of the two-step procedure previously illustrated is carried out. The structural systems have been subjected to elastic numerical analyses (static and dynamic) with different hypotheses about the modelling of the roofing system. The analyses on these buildings have allowed to characterize the seismic behaviour, to find out points of greater vulnerability, to identify the distribution of stresses among different structural elements and the out of the plane contribution of the elements orthogonal to the direction of seismic forces.

## 2. STRUCTURE, MATERIAL AND SEISMIC ACTION

The masonry buildings have been analyzed in the linear field through the Finite Element Method, using the commercial computer code SAP2000 [CSI, 2000]. Library elements have been used to model the structure: shell elements for vertical walls and frame elements for roof trusses, columns and arches.

The three dimensional models of the four basilicas are reported in Fig. 1 and are composed respectively of 5924 shells, 8 frames and 6401 nodes for the church of S. Giovanni a Mare (SGMR); 5572 shells, 56 frames and 5941 nodes for the church of S. Ippolisto (SI); 13966 Shells, 256 frames and 16126 nodes for the church of S. Giovanni Maggiore (SGMG); 12349 shells, 1051 frames and 13777 nodes for the church of S. Paolo Maggiore (SP).

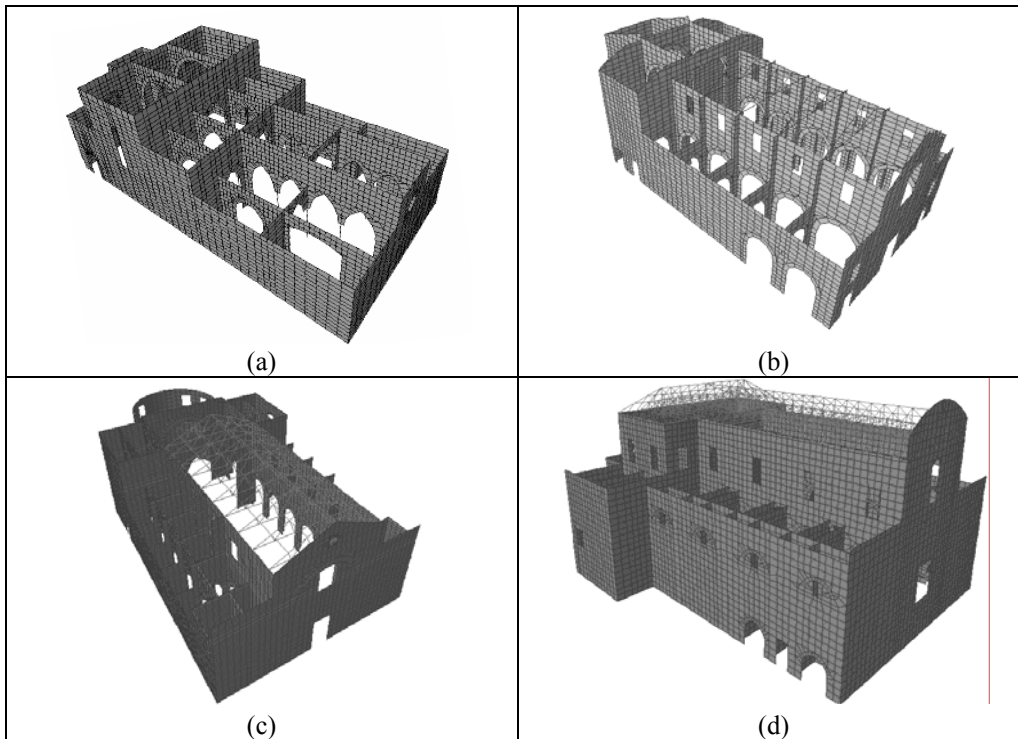


Figure 1. Three-dimensional models – a) SGMR, b) SI, c) SGMG, d)SP.

For masonry tuff elements the hypothesis of linear elastic behaviour (elastic module  $E = 1100 \text{ MPa}$ , Poisson's coefficient  $\nu = 0.071$ , self weight  $W = 17 \text{ kn/m}^3$ ) has been adopted. For the steel elements,  $E=210000 \text{ MPa}$ ,  $\nu = 0.3$  and  $W = 77 \text{ kn/m}^3$  have been assumed.

In order to simulate the effects of the horizontal structural elements, two different hypotheses have been made: in the first one, roof elements in wood, steel or vaulted systems have been modelled with simple frame elements; in the second one, rigid diaphragms at different heights have been considered.

The self weight of the buildings has been automatically applied onto the shell elements according to the weight density. The dead loads, coming from the self weight of vaults and trusses roof, have been imposed onto the structures. Depending on the load type, uniform and point loads have been considered along the elements or in correspondence of the wall crossing. In the SAP models, when the loads are distributed along the wall development, the values per unit per area (automatically applied to the thickness of the shell) have been applied. Furthermore the concentrated loads, such as the trusses weight, have been imposed directly on the joints.

In addition to vertical loads, coming from the self weight and the dead load, in static analyses, horizontal actions equivalent to seismic loads have been applied according to DM96 [M.LL.PP., 1996] and EC8 [CEN, 2002]. Two load cases have been considered, applying the horizontal actions separately in the longitudinal and transversal directions.

Furthermore, in order to investigate the response to seismic actions, dynamic analyses using the DM96 spectra and the EC8 design spectra have been carried out. Again, seismic actions have been considered acting not contemporarily in the two principal directions of the building. In Figure 2, values of the first period of the buildings with the presence or not of the rigid slab are reported.

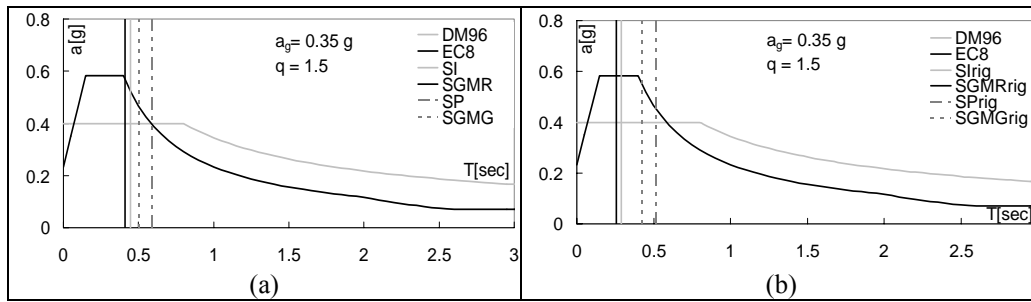


Figure 2. Seismic actions – DM96 and EC8 Design Spectra: a) actions on buildings without rigid slabs; b) actions on building with rigid slab.

### 3. DYNAMIC BEHAVIOUR OF CHURCHES

#### 3.1. “AS IS” MODELS

In Figures 3,4,5,6 the first three modal shapes and the corresponding value of the period of churches without rigid diaphragms (in the following labelled “as is” models) not considering local deformations, are reported; in Tables 1,2,3 and 4 the modal participating mass ratios (individual mode and cumulative percent) are plotted.

From the analyses of the deformed shapes some aspects are visible. Out of the plane deformation of some alignments, reveal a contribution of these elements to the absorption of seismic actions along the transversal direction. Torsional deformations of the whole three-dimensional complex show a low torsional stiffness of the buildings, deriving from the lack of “box behaviour”. The values of the first significant periods vary between 0.41 and 0.45 seconds for the smaller churches (SGMR and SI) and between 0.51 and 0.59 seconds for the bigger churches (SGMG and SP).

Evaluating the total participating mass factor (expressed as the ratio between the participating mass of the single mode  $M_i$  and the total mass  $M_{tot}$ ) it is noticeable that not many vibration modes (compared to the freedom grades) have to be summed up to excite a significant amount of the total mass.



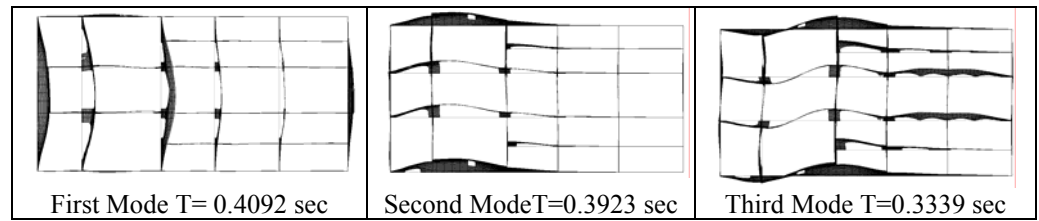


Figure 3. S. Giovanni a Mare “as is” – Modal shapes of the building.

TRANSVERSAL DIRECTION (X axe)				LONGITUDINAL DIRECTION (Y axe)			
MODE	PERIOD [sec]	$M_i/M_{tot}$ [%]	$\Sigma M_i/M_{tot}$ [%]	MODE	PERIOD [sec]	$M_i/M_{tot}$ [%]	$\Sigma M_i/M_{tot}$ [%]
2	0.3923	37.2412	37.3496	1	0,4029	41.4730	41.4730
3	0.3339	13.3174	50.667	6	0,2735	6.5533	48.2338
4	0.3177	6.7272	57.3942	16	0,1612	4.7107	53.3756
7	0.2365	2.2775	59.7409	17	0,1577	9.1321	62.5077
12	0.1935	4.0774	63.9416	20	0,1482	5.1420	67.7137
14	0.1763	2.1879	66.3523	58	0,0933	1.0679	75.6468
15	0.1673	4.2064	70.5588				
29	0.1285	1.0476	73.0894				
41	0.1091	3.2464	76.9225				
48	0.1009	1.8576	80.1407				

Table 1. S. Giovanni a Mare “as is” – Modal Participating mass ratios

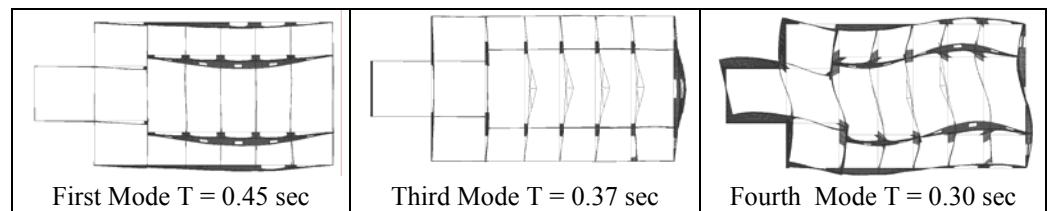


Figure 4. S. Ippolisto “as is” – Modal shapes of the building.

TRANSVERSAL DIRECTION (X axe)				LONGITUDINAL DIRECTION (Y axe)			
MODE	PERIOD [sec]	$M_i/M_{tot}$ [%]	$\Sigma M_i/M_{tot}$ [%]	MODE	PERIOD [sec]	$M_i/M_{tot}$ [%]	$\Sigma M_i/M_{tot}$ [%]
1	0.4470	42.6703	42.6703	3	0.3403	53.3264	53.5476
2	0.3698	10.3297	53.0000	12	0.2272	8.9648	64.3640
4	0.2982	1.0975	54.1439	13	0.2146	1.4342	65.7983

10	0.2649	9.2096	63.5956	21	0.1568	2.1460	68.8336
14	0.2079	4.2496	68.7096	27	0.1387	1.6479	72.4708
15	0.1889	3.3240	72.0336	29	0.1285	3.5134	76.0017
17	0.1819	1.0010	73.8673	34	0.1100	1.0546	78.0047
18	0.1764	1.7495	75.6168	48	0.0968	2.5551	82.3961
30	0.1213	1.3443	80.8956				
45	0.1001	1.5998	83.9021				

Table 2. S. Ippolisto “as is” – Modal Participating mass ratios

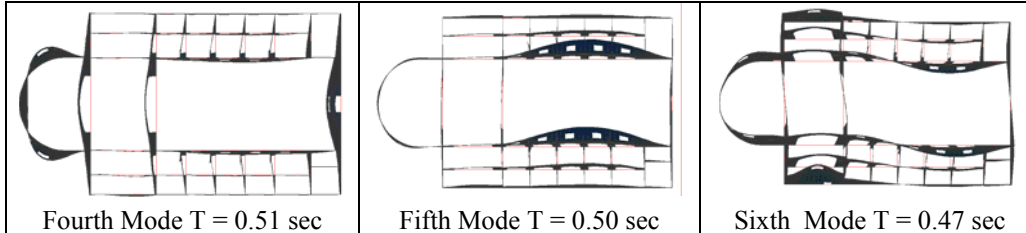


Figure 5. S. Giovanni Maggiore “as is” – Modal shapes of the building.

TRANSVERSAL DIRECTION (X axe)				LONGITUDINAL DIRECTION (Y axe)			
MODE	PERIOD [sec]	$M_i/M_{tot}$ [%]	$\Sigma M_i/M_{tot}$ [%]	MODE	PERIOD [sec]	$M_i/M_{tot}$ [%]	$\Sigma M_i/M_{tot}$ [%]
5	0.5013	28.4619	29.2625	4	0.5072	50.2205	51.4709
6	0.4684	22.6369	51.8994	12	0.3592	8.2557	61.7957
11	0.3810	3.3445	55.7767	28	0.2885	4.9935	67.6308
27	0.2943	3.4507	60.1516	30	0.2737	6.7693	74.5578
29	0.2827	5.9720	66.1403	59	0.1430	0.2878	81.0464
31	0.2711	8.9508	75.1322				
35	0.2349	1.1053	76.4739				
60	0.1402	0.7184	82.8708				

Table 3. S. Giovanni Maggiore “as is” – Modal Participating mass ratios

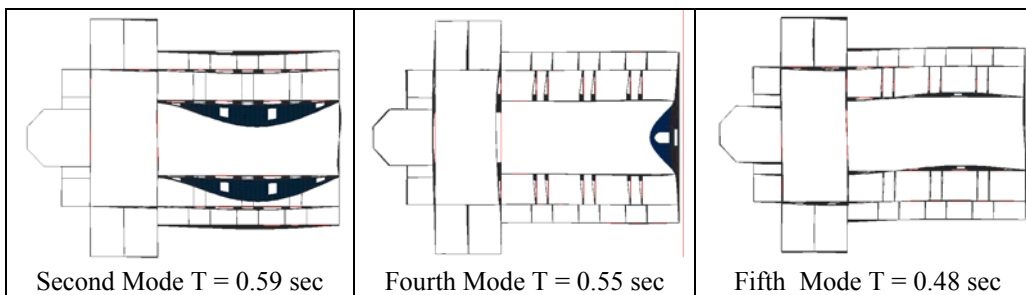


Figure 6. S. Paolo Maggiore “as is” – Modal shapes of the building.

TRANSVERSAL DIRECTION (X axe)				LONGITUDINAL DIRECTION (Y axe)			
MODE	PERIOD [sec]	M <sub>i</sub> /M <sub>tot</sub> [%]	Σ M <sub>i</sub> /M <sub>tot</sub> [%]	MODE	PERIOD [sec]	M <sub>i</sub> /M <sub>tot</sub> [%]	Σ M <sub>i</sub> /M <sub>tot</sub> [%]
2	0.5909	17.5115	17.5135	1	0.6493	7.6043	7.6043
9	0.4196	20.7699	39.6810	3	0.5514	1.5782	9.1944
14	0.3580	2.5988	43.6750	4	0.5511	11.6010	20.7954
15	0.3584	8.4881	52.1631	6	0.4581	25.6356	46.4528
22	0.3408	1.1424	53.8622	7	0.4465	1.4861	47.9389
25	0.3314	6.6361	61.3447	17	0.3547	1.8963	50.0004
41	0.2840	3.1567	66.4612	24	0.3348	1.5099	51.8201
54	0.2273	1.0180	69.1719	26	0.3284	5.8488	58.1490
				27	0.3272	1.1108	59.2598
				39	0.3078	3.9930	64.7309
				45	0.2620	2.3950	66.7091
				60	0.2075	2.7389	74.1130

Table 4. S. Paolo Maggiore “as is” – Modal Participating mass ratios

### 3.2. RIGID DIAPHRAGMS MODELS

Examining the more representative modal shapes of buildings with rigid diaphragms, a clearly different behaviour with respect to buildings without rigid diaphragms can be noticed in Fig. 7, 8, 9 and 10.

Analyzing the first modes, rigid deformations in the transversal directions do not show the out of plane behaviour observed in the previous models. In particular, the structural schemes are stiffer and more monolithic than the previous ones, as suggested by the marked reduction of vibration periods as well (SGMR: T=0.26 s; SI: T=0.29 s; SGMG: T=0.42 s, SP: T=0.52 s).

This variation is also visible in the total mass participating factors since fewer modes are needed to reach significant participating masses (Tab. 5-6-7-8).

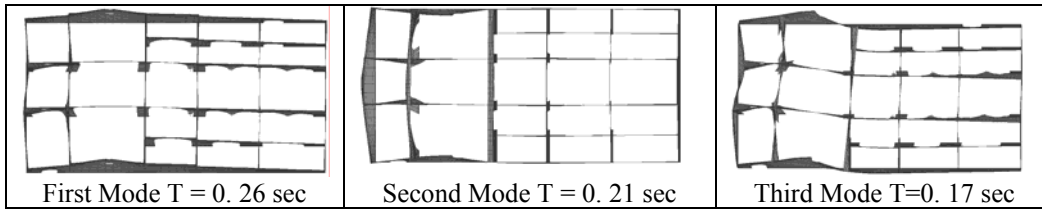


Figure 7. S. Giovanni a Mare with rigid slabs – Modal shapes of the building.

TRANSVERSAL DIRECTION (X axe)				LONGITUDINAL DIRECTION (Y axe)			
MODE	PERIOD [sec]	$M_i/M_{tot}$ [%]	$\Sigma M_i/M_{tot}$ [%]	MODE	PERIOD [sec]	$M_i/M_{tot}$ [%]	$\Sigma M_i/M_{tot}$ [%]
1	0.2576	72.0278	72.0278	2	0.2108	54.8590	54.8617
3	0.1733	1.1963	73.2339	4	0.1498	14.1895	69.0808
9	0.1134	3.181	77.6987	5	0.1352	2.3948	71.4755
15	0.08876	7.2941	85.3091	6	0.1341	6.4473	77.9228
				11	0.0982	3.9994	82.3417

Table 5. S. Giovanni a Mare “rigid slab” – Modal Participating mass ratios.

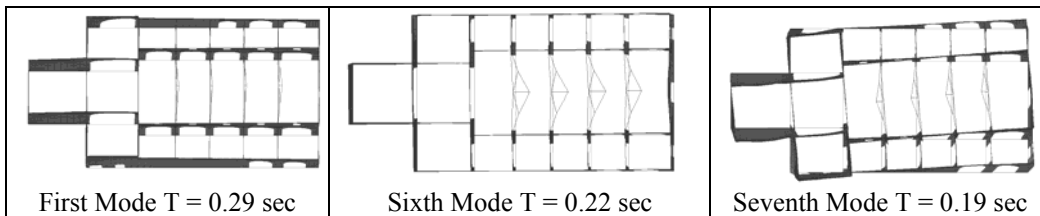


Figure 8. S. Ippolisto with rigid slabs – Modal shapes of the building.

TRANSVERSAL DIRECTION (X axe)				LONGITUDINAL DIRECTION (Y axe)			
MODE	PERIOD [sec]	$M_i/M_{tot}$ [%]	$\Sigma M_i/M_{tot}$ [%]	MODE	PERIOD [sec]	$M_i/M_{tot}$ [%]	$\Sigma M_i/M_{tot}$ [%]
1	0.2898	79.4699	79.4699	2	0.2731	1.0973	1.2151
11	0.1077	4.3497	84.6323	4	0.2644	1.2673	3.4543
				6	0.2151	72.8354	76.2897
				7	0.1859	6.4112	82.7009

Table 6. S. Ippolisto “rigid slab” – Modal Participating mass ratios.

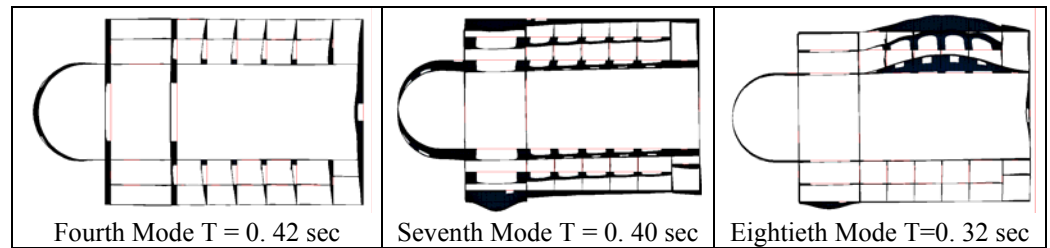


Figure 9. S. Giovanni Maggiore with rigid slabs – Modal shapes of the building.

TRANSVERSAL DIRECTION (X axe)				LONGITUDINAL DIRECTION (Y axe)			
MODE	PERIOD [sec]	$M_i/M_{tot}$ [%]	$\Sigma M_i/M_{tot}$ [%]	MODE	PERIOD [sec]	$M_i/M_{tot}$ [%]	$\Sigma M_i/M_{tot}$ [%]
7	0.4002	70.1181	70.3515	4	0.4242	64.7336	65.8515
8	0.3215	3.5853	73.9368	6	0.4063	8.4173	74.2794
9	0.3198	3.1766	77.1134	40	0.1984	1.0515	76.6279
44	0.1763	1.2113	80.1854	49	0.1625	1.9965	80.5213

Table 7. S. Giovanni Maggiore “rigid slab” – Modal Participating mass ratios

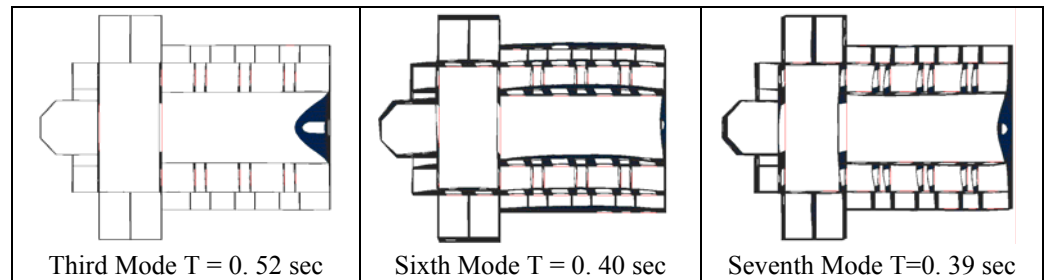


Figure 10. S. Paolo Maggiore with rigid slabs – Modal shapes of the building.

TRANSVERSAL DIRECTION (X axe)				LONGITUDINAL DIRECTION (Y axe)			
MODE	PERIOD [sec]	$M_i/M_{tot}$ [%]	$\Sigma M_i/M_{tot}$ [%]	MODE	PERIOD [sec]	$M_i/M_{tot}$ [%]	$\Sigma M_i/M_{tot}$ [%]
4	0.4784	2.4545	2.4675	1	0.6335	2.7973	2.7973
6	0.3976	50.7869	53.2544	3	0.5169	5.9929	8.7902
7	0.3906	6.3610	59.6154	6	0.3976	7.2138	16.1220
8	0.3790	6.1488	65.7642	7	0.3906	49.1364	65.2584
44	0.2129	1.9213	70.9710	32	0.2932	2.5973	68.9197
58	0.1680	1.7771	76.5010	50	0.2033	0.2439	76.2620

Table 8. S. Paolo Maggiore “rigid slab” – Modal Participating mass ratios.

#### 4. SEISMIC ACTIONS DISTRIBUTION

Linear analyses of the whole structural complex allow individuating the stress distribution among the macroelements constituting the church.

The results of the linear static and modal analyses, carried out on three-dimensional models of buildings, with and without rigid slabs, are reported in Fig. 11, 12 and 13.

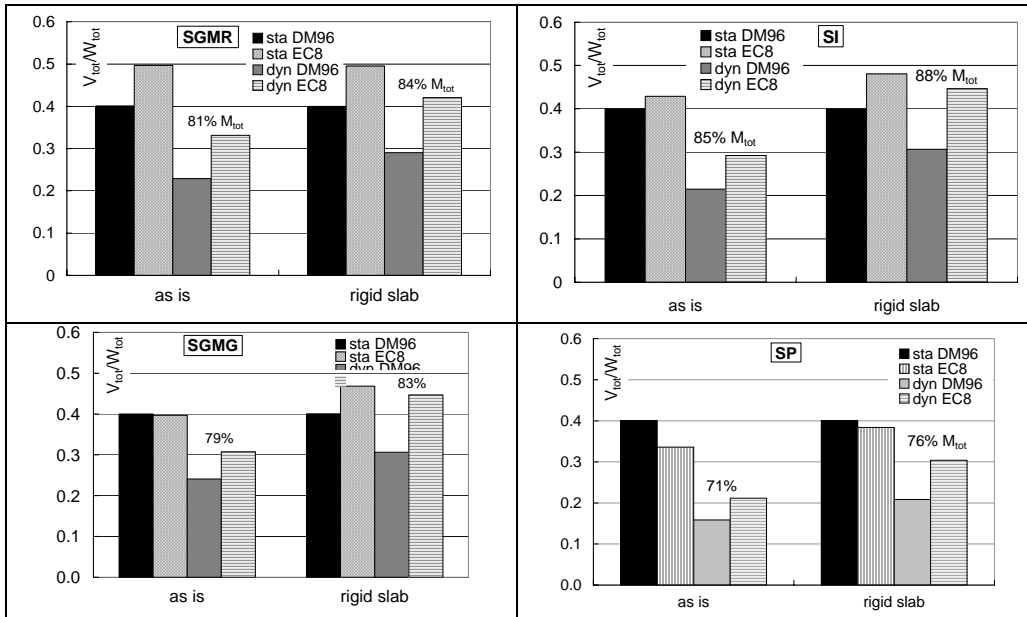


Figure 11.  $V_{tot}/W_{tot}$  – Total shear at the base of the buildings normalized to the total weight.

In Figure 11, on the horizontal axis two groups of bars are reported: “as is” and rigid slab models; on the vertical axis, the total base shear  $V_{tot}$  normalized to the total weight  $W_{tot}$  is indicated. In the histograms four bars per each model are reported; they are related to the case of equivalent static analysis with values of forces provided by DM96 and EC8 codes and of modal analyses with DM96 and EC8 spectra. The values of the total participating masses of the structures on which the analyses have been done are also reported. As it can be seen, the range varies from a

minimum of 71% to a maximum of 88%, never reaching the whole 100% as deduced from the static equivalent analyses. This is the reason why, in the modal analyses the values of  $V_{tot}/W_{tot}$  are always inferior to the static analyses.

The results reported in the histograms of Figure 11 show a marked reduction of base shear passing from static analyses to dynamic analyses. This obvious reduction contextually points out the need of taking into account the largest possible number of vibration modes.

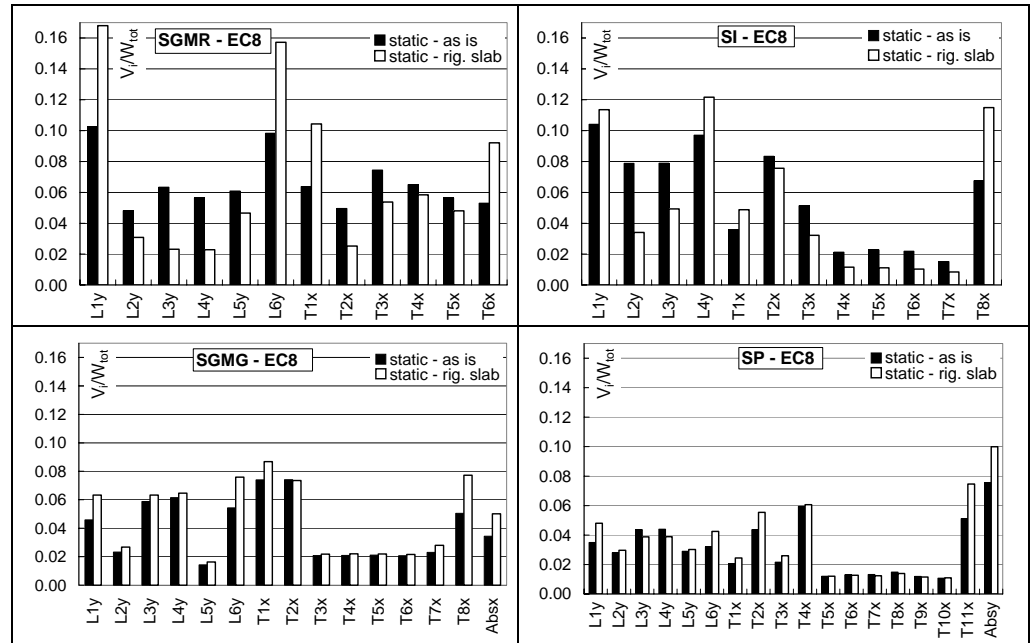


Figure 12.  $V_i/W_{tot}$  – Shear in the single elements normalized to the total weight.

In Fig. 12, the total amount of shear (plotted in Fig. 11) is distributed among the macro-elements. Because in each diagram the transversal and the longitudinal elements are both present, their sum will not be equal to the value reported in the last pictures. On the other side, it is noticeable that the macroelements placed in the same direction of the seismic action absorb more stresses than the elements out of plane.

The histograms in Fig. 13 and 14, report for the four study cases (SGMR, SI, SGMG, SP), the shear absorbed by the single elements  $V_i$  normalized to the total

shear  $V_{tot}$  for a seismic action coming from the transversal direction (X) and the longitudinal one (Y). In the histograms two bars per each structural element are reported, related respectively to the static analyses without and with the rigid diaphragms.

The analyses of the results reported in Fig. 13 and 14 allow deriving information on the stress distribution of churches in the two modelling hypotheses.

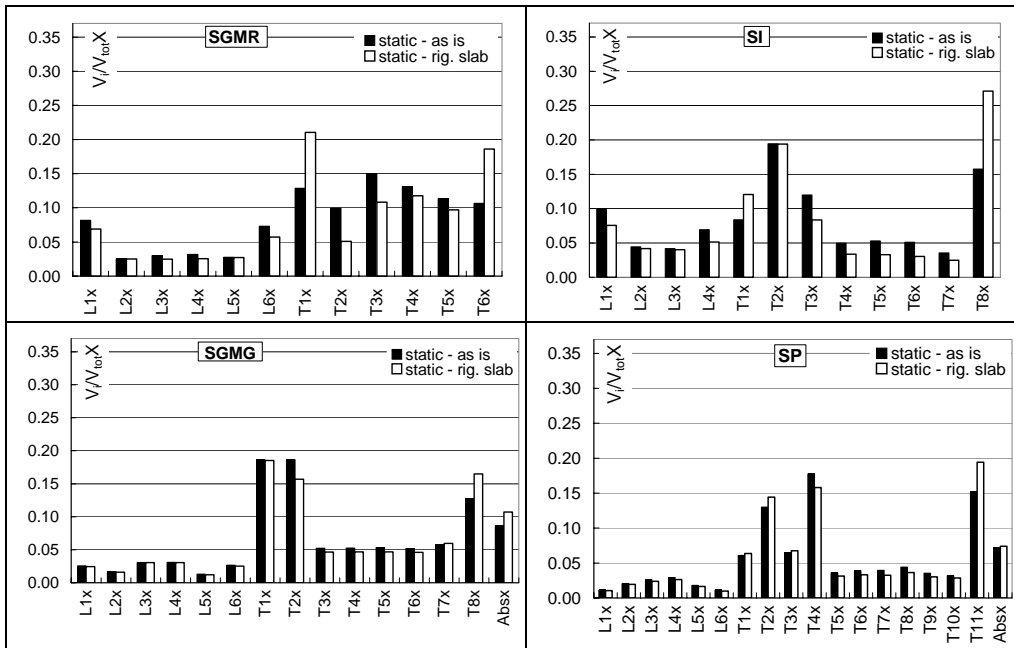
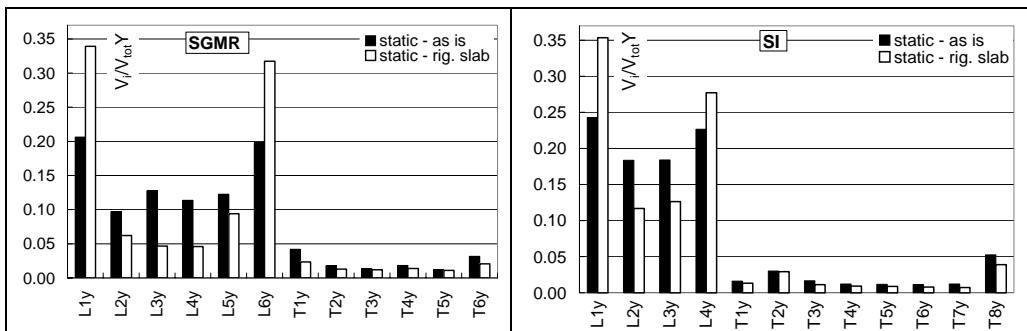


Figure 13.  $V_i/V_{tot}$  – Shear of the single elements normalized to the total shear along X.





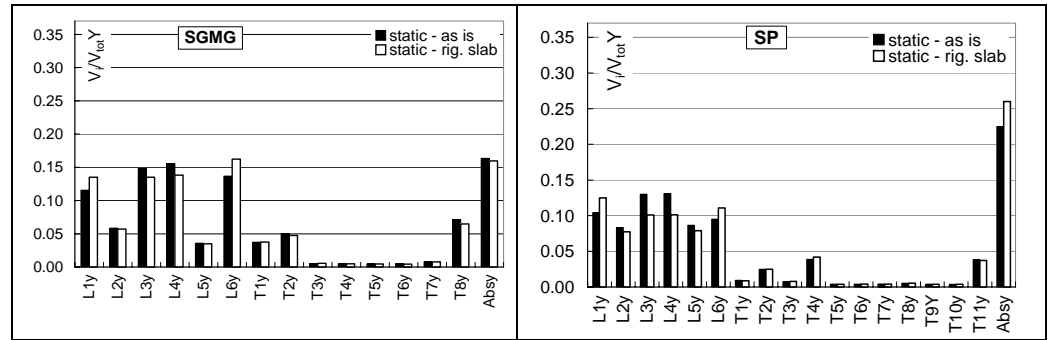


Figure 14.  $V_i/V_{tot}$ – Shear of the single elements normalized to the total shear along Y.

Generally, it is fairly evident that in the X direction, the transversal elements absorb larger amount of base shear and that in the Y direction, the values of shear for longitudinal macroelements are greater than in the perpendicular direction. More comments are possible going into detail for the different church models.

#### 4.1. STRUCTURES WITHOUT RIGID DIAPHRAGMS

In the structures without rigid diaphragms, static and dynamic analyses in both directions show a stress concentration in the stiffer elements. In the transversal direction, they are the external elements such as the façade and the apse (macroelements T1X and T6X in SGMR; T1X, T2X and T8X in SI; AbsX, T1X and T8X in SGMG; AbsX, T1X, T2X and T11X in SP) and the transept area (SGMR hasn't got it, T3X in SI, T2X in SGMG; T4X in SP). In the longitudinal direction, they are located in correspondence of the external elements (L1Y and L6Y in SGMR; L1Y and L4Y in SI; L1Y and L6Y in SGMG; L1Y and L6Y in SP) and in the arcades which separate the principal nave from the lateral ones (L3Y and L4Y in SGMG; L3Y and L4Y in SP).

## 4.2. STRUCTURES WITH RIGID DIAPHRAGMS

The analyses on buildings with rigid diaphragms highlight the transfer of the actions from less stiff to stiffer elements. Generally, external elements absorb a larger amount of base shear in the model without rigid diaphragms.

earthquake in the TRANSVERSAL direction			
Church	macroelement	“as is”	Rigid slab
<b>SGMR</b>	T1X	13%	→ 21%
	T6X	11%	→ 19%
<b>SI</b>	T1X	8%	→ 12%
	T8X	16%	→ 27%
	T3X	12%	← 8%
<b>SGMG</b>	ABSX	9%	→ 11%
	T8X	13%	→ 17%
	T2X	19%	← 16%
<b>SP</b>	T2X	13%	→ 14%
	T11X	15%	→ 19%
	T4X	18%	← 16%

Table 9. Stress transfer from less stiff to stiffer elements in the transversal direction.

earthquake in the LONGITUDINAL direction			
Church	macroelement	“as is”	Rigid slab
<b>SGMR</b>	L1Y	21%	→ 34%
	L6Y	20%	→ 32%
<b>SI</b>	L1Y	24%	→ 35%
	L4Y	23%	→ 28%
<b>SGMG</b>	L1Y	12%	→ 14%
	L6Y	14%	→ 16%
	L3Y	15%	← 14%
	L4Y	16%	← 14%
<b>SP</b>	L1Y	10%	→ 13%
	L6Y	10%	→ 11%
	L3Y-L4Y	13%	← 14%

Table 10. Stress transfer from less stiff to stiffer elements in the longitudinal direction.

In Tab.9 and 10 the variation of shear absorbed by the elements for each church is reported. The elements which have an increase of stresses due to the rigid diaphragms in the plane are the external ones, while all the others, less stiff, present a reduction of the stresses. Also in the buildings with rigid slabs the dynamic analyses confirm substantially the results of the static analyses.

### 4.3. OUT OF PLANE CONTRIBUTION

From the analyses on buildings with and without rigid elements, the contribution of the orthogonal elements in the direction of the earthquake can be derived as well. They are depicted in Figures 13 and 14 and summarized in Tab. 11.

Church	Transversal direction		Longitudinal direction	
	“as is”	Rigid slab	“as is”	Rigid slab
<b>SGMR</b>	14%	→ 9%	27%	→ 23%
<b>SI</b>	16%	→ 13%	26%	→ 21%
<b>SGMG</b>	19%	→ 18%	14%	↔ 14%
<b>SP</b>	14%	↔ 14%	12%	→ 11%

Table 11. Transfer of the contribution of the orthogonal elements – transversal and longitudinal direction.

It can be affirmed that the contribution of the orthogonal elements in the schemes with rigid diaphragms is slightly inferior to those without diaphragms and that in the transversal direction a larger contribution than longitudinally can be noticed.

### 5. STRENGTH DEMAND

The results of the analyses in terms of strength demand (that seismic action imposes to the structural elements) are provided in Figure 15 and 16.

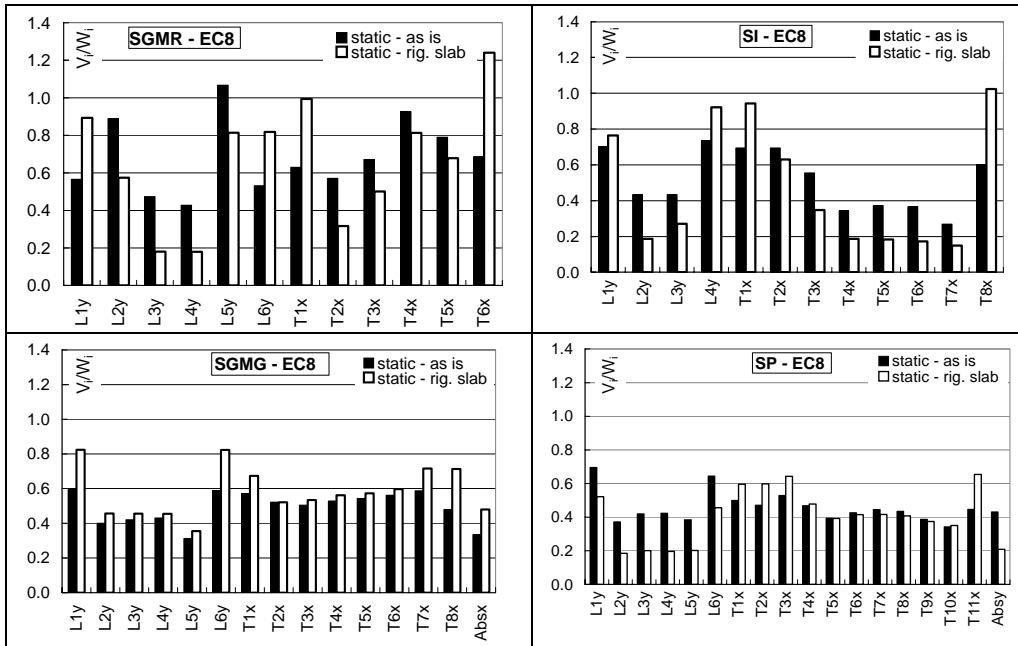


Figure 15.  $V_i/W_i$  – Shear of the single elements normalized to their weight.

In both the Figures, on the abscissa axis the label of the macroelements and on the ordinate axis the value of the shear absorbed from the single element is reported. In Figure 15 these shear values are normalized to the vertical load acting on the element  $W_i$ , and in Figure 16 to the total weight  $W_{tot}$ . In each diagram only the contribution of the elements in the direction of the earthquake is reported; for each element the two bars refer to the “as is” and with diaphragms.

Examining the Figure in more detail, it can be noticed that larger strength demands are generally concentrated in the external elements. In the scheme with rigid diaphragms there is an even larger concentration in the stiffer elements. In Tables 12 the range of variability for models with and without rigid diaphragms in both directions is reported.

<b><math>V_i/W_i</math> RANGE OF VARIABILITY</b>				
Church	“as is” models		rigid slab models	
	Long. Dir.	Trans. Dir.	Long. Dir.	Trans. Dir.
<b>SGMR</b>	43% ÷ 107%	57% ÷ 93%	18% ÷ 89%	32% ÷ 54%
<b>SI</b>	43% ÷ 74%	27% ÷ 70%	17% ÷ 85%	17% ÷ 94%
<b>SGM G</b>	31% ÷ 59%	33% ÷ 59%	36% ÷ 82%	52% ÷ 72%
<b>SP</b>	37% ÷ 70%	34% ÷ 53%	18% ÷ 52%	21% ÷ 65%

Table 12.  $V_i/W_i$  – Range of variability in the “as is” and Rigid slab models.

<b>MINIMUM STRENGTH DEMAND</b>				
Church	“as is” models		rigid slab models	
	Long. Dir.	Trans. Dir.	Long. Dir.	Trans. Dir.
<b>SGMR</b>	6% ÷ 97%	20%÷104%	17%÷102%	3%
<b>SI</b>	30% ÷ 93%	19%÷111%	33%÷134%	--
<b>SGM G</b>	2% ÷ 66%	3% ÷ 63%	19%÷ 96%	--
<b>SP</b>	9% ÷ 83%	28% ÷ 74%	32%÷ 90%	--

Table 13. Range of variability of the minimum strength demand.

Furthermore, in Table 13 the strength demand in terms of minimum and maximum values is provided. These values are substantially confirmed in Figure 16, in which the shear values  $V_i$  are normalized to the total vertical weight  $W_{tot}$ . These representation provides qualitative indications, concerning the repartition of global actions, and quantitative indications, on the entity of the seismic action on the building in the two cases (with and without rigid slab).

## 6. CONCLUSIONS

In this chapter the seismic behaviour of the four study cases has been analyzed. This study has been developed through static and dynamic analyses on models of the buildings with and without rigid diaphragms. The analyses on the schemes in the hypothesis of absence of the rigid diaphragm have highlighted the complexity of the dynamic behaviour of this typology and the particular vulnerability to seismic actions. The modal shapes for the analyzed buildings, furthermore, have shown low

torsional and transversal stiffness of the buildings and great out of the plane deformation.

These problems are subdued in the behaviour of buildings with rigid slabs, characterized by a greater global stiffness (especially in torsional terms) and a more monolithic behaviour. The introduction of rigid diaphragms implies a global improvement of the buildings, even if this effect is not completely beneficial. Because the heights at which the roofs are located are different (principal naves are, generally, higher than the secondary naves) it is possible to notice some discontinuities. It has been noticed, furthermore, a stress concentration in the stiffer elements of the buildings (façade elements and in the transept zone) which absorb a greater amount of the total shear compared to the scheme without rigid diaphragms. In the longitudinal direction the external elements, stiffer than the internal ones, are more stressed than in the case without diaphragms, whilst internal elements are almost unloaded.

## **CHAPTER 4:**

### ***FEM NON LYNEAR ANALYSES***

#### **1. INTRODUCTION**

The mathematical modelling of masonry shows several difficulties that rise from the need to take into account the non linear behaviour and the progressive degradation of the stiffness when strains increase. In case of old stone masonry other irregularities are added. Different dimension and location of the stones, non homogeneity in the distribution of the mortar, great scattering of the mechanical characteristics of the elements and uncertainty on the structural complex have to be considered.

In this chapter, non linear analyses on bi-dimensional elements are carried out through the computer code ABAQUS [HKS, 2004]. On the base of the results of these analyses, some considerations are made with reference to the confidence of the adopted model.

## 2. MODELLING THROUGH ABAQUS

All the macroelements constituting the basilicas have been subjected to non linear analyses using a smeared cracking approach as implemented in the computer code ABAQUS. The computational mechanic of the brittle structures has been approached in the past through two different ways: discrete and smeared cracked models. In the first one, the cracking is considered through modifying the geometry whether the internal parts of the body are linear elastic [Alexandris A. et Al., 2004; Azevedo et Al. 2000; Lemos, 2004; Schlegel R. & Rautenstrauch K., 2004; Tzamtis A.D. & Asteris P.G., 2004]; the second one considers fixed the geometry and introduces the cracking process only through constitutive law. In big or complex structures, the smeared model is preferred to the discrete one for the difficulties into following the developing of all the cracks. In the smeared models the cracking process is entirely introduced through constitutive laws and some important phenomenon like the tension stiffening, rotating or fixed multiple cracks, softening in tension and compression have been introduced.

On the other side, this model has the disadvantage of being mesh-dependent. Two types of mesh dependency can be highlighted: 1) mesh organization: mechanisms of localization can be captured or addressed by the topology of the elements; 2) mesh dimensions. The last problem can be overcome putting into relation some constitutive model parameters with the dimension of the elements (i.e. fracture energy has to remain constant). The first one has been avoided by adopting some regularization technique.

Caporale [A. Caporale, R. Luciano, 2002] shows how the post peak behaviour is influenced by the deformation localization phenomena so that the numerical solution is mesh and arc-length dependent.

The smeared cracking model proposed in ABAQUS is called “concrete” and it is good for relatively monotonic loadings under fairly low confining pressure. Cracking is assumed to be the most important aspect of the behaviour and dominates the



modelling. It is assumed to occur when the stresses reaches a failure surface called “crack detection surface”. The presence of cracks enters into these calculations by the way the cracks affect the stress and the material stiffness associated with the integration point. When the principal stress components are dominantly compressive, the response of the concrete is modelled by an elastic-plastic theory using a simple form of yield surface written in terms of the first two stress invariants. Associated flow and isotropic hardening are used.

The cracking and compression responses are illustrated by the uni-axial response depicted in Fig. 1.a. When the material is loaded in compression, it initially exhibits elastic response. As the stress is increased, some inelastic straining occurs and the response of the material softens. The softer unloading response is neglected by the model. When an uni-axial specimen is loaded into tension, it responds elastically until, at a stress that is around the 10% of the ultimate compressive stress, the material loses strength through a softening mechanism. This is a damage effect and the model neglects any permanent strain associated with cracking.

In multi-axial stress states, these observations can be generalized through the concept of surfaces of failure and of ultimate strength in stress space (Fig. 1.b).

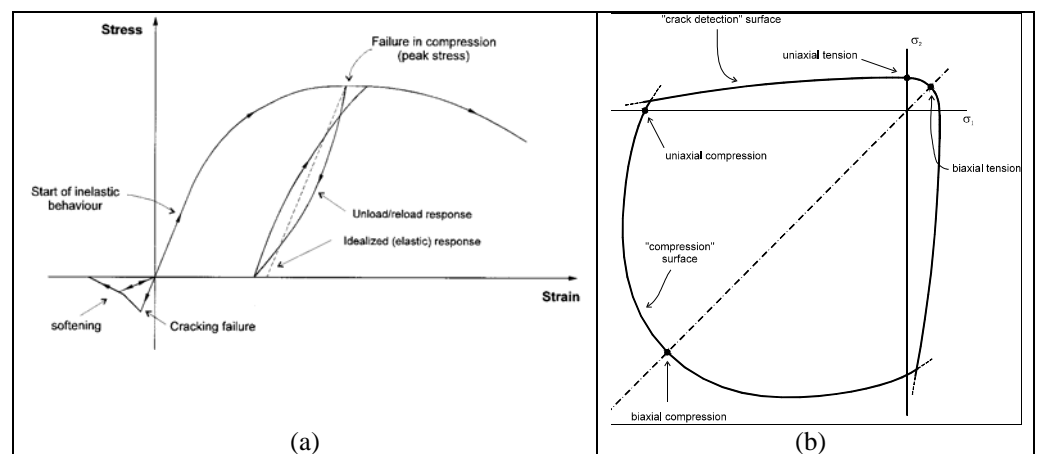


Figure 1. a) Uni-axial behaviour of plain concrete; b) Concrete failure surface in plane stress.

Since ABAQUS is a stiffness method code and the material calculations used to define the behaviour of the material are carried out independently at each integration point, the solution is known at the start of the time increment. The constitutive calculations (based on the current estimate of the kinematic solution for the response at the spatial integration point during the increment) provide values of stress and material stiffness at the end of the increment. Once cracks exist at a point, the component forms of all vector and tensor quantities are rotated so that they lie in the local system defined by the crack orientation vectors.

The model, thus, consists of a compressive yield/flow surface to model the response in predominantly compressive states of stress, together with damaged elasticity to present cracks that have occurred at a material calculation point.

The model uses the classical concepts of plasticity theory: strain rate decomposition into elastic and inelastic strain rates, elasticity, flow and hardening.

In the definition of the compression yield, the value of the magnitude of each nonzero principal stress in biaxial compression and the stress magnitude in uni-axial compression ( $\sigma_b/\sigma_c$ ) is given on the 1° FAILURE RATIO data line. In the same way, the ratio of the uni-axial tensile stress at failure to the uni-axial compressive stress at failure ( $\sigma_t/\sigma_c$ ) is given on the 2° FAILURE RATIO data line.

In the definition of the flow, the value given on the 3° FAILURE RATIO option is representative of the ratio of  $\epsilon^{pl}$  in a monotonically loaded biaxial compression test to  $\epsilon^{pl}$  in a monotonically loaded uni-axial compression test.

In tension, cracking dominates the material behaviour. The model uses a “crack detection” plasticity surface in stress space to determine when cracking takes place and the orientation of cracking. Damaged elasticity is then used to describe the post-failure behaviour of the material with open cracks. About the crack orientation, although some models have been proposed (fixed model with orthogonal cracks, rotating model, fixed model with multidirectional cracks), the used model by ABAQUS is the first one. The perpendicular to the first crack that occurs in a point is

parallel to the maximum principal tension stress; the model remembers this direction so that the following cracks could form only in direction perpendicular to the first one.

The value of the tensile failure stress  $\sigma_I$  in a state of biaxial stress when the other nonzero principal stress  $\sigma_{II}$ , is at the uni-axial compression ultimate stress state is defined by the 4° FAILURE RATIO.

Another important aspect of the model is the TENSION STIFFENING, which consists in the hypothesis that once the cracking tension stress is reached, the strength doesn't decay suddenly; the stress-strain curve will be zero covering a descending rectilinear or curved path, definable by the user.

After all, the utilization of the “concrete” model in ABAQUS requests the definition of the following parameters by the user:

1. **Young module** (normal elasticity module);
2. **Poisson module** (transversal contraction coefficient);
3. (whatever) **Constitutive model** assigned for values of tension and correspondent plastic strain rates;
4. **Tension Stiffening** or the tension strength decay once the cracking is reached;
5. **Failure ratios:**
  - 1: ratio of the ultimate biaxial compressive stress to the uni-axial compressive ultimate stress.
  - 2: absolute value of the ratio of uni-axial tensile stress at failure to the uni-axial compressive stress at failure.
  - 3: ratio of the magnitude of a principal component of plastic strain at ultimate stress in biaxial compression to the plastic strain at ultimate stress in uni-axial compression.
  - 4: ratio of the tensile principal stress value at cracking in plane stress, when the other nonzero principal stress component is at the ultimate compressive stress value, to the tensile cracking stress under uni-axial tension.

### 3. MODEL CALIBRATION

In order to correctly calibrate the model parameters, a curve fitting procedure was made by [Giordano A., 2002] using the results of the experimental tests on masonry tuff walls conducted at the ISMES in Bergamo. The natural stone blocks, deriving from the demolition of ancient Neapolitan buildings, were subjected to different set loadings, both monotone and cyclic, in order to determine the values of the elastic modules and the ultimate resistance. These data have been used in a finite element model to define the parameters in the  $\sigma$ - $\varepsilon$  curve. Extended sensibility analyses have been conducted again by [Giordano A., 2002] to improve the correspondence between the experimental results and those numerically obtained. The model, applied to masonry with very low strength values, appears extremely sensitive even to small variation.

About the TENSION STIFFENING option, although it could appear a non-sense in the case of masonry, small tension strength has been maintained in the cracking process in order to stabilize the numerical algorithm. The Riks algorithm has been used to push the analysis towards the descending load branch, without the need to carrying out simulations in displacement control.

The following parameters have been used in the adopted model.

1. **Young module:**  $E=1.1 \text{ E}+9 \text{ (N/m}^2\text{)}$ ;
2. **Poisson module:**  $\nu= 0.1$ ;
3. **Constitutive model:** as reported in Fig. 2;

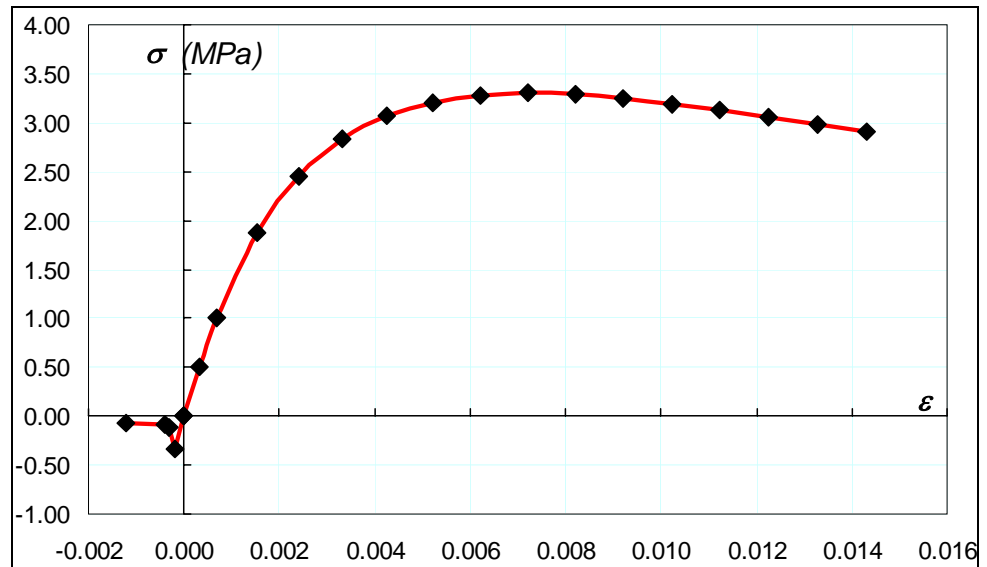


Figure 2. Constitutive model adopted into the definition of the “concrete” properties.

4. **Tension Stiffening:** displacement = 3mm;
5. **Failure ratios:**
  - 1: 1.16 (by default);
  - 2: 0.1 (0.09 by default);
  - 3: 1.33 (1.28 by default);
  - 4: 0.3 (0.33 by default).

#### 4. BEARING CAPACITY IN THE FOUR STUDY CASES

##### 4.1. S. GIOVANNI A MARE

The plan of the church with the individualization of the macroelements is reported in Fig. 3. From Fig. 4 to Fig. 13 a summary of the non linear analyses per each macroelement is reported. The visualization of the plastic strain tensor for forces coming from both directions and the plot of the force/displacement curve are depicted. On these curves, the maximum value reached by the collapse multiplier for each analysis is highlighted.

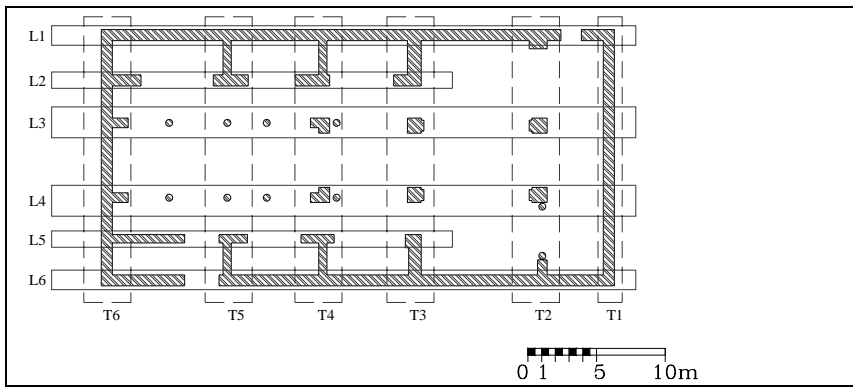


Figure 3. SGMR – individuation of the macroelements in plan.

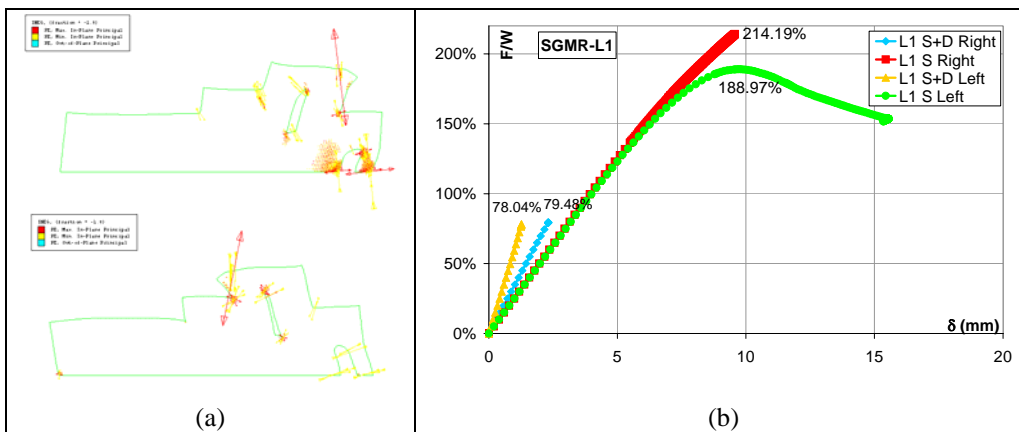


Figure 4. L1 macroelement – a) Plastic strain tensor; b) Force/Displacement curve.

This macroelement is not symmetric in geometry and load condition so that four analyses have been carried out (two of them for the self weight with horizontal actions in the right and left verse and other two for the self weight plus the dead load with seismic actions again in the two verses in the plane). Two aspects of these analyses can be clearly noticed: the first one is that the two curves relevant only to the self weight reach values that are double the ones of the analyses with the dead load included. Furthermore, the plastic branch is reached only in the analysis with horizontal forces coming from the left verse considering the self weight. Then, the

horizontal stiffness is fairly different. Surprisingly, in the analyses with self weight plus the dead load the values are bigger than the analyses with only the self weight and they are dependent on the verse of the force.

When the forces are coming from the left side, the analysis stops when the collapse of the pier is obtained; in the opposite direction the condition for which the collapse occurs is for the opening of the cracks at the top of the panel in correspondence of the roof transmission loads.

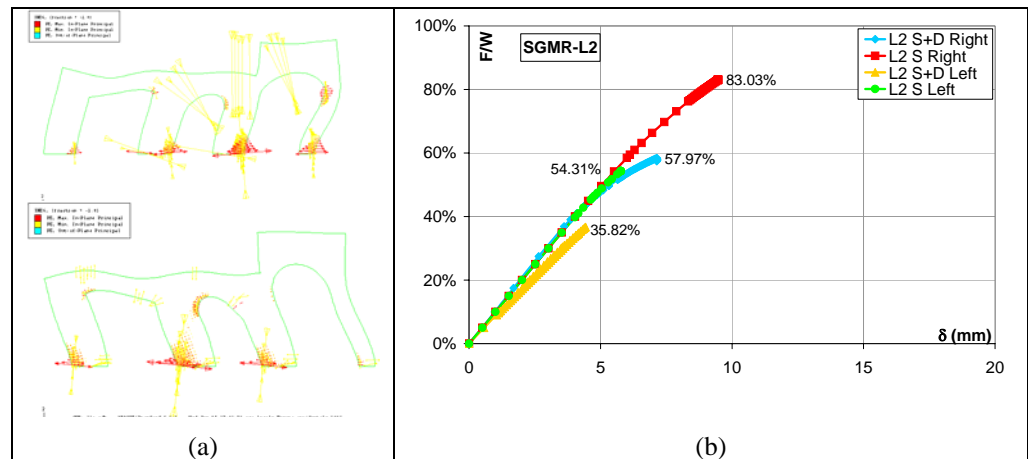


Figure 5. L2 macroelement – a) Plastic strain tensor; b) Force/Displacement curve.

Also in this macroelement, four different analyses have been carried out. In the right verse the two curves (with and without the dead loads) seems to tend to the plastic branch; on the contrary, when the horizontal actions come from the left side, the analyses stop during the crescent phase. The horizontal stiffness is almost the same (independently from the load condition) except when the forces come from the left. In terms of strength the results are quite different. For left forces, the collapse of the pier sustaining the main arcade is determinant for the collapse. This happens because the horizontal thrust of the arch sums to the seismic force and there is no contrast from the following arcades. On the contrary, when the forces are coming from the

right direction, an effective contribute of the other arcades can be noticed so that the values of the collapse multiplier are higher than the previous ones. In both cases, anyway, the analyses stop for the opening of the cracks at the top of the main pier or at the base of the small piers.

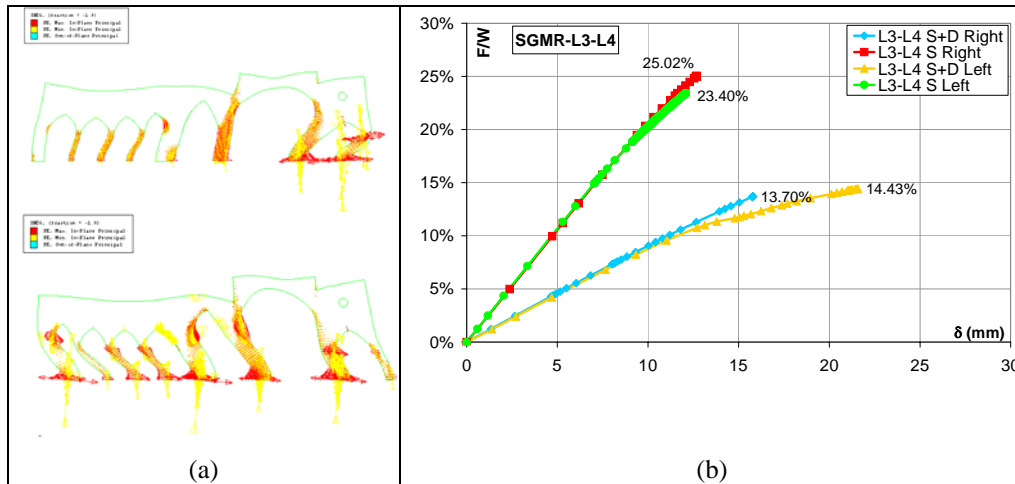


Figure 6. L3 and L4 macroelement – a) Plastic strain tensor; b) Force/Displacement curve.

A decrease in the horizontal stiffness and in the collapse multiplier can be noticed in the model with self weight and dead load. At the same time the stiffness and the value of the bearing capacity are consistent in the models independently from the verse of the seismic action. The collapse conditions are due to the crack openings at the base of the piers with a linear behaviour until the reaching of the maximum strength.

In Fig. 7 Although the collapse mechanism is close to the storey one, the great discrepancy between the dimensions of the pier on the left and the other ones on the right leads to great differences in terms of collapse multiplier depending from the verse of the force. When the forces come from the left part, in the first pier on the right the seismic action sums to the horizontal thrust of the arch. Independently from



the presence of the dead load, the analyses with seismic force coming from right give larger values than the analyses with forces coming from left.

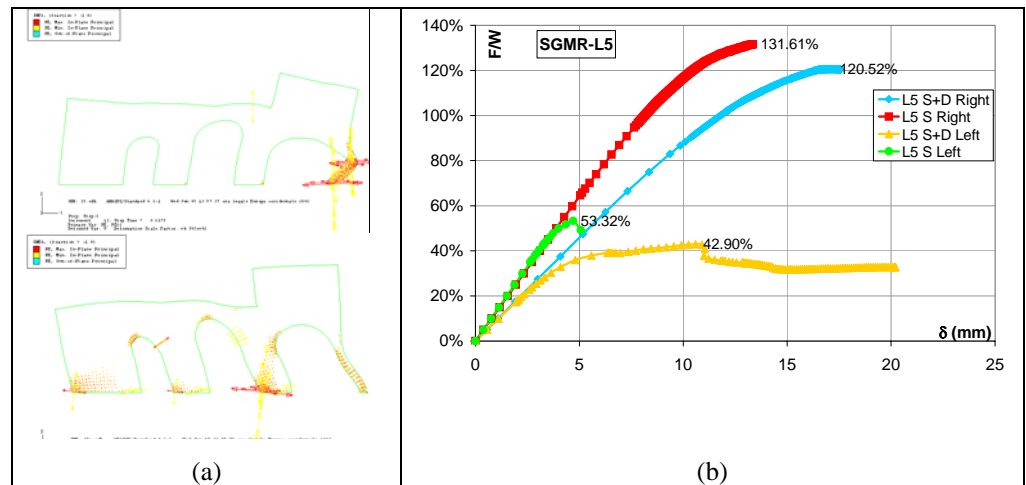


Figure 7. L5 macroelement – a) Plastic strain tensor; b) Force/Displacement curve.

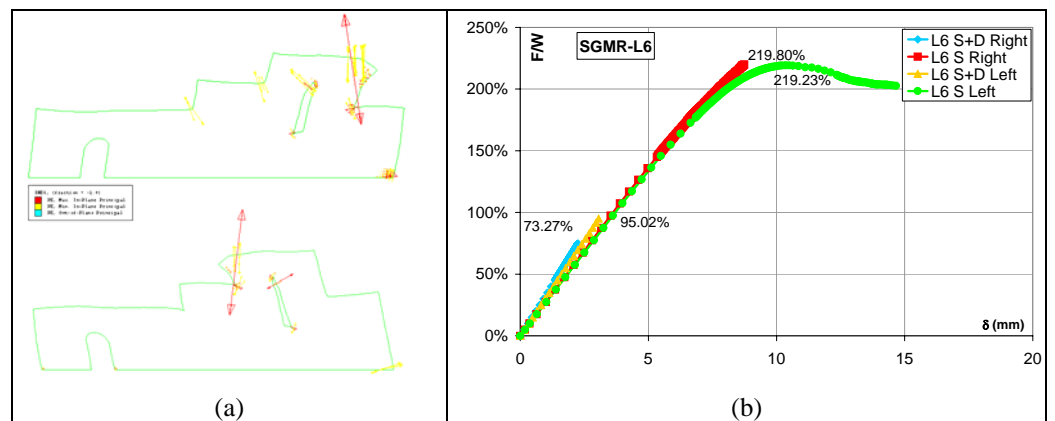


Figure 8. L6 macroelement – a) Plastic strain tensor; b) Force/Displacement curve.

The analyses carried out on the model with the sole self weight give results somehow larger than the analyses with the included dead load. The horizontal stiffness is fairly the same in the four load conditions. The analysis stops for local cracking phenomenon at the top of the panel in correspondence of the loads coming from the

roof. The percentage of the dead load compared to the self weight is only of the 17% but the curves with the dead load break when they are still in the linear branch.

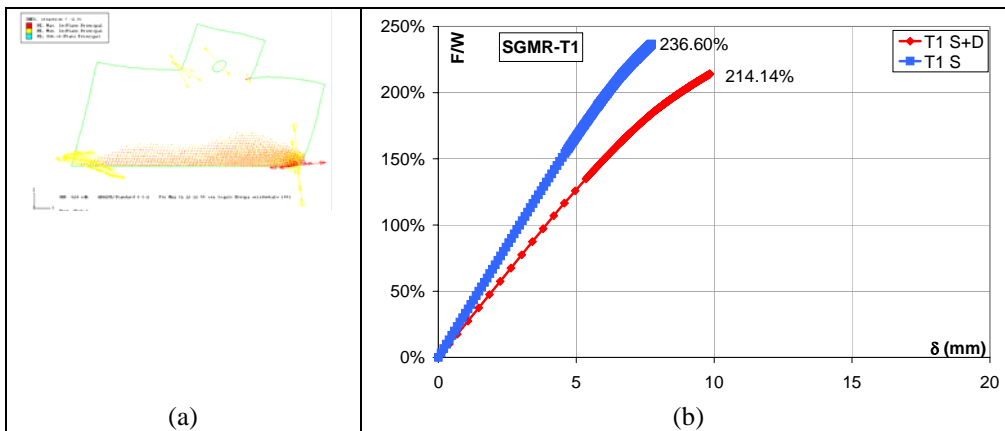


Figure 9. T1 macroelement – a) Plastic strain tensor; b) Force/Displacement curve.

The macroelement shows the classic behaviour of the stocky panel. The formation of compressed areas in correspondence of the corners at the bottom of the panels, with forces in the alternative directions, is individuated. Smaller values of the collapse multiplier and of the horizontal stiffness can be seen in the diagram in presence of the self weight and the dead load. The linear behaviour of the curves is shown until the reaching of the maximum values, although a starting of the plastic branch is detectable.

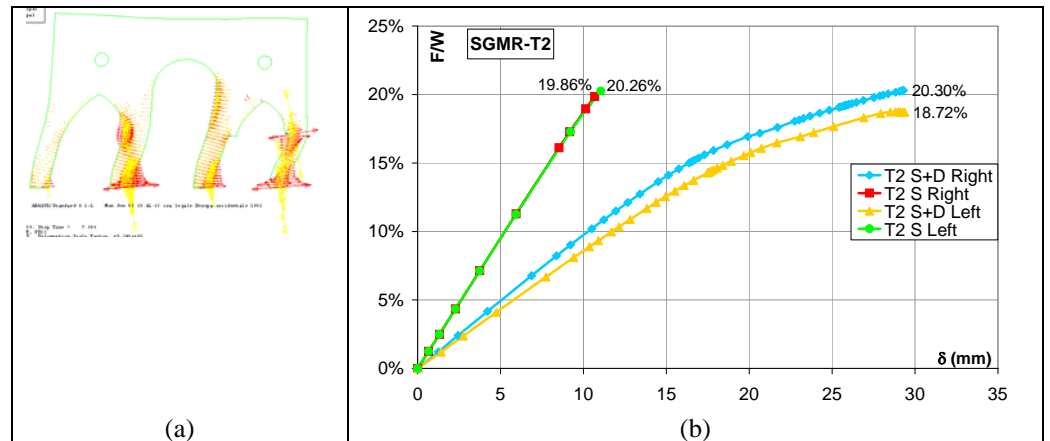


Figure 10. T2 macroelement – a) Plastic strain tensor; b) Force/Displacement curve.

In this macroelement, only a decrease of the stiffness can be noticed in the model with the self weight and the dead load. Because of the clear storey mechanism of this panel, the collapse occurs for a series of plastic hinges at the top and the bottom of the piers. The plastic branch is more visible in the cases with the dead load instead of the cases with the self weight only.

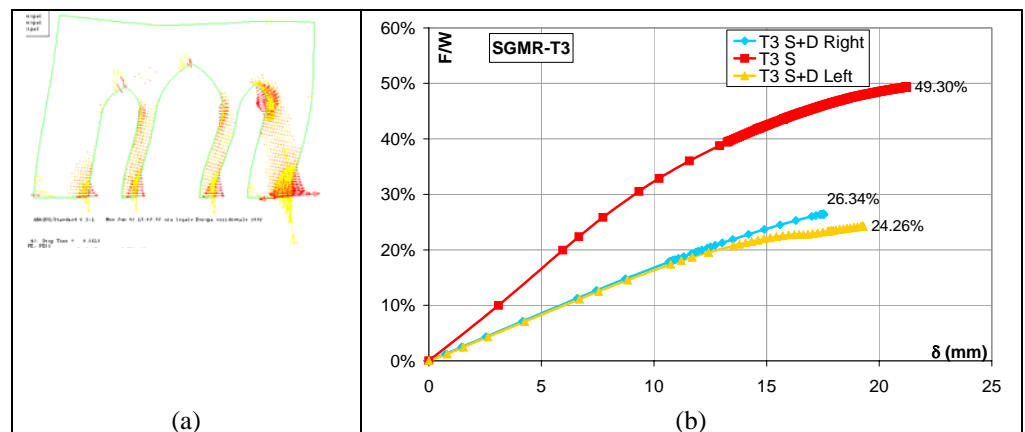


Figure 11. T3 macroelement – a) Plastic strain tensor; b) Force/Displacement curve.

This macroelement is symmetric only for the geometry but not for the load condition; this is the reason why three curves are depicted in the plot. A decrease of strength and stiffness can be noticed in the diagrams in the case of self weight plus dead load model; indeed the ratio between the dead load and the self weight is equal to 0.865 so fairly close to unity.

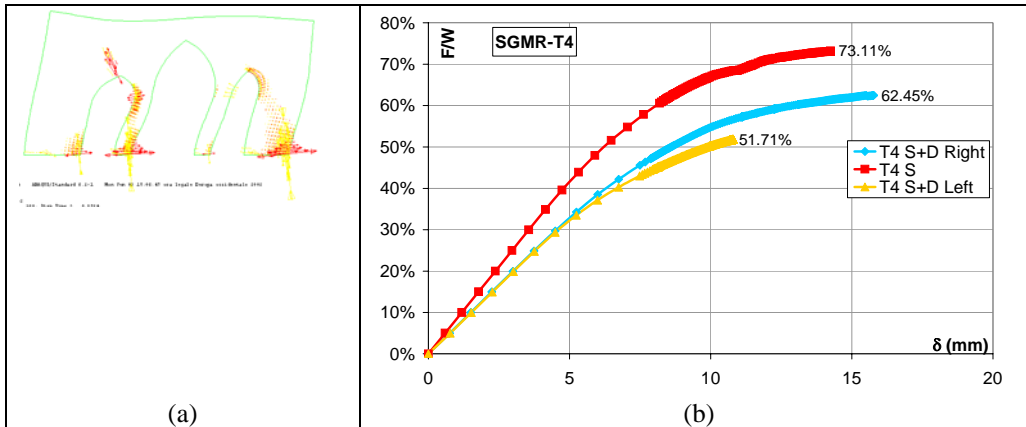


Figure 12. T4 macroelement – a) Plastic strain tensor; b) Force/Displacement curve.

This macroelement is very similar to the previous one in terms of geometric shape but is differently loaded. Horizontal stiffness and collapse value are different according to the load considered case. After the linear behaviour, increasing displacements more than the loads can be detected until the collapse.

In Fig. 13 the symmetrical geometrical structure is loaded in a non symmetric way. This is the reason why three curves are shown. In terms of strength, the models inclusive of the dead load stop in the elastic branch with small values compared to the analysis with only the self weight which clearly reaches the horizontal branch. The discrepancy in the collapse values can be found also in the ratio between the intensity of the dead load on the self weight of the element that is 77.4 %.

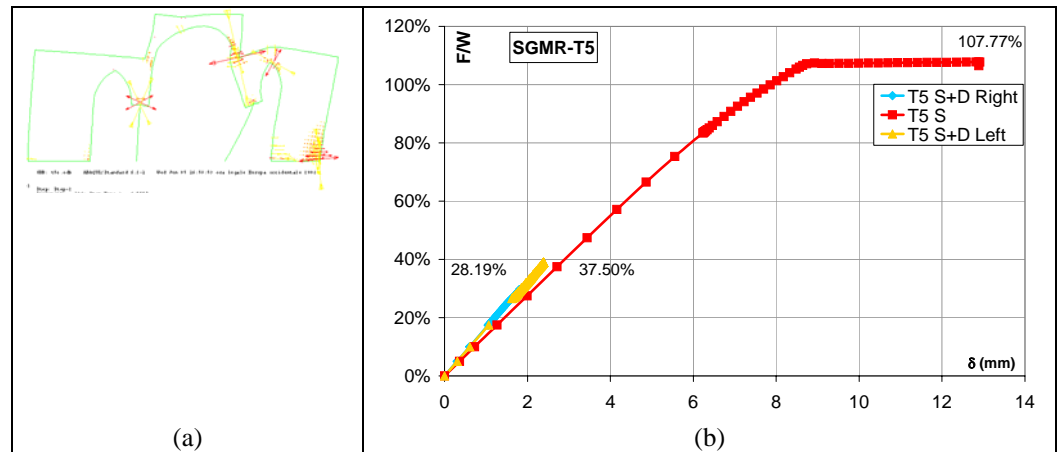


Figure 13. T5 macroelement – a) Plastic strain tensor; b) Force/Displacement curve.

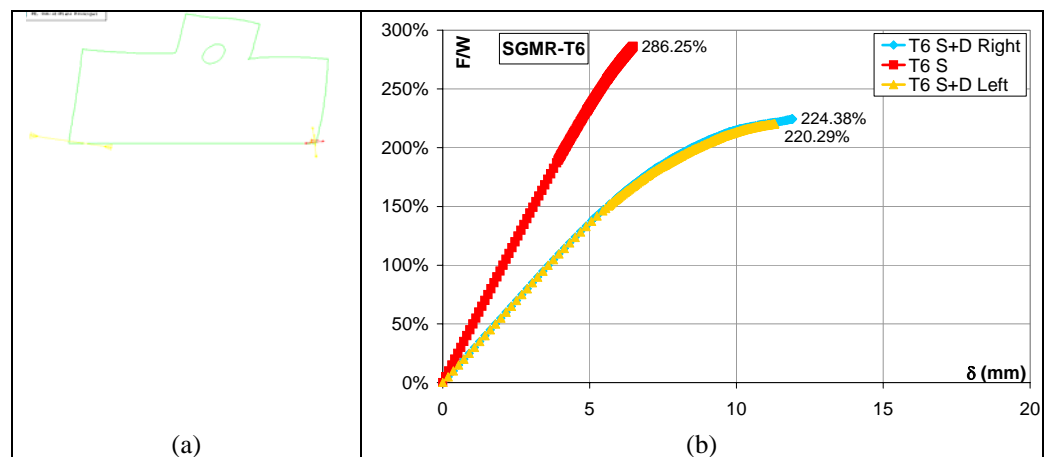
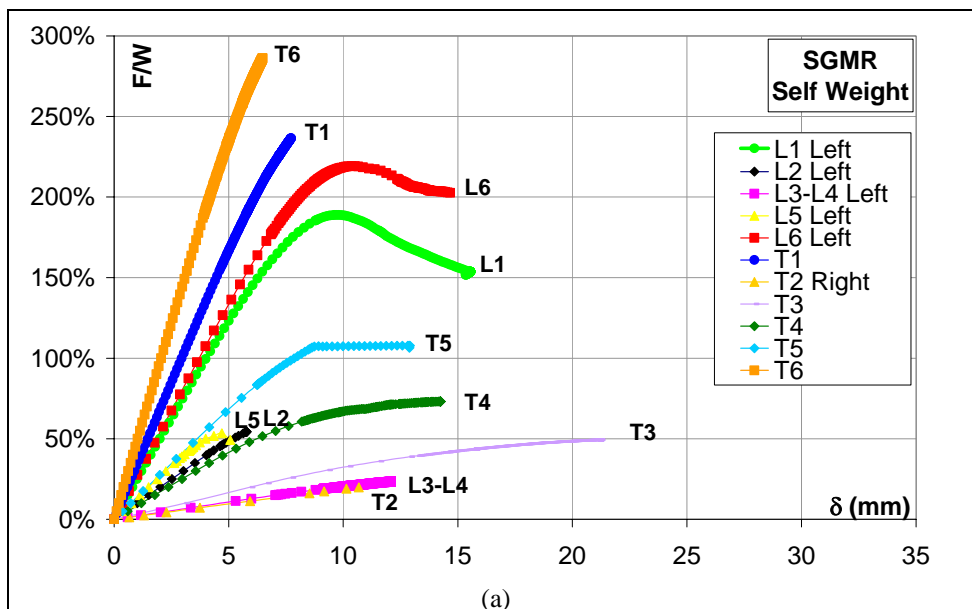


Figure 14. T6 macroelement – a) Plastic strain tensor; b) Force/Displacement curve.

A decrease in terms of strength and collapse values can be detected in the models comprehensive of the dead load. The stocky panel lacks openings and indeed, the formation of compressive areas in correspondence of the corners at the bottom of the element is the cause of the collapse for forces coming in both the directions.

**4.1.1. SUMMARY OF THE RESULTS IN SGMR**

In Figure 15 the summary of the smallest collapse multipliers for each macroelement is reported. In the picture on the top the results for the only self weight condition and in the picture on the bottom for the load condition of self weight plus dead load are reported. In both the pictures, the values assumed by the horizontal stiffness are clear: the external elements (L1, L6, T1, T6) which are lacking openings and fairly stocky shape have a greater stiffness than the internal elements. More into the detail, it can be noticed that the curves for the self weight reach more easily the plastic branch than the curves of the models with the self weight and the dead load. Furthermore, the collapse multiplier values of the first figure are generally larger and bear smaller displacements than the second one.



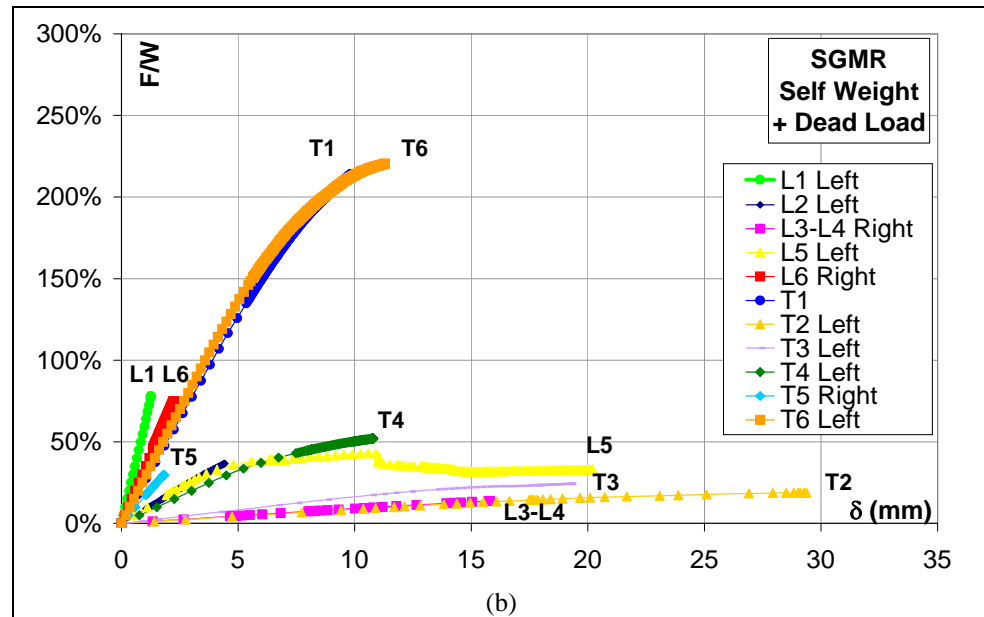


Figure 15. Summary of the curves in SGMR.

#### 4.1.2. STRENGTH VS CAPACITY IN SGMR

In order to assess the seismic vulnerability of the macroelements constituting the churches, two values descending from different analyses can be compared. They are the strength demand (coming from linear analyses and already exposed in the previous chapter) and the bearing capacity (coming from non linear analyses and herein illustrated). Already [Abrams D.P., 1997, 2000], conducting some experiments on two reduced-scale, unreinforced clay-unit masonry buildings subjected to simulated earthquake motions on a shaking table, measured the response of estimated base shear demand versus capacity.

In Fig. 16 the comparison between the two values of each macroelement is reported. In other words, from the linear analyses it is possible to determine the amount of shear stress each element needs when a seismic wave acts in its direction. More in detail the results for the two models in presence of a rigid diaphragm or “as is” can be compared to the results obtained from the non linear analyses which show

the bearing capacity of the element. In particular, two bars representing the minimum and the maximum capacity in presence of self weight and dead load are reported. It is noticeable that, the internal macroelements are easily subjected to damages in case of horizontal action because of the smaller values of the capacity compared to the strength. On the contrary, the external macroelements (the façade and the longitudinal walls) have shown a good behaviour in the non linear analyses so that, it seems they are able to bear the action.

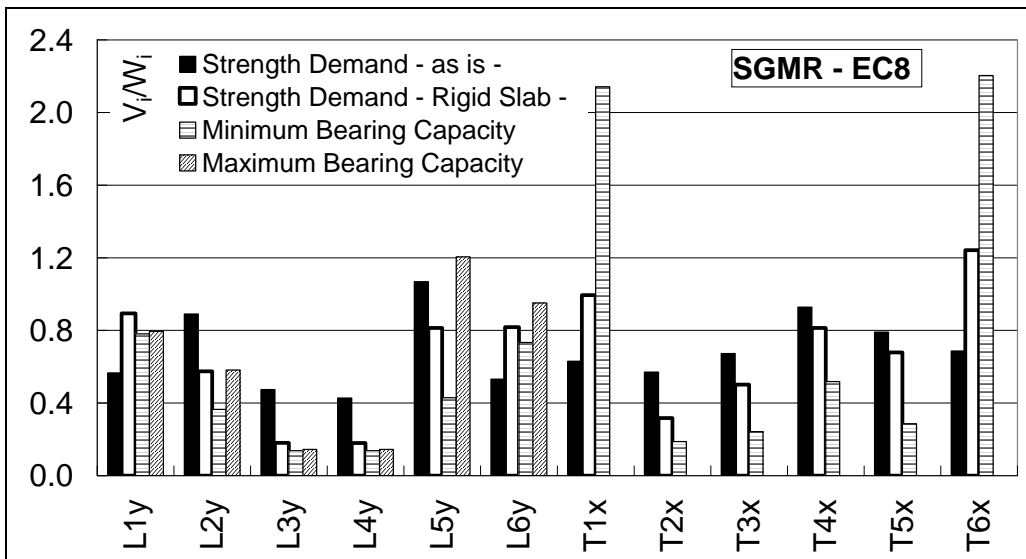


Figure 16. Strength against capacity in SGMR.



**4.2.S. IPPOLISTO**

The same scheme followed in SGMR has been adopted for the other churches. Therefore, in Fig. 16 there is the plan with the macroelements and in the following pictures (from Fig. 17 to Fig. 25) the analyses of the single macroelements are reported in detail.

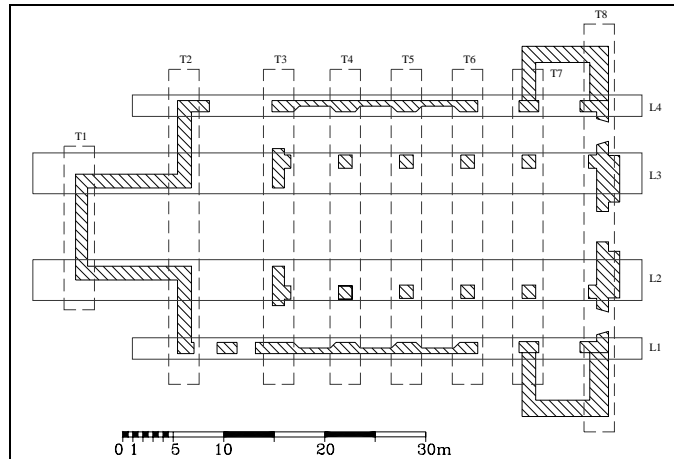


Figure 17. SI - Individuation of the macroelements in plan.

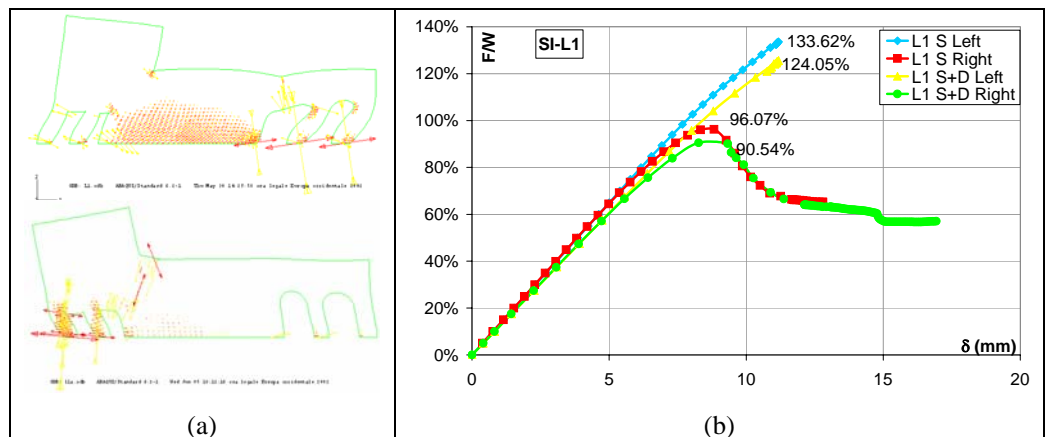


Figure 18. L1 macroelement – a) Plastic strain tensor; b) Force/Displacement curve.

The small incidence of the dead load compared to the self weight shows similar results for the modelling with and without the dead load. The collapse multipliers for forces coming from the left side are bigger than the values coming from the right side. This is clearly explained noticing that a severe damage will form in correspondence of the connection between the high panel and the remaining part of the element. All the analyses will stop in consequence of the crack openings.

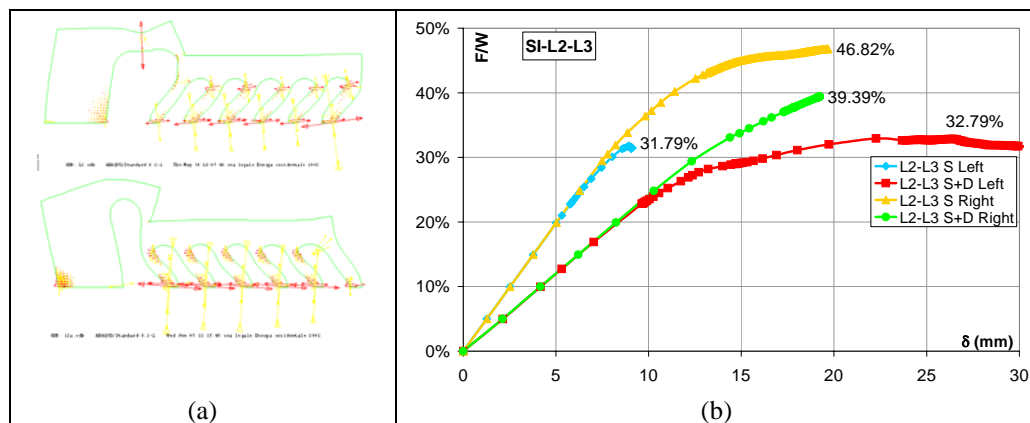


Figure 19. L2 & L3 macroelements – a) Plastic strain tensor; b) Force/Displacement curve.

In this macroelement the coupling of the two collapse mechanisms of storey in the right part and panel in the left part is shown. This particularity can be evidenced in the different strength values according to the verse of the seismic action. When forces are coming from the left side, there isn't enough contrast in the last pier such as when the forces are coming from the right side where a stocky panel can better absorb the actions. This is the reason why the values of the collapse multiplier are bigger for forces coming from the right side (independently from the load condition). The presence of the dead load influences, on the contrary, the horizontal stiffness of the panel as can be noticed in the plot. The plastic branch develops in almost all the four curves.

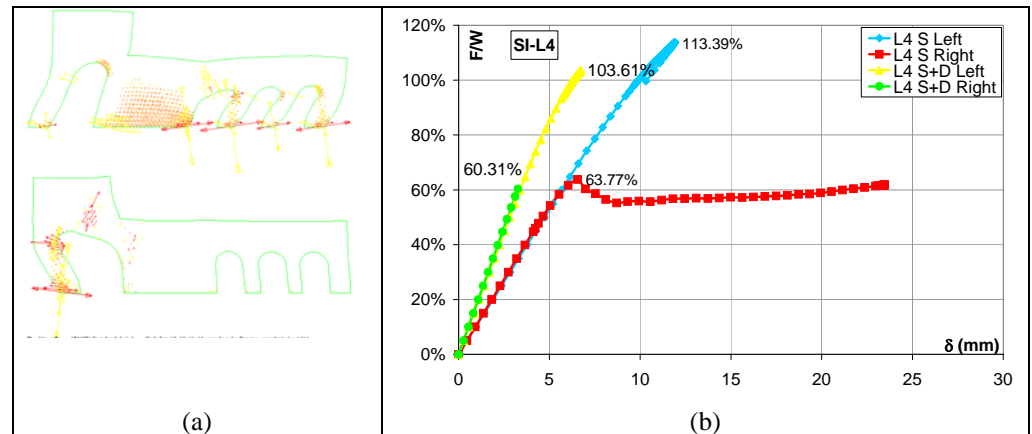


Figure 20. L4 macroelement – a) Plastic strain tensor; b) Force/Displacement curve.

This macroelement is characterized by the presence of three zones with different mechanical behaviour. The two external parts are close to the storey mechanism, while the central part is a stocky element. This configuration has an implication in the collapse multipliers: for forces coming from left a strength contribution is provided both from the central panel and the two external frames. When the forces are coming from right, the severe damage in correspondence of the beginning of the high panel on the left limits the value of the bearing capacity. This aspect reflects also in the horizontal stiffness which assumes different values according to the verse of the force independently from the load condition.

In Fig. 21, the apse of the church, lacking openings, shows the classical behaviour of the stocky panel. The typical stress concentration for compression in correspondence of the hypothetical rotation hinge and the cracks' opening in the opposite side is the cause of the collapse. The small ratio of the dead load over the self weight influences only in a small part the value of the collapse multiplier and not at all the value of the horizontal strength.

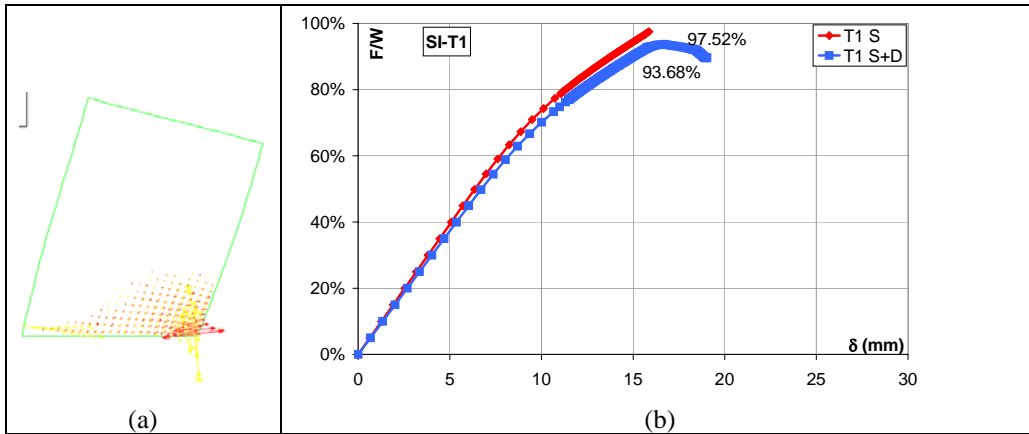


Figure 21. T1 macroelement – a) Plastic strain tensor; b) Force/Displacement curve.

In Fig. 22, for the triumphal arch the storey mechanism is assumed to form in the collapse process. The two piers show slender cantilever behaviour: at the base of the columns tension and compression stresses in the opposite sides are evident. Oddly, the model provided of self weight and dead loads has a strength value smaller than the model with the self weight only, but the stiffness is bigger than the other one.

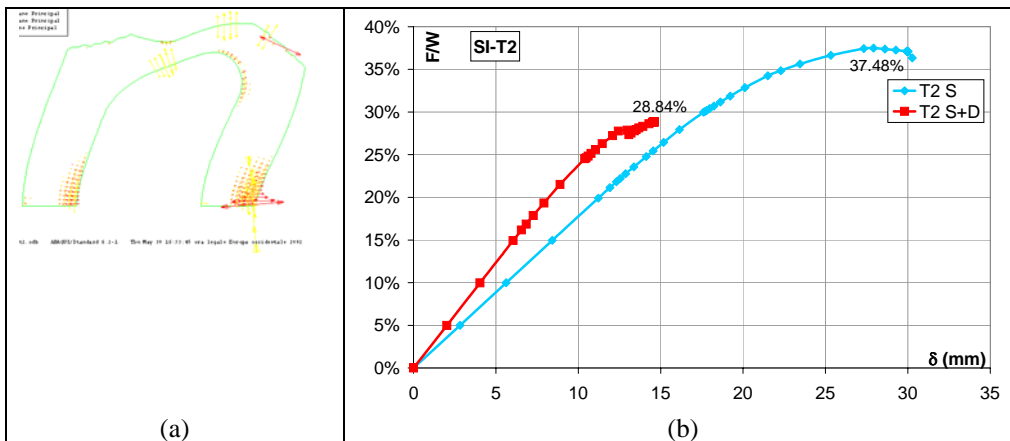


Figure 22. T2 macroelement – a) Plastic strain tensor; b) Force/Displacement curve.

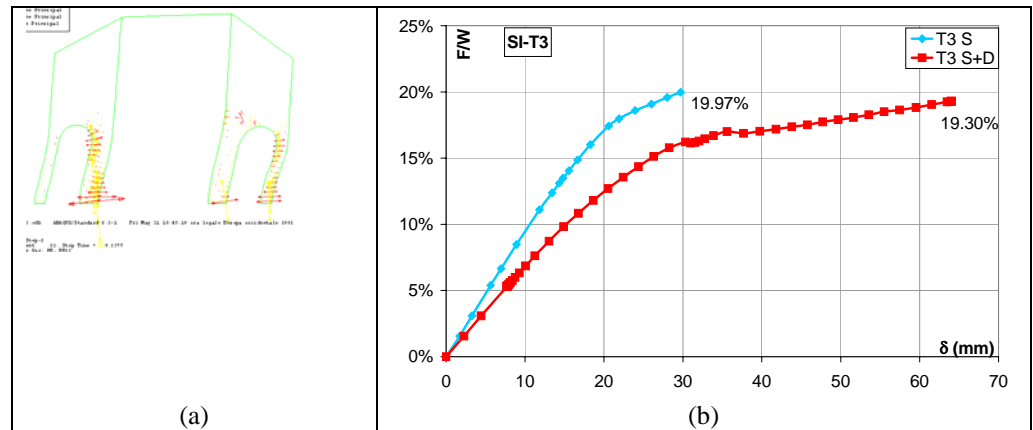


Figure 23. T3 macroelement – a) Plastic strain tensor; b) Force/Displacement curve.

The symmetry of the geometry and the loads lead to the tracing of only two curves (one with the self weight and another one with self weight and dead load). The macroelement is constituted of two coupled elements which present the classic storey mechanism for the presence of column elements in the inferior part and the beam element in the upper part. The conventional load-displacement curve shows a linear behaviour until the non linearity with displacements bigger than the loads reach the maximum strength. Although the dead loads are the almost the 15% of the self weight, the strength value are very close the different stiffness can be noticed.

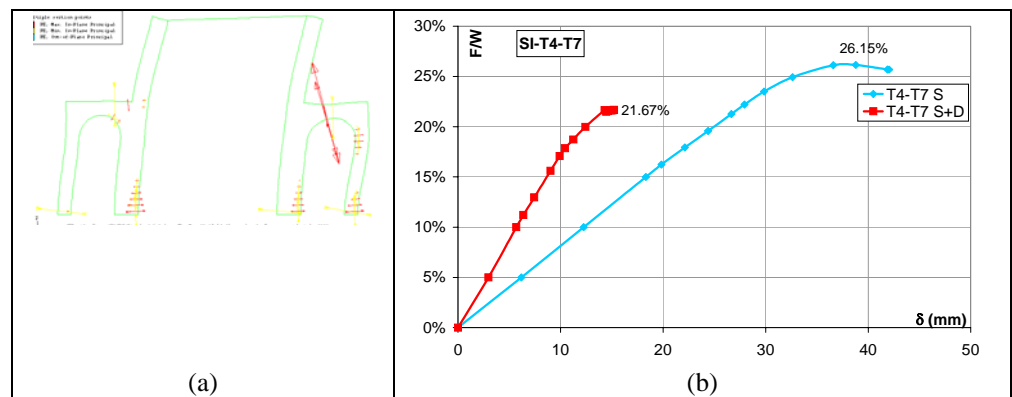


Figure 24. T4 – T5 – T6 – T7 macroelements – a) Plastic strain tensor; b) Force/Displacement curve.

Similarly to the previous macroelement, in Fig. 24 the repetitive elements along the development of the church have been assimilated to the storey mechanisms. Again, a greater stiffness and smaller bearing capacity are assumed by the model with the self weight and the dead load.

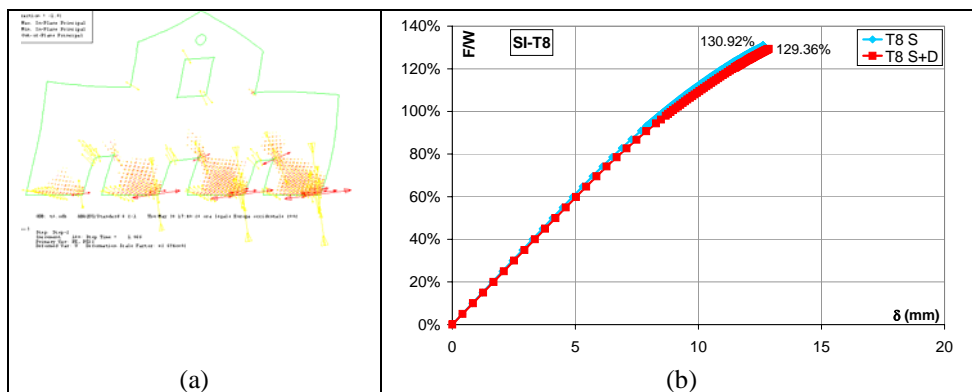


Figure 25. T8 macroelement – a) Plastic strain tensor; b) Force/Displacement curve.

Although in the panel some openings are present, the general behaviour of the element can be assumed as a stocky one. The course of openings at the base of the element defines some panels with a storey mechanism. Evident are the areas, close to the rotation corners where compression stresses are concentrated. A small plastic branch can be detected after the linear behaviour. The small amount of the dead load does not influence the horizontal stiffness and the bearing capacity of the panel.

#### 4.2.1. SUMMARY OF THE RESULTS IN SI

Again, the summarized values of the two analyses types are reported in Fig. 26.a and b. When the self weight and the dead load are considered, plastic branch and greater displacements are reached more easily. Again, the stockier elements have a greater stiffness than internal elements whose collapse is closer to the storey mechanism with a series of columns and a beam on the top.

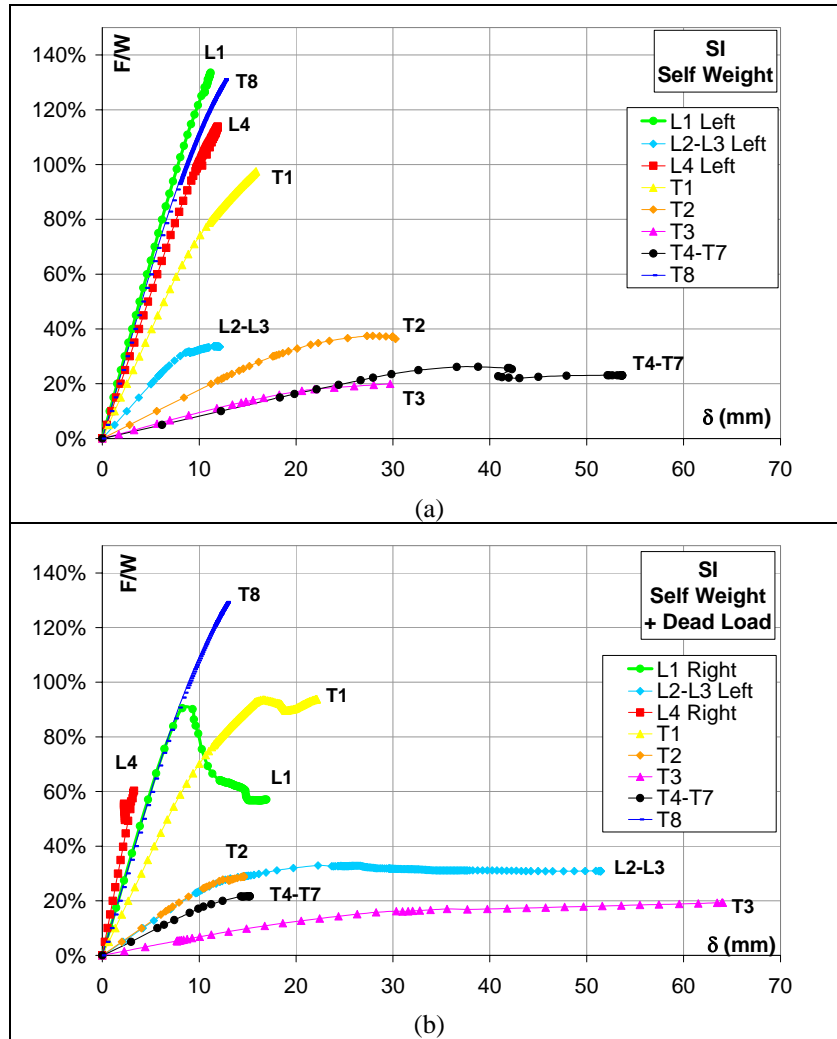


Figure 26. Summary of the curves in SI

#### 4.2.2. STRENGTH VS CAPACITY IN SI

In fig. 27 the comparison between strength and capacity is plotted. Again, the first two bars represent the strength in the two models (“as is” and with rigid slab) and the last two the capacity (minimum and maximum). For symmetrical elements only one bar is reported in terms of bearing capacity (being the seismic action equal in both

the directions). The seismic vulnerability of the internal elements compared to the external ones can be noticed as well.

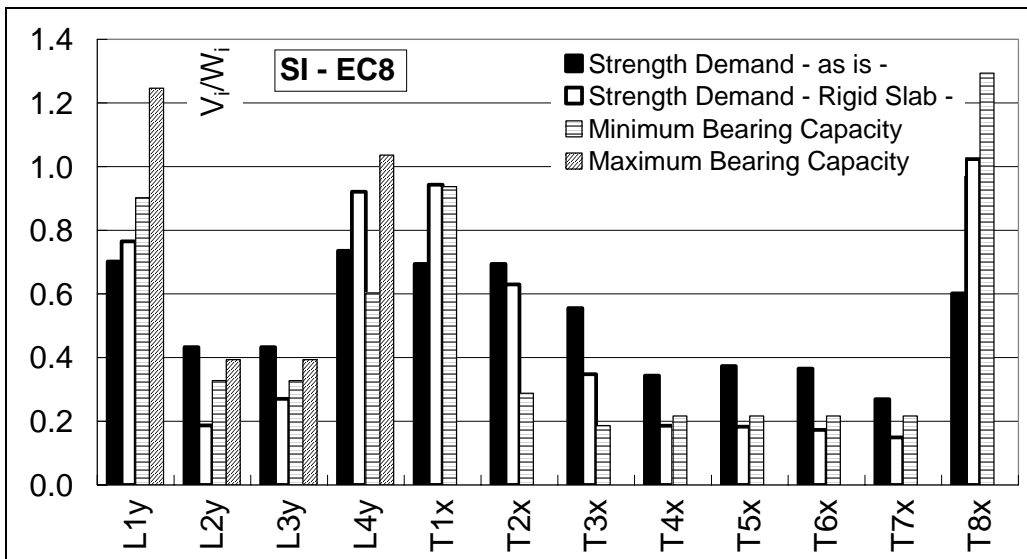


Figure 27. Strength against capacity in SI



### 4.3. S. GIOVANNI MAGGIORE

The macroelements of this church are visualized in the plan of Fig. 28 and are analyzed into detail from Fig. 29 to Fig. 36.

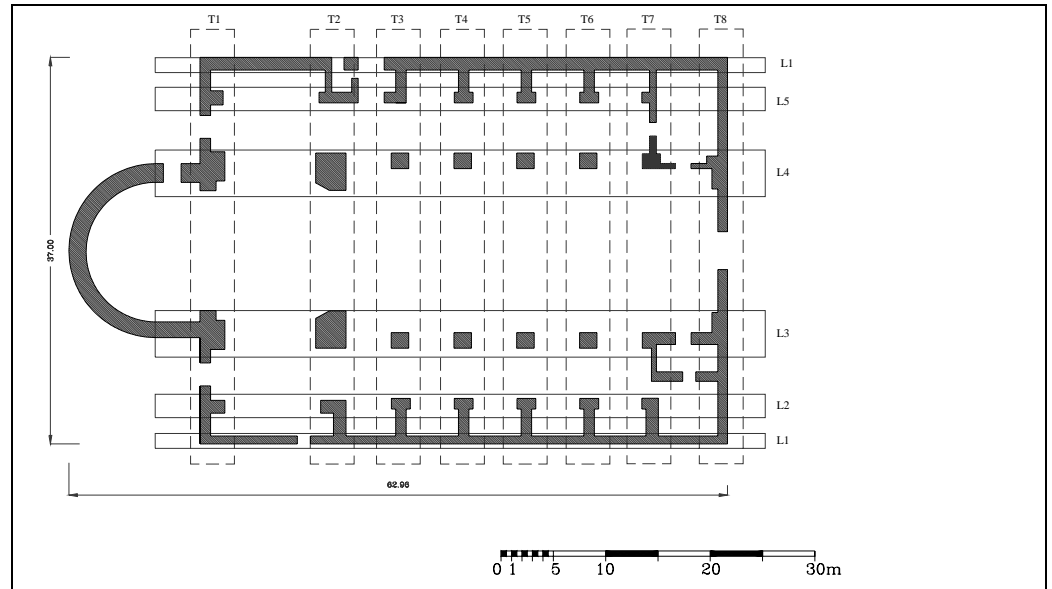


Figure 28. SGMG - Individuation of the macroelements in plan.

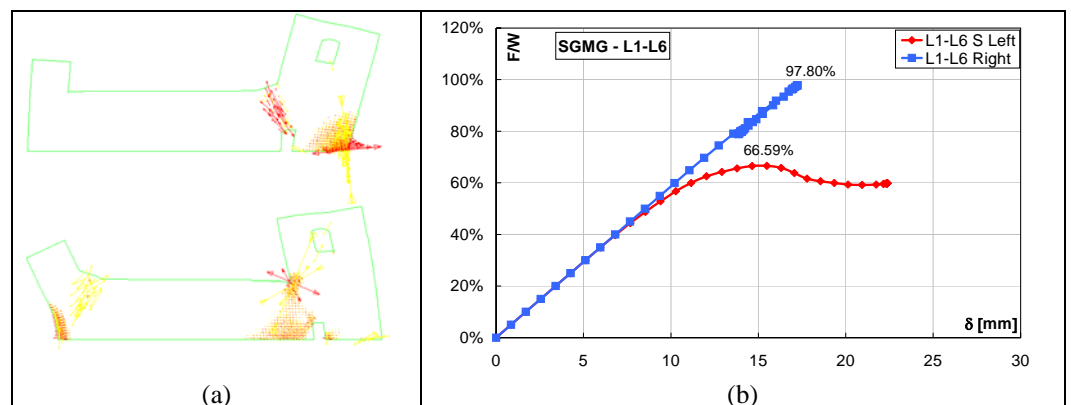


Figure 29. L1 & L6 macroelements – a) Plastic strain tensor; b) Force/Displacement curve.

From the observation of the deformed shape three different areas with different behaviour can be individuated. In particular, the two external panels are characterized by the typical rocking mechanism with the concentration of compression stresses in correspondence of a corner and tension stresses in the opposite one. The central panel, with a lengthened shape, will have the tendency to collapse due to shear. The dead load condition has been neglected due to very small value. When forces are coming from the left side, the damage in correspondence of the development of the high panel on the right can be detected. Again, when the horizontal forces are coming from the right verse, a crack will form at the beginning of the other high panel. Therefore, when forces are coming from whenever verse, the opening of a crack will be noticed in the opposite part; once the high panel on the right and once on the left, characterized by different dimensions and so different strengths will cause the collapse. For this reason, the collapse multiplier with forces coming from the left verse is smaller than with forces in the opposite verse. The horizontal stiffness is the same in both the directions.

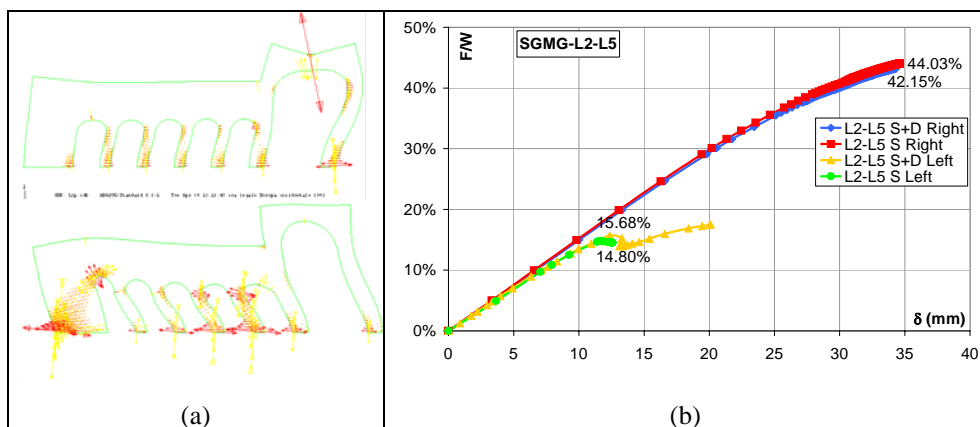


Figure 30. L2 & L5 macroelement – a) Plastic strain tensor; b) Force/Displacement curve.

This macroelement assumes the classic behaviour of a frame with the formation of hinges at the base of the pillars with tension and compression areas in the opposite

sides. Independently from the load condition, for seismic action coming from the left side, the strength factors are smaller than the other ones coming from the right side because of the lacking of an opposition of some structural elements at the end of the slender right column and the crack opening between the high and the low part. This phenomenon does not occur with forces in the other direction where the horizontal thrust is better absorbed by the left side. The stopped analysis is due to the cracks opening at the top of the biggest pier or at the base of smaller piers. The small amount of the dead load compared to the self weight does not influence the values of the collapse multiplier and the horizontal stiffness.

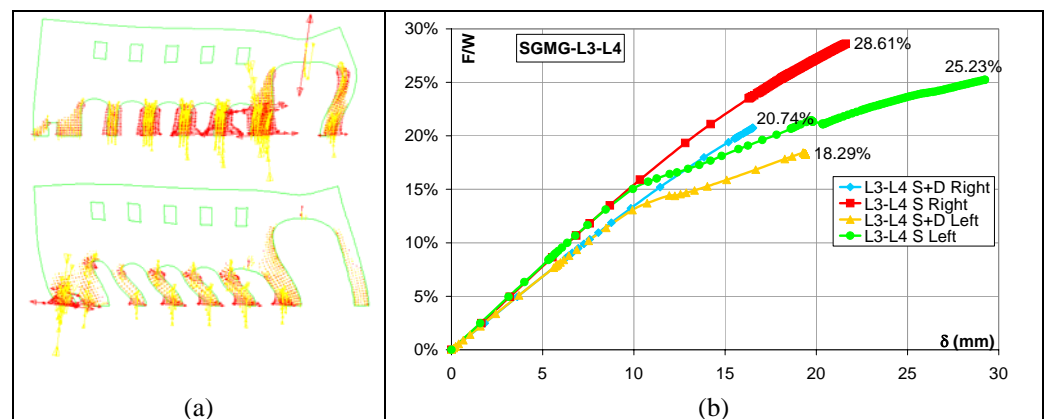


Figure 31. L3 & L4 macroelement – a) Plastic strain tensor; b) Force/Displacement curve.

This macroelement has the same behaviour of the former one, but in the right part of the panel there is the presence of some external walls. For this reason, although the storey mechanism is the same, there is less discrepancy in the strength values. The opening of a crack in the corner between the high and the low part can not occur anymore and the analysis stops due to the cracks opening at the top of the biggest pier or at the base of smaller piers. The 11% of the dead load compared to the self weight influences significantly the values of the collapse multiplier and the stiffness.

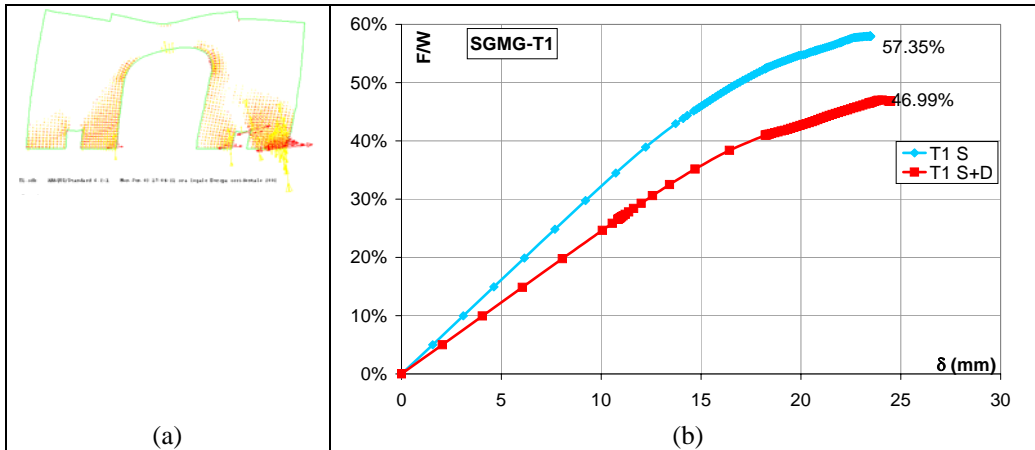


Figure 32. T1 macroelement – a); b) Force/Displacement curve.

Although some small openings are present at the base of the element, the macroelement is constituted of two big lateral panels joined through the arch. Therefore, the rocking collapse mechanism can be observed. The symmetry of the geometry and loads has implied only two analyses. The 17% of the dead load over the self weight has involved, in the analysis with the self weight plus the dead load, a smaller value of the collapse multiplier and of horizontal stiffness.

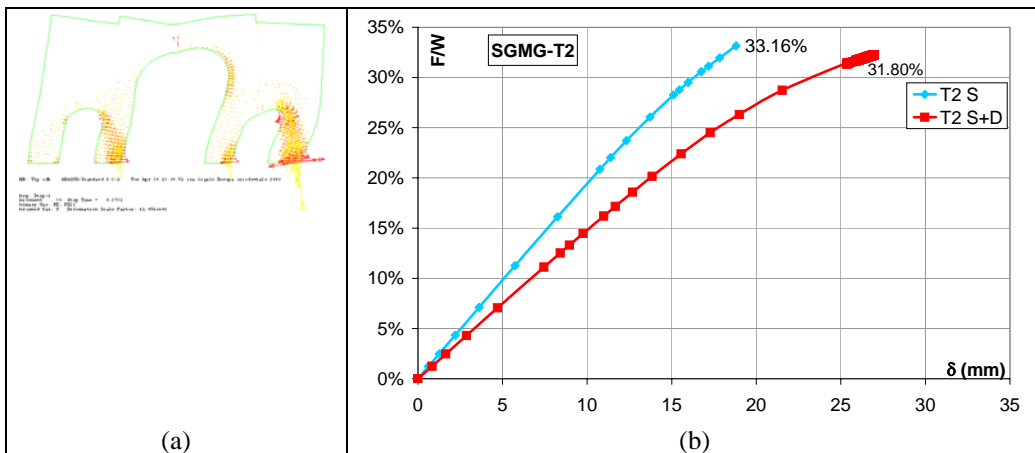


Figure 33. T2 macroelement – a) Plastic strain tensor; b) Force/Displacement curve.

Unlike the previous macroelement, this panel has got two big openings on the sides so that in the deformed shape a transversal beam and some longitudinal piers can be individuated. Therefore, the panel collapse can be assimilated to a storey mechanism where the dead loads influence the stiffness and the strength. The two curves are close to the beginning of the plastic branch so that the values are fairly close to the maximum capacity of the element.

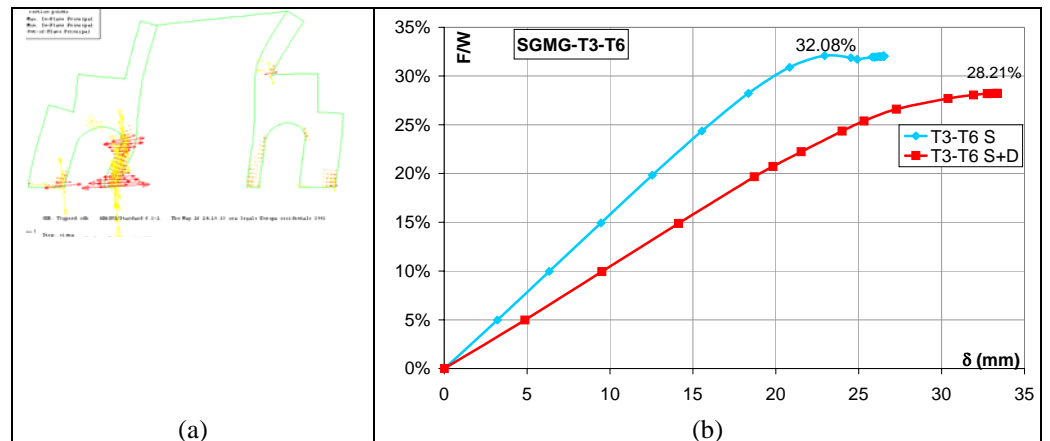


Figure 34. T3 – T4 – T5 – T6 macroelements – a) Plastic strain tensor; b) Force/Displacement curve.

From the study of the deformed shape, hybrid behaviour between the storey mechanism (for the presence of some columns) and the rocking mechanism (for the two external cantilevers bigger than the internal pillars) can be detected. Again, stiffness and strength are penalized in the model with the addition of dead loads to the self weight.

In Fig. 35 the macroelement presents the typical mechanism of partial rocking of the upper part of the panel. The plastic hinge formation at the base of the upper piers is detected. The ratio of the dead loads over the self weight of 24% reflects significantly on the horizontal stiffness and the collapse value.

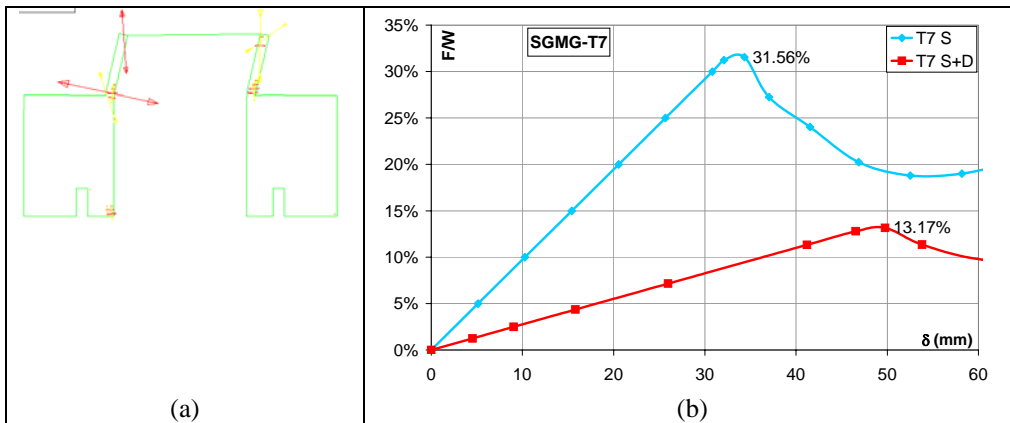


Figure 35. T7 macroelement – a) Plastic strain tensor; b) Force/Displacement curve.

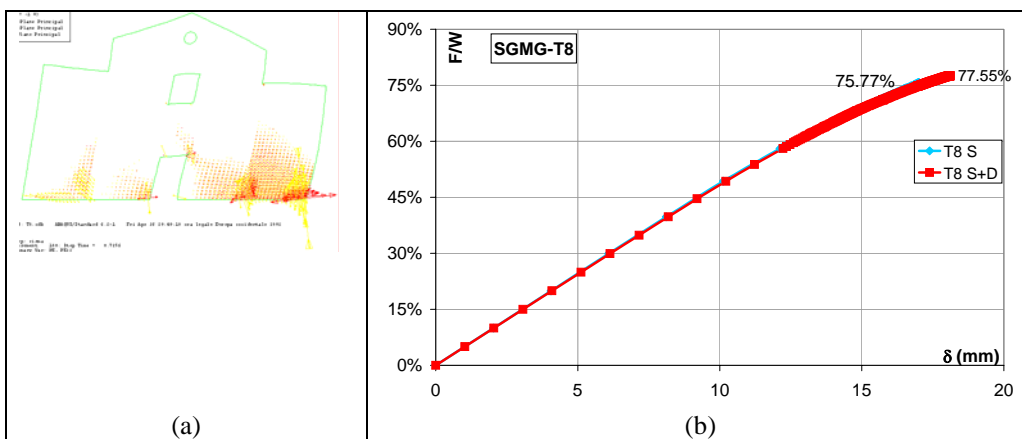


Figure 36. T8 macroelement – a) Plastic strain tensor; b) Force/Displacement curve.

The macroelement is the assemblage of three stocky blocks with different thickness: the non linear analysis evidences that at each right corner the rotation centre of the compression forces occur. The small amount of overload doesn't influence the models with the dead load and the two curves tend to the horizontal branch.

### 4.3.1. SUMMARY OF THE RESULTS IN SGMG

In Figure 37 the comparison of all the collapse values with and without dead load condition is reported. Generally, it can be noticed a decrease of the stiffness in the

models provided of the dead load. Inside the same diagrams, more stocky are the elements stiffer is the response.

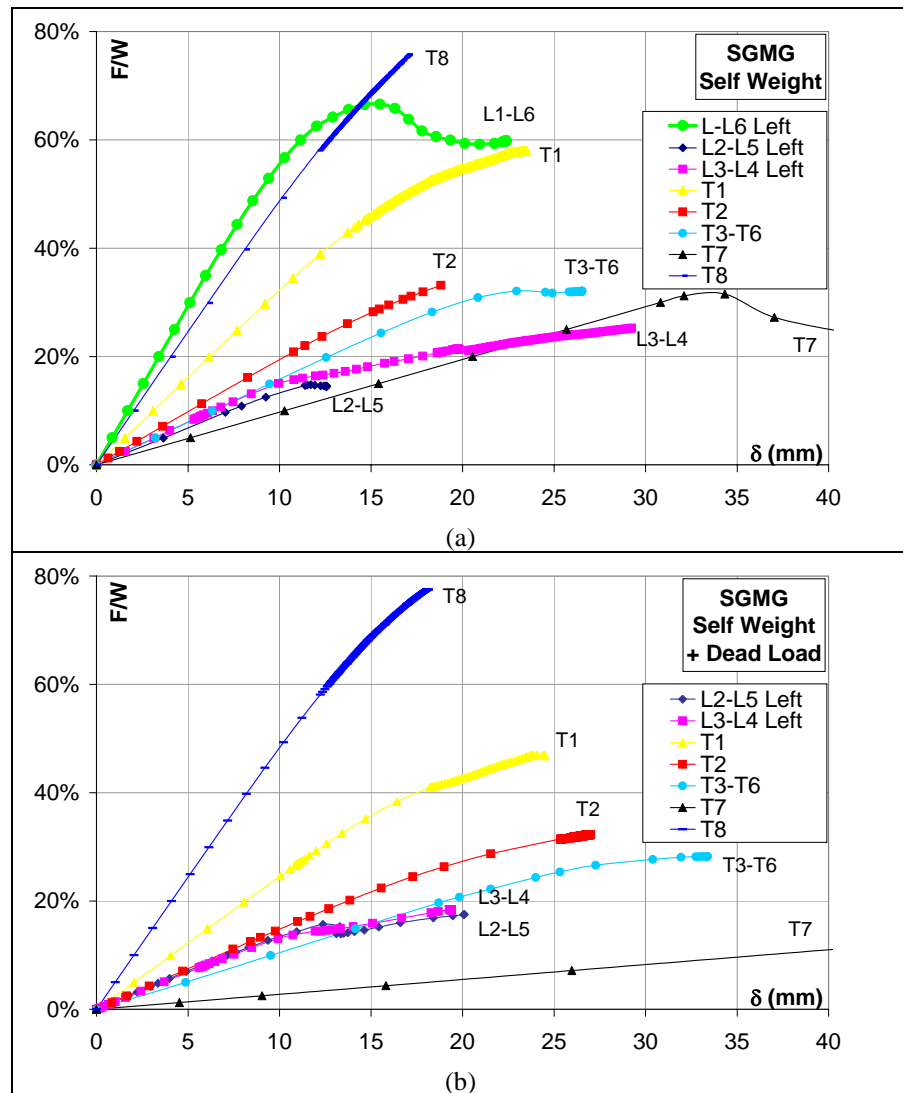


Figure 37. Summary of the curves in SGMG.

4.3.2. STRENGTH VS CAPACITY IN SGMG

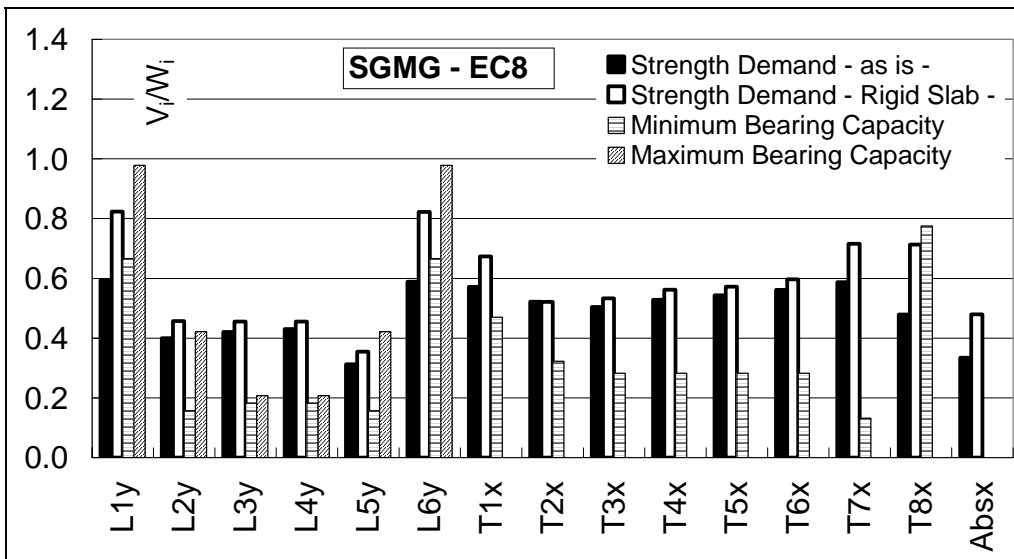


Figure 38. Strength against capacity in SGMG.

As in the previous study cases, the comparison between strength and demand is plotted in Fig. 38. Of course, the crisis points are individuated in the internal elements as already pointed out previously.



#### 4.1. S. PAOLO MAGGIORE

For the SP basilica the macroelement are indicated in Fig. 39. In Fig. 40 to Fig. 49 the detailed analysis of each macroelement is reported.

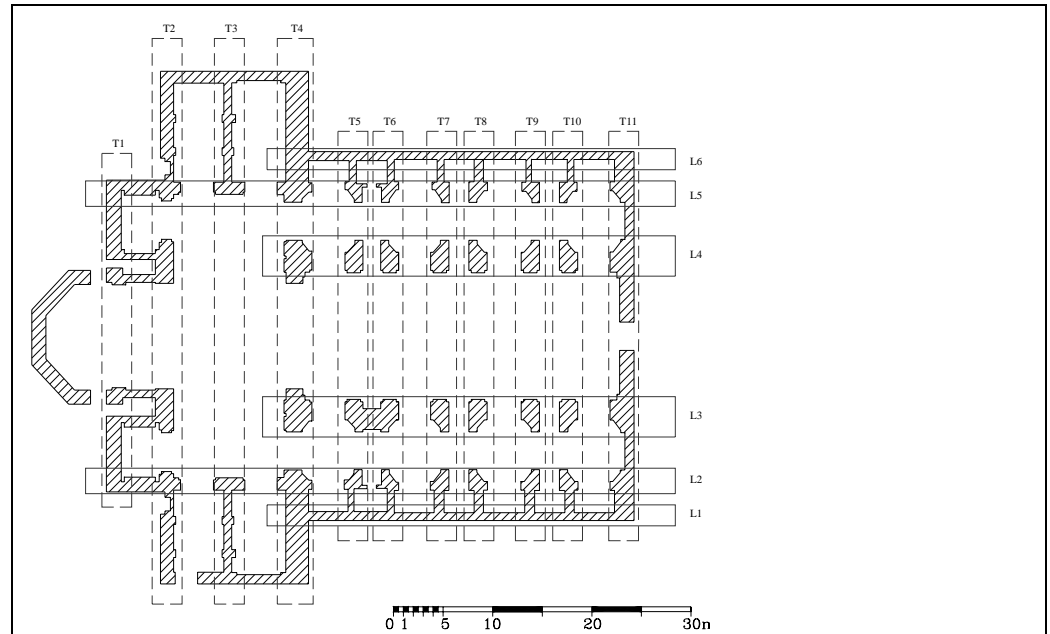


Figure 39: SP - individuation of the macroelements in plan.

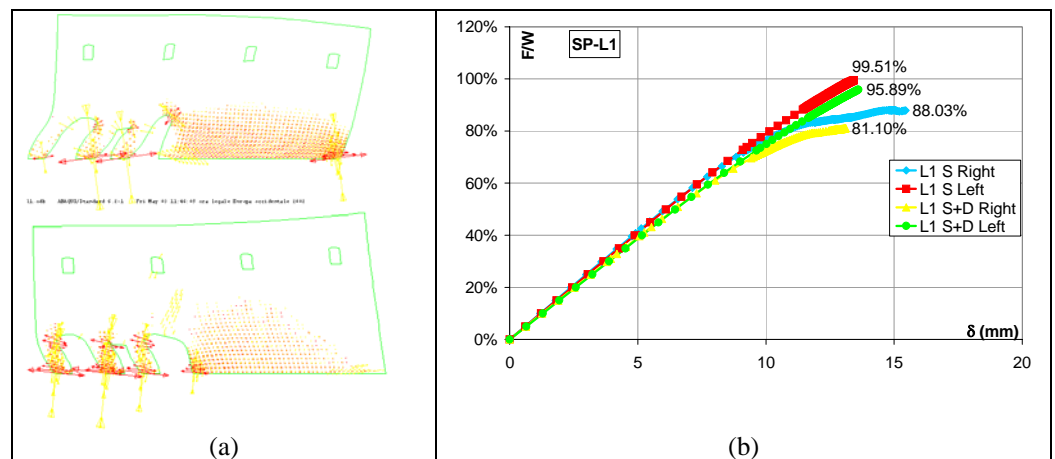


Figure 40: L1 macroelement – a) Plastic strain tensor; b) Force/Displacement curve.

The macroelement can be divided into two zones with different behaviour. The right part is a stocky panel with a stress concentration in correspondence of the corners when subjected to lateral loads; the left part, dominated by the presence of some openings, defines slender cantilever behaviour in the arch columns with zones of tension and compression in opposite parts. When horizontal forces are coming from the right verse, the collapse multipliers are smaller than in the other verse. The small percentage of the dead load slightly influences the strength values and not at all the stiffness.

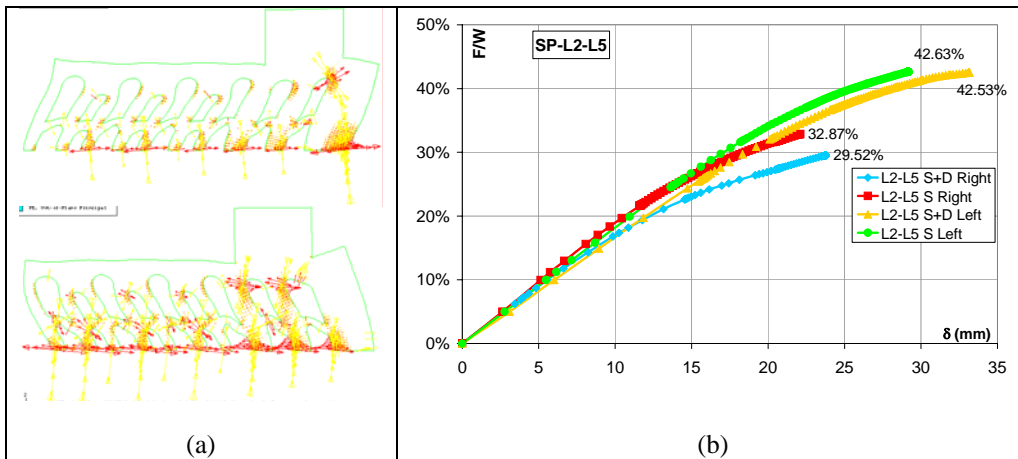


Figure 41. L2 – L5 macroelements – a) Plastic strain tensor; b) Force/Displacement curve.

From the observation of the deformed shape, the main collapse mechanism of this element is a storey mechanism, even if there is a stocky cantilever in the right part. The left part, characterized by the sequence of two levels of arches, constitutes a frame in which pillars and beams can be distinguished. For the first ones, in particular, slender cantilever behaviour can be detected. The analyses stop before when horizontal forces come from the right side where the last arches on the left are not contrasted like the arches on the right. The horizontal stiffness is almost the same, whilst smaller collapse values are reached when the dead load is considered.

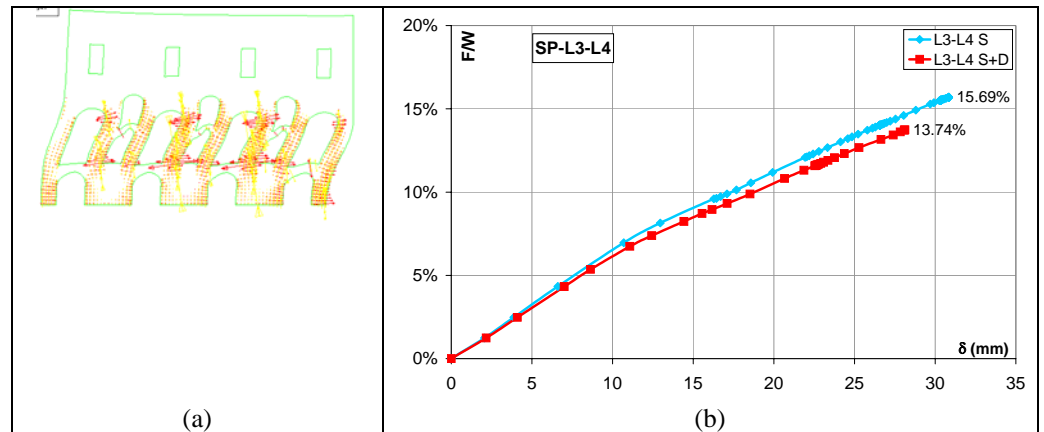


Figure 42. L3 – L4 macroelements – a) Plastic strain tensor; b) Force/Displacement curve.

The deformed shape of this macroelement clearly shows the typical storey collapse mechanism. Indeed, for the particular geometric configuration, masonry frame can be defined. The translation mechanism of the superior beam and the rotation of the inferior piers are clearly evidenced. The small amount of dead load slightly influence the strength value even if in both the cases the horizontal branch is not reached.

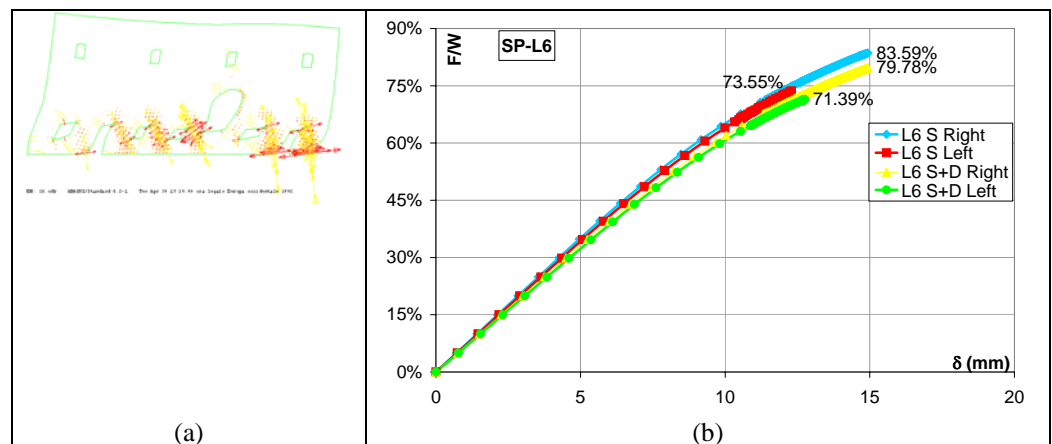


Figure 43. L6 macroelement – a) Plastic strain tensor; b) Force/Displacement curve.

Although some openings are present in the macroelement, because of their small dimensions, the whole panel can be considered stocky. In other words, the panel acts like a unique element subjected to horizontal forces. Nevertheless, in both the directions, plastic concentrations in the areas close to the corners of the openings can be noticed. As a confirmation, symmetric behaviour of the element in terms of stiffness and smaller values of the collapse when forces are coming from the left side can be noticed.

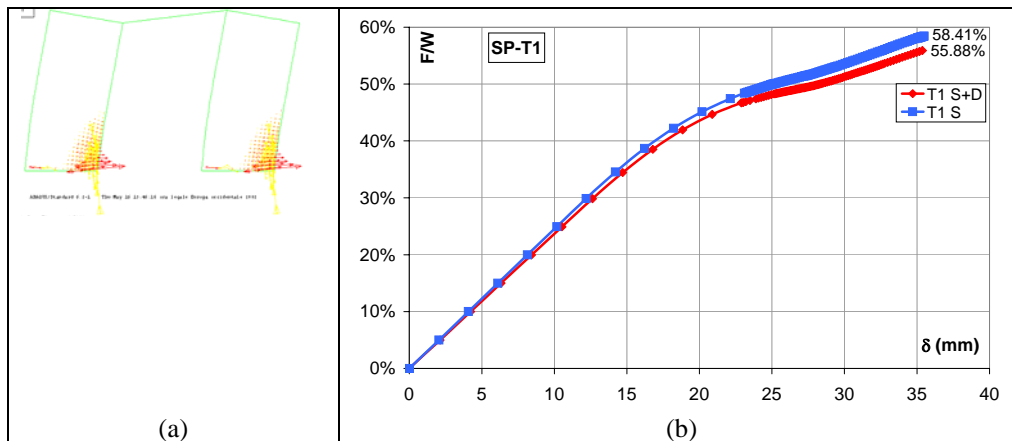


Figure 44. T1 macroelement – a) Plastic strain tensor; b) Force/Displacement curve.

This macroelement is formed by two panels completely lacking openings. The mechanism could be rocking with stress concentration on the corners at the base of the elements. The two non linear curves, although reaching the non linear field, do not seem to have reached the full developed capacity.

In Fig. 45 the macroelement, as confirmed by the deformed shape presents a collapse mechanism given by the combination of a storey mechanism in the central part and the rocking of the two rigid panels formed by the two lateral walls. Because of the geometrical and load condition symmetries of the element, only two analyses have been performed with and without the dead load. A decrease in terms of collapse

value and horizontal stiffness can be noticed in the model with self weight and dead load. In both the analyses, the plastic branch is fairly reached.

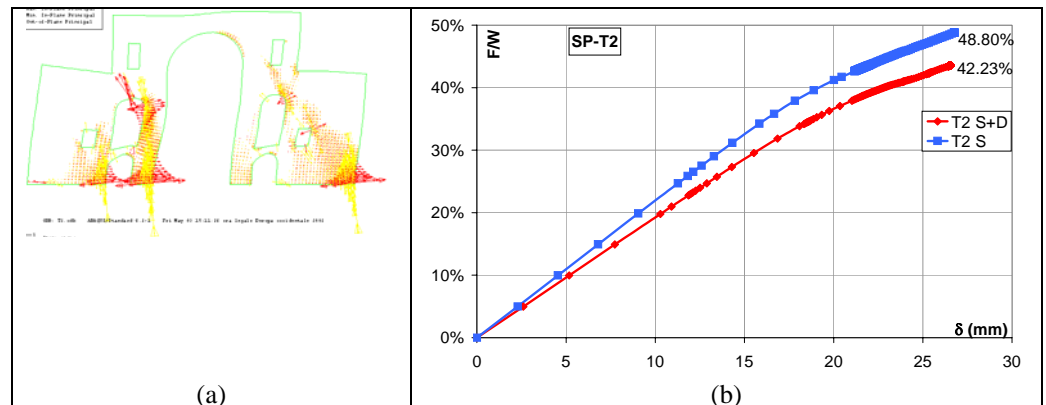


Figure 45. T2 macroelement – a) Plastic strain tensor; b) Force/Displacement curve.

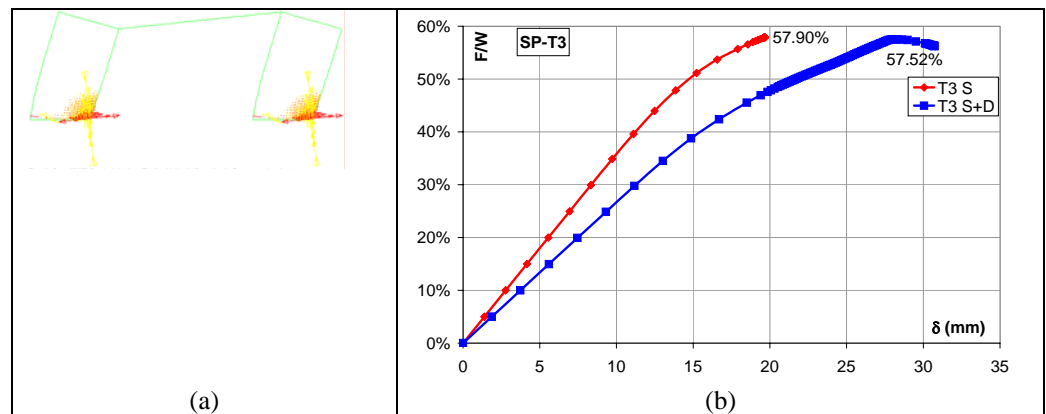


Figure 46. T3 macroelement – a) Plastic strain tensor; b) Force/Displacement curve.

This macroelement is constituted of two lacking openings elements, whose typical failure is by rocking. A stress concentration in the hypothetical hinge locations can be noticed in the plastic strain tensor so that the analysis stops for the cracks opening in the opposite side. Again, a decrease in horizontal stiffness and collapse value is shown in the model including the self weight and the dead load.

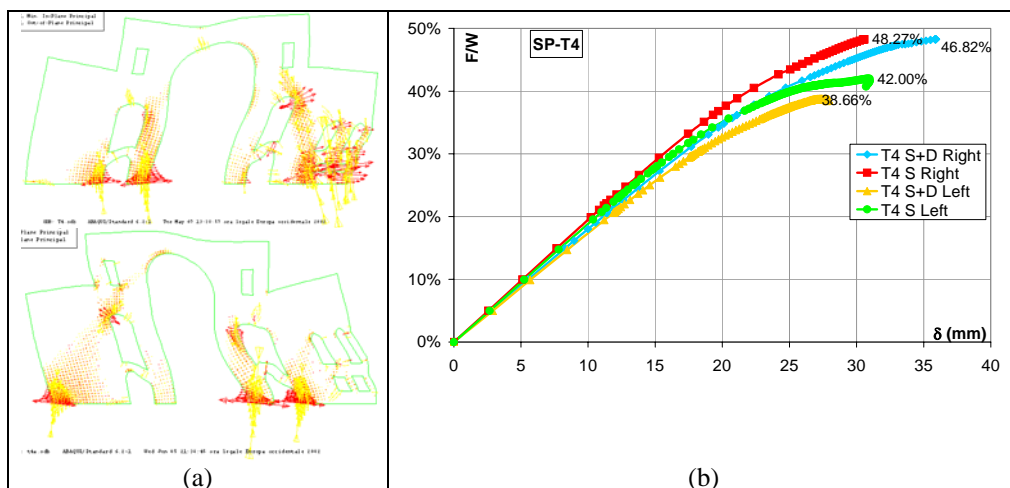


Figure 47. T4 macroelement – a) Plastic strain tensor; b) Force/Displacement curve.

Because of the presence of some openings on the right side of the element, the structure is not symmetric anymore like the T2 macroelement. This is the reason why, on the right side a storey mechanism will develop and on the left side the panel behaviour still occurs. This asymmetry can be seen through the curves as well. Independently from the load condition (presence or not of the dead load), the models with forces acting from the left side can bear less seismic load. On the contrary, analyzing the models in function of the load conditions, the horizontal stiffness is the same in the four analyses, while the collapse values vary according to the presence of the dead load.

In Fig. 48, for these transversal macroelements, hybrid behaviour can be noticed for the presence of the inner columns and the external cantilevers wider than the previous ones. For this reason in the slender elements tension and compression zones forming in the opposite sides occur before the rocking of the two stocky elements. The geometrical and load condition allow the performing of two analyses with different horizontal stiffness and failure values.

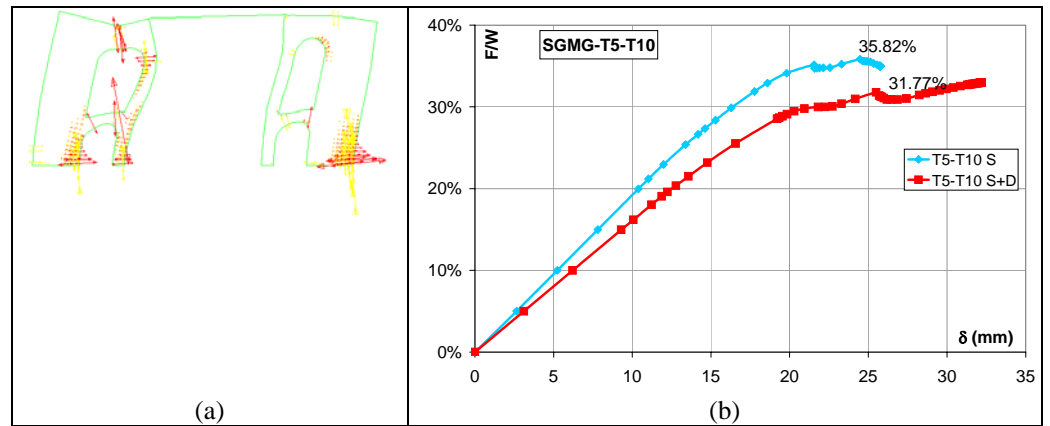


Figure 48. T5 – T6 – T7 – T8 – T9 – T10 macroelement – a) Plastic strain tensor; b) Force/Displacement curve.

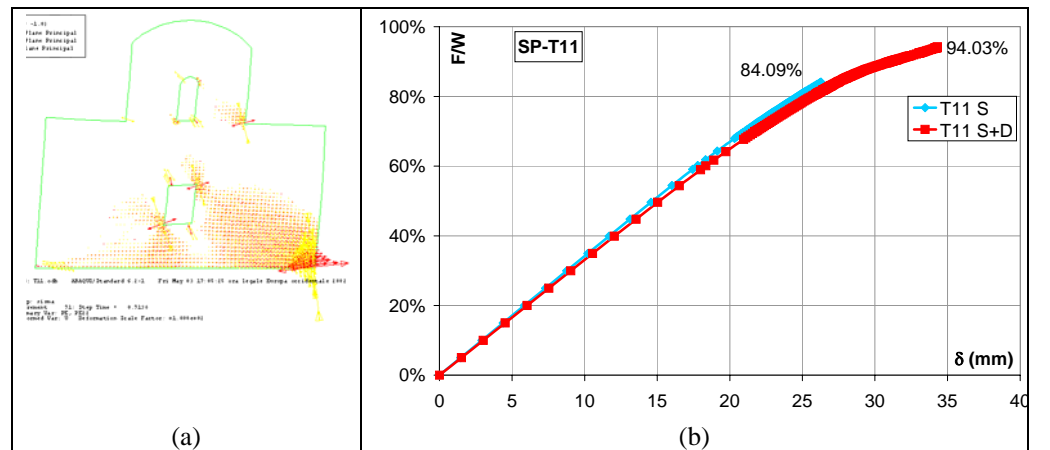


Figure 49. T11 macroelement – a) Plastic strain tensor; b) Force/Displacement curve.

Because of the small presence of openings, the behaviour of this macroelement is monolithic. The formation of a hinge rotation around the corner at the bottom can be clearly noticed in the plot. Same stiffness but different collapse values are obtained from the analyses. Strangely, the value of the model with self weight plus the dead load is bigger than the one of the model only with the self weight.

4.4.1. SUMMARY OF THE RESULTS IN SP

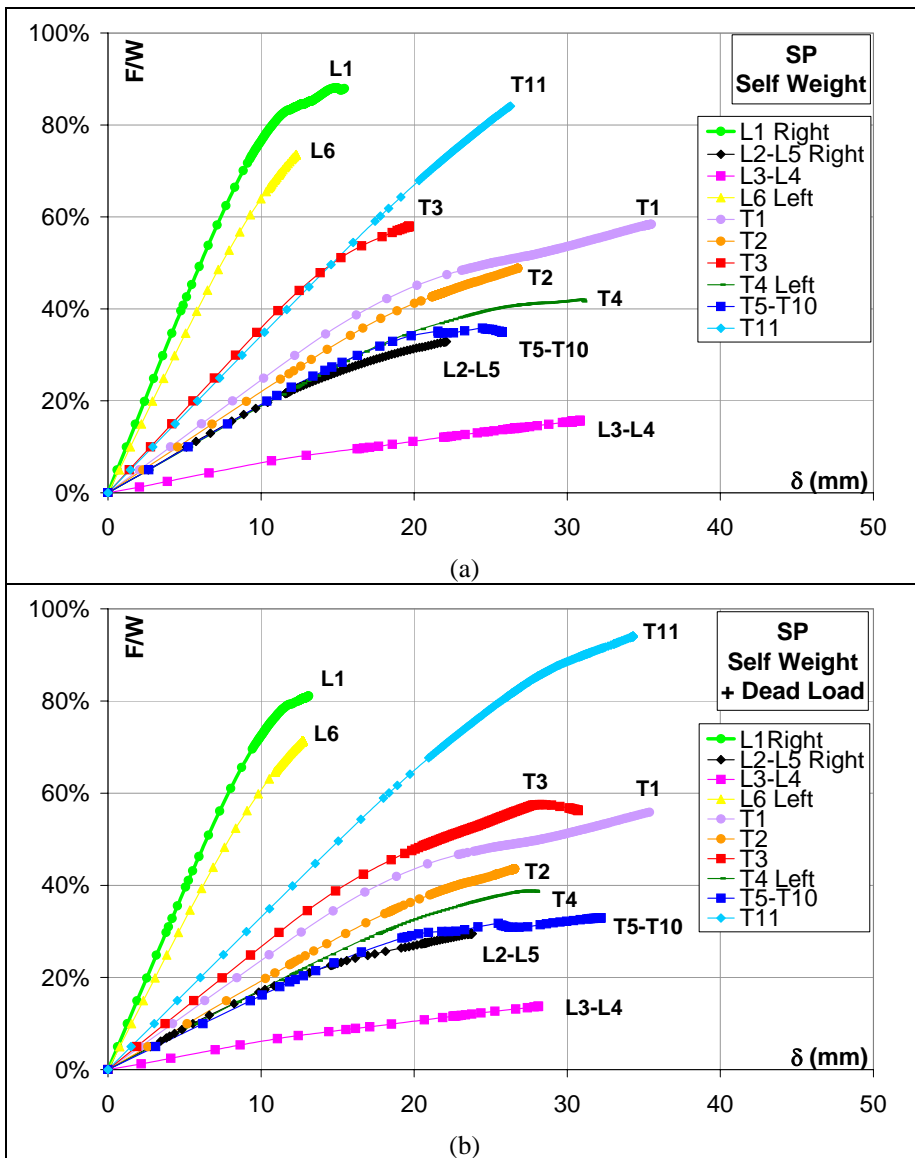


Figure 50. Summary of the macroelements in SP.

The summary of the curves of all the macroelements are reported in Fig. 49. As also derived in the previous cases, the external elements are the stiffest and able to bear



the largest amount of horizontal forces before the collapse. The internal arcades, on the contrary, are the least stiff and with the smallest value of bearing capacity.

#### 4.4.2. STRENGTH VS CAPACITY IN SP

Finally, in Fig. 51 strength demand against capacity is reported. The conclusions made for the first three study cases are still valid in this church with some exceptions in the first transversal elements.

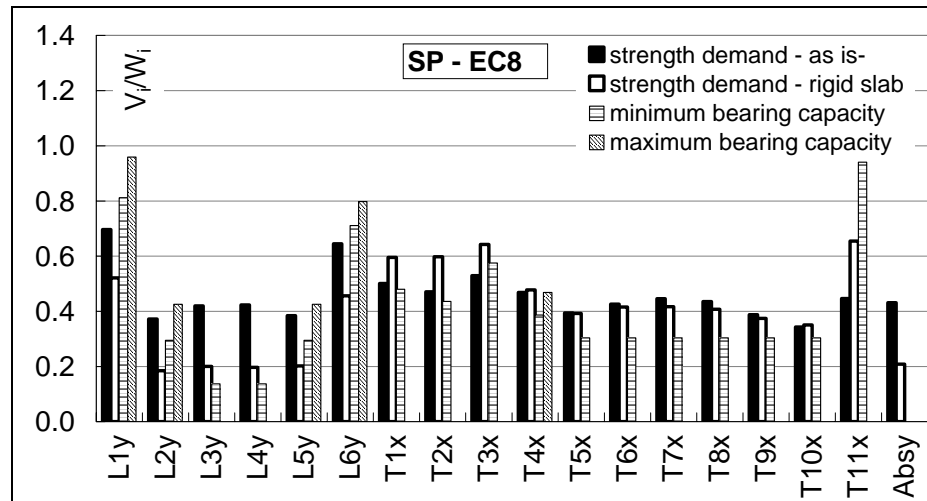


Figure 51. Strength against capacity in SP.

## 5. CONCLUSIONS

In this chapter non linear analyses on bi-dimensional elements have been performed. Such analyses are aimed at determining the collapse behaviour of the structural elements, and in particular the ultimate load bearing capacity. It can be argued that a direct evaluation of the ultimate condition at collapse is useful since the definition of the seismic forces for masonry structures according to different code provisions is not unique, as stated in §1.

The study cases have been analyzed adopting a smeared cracking approach as implemented in the computer code ABAQUS. The use of such a constitutive model has firstly required a curve-fitting procedure based on experimental tests for the choice of some parameters defining the material properties.

Load-displacement curves, indicating the initial stiffness and the trend of the displacements of some points on the structure chosen as control points have been plotted. A full developed curve will have the first part in the linear field and the second part in the non linear one until the achievement of the plastic line leading to the vertical collapse of the element. The results will not be unique if the element is not symmetrical (so that two curves will represent the different response of the structure according to the verse of the seismic action) and if some dead loads are applied on it (so that one curve will be representative of the behaviour of the macroelement only for its shape and the other one will take into account the influence of the dead load). In safety terms, under the same load condition, the curve with the smaller value of the collapse multiplier should be the governing one.

When the trend is quasi-linear and the analyses are stopped early due to numerical instability or slow rate of convergence, some issues arise about the reliability of the computed collapse multiplier value. In fact, it can be argued that the numerical algorithm may not be able of following the actual equilibrium path towards a further branch, so that the collapse multiplier may be larger to some extent. Besides, in case of stocky elements, failure may occur as a result of mechanisms that can not be simulated with such constitutive theory and homogenized approach. For example, sliding at joint level introduce such an anisotropy that can not be taken into account using smeared cracking approach.

For each study case, all curves are plotted together for comparison purposes.

Finally, the comparison between strength demand (from linear analyses) and bearing capacity (from non linear analyses) has been reported. It can be noticed that, generally, the bearing capacity of these elements is smaller than the strength demand.

Therefore these constructions are prone to damage and effective retrofit techniques are necessary.

In the light of the analyses conducted on these complex constructions it can be said that is quite hard following a unique procedure able to define with consistency the most influencing quantities. Undoubtedly churches are more sensitive to damages than other structures for the reasons illustrated in the previous chapters, but at the same time the necessity of defining a handy and suitable methodology for designers is strongly felt.



## CHAPTER 5: *THE MASONRY PORTAL FRAME*

### 1. INTRODUCTION

Masonry portals, made of two vertical elements and a rectilinear horizontal element, are very often found in any masonry structures (Fig.1) and can be considered as the basic structural element in historical multistory buildings; further, more complex structural elements of masonry constructions, such as churches, can be geometrically simplified and reduced to portal frames [De Luca A. et Al., 2004].

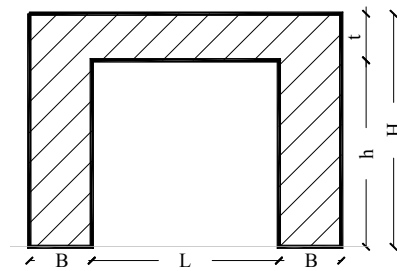


Figure 1. Geometry and loads of a masonry portal.

By adopting the same hypotheses made by [Heyman J., 1966], limit analysis is applied for determining the collapse multiplier of an horizontal concentrated force in presence of self weight loads; on account of the additional hypothesis that crack hinges can only occur at the piers-to-spandrel connections, different possible mechanisms are identified and the corresponding horizontal collapse load evaluated. Eventually, as a result of a wide parametric analysis performed using the derived exact expressions, a simple approximated formula for computing the collapse multiplier is proposed.

Some other authors have analyzed structures with one degree of freedom: in [Sinopoli A., 1985] arches and portals are evaluated in terms of equilibrium quality, safety assessment, analysis of free dynamic, impulsive phenomena and following action modes; [Como et Al., 1983;] dealt with portal frames through limit analysis approach. In particular the last work is reviewed and discussed enlightening the differences, since the results presented by the cited authors are obtained for portal outfitted with reinforcing ties in the spandrel and under slightly different assumptions about the mechanisms shapes.

## 2. A LIMIT ANALYSIS APPLICATION

In this chapter, a fully geometrical formulation for the evaluation of horizontal collapse load is proposed. Direct geometrical approach, indeed, can be easy to use and the procedure fast to implement.

Within the framework of the limit analysis, collapse multiplier of the distribution given in Figure 2 for a single rocking panel is derived through trivial equilibrium equation:

$$\frac{F}{W} = \frac{B}{2 \cdot H} \quad (1)$$

where  $F$  is the applied force,  $W$  the total weight,  $B$  the width and  $H$  the height of the masonry panel.

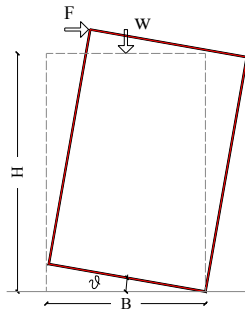


Figure 2. Rocking of the panel.

For portal frames an analogy can be observed with the single panel rocking behaviour if the possible mechanisms are sketched. Four mechanism classes are chosen, in the following regarded as I mechanism (*frame mech.*), II and III mechanism (*mixed mech.*) and IV mechanism (*storey mech.*) as represented in Fig. 3.

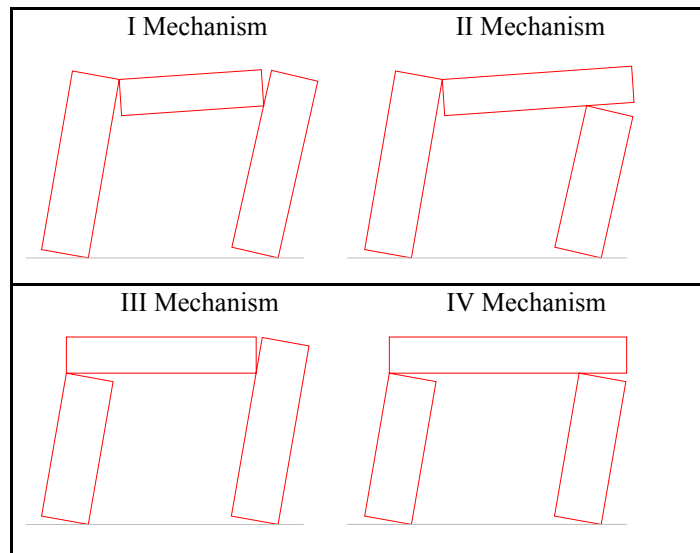


Figure 3. Masonry portal – collapse mechanisms.

Each mechanism features 4 hinges that give the structure a single lagrangian degree of freedom. Once the kinematic chain has been drawn, the principle of virtual

works can be applied to each mechanism, stating an equilibrium equation which gives the load multiplier  $F/W_{tot}$ . The minimum of the four multipliers is assumed to be the collapse multiplier for the portal  $F/W_{tot,real}$ .

The approach adopted clearly turns out to be a straightforward application of the kinematic theorem, which can be here synthetically expressed as follows:

*“If a collapse mechanism can be found such that the equilibrium condition (through the principle of virtual works) is satisfied, then the mechanism is kinematically sufficient and the corresponding load system is greater than or equal to the true collapse load”.*

### 3. EXPRESSIONS FOR KINEMATIC MULTIPLIERS

On account of the hypotheses of limit analysis and within the chosen set of collapse mechanisms, expressions for the evaluation of the horizontal collapse load are here provided as function of the geometry alone.

#### 3.1. MECHANISM I (FRAME MECHANISM)

Figure 4.a shows geometrical configuration and loads of the portal, while in figure 4.b the kinematic chain of the mechanism is represented:

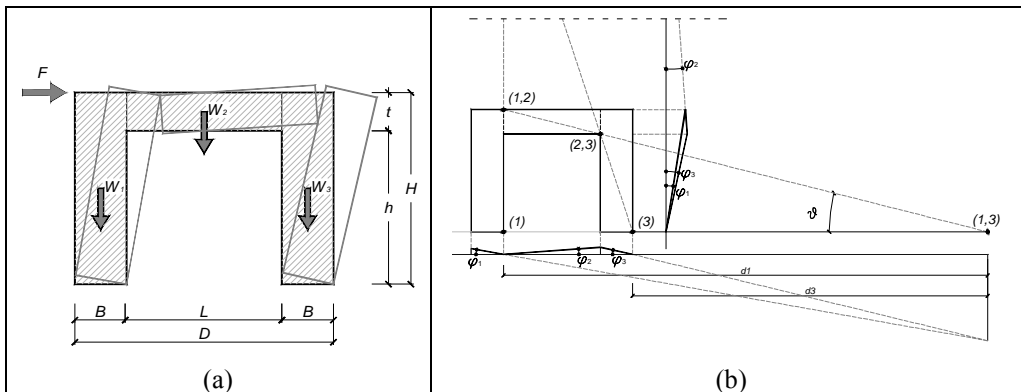


Figure 4. I mechanism – a) geometry and loads; b) kinematic chain.

Operating on the kinematic chain, simple geometrical considerations give:



$$\varphi_3 B = \varphi_2 L; \quad \varphi_1 d_1 = \varphi_3 d_3 \quad (2)$$

$$g d_1 = H \quad \Rightarrow \quad d_1 = \frac{H}{g} \quad \Rightarrow \quad d_1 = \frac{H \cdot L}{t} \quad (3)$$

$$d_3 = d_1 - B - L \quad \Rightarrow \quad d_3 = \frac{HL}{t} - B - L \quad \Rightarrow \quad d_3 = \frac{HL - Bt - Lt}{t} \quad (4)$$

substituting the expressions of  $d_1$  and  $d_3$  in (2):

$$\varphi_1 \frac{HL}{t} = \varphi_3 \frac{HL - Bt - Lt}{t} \quad (5)$$

Let:

$$\psi = \frac{HL}{HL - Bt - Lt} \quad (6)$$

then:

$$\varphi_1 \psi = \varphi_3; \quad \varphi_2 = \frac{B}{L} \varphi_1 \psi \quad (7)$$

The principle of virtual work then gives:

$$F \varphi_1 H = W_1 \varphi_1 \frac{B}{2} + W_2 \varphi_2 \frac{L}{2} + W_3 \varphi_3 \frac{B}{2} \quad (8)$$

From which the collapse multiplier for type I mechanism can be derived:

$$\boxed{\frac{F}{W_{tot}} = \frac{B}{2H} \left( \frac{W_1 + W_2 \psi + W_3 \psi}{W_{tot}} \right)} \quad (9)$$

Where  $W_{tot} = W_1 + W_2 + W_3$ .

### 3.2. MECHANISM II (MIXED MECHANISM)

Following the same procedure as outlined above, the collapse multiplier for the other mechanisms is here derived.

As in the previous case, figure 5.a shows geometrical configuration and loads of the portal, while in figure 5.b the kinematic chain of the mechanism is shown.

Geometrical relations are the same as for type I mechanism, and the equilibrium condition, written the principle of virtual works, is:

$$F\varphi_1 H = W_1\varphi_1 \frac{B}{2} + W_2\varphi_2 \frac{B+L}{2} + W_3\varphi_3 \frac{B}{2} \tag{10}$$

The collapse multiplier for II mechanism is then:

$$\frac{F}{W_{tot}} = \frac{B}{2H} \left( \frac{W_1 + W_2\psi \frac{B+L}{L} + W_3\psi}{W_{tot}} \right) \tag{11}$$

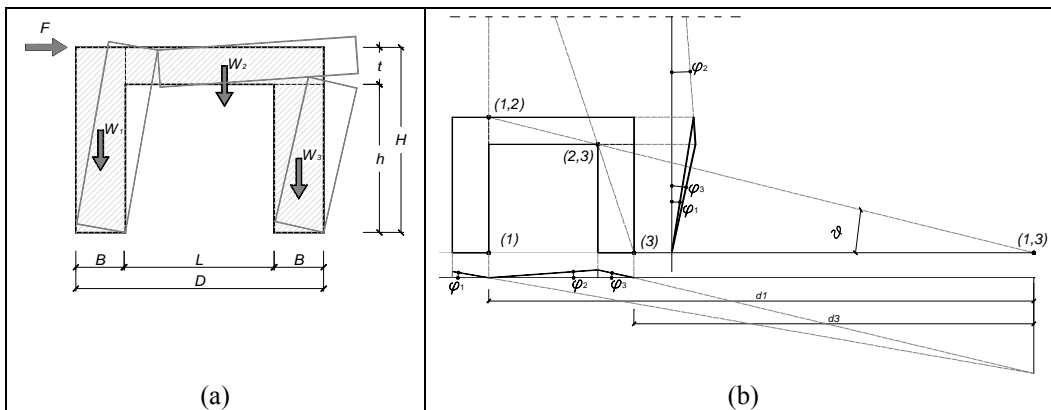


Figure 5. II mechanism – a) geometry and loads; b) kinematic chain.

**3.3. MECHANISM III (MIXED MECHANISM)**

Figures 6.a and 6.b respectively show the geometrical/loads configuration of the portal and the kinematic chain for the mechanism.

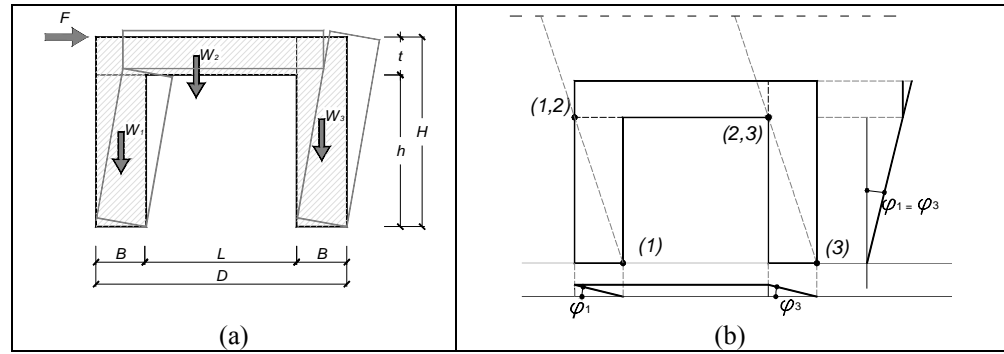


Figure 6. III mechanism – a) geometry and loads; b) kinematic chain.

The following geometrical relations can be written:

$$\varphi_1 = \varphi_3 ; \quad \varphi_2 = 0 \quad (12)$$

The equilibrium condition is:

$$F \varphi_1 (H - t) = W_1 \varphi_1 \frac{B}{2} + W_2 \varphi_1 B + W_3 \varphi_3 \frac{B}{2} \quad (13)$$

and then the collapse multiplier is:

$$\boxed{\frac{F}{W_{tot}} = \frac{B}{2h} \left( \frac{W_1 + 2W_2 + W_3}{W_{tot}} \right)} \quad (14)$$

### 3.4. MECHANISM IV (STOREY MECHANISM)

For this mechanism, geometrical configuration, loads of the portal and the kinematic chain of the mechanism are represented in figure 7.a and 7.b.

Geometrical relations are the same as for III mechanism. The principle of virtual works gives:

$$F \varphi_1 (H - t) = W_1 \varphi_1 \frac{B}{2} + W_2 \varphi_1 B + W_3 \varphi_3 \frac{B}{2} \quad (15)$$

from which the collapse multiplier can be derived:

$$\frac{F}{W_{tot}} = \frac{B}{2h} \left( \frac{W_1 + 2W_2 + W_3}{W_{tot}} \right) \tag{16}$$

or:

$$\frac{F}{W_{tot}} = \frac{B}{2h} \left( 1 + \frac{W_{beam}}{W_{tot}} \right) \tag{17}$$

where:  $W_{beam}=W_2$ .

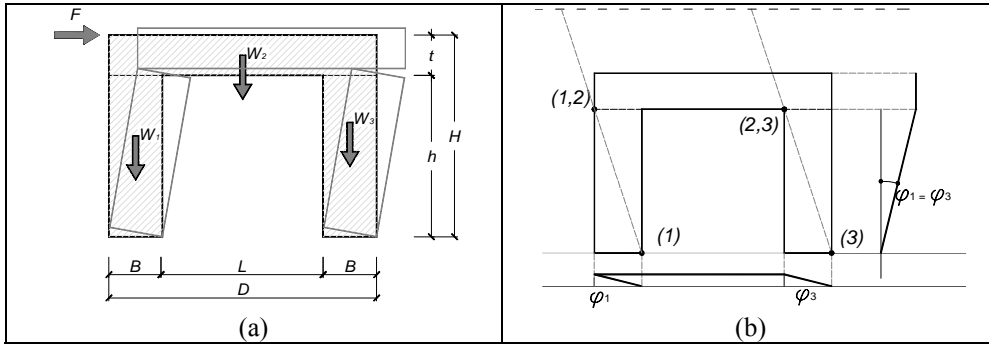


Figure 7. IV mechanism – a) geometry and loads; b) kinematic chain.

#### 4. NORMALIZATION

In order to compare the collapse multiplier from the four selected mechanism and to unify the obtained expressions, let us identify the starting geometry as shown in figure 8, in which also the nodal panels are highlighted.

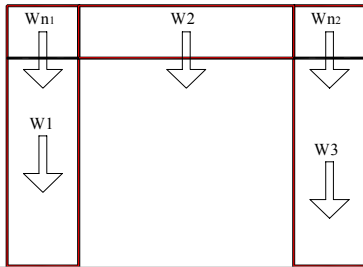


Figure 8. Portal geometry with nodal panels.

Collapse multiplier expressions can be then modified as follows:

Mechanism I:

$$\left( \frac{F}{W_{tot}} \right)_1 = \frac{B}{2H} \left[ 1 + \frac{(\psi - 1)(W_2 + W_{n2} + W_3)}{W_{tot}} \right] \quad (18)$$

Mechanism II:

$$\left( \frac{F}{W_{tot}} \right)_2 = \frac{B}{2H} \left[ 1 + \frac{(\psi - 1)(W_2 + W_{n2} + W_3) + \left( \frac{L+B}{L} \psi \right) W_{n2}}{W_{tot}} \right] \quad (19)$$

Mechanism III:

$$\left( \frac{F}{W_{tot}} \right)_3 = \frac{B}{2h} \left( 1 + \frac{W_{n1} + W_2}{W_{tot}} \right) \quad (20)$$

Mechanism IV:

$$\left( \frac{F}{W_{tot}} \right)_4 = \frac{B}{2h} \left( 1 + \frac{W_{n1} + W_2 + W_{n2}}{W_{tot}} \right) = \frac{B}{2h} \left( 1 + \frac{W_{beam}}{W_{tot}} \right) \quad (21)$$

In the expression given for IV mechanism,  $W_{beam}$  denotes the weight of the horizontal element including nodal panels, i.e.  $W_{beam} = W_2 + W_{n1} + W_{n2}$ .

The expressions for I and II mechanism only differ in an addendum at second member. It is easy to recognize that, in those expressions, the collapse multiplier derived for I mechanism is always smaller than the one for II mechanism.

Similarly, expressions for III and IV mechanisms are the same except of the addendum regarding the second nodal panel. As a result, the collapse multiplier for III mechanism is smaller than the one for IV mechanism.

The formulation proposed provides simple and clear expressions for all the four mechanisms. In particular the parameter  $B/2H$ , which provides an indication of capacity of a single column, is factored out. The multiplier of this factor clearly expresses the effect of the weight of the other parts of the portal (beam and panel of intersection of beam to column).

### 5. PARAMETRIC ANALYSES

From a geometrical point of view, the portal is identified by the quantities  $B$ ,  $D$ ,  $H$  and  $t$  as shown in Fig. 9. The geometry of the portal can be identified once the ratios  $B/D$ ,  $H/D$  and  $t/H$  (in the following regarded as fundamental ratios) have been fixed and the value of a parameter, say  $H$ , chosen.

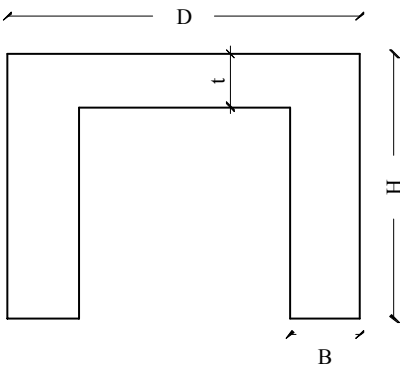


Figure 9. Geometrical characteristics of the portal.

It can be argued that all portal classes obtained fixing any combination of the fundamental ratios show the same collapse multiplier, so that the three chosen ratios are necessary and sufficient for characterizing the portal.

In order to derive the collapse multiplier for the most commonly portals found in monumental structures, parametric analyses have been carried out on a wide class of portals obtained with the following ranges for the fundamental ratios:

- **H/D** step-wise variability: 0,50 – 1,00 – 1,50 – 2,00 (height of the portal ranging between half total width and twice the total width);
- **t/H** step-wise variability: 0,10 – 0,20 – 0,30 – 0,40 – 0,50 (height of the horizontal element ranging between 10% and 50% of the total height of the portal);
- **B/D** step-wise variability: 0,10 – 0,20 – 0,30 – 0,40 (width of the vertical elements ranging between 10% and 40% of the portal total width).

The collapse multiplier of the four mechanisms  $F/W_{tot}$  has been plotted as function of the fundamental ratios  $B/D$ ,  $t/H$  e  $H/D$ , alternatively fixing two of them and studying the variability of  $F/W_{tot}$ .

In figures 10 to 13, the collapse multipliers for the four mechanisms are plotted as functions of variable  $H/D$  and  $t/H$  with **B/D** respectively equal to 0.1, 0.2, 0.3 and 0.4.

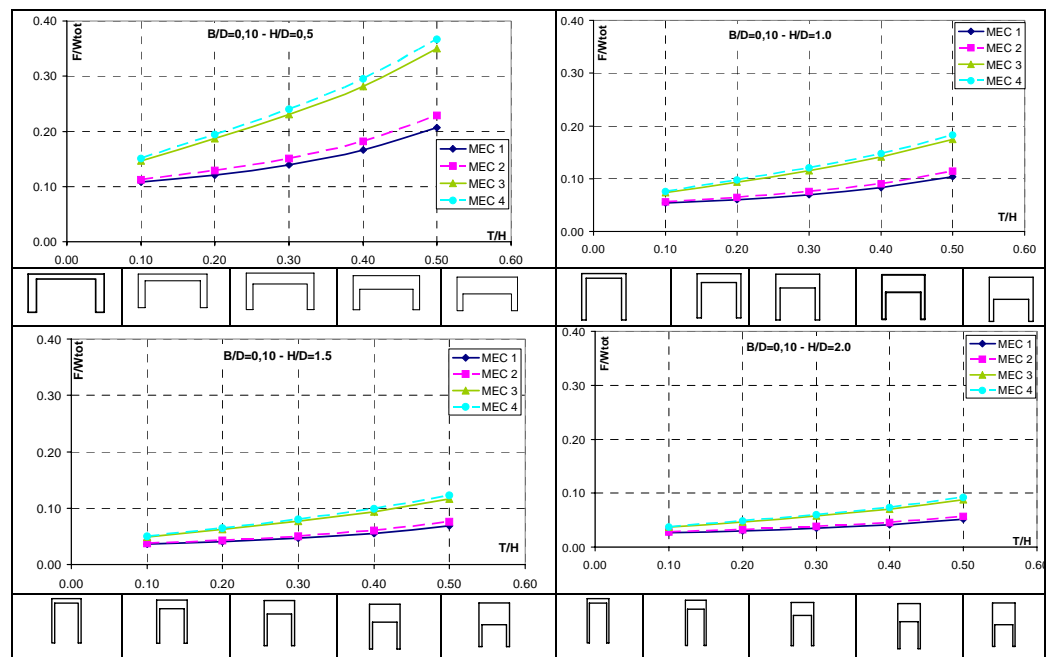


Figure 10. Collapse multipliers for  $B/D=0.1$ .

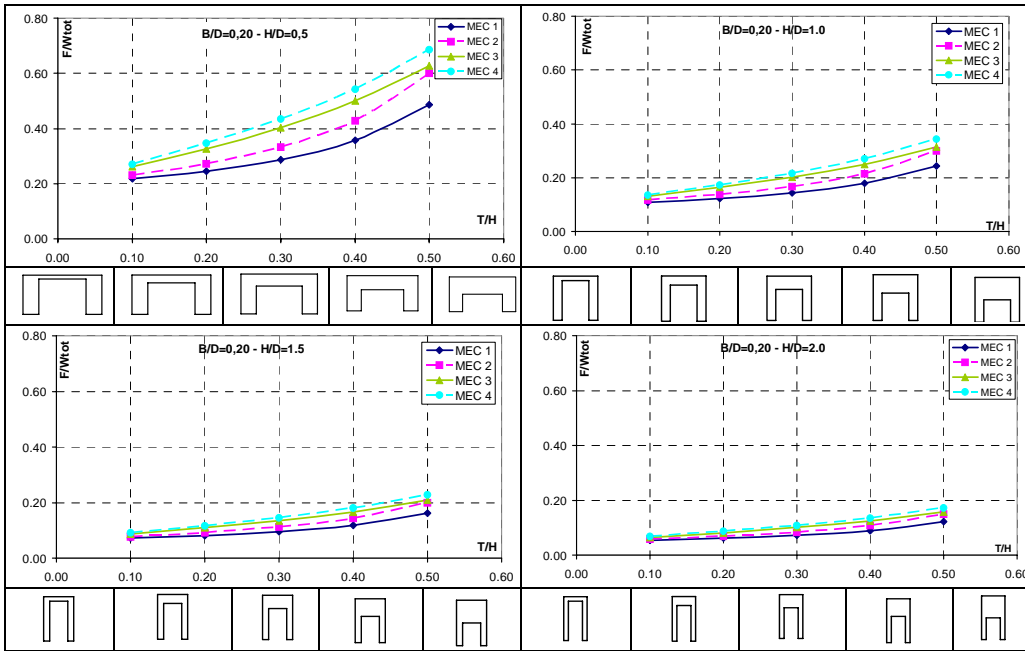


Figure 11. Collapse multipliers for B/D=0.2.

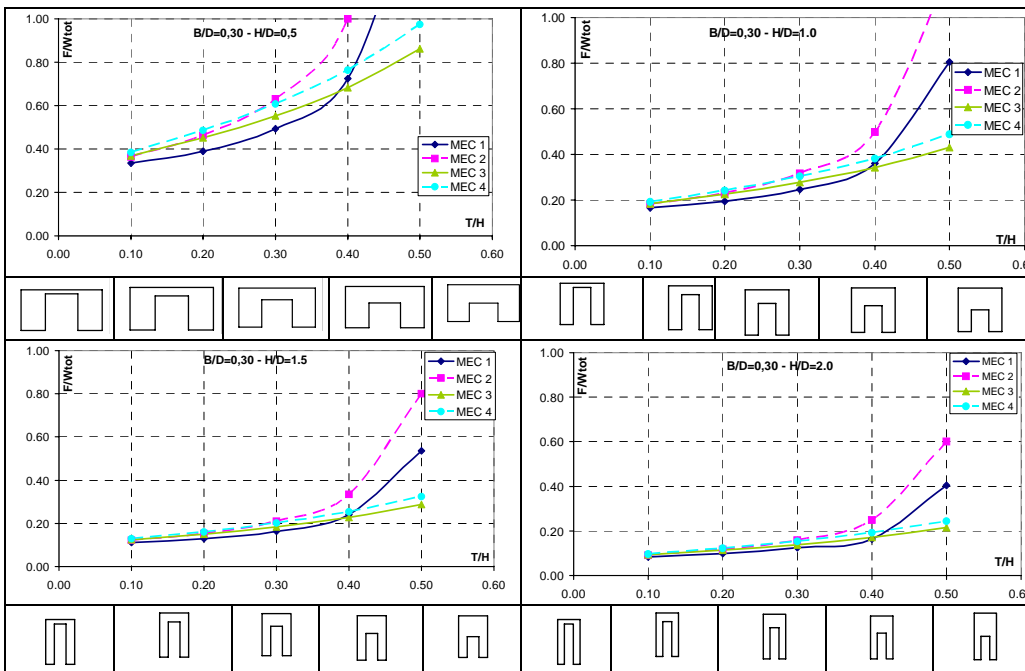


Figure 12. Collapse multipliers for B/D=0.3.



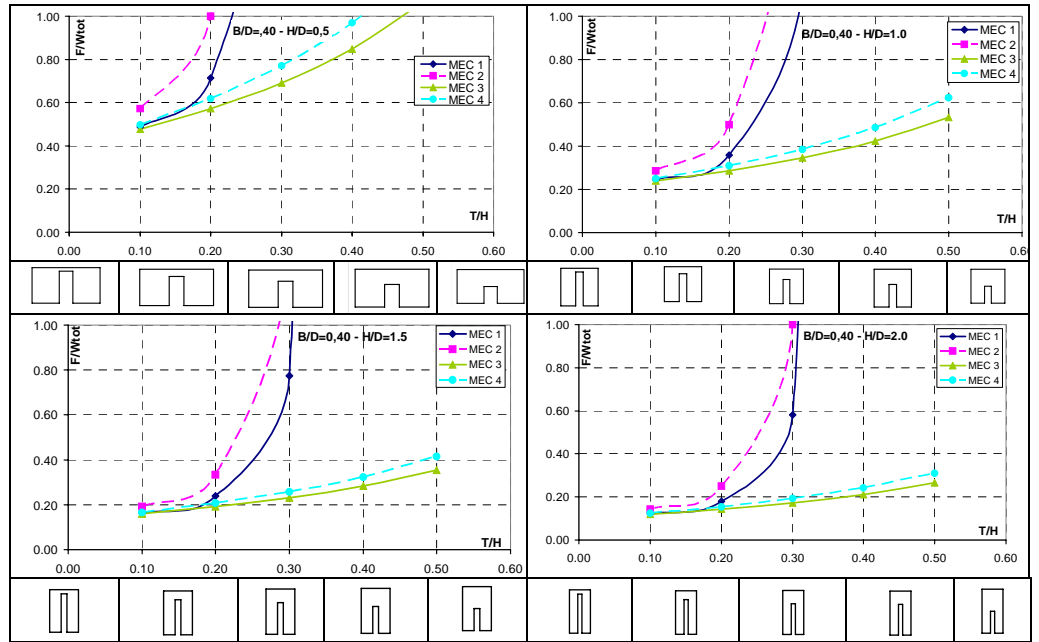
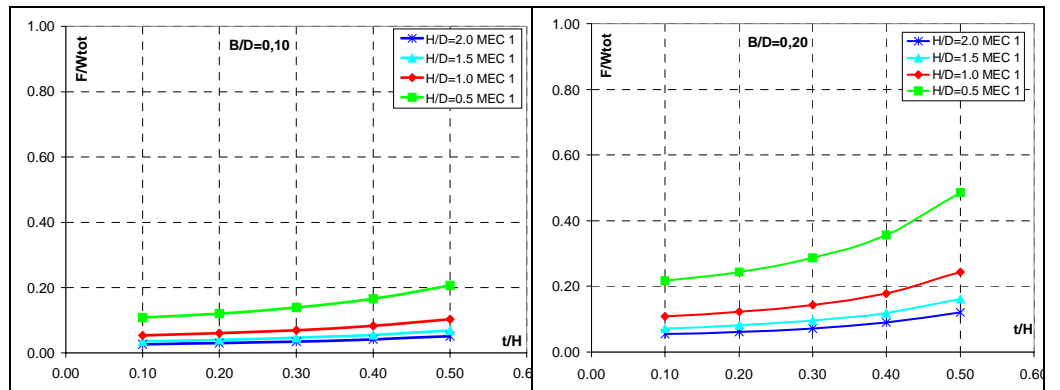


Figure 13. Collapse multipliers for  $B/D=0.4$ .

As already stated in a previous paragraph, it is easy to recognize that I mechanism systematically leads to smaller values of the collapse multiplier with respect to II mechanism, and the same happens for III mechanism with respect to IV mechanism.



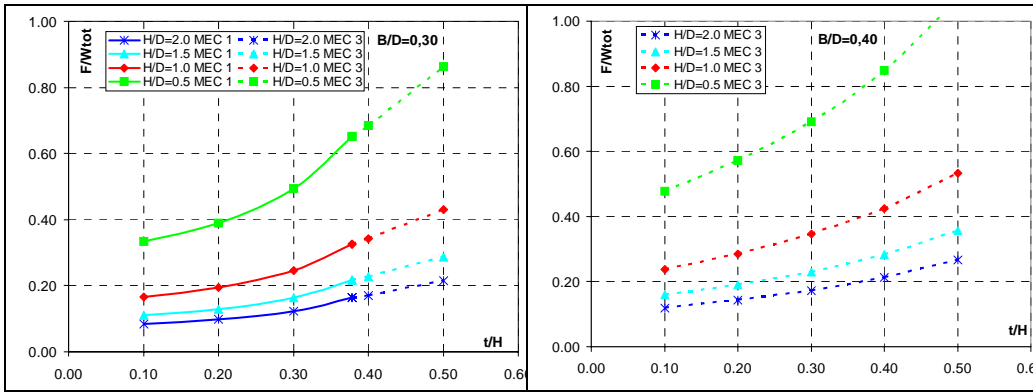
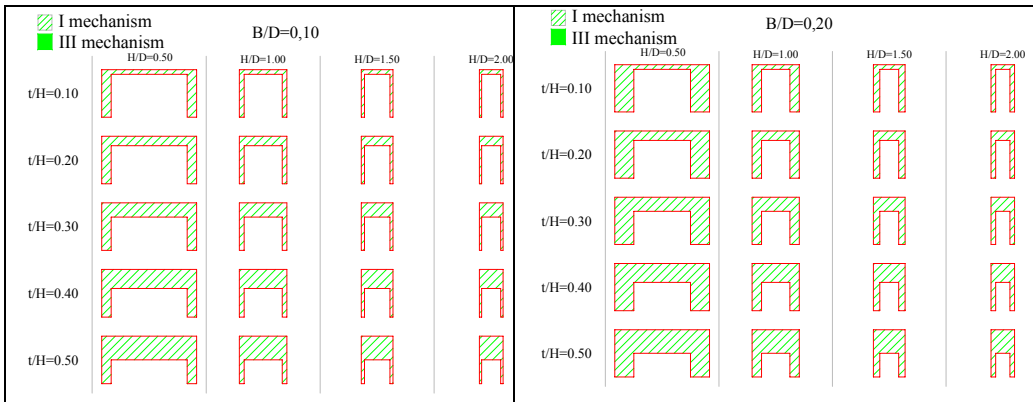


Figure 14. Synthetic diagrams.

In Figure 14, the minimum multipliers, regardless of the particular mechanism, are plotted as a function of  $t/H$ , for different  $H/D$  ratios, having fixed the value of  $B/D$ .

Further, it is possible to define ranges of the fundamental ratios in which a mechanism prevails upon the others. In the following figure 15, the above described ranges, with prevalence of I or III mechanism, are represented in a graphical way.



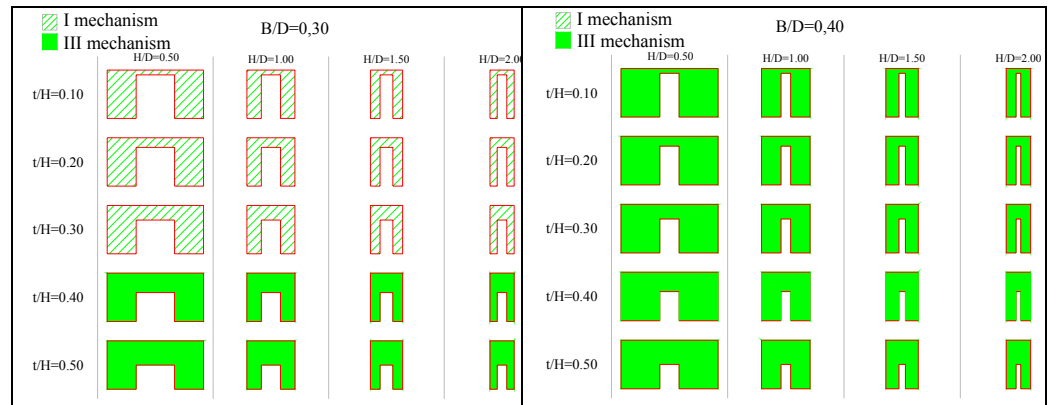


Figure 15. Geometrical configurations for different geometrical ratios values; prevalence of I or III mechanism: B/D=0.1; 0.2; 0.3; 0.4.

$B/D \leq 0,20$		mechanism type 1	
$B/D = 0,30$	and	$t/H \leq 0,30$	mechanism type 1
$B/D = 0,30$	and	$t/H \geq 0,40$	mechanism type 3
$B/D \geq 0,40$		mechanism type 3	

## 6. AN ABAQUS FOR EVALUATING THE COLLAPSE MULTIPLIER

The formulation in a closed form of all the possible mechanism of the portal frame subjected to vertical load and horizontal load at the top allows obtaining the ultimate multiplier for any given geometry of a masonry portal frame. In order to catch in a more immediate manner this value in the design process, abacuses have been provided for the different parameters chosen defining the geometry of the portal: B/D, H/D and t/H. In particular each abacus is relative to a B/D value (0.1, 0.2, 0.3, 0.4) in Fig. 16. In each of them iso-limit curves providing the  $F/W_{tot}$  values for different H/D abscissa and t/H ordinate values are then plotted.

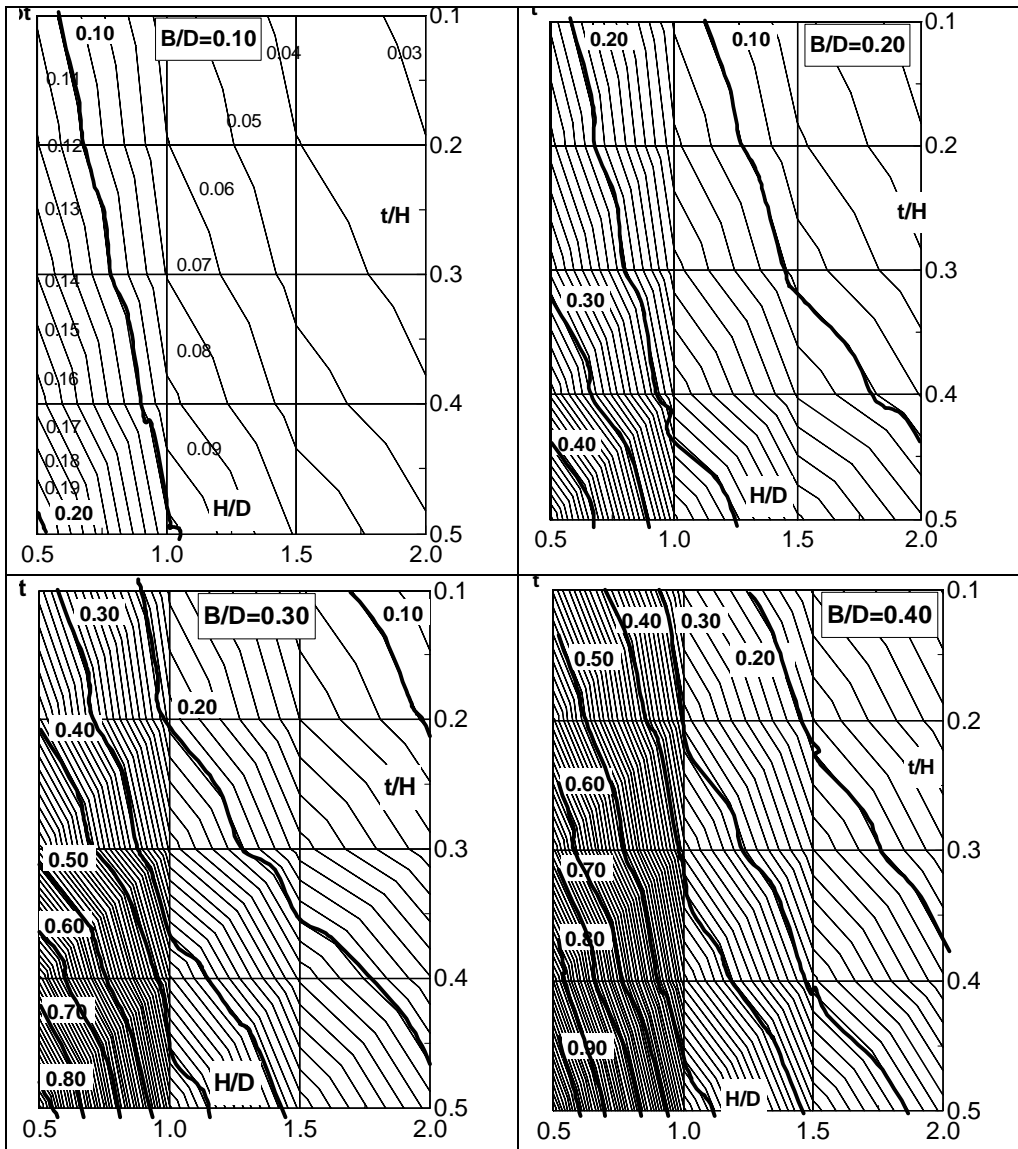


Figure 16. Iso-limit curves with fixed B/D ratio; B/D=0.1, B/D=0.2, B/D=0.3, B/D=0.4.

As an example, let us consider a portal with the following fundamental ratios: B/D=0.2, t/H= 0.15 e H/D=1.7. Using the abacus of Figure 16, the plot corresponding to the actual B/D value has to be selected and in that one the point of coordinates (H/D, t/H) detected (Fig. 17). Such point represents the collapse

multiplier, obtainable by interpolating the iso-limit curves 0.06 and 0.07. As a verification, for the chosen fundamental ratios the collapse multiplier results  $F/W_{\text{tot}} = 0.0684$ .

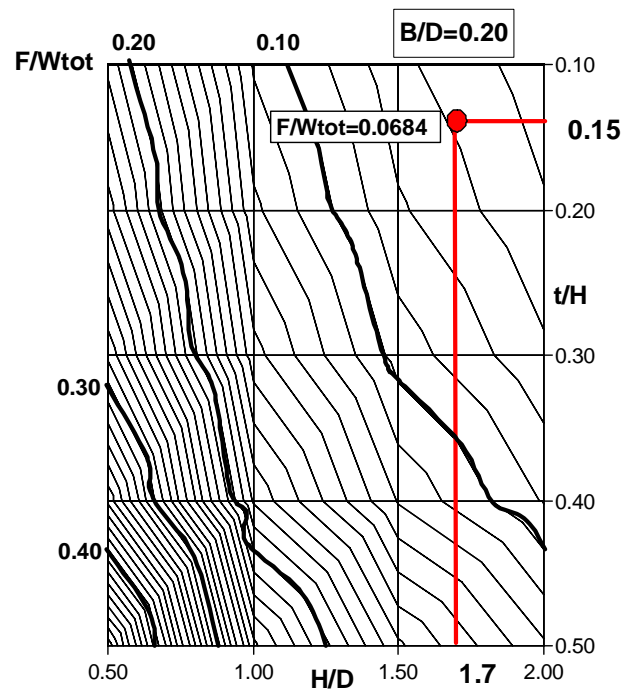


Figure 17. Example of use of the abacus.

## 7. ADVANCES WITH RESPECT TO PREVIOUS FORMULATIONS

Previous studies on similar portal frames can be found in [Como M. et Al., 1983], where horizontal load multipliers are derived under the hypotheses of non-zero bending capacity ( $M_0$ ) of the masonry spandrel beam, made possible by the presence of reinforcing ties.

The expressions provided by [Como M. et Al., 1983] for the horizontal multipliers are derived for three mechanism shapes (Figure 18) comparable with the ones here denoted as mechanisms I, III and IV, though some differences exist regarding hinge positions and loads configuration.

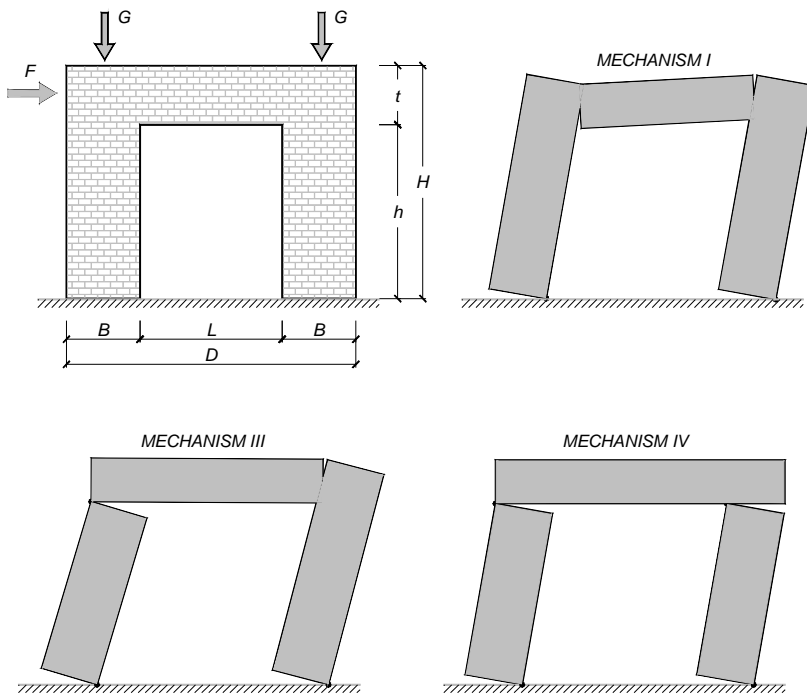


Figure 18. Configuration and mechanism shapes in [Como M. et Al., 1983].

Those expressions, as a function of geometry, applied vertical loads  $2G$ , and spandrel bending capacity  $M_0$ , are reported in Table 1. In those formulas, some algebra has been applied to the ones originally presented in the cited reference, in order to introduce the same symbols as here adopted.

Since in the present approach any vertical/horizontal loads configuration can be easily taken into account, the formulas provided in the previous sections are here modified for the load assembly of Figure 18, and the expressions for mechanisms I to IV also shown in Table 1.

	Cited reference	Present proposal (load configuration asin figure 18)
“Frame” mechanism (mechanism I)	$\frac{F}{2G} = \frac{B}{2\left(h + \frac{t}{2}\right)} \left(1 + \frac{2M_0 \cdot (1 + B/L)}{G}\right)$	$\frac{F}{2G} = \frac{B}{4\left(h + \frac{t}{2}\right)} (1 + \psi)$
“Mixed” mechanism (mechanism II)		$\frac{F}{2G} = \frac{B}{4 \cdot \left(h + \frac{t}{2}\right)} \left(1 + \psi \frac{2L + B}{L}\right)$
“Mixed” mechanism (mechanism III)	$\frac{F}{2G} = \frac{B}{2h} \left(\frac{1 + \frac{L}{B}}{1 + \frac{t}{2h}}\right) \cdot \left(\frac{\frac{3}{2} + \frac{t}{2h}}{1 + \frac{L}{B} + \frac{t}{2h}}\right) + \frac{t}{2h} \cdot \left(1 + \frac{M_0}{BG \cdot \left(\frac{3}{2} + \frac{t}{2h}\right)}\right)$	$\frac{F}{2G} = \frac{3B}{4h}$
“Storey” mechanism (mechanism IV)	$\frac{F}{2G} = \frac{B}{h}$	$\frac{F}{2G} = \frac{B}{h}$

Table 1. Comparison of present and cited formulas.

For comparison, the following Table 2 reports the non-dimensional collapse loads calculated through the present and cited proposals, in which null bending capacity ( $M_0 = 0$ ) has been assumed, for the different geometrical configurations shown in Figure 19.

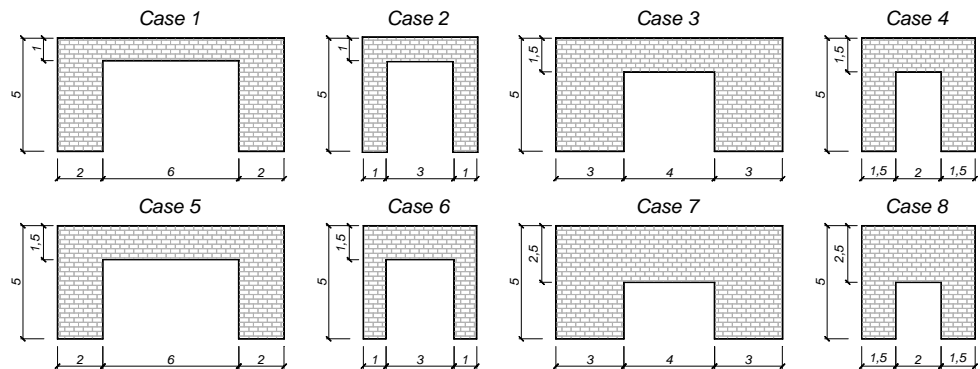


Figure 19. Geometrical configurations for comparison.

Case	Cited reference	Present proposal (load configuration as in figure 18)
1	0.222	0.263
2	0.111	0.131
3	0.353	0.548
4	0.176	0.274
5	0.235	0.314
6	0.118	0.157
7	0.4	0.9
8	0.2	0.43

Table 2. Comparison among present and cited proposals.

Quite evidently, differences arise between the two proposals, with the present expressions always giving higher values of the collapse load, although no reinforcing tie is taken into account. The largest scatters are obtained for the stockiest schemes. In particular, for cases 7 and 8, the cited reference provides values that are less than half those relevant to the present proposals. This is mainly due to the slightly different shapes of the collapse mechanisms, which reflects on the virtual displacements read from the kinematic chain. Actually, in case of non slender elements, small rotation differences drive to large displacement differences.

A few issues arise about the conceptual differences with regard to the present proposal. Firstly, as far as loads are concerned, the horizontal force is applied at mid height of the spandrel beam, while in this study it is assumed at full height of the portal. This difference is generally negligible and may drive to considerable disagreement only for unrealistically large beam heights. Besides, vertical loads are limited to two forces, named G in Figure 18, acting on top of the portal, so that self-weight is neglected. As a consequence, the stabilising effect of the weights of spandrel and panel zones, which is instead thought to be important, is not accounted



for. Presence of the beam is substantially accounted for by the way its bending capacity (when present) provides a contribution to the equilibrium.

Arguably, the hypothesis of negligible self-weight with respect to the external vertical load can be reasonable when the portal is located at lowest levels of multi-storey buildings, while it may not be realistic for some monumental buildings typologies, like churches, in which masonry weight almost fills out the total vertical load.

A further conceptual difference regards the position of the adopted hinges. In the cited references, the upper part behaves as a beam, so that the bending capacity due to the presence of reinforcing ties (or possibly platbands) is assumed to be an equivalent plastic moment; as a consequence, hinges are regarded as plastic hinges and this circumstance involves a certain geometrical compenetration in the zones that mutually rotate in the deformed shape. This is not possible in the present approach, which considers infinite compressive strength in the blocks.

The present study, indeed, do not need the presence of reinforcing ties, and the expression proposed are easily adaptable to any load condition.

## **8. PROPOSAL FOR A SIMPLE APPROXIMATE EXPRESSION**

The deep insight obtained in the analysis and behaviour of portal frames, gained through the extensive parametric analysis developed on 80 different schemes characterized by strongly varying geometrical proportion, allow to define the mechanical parameters governing the behaviour and consequently the value of  $F/W_{tot}$ . The behaviour is in fact governed by:

- a) Column geometrical proportion  $B/2h$  which represents the multiplier of a single panel;
- b) Effect of the weight of the beam which stabilizes the column;
- c) Percentage of openings which drives the behaviour respectively to a stocky global panel or to the one characterized by two slender columns.

These considerations have allowed us to propose a simple formula which includes all the previously reported three effects. The formula is:

$$\frac{F}{W_{tot}} = \frac{B}{2 \cdot h} \left( 1 + \frac{W_{beam}}{W_{tot}} \right) \left( 0,50 + \frac{B}{D} \right) \quad (22)$$

where the symbols are given in figure 20:

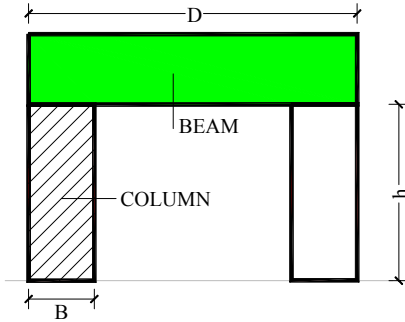


Figure 20. Effects considered in the approximated formula.

It's easy to understand the meaning of the three multipliers:

$\frac{B}{2h}$	Column behaviour as single panel element
$\left( 1 + \frac{W_{beam}}{W_{tot}} \right)$	Stabilizing effect of beam
$\left( 0,50 + \frac{B}{D} \right)$	Effect of openings

In Figure 21, for all the cases ( $B/D=0.1\div 0.4$ ), the *exact* collapse multipliers computed through the equations (18), (19), (20) and (21), are compared with the results obtained from expression (22).

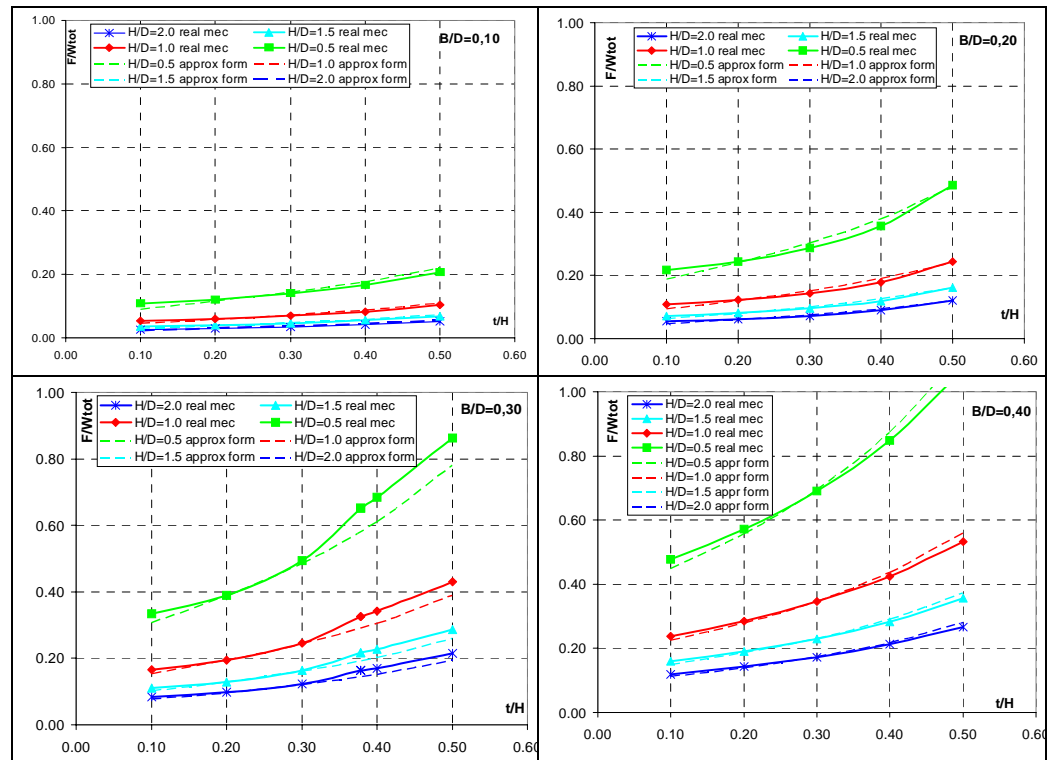


Figure 21. Actual mechanism and approximated formula. Comparison.

A more extensive comparison is given in Fig. 22 where for all the 80 cases of portal frames are compared the exact value against the approximate ones. The approximation is excellent since the errors are always less than 6 % except for two cases:

- 1)  $H/D=0.5$ ;  $t/H=0.4$ ;  $B/D=0.3$ ;
- 2)  $H/D=0.5$ ;  $t/H=0.5$ ;  $B/D=0.3$ ;

in which the maximum error is anyway less than 8.5%.

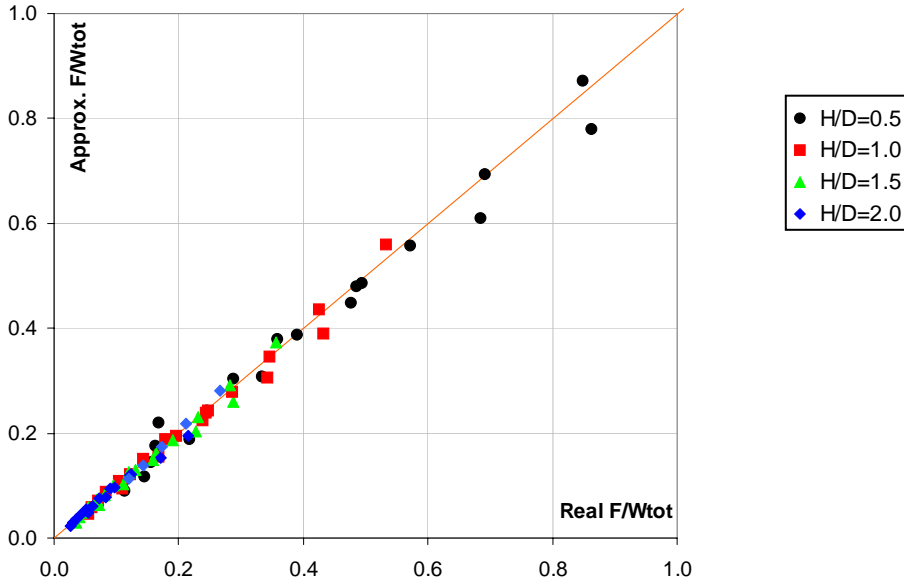


Figure 22. Errors of the approximated formula for different portal configurations.

## 9. CONCLUSIONS

In this chapter an exhaustive analysis of masonry portals through limit approach has been presented. In this aim, by adopting the hypotheses made in [Heyman J., 1966], the analysis is extended to the portal frame which is a very recurrent element in historical buildings and is analyzed under the loading case of horizontal actions.

The formulation proposed in this paper removes the hypotheses made in previous studies [Como M. et Al., 1983] on similar structures. In this manner, the formulation allows the possibility of deriving in a closed form solution, the horizontal capacity of portal masonry frames in absence of reinforcing ties.

The closed form solution has been then used for performing an extensive parametric analysis on 80 structural schemes characterized by considerably varying geometrical proportions.

Abacuses are given for an immediate use for design purposes.

Finally, an approximate solution is proposed for evaluating the horizontal capacities of such schemes. The approximate formula has a very sound mechanical basis since it splits the multiplier in three factors each of them being very simple and immediate in its mechanical significance.

The formula has been tested for all the 80 cases providing excellent results with errors always less than 6%.

The results provided both in terms of closed form and approximated solutions might be very valuable for the designer in evaluating the capacity of portal masonry frames of historical buildings to horizontal action which is related to their seismic strength.



## **CHAPTER 6:**

### ***SIMPLIFIED ANALYSIS OF MACROELEMENTS***

#### **1. INTRODUCTION**

One of the objects of this study is the possibility of defining a suitable methodology to obtain an approximate valuation of the bearing capacity of single macroelements, with few calculations and without time consuming and complex analyses.

In this chapter, in the light of the simplified approach described in the previous chapter, an application of limit analysis to some elements of the four study cases is made.

Furthermore, a comparison between simplified calculations and non linear analyses carried out in §4 is exposed and discussed.

## 2. EXTENSION OF THE SINGLE PORTAL FRAME TO THE MULTI-BAY FRAME.

The formulas showed in the previous chapter can be somehow adapted in the case of multi-bay frames. Obviously, the kinematic chain will be more complicated but still constructible. In Fig. 1 the kinematic chain for the I - frame mechanism- and the IV – storey mechanism- type are depicted.

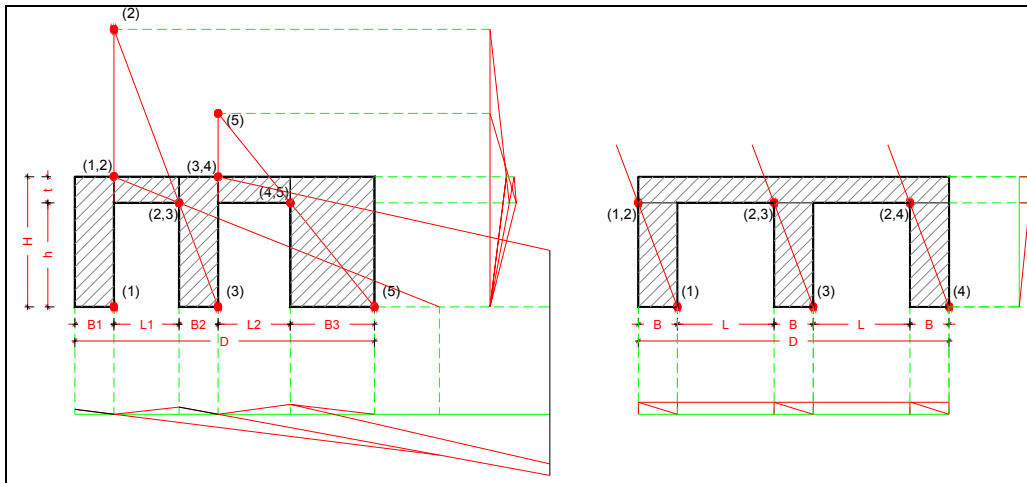


Figure 1. Frame and Storey kinematic chains in the multi-bay frames.

Internal macroelements of churches, featuring a series of piers and a superior horizontal beam, are similar to the multi-bay frames. The non-linear analyses have shown that, generally, the columns rotate around a point on the base and the beam will shift horizontally. In other words, if a series of elements like columns can be individuated, the collapse occurs for the formation of a storey mechanism rather than a frame or a mixed mechanism (Fig.2).

About the dimensions of the piers, the B value in the formula has to be specified. It has to be underlined that no kinematic chain can be constructed for different values of the base because of the non uniqueness of the fixed centre (2). For this reason a unique value has to be selected and, because it represents also the



contribution of the panel to the rocking, it could assume the value of the maximum, the minimum or the average dimension. Therefore, in the storey mechanism, passing from the portal frame to the multi-bay frame no change is individuated in the collapse multiplier; the formula adopted is then:

$$\frac{F}{W_{tot}} = \frac{B}{2 \cdot h} \left( 1 + \frac{W_{beam}}{W_{tot}} \right) \quad (1)$$

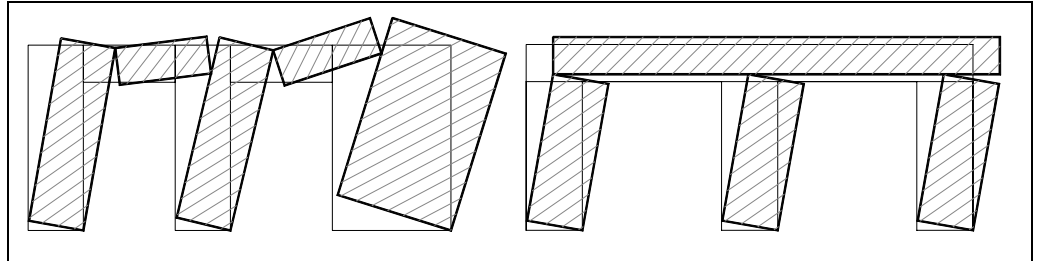


Figure 2. Frame and Storey mechanism in the multi-bay frames.

In case of presence of dead loads coming from the over-structures such as roof systems or vaults, their stabilizing effect is considered as additional loads in the term  $W_{beam}$ .

Of course, these macroelements could feature non-uniform shapes so that the mechanism considered can not occur: this is a very delicate aspect of the simplified approach so that a confident statement can hardly be expressed.

### 3. FEM – LIMIT ANALYSIS: COMPARISON

In the following Figures, the internal churches macroelements are illustrated. In each of them, the comparison of the results of non linear and simplified analyses is reported. In the section *a* of the figures, the mesh and the deformed shape of the bi-dimensional element in the non linear analysis are shown; in the *b* part the simplified geometry of the macroelement is depicted and in *c* part the numerical values used in the simplified analysis are reported. Finally, in the *d* and *e* section the comparison

between the non linear and limit analysis, as function of the applied loads (only dependent on the self weight in the first one and self weight plus dead load in the second one), are depicted in a graph. These plots represent the conventional load displacement curves obtained through non-linear analysis using ABAQUS. This curve will provide the initial stiffness with respect to the horizontal actions and the trend of the displacements of some points on the structure chosen as control points. As it has already been shown, a typical curve will have the first part in the linear field and the second part in the non linear range up to the achievement of the plastic branch; again, the results will not be unique if the element is not symmetrical in the vertical axis, so that two curves represent the different response of the structure according to the verse of the seismic action (from right or left). About plastic analyses no differences are pointed out as function of the verse of the horizontal force. On the other side, two plots have been diagrammed according to the presence or not of the dead load. Furthermore, when piers are not uniform in their dimensions three values of the collapse multiplier for each diagram, corresponding to the maximum, medium and minimum magnitude, have been calculated.

Reasoning in safety terms, the curve with the smallest value of the collapse multiplier should be the reference in the comparison with the limit analysis represented by an horizontal line. The comparison between the results, representative of two different methodologies, consists into the evaluation of their scatter. Small error percentages mean that the results match well, or in other words, a good modelling of the structure has been performed. Differently, great scatters evidence that the model is not able to grasp the real behaviour of the structure.

**3.1. S. GIOVANNI A MARE**

In Figure 3 the macroelements of SGMR comparable to multi-bay frames and considered in the simplified analyses are enlightened.

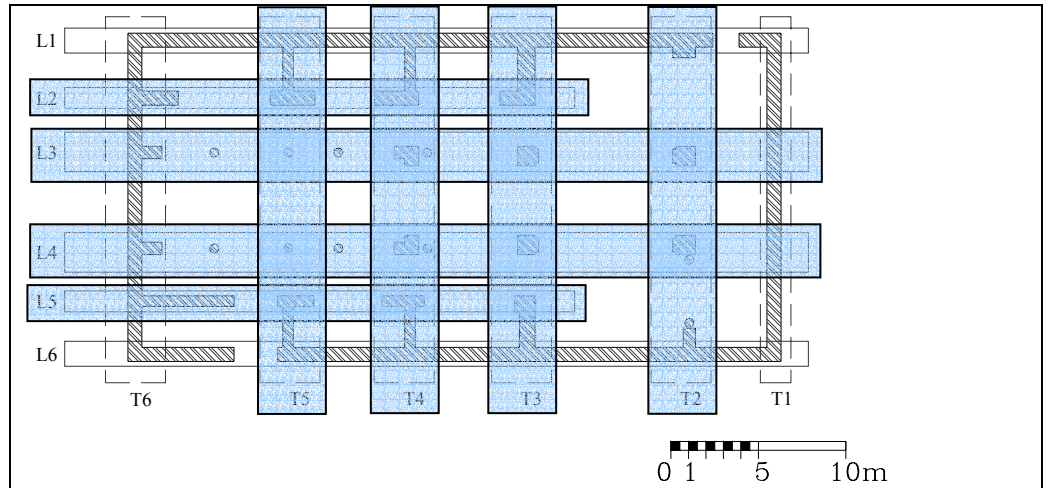
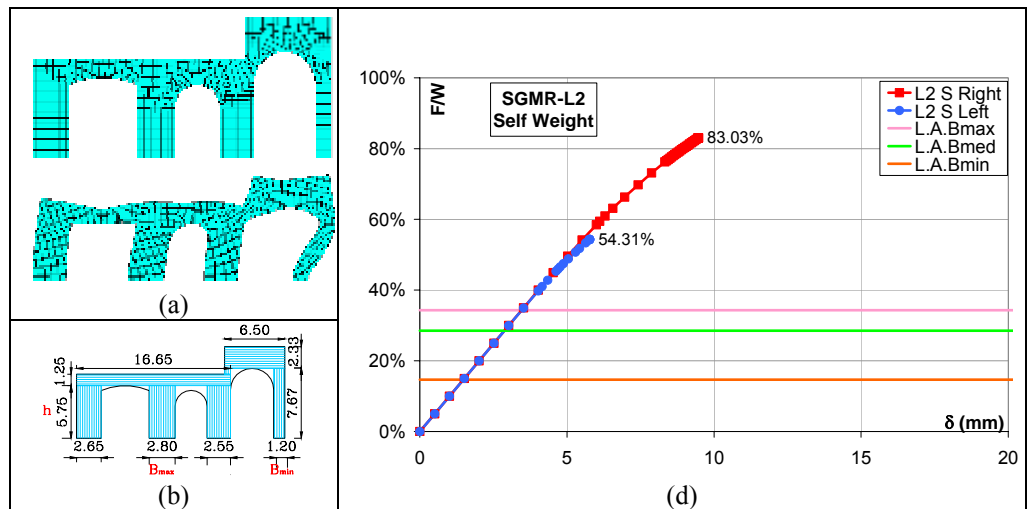


Figure 3. SGMR – Individuation of the macroelements in plant.



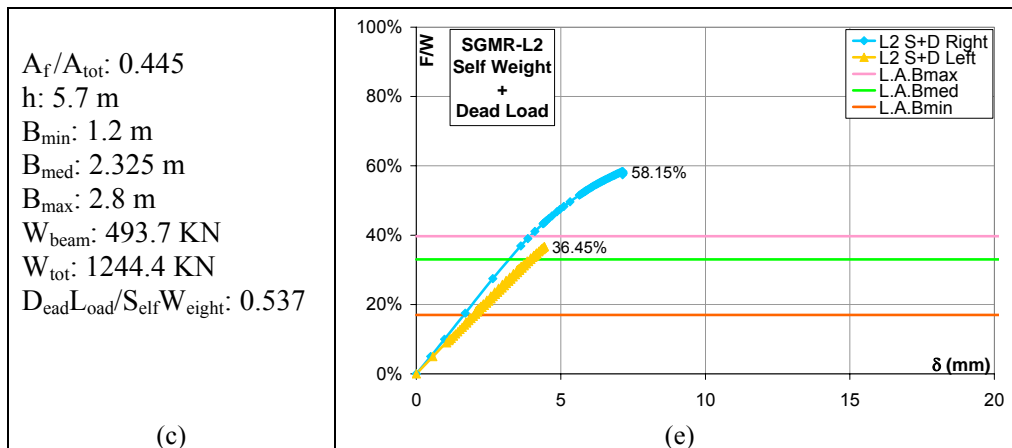


Figure 4. L2 macroelement – a) Mesh; b) Modelling; c) Simplified analysis data; d & e) Force/Displacement curves.

This non symmetrical macroelement, both in geometry and loads, has implied the execution of four non linear analyses. The deformed shape in the non linear analysis has suggested the choice of a storey collapse mechanism in the simplified analysis. Due to the significant presence of dead load on the structure, the simplified value of the collapse multiplier varies according to the loads considered. Because of the non uniformity of the piers in the macroelement, three values of the collapse multiplier for each diagram have been calculated. In the “self weight diagram” the comparison between the FEM and simplified analyses show large difference. Smaller values of the limit analyses are reached compared to the non linear curves. Quite different is the behaviour when dead loads are applied. In Fig. 4.e the scatter between the simplified analysis considering a medium value of the base and the collapse value due the horizontal force coming from the left is small.

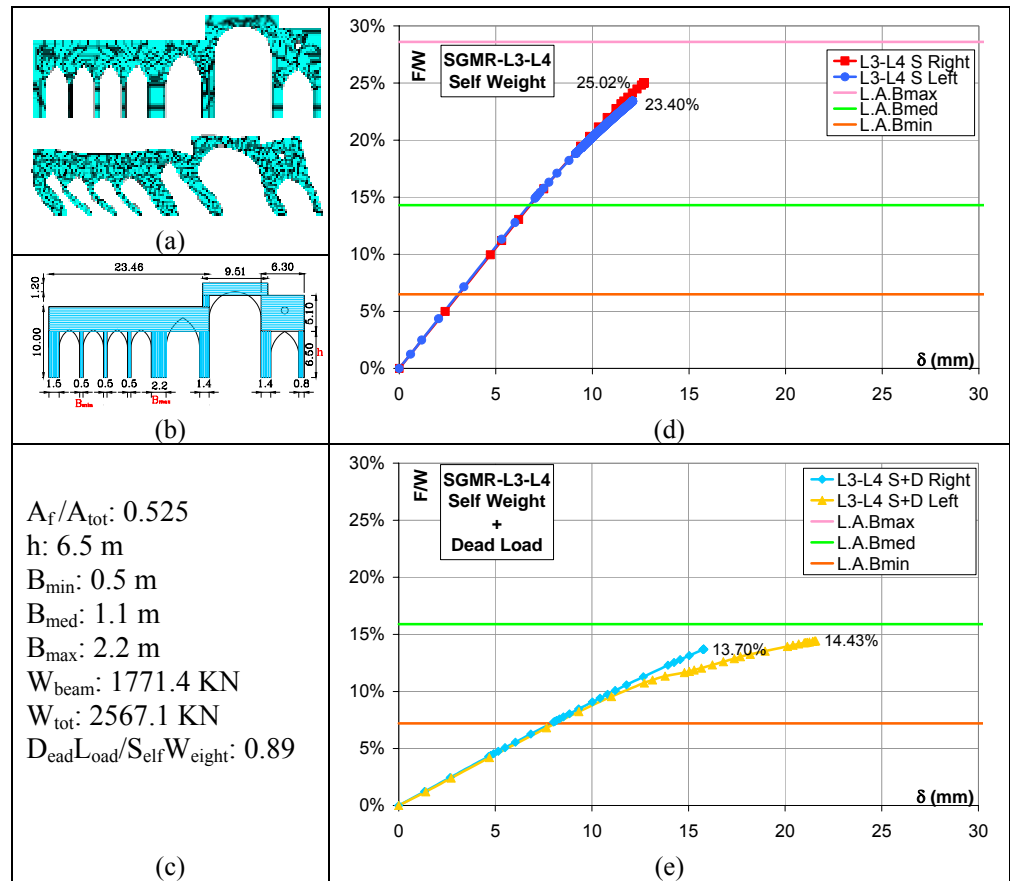


Figure 5. L3-L4 macroelement – a) Mesh; b) Modelling; c) Simplified analysis data; d & e) Force/Displacement curves.

The inner arcade of the church bears the dead loads on both the sides, so that the percentage of these actions compared to the self weight is close to the unity. This point reflects also in the shape of the two diagrams. Considering a collapse mechanism of storey type, in the first plot the two collapse value derived from the non linear analyses are closer to the value obtained assuming in the formula the maximum dimension of the columns, whilst in the second one the two values are close to the middle one relevant value of the pier base.

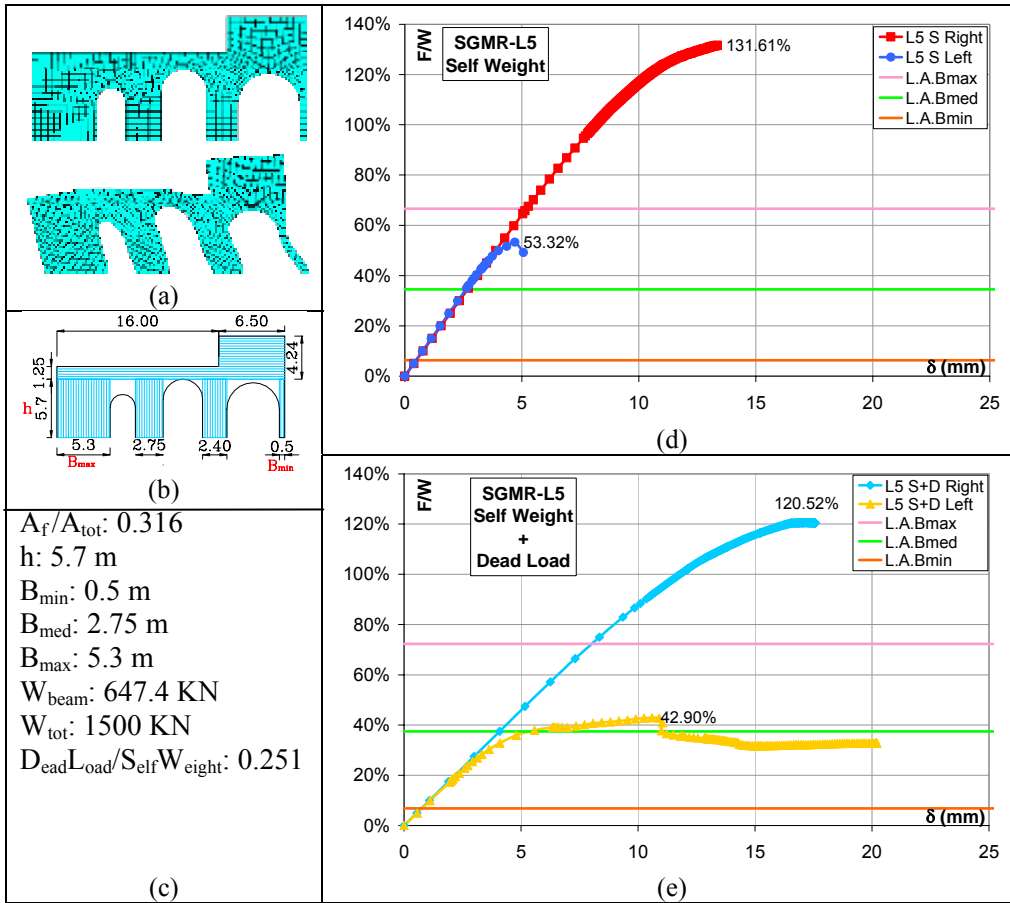


Figure 6. L5 macroelement – a) Mesh; b) Modelling; c) Simplified analysis data; d & e) Force/Displacement curves.

Great scatter of non linear behaviour of the macroelement are noticeable in both the diagrams according to the verse of the horizontal action. This is due to the small dimension of the first pier on the left. The shape of the element has suggested a storey mechanism type and in both the cases, the medium base values in the simplified analyses are close to the values of the collapse multiplier for forces coming from the left side.

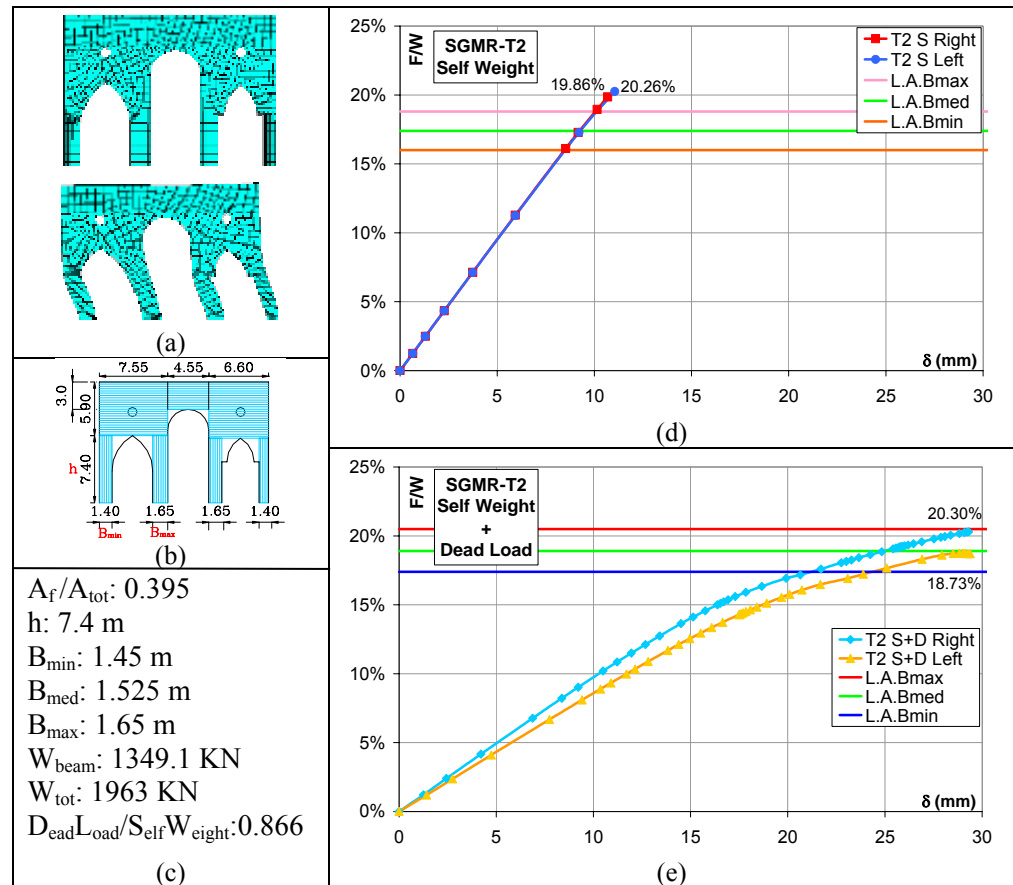


Figure 7. T2 macroelement – a) Mesh; b) Modelling; c) Simplified analysis data; d & e) Force/Displacement curves.

The inner macroelements, like this triumphal arch, have larger openings than the external elements and are strongly loaded, with values sometimes comparable to the self weight. The comparison of the non linear analyses under self weight only with simplified limit analyses is somehow uncertain due to sudden stop of the numerical curves. On the contrary, the case with dead loads also show more meaningful interpretability.

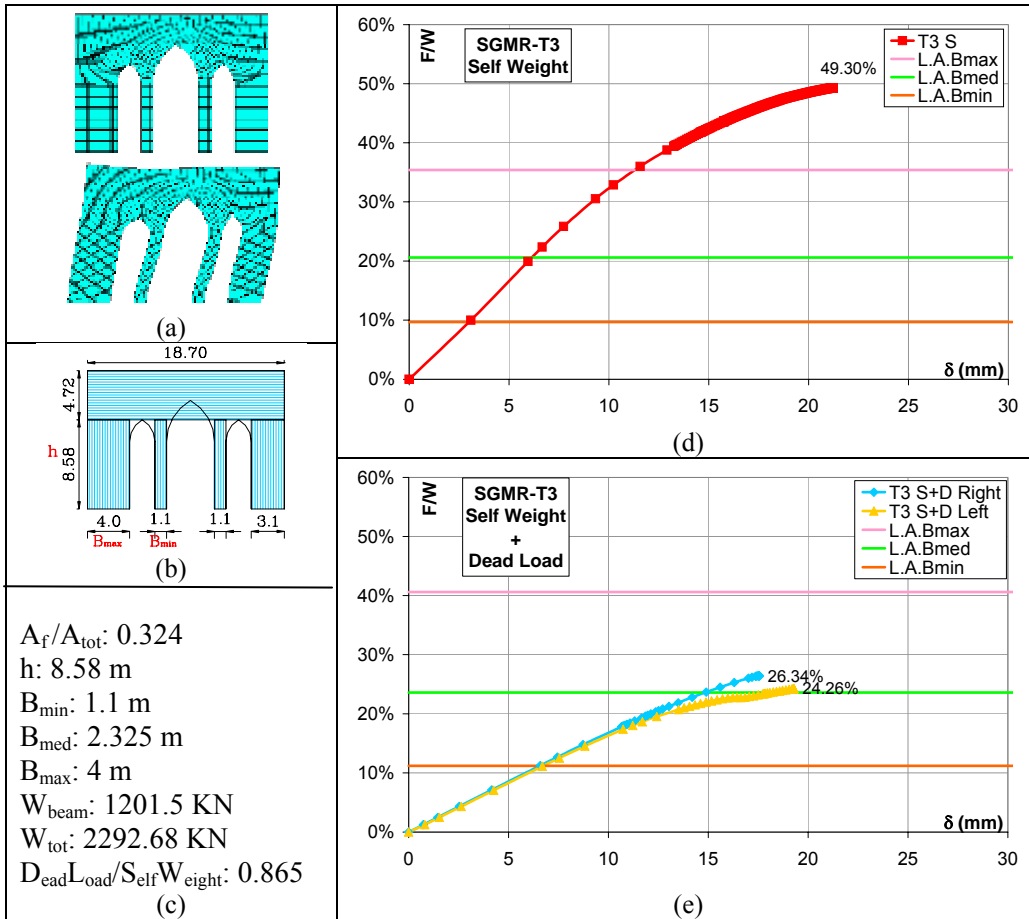


Figure 8. T3 macroelement – a) Mesh; b) Modelling; c) Simplified analysis data; d & e) Force/Displacement curves.

Like the previous element, this second triumphal arch has small values scatter in the model with the dead load and bad matching for the case of self weight only.



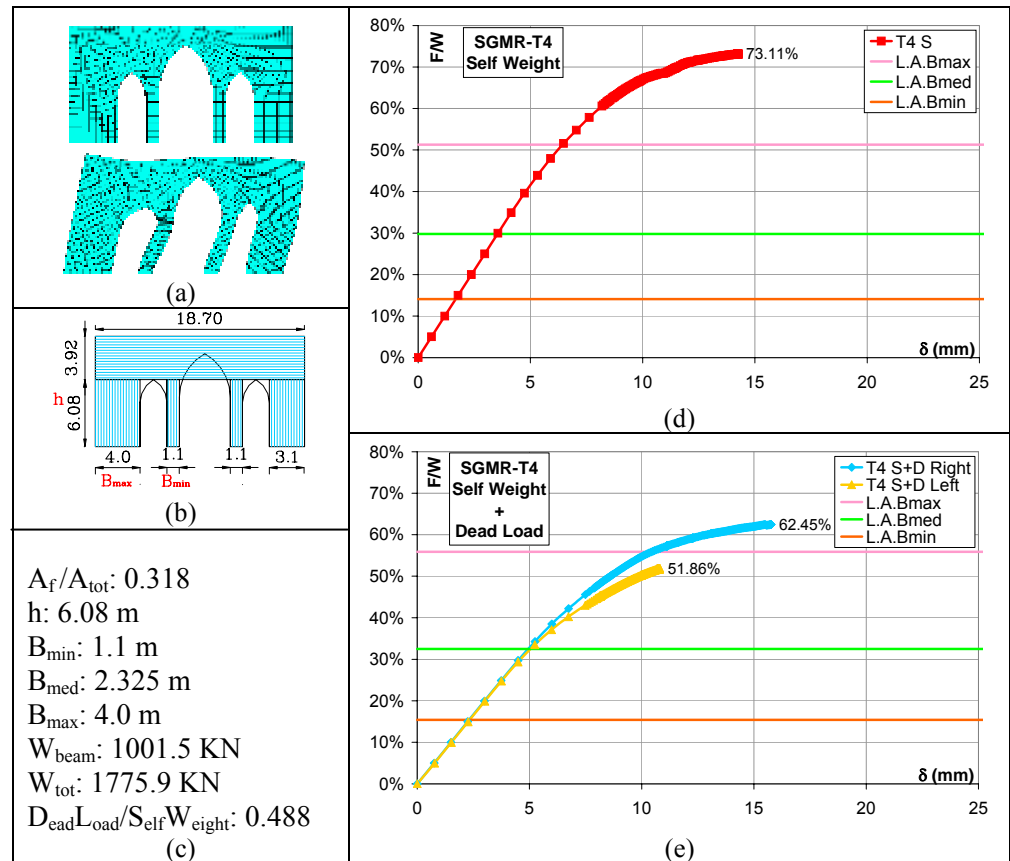


Figure 9. T4 macroelement – a) Mesh; b) Modelling; c) Simplified analysis data; d & e) Force/Displacement curves.

The T4 element shows a no matching behaviour between the carried out analyses in both the modelling. More in detail, in case of only self weight load distribution, the values of limit analysis are sufficiently below the non linear curve. In the other model, the two ABAQUS curves give values closer to the one obtained using in the formula the maximum dimension of the columns.

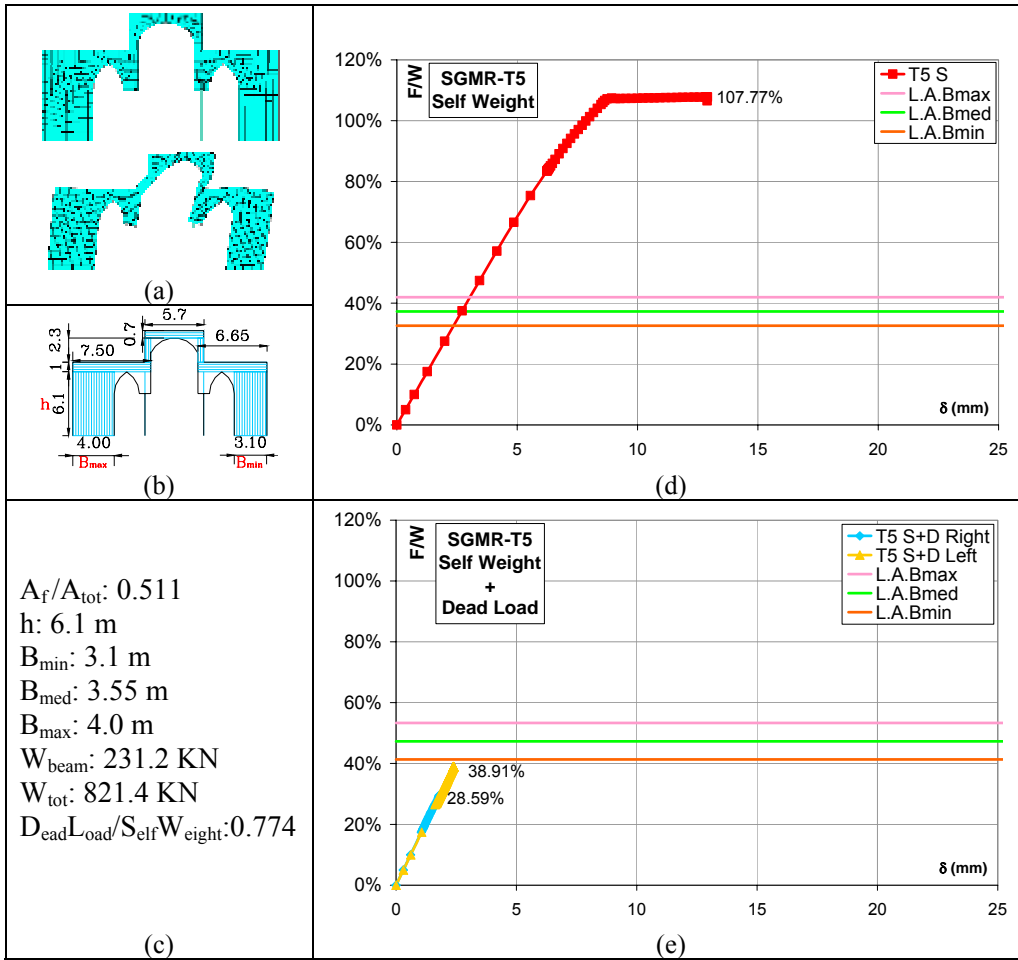
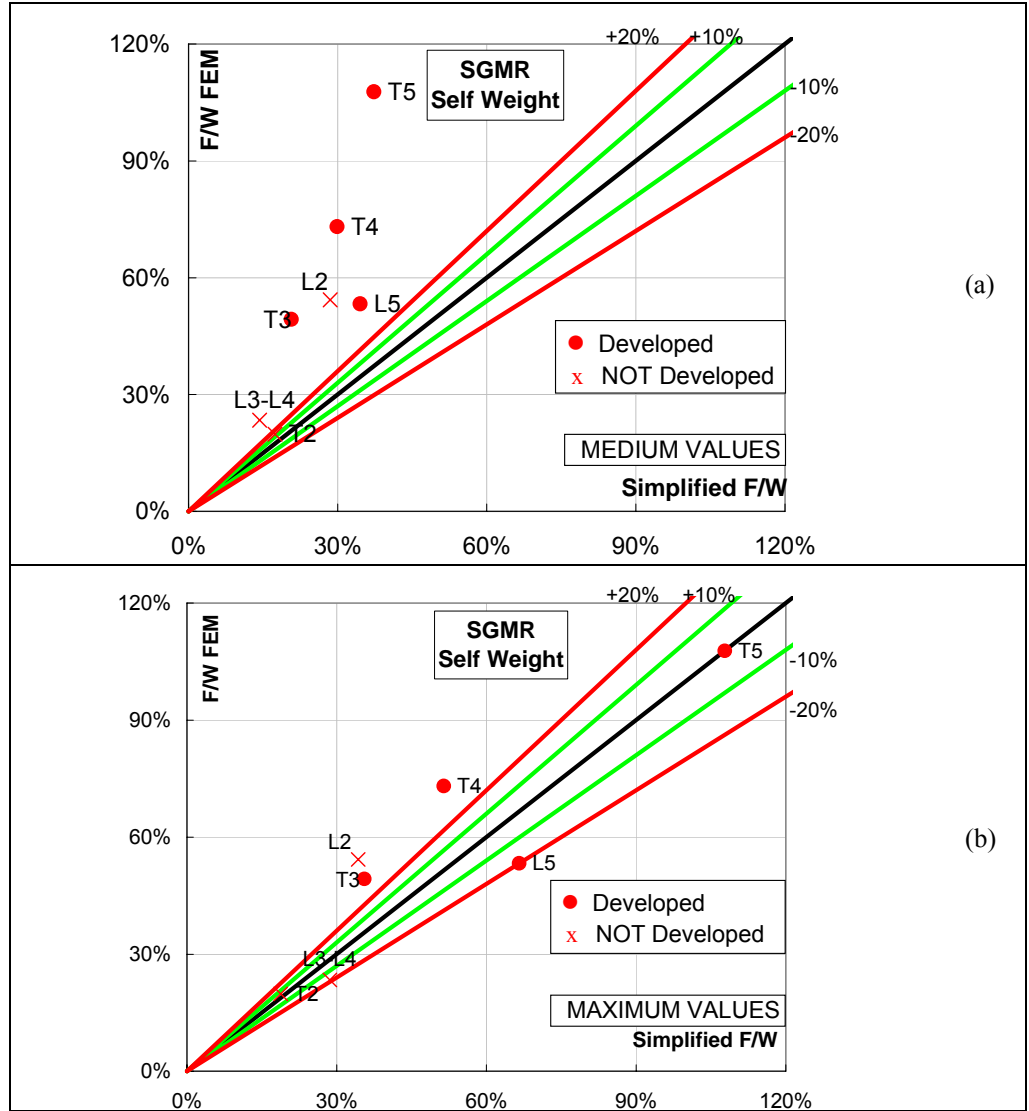


Figure 10. T5 macroelement – a) Mesh; b) Modelling; c) Simplified analysis data; d & e) Force/Displacement curves.

In this macroelement, two marble columns are present. The non linear curve in the “self weight” diagram reaches an horizontal branch but the values given by limit analysis are three time smaller. In the second diagram, the two methodologies provide close values but the non linear curves have stopped still in the crescent branch, so that the values are not necessarily reliable.

**3.1.1. SUMMARY OF THE SGMR RESULTS**

In Figure 11 the comparison between the result obtained with the non linear analyses and the simplified approach for all the considered macroelements is depicted.



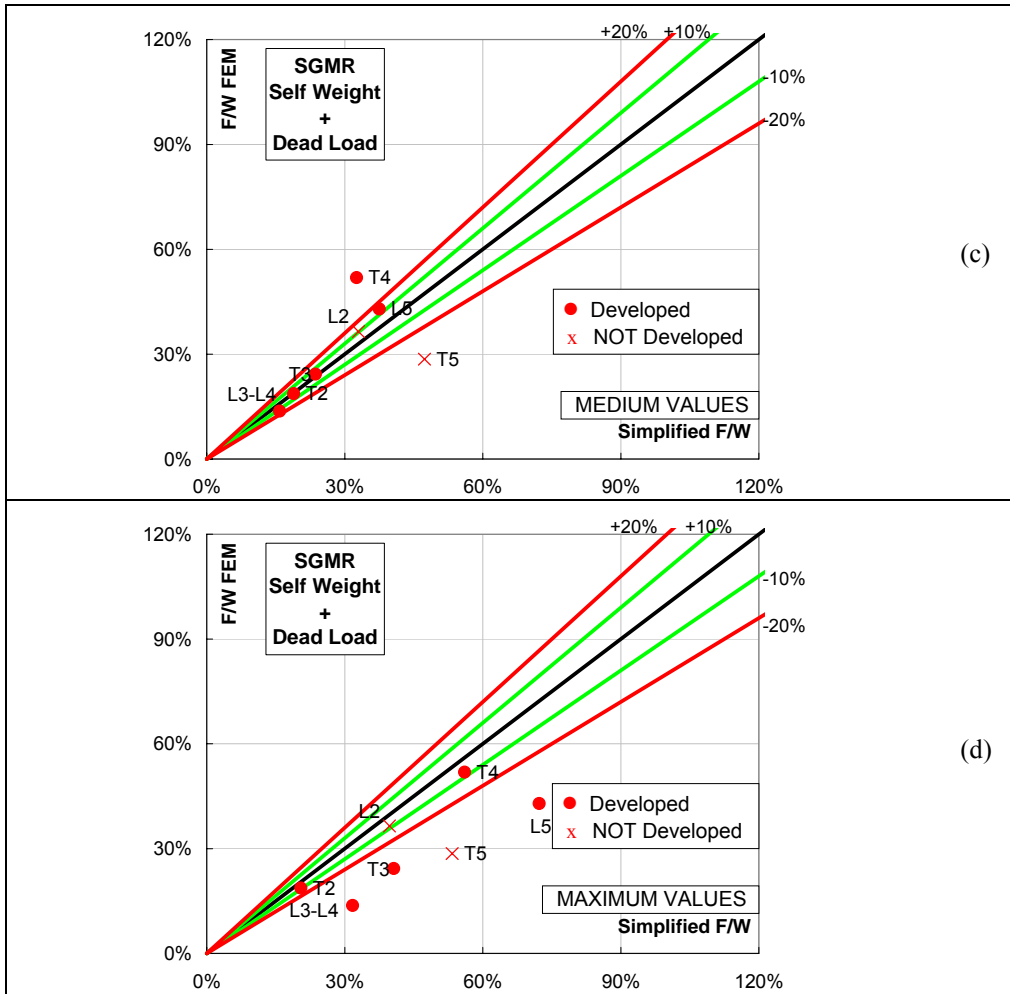


Figure 11. SGMR – Summary of the results.

Fig. 11.a and 11.b report the results relevant to the case with only the self weight varying the chosen dimension for piers in the simplified analysis. Therefore, in the two plots, the values of non linear analysis will be the same (ordinate value) whilst the limit analysis values (on the abscissa), moving from one diagram to the other one, will assume greater values. Likewise, in Fig. 11.c and 11.d the diagrams with self weight plus dead load are reported. The diagonal line represents zero scatter between the two analyses while the other ones progressively less close represent  $\pm 10\%$  and

$\pm 20\%$  scatters. A point inside the domain defined by the constant scatter lines will mean that a small percentage of error exists. Two symbols have been chosen to represent the placing of the macroelements: according to the opinion of the author, the dot is for the developed curves and the cross when the curve is not considered wholly developed. It is fairly clear that in Fig. 11.a the values are generally in the upper part of the diagram (meaning that the non linear analyses give greater collapse multipliers than in the simplified approach) and move inside the domain if the maximum values of the piers are considered. In the following plot (Fig. 11.c), on the contrary, smaller scatters are evidenced between the two approaches. Therefore, when the maximum size of the piers is considered, the values move on the right part on the bottom.

### 3.2 S. IPPOLISTO

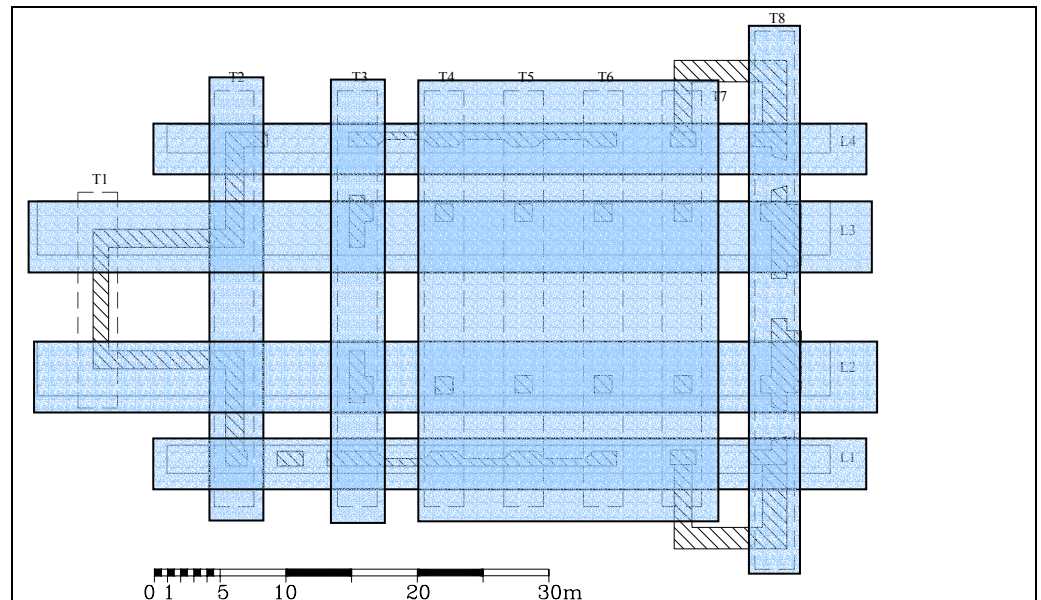


Figure 12. SI – Individuation of the macroelements in the plant.

The plan of SI with the individuation of the considered macroelements is shown in Fig. 12.

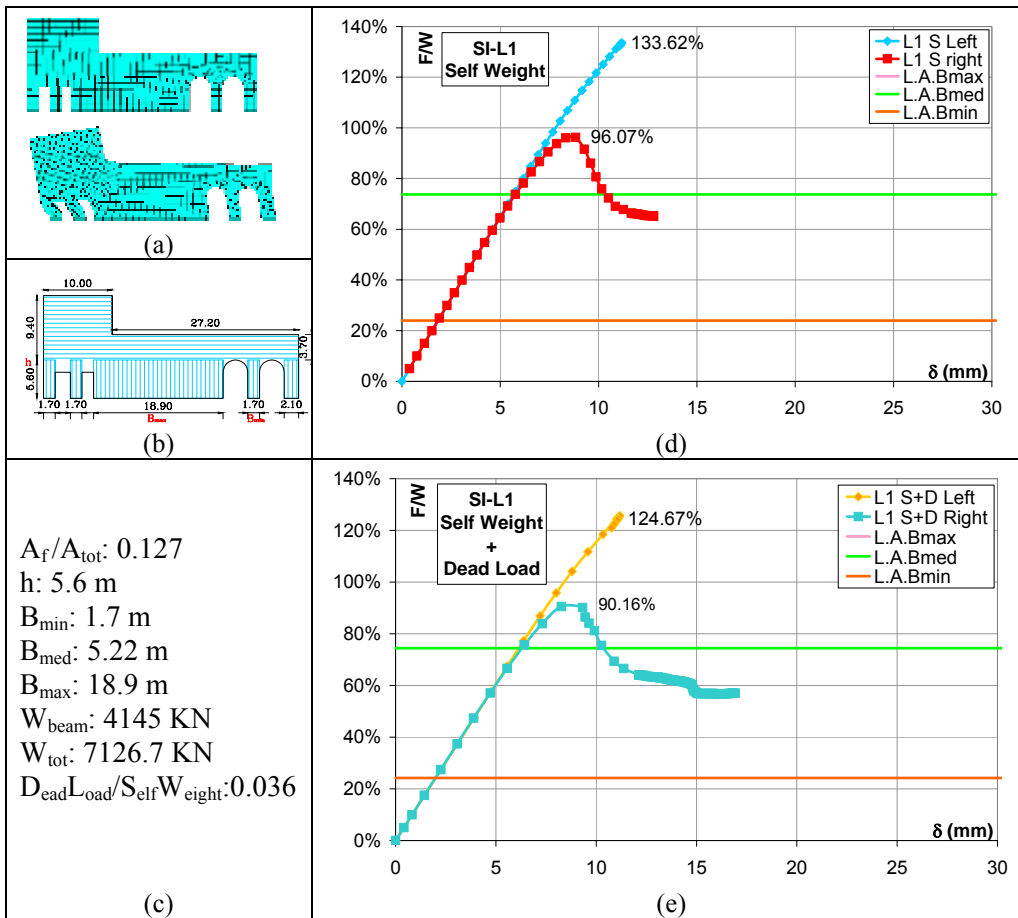


Figure 13. L1 macroelement – a) Mesh; b) Modelling; c) Simplified analysis data; d & e) Force/Displacement curves.

The L1 macroelement is so slightly loaded by the dead load that the non linear curves and the simplified values in both the graphs are similar. As it can be noticed in the two plots, the weakest behaviour is when the forces come from the right verse. The values at the collapse are close to the simplified evaluation when the medium base is considered.

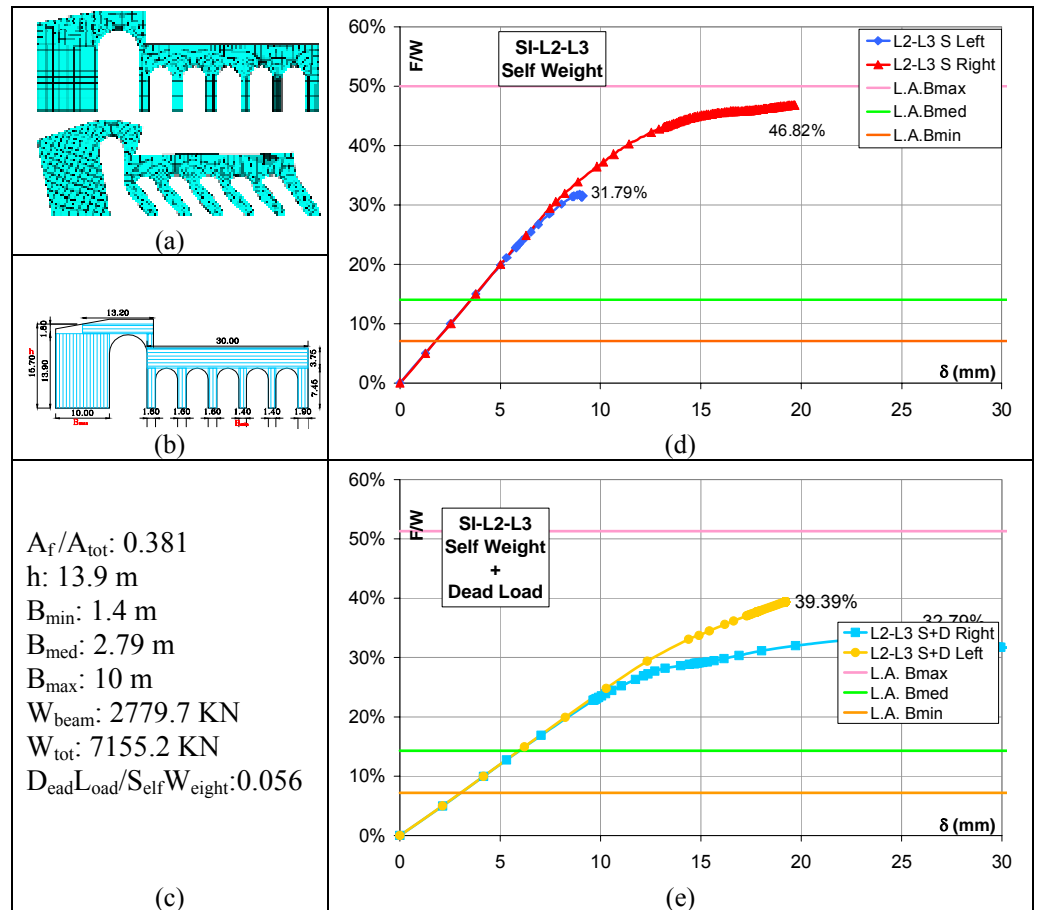


Figure 14. L2-L3 macroelements – a) Mesh; b) Modelling; c) Simplified analysis data; d & e) Force/Displacement curves.

The L2 and L3 macroelements present the classical mixed mechanism for the presence of a series of small piers along the nave of the church and a stocky panel in correspondence of the apse. It's evident how the simplified methodology is not able to catch the real behaviour of the element, because of the choice of a unique mechanism (the storey one in this case). The values reached with the non linear analyses are inside the range of the simplified formula evaluated with medium and maximum value of the base.

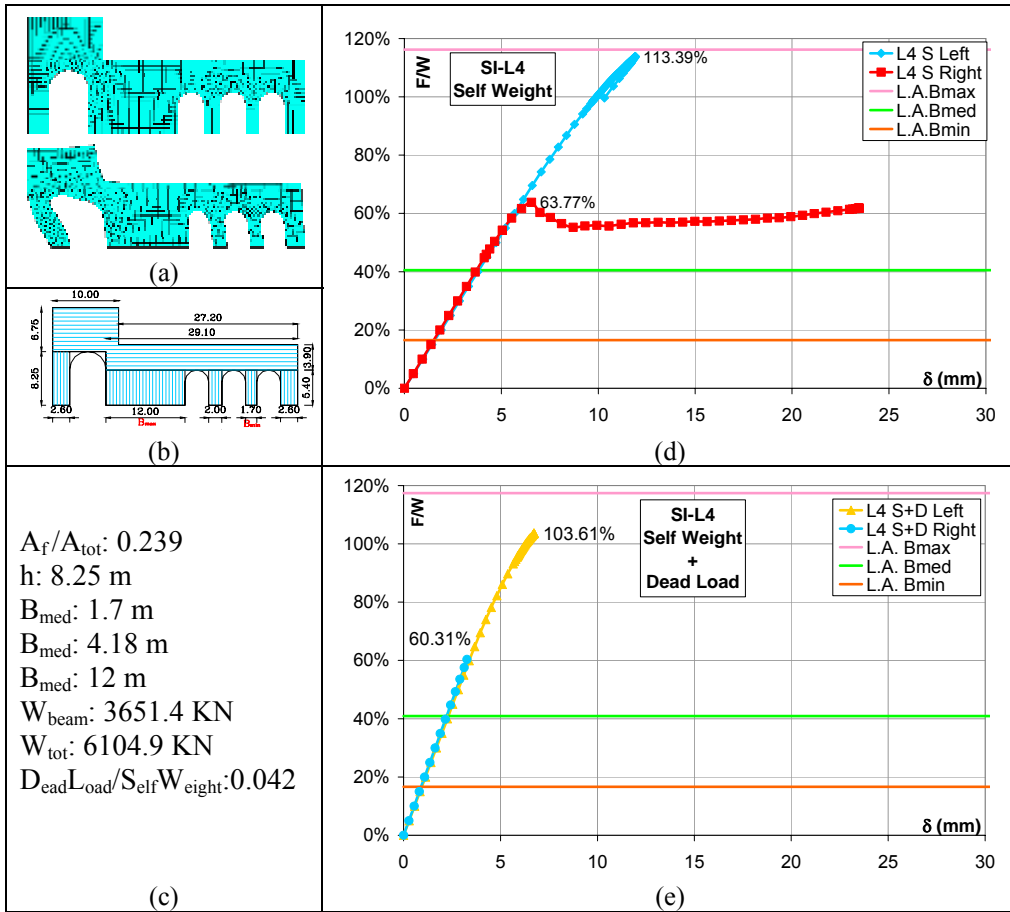


Figure 15. L4 macroelement – a) Mesh; b) Modelling; c) Simplified analysis data; d & e) Force/Displacement curves.

In Fig. 15, although the difference of the two cases is just of 4.2%, the two curves for horizontal forces coming from the right side are different. While in the first one, the plastic branch is reached, in the second one the analysis stops some steps before reaching the horizontal plateau. The two cases don't match well with the simplified analyses



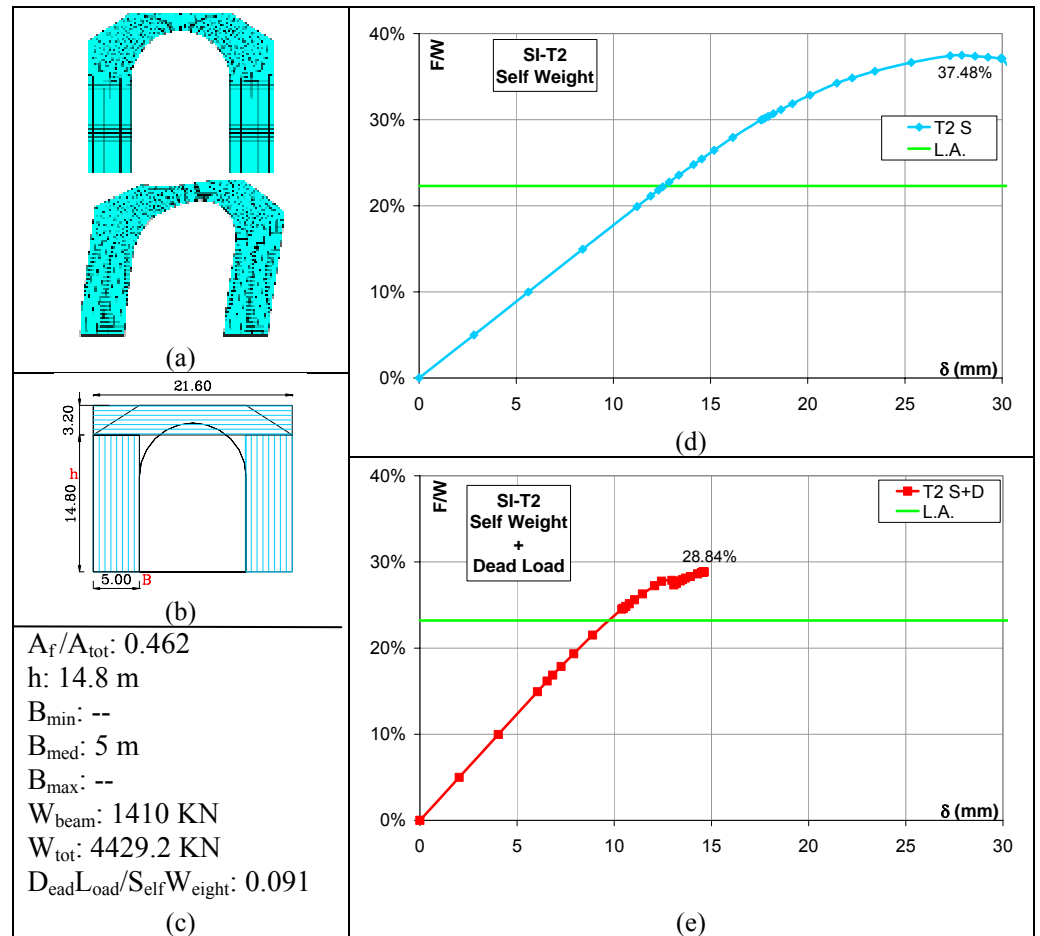


Figure 16. T2 macroelement – a) Mesh; b) Modelling; c) Simplified analysis data; d & e) Force/Displacement curves.

Although the triumphal arch in Fig. 16 is similar to a simple portal, the limit analysis values are smaller than the collapse multiplier calculated with the non linear analysis. In the second graph the values match better than the first one because of the smaller response given by ABAQUS.

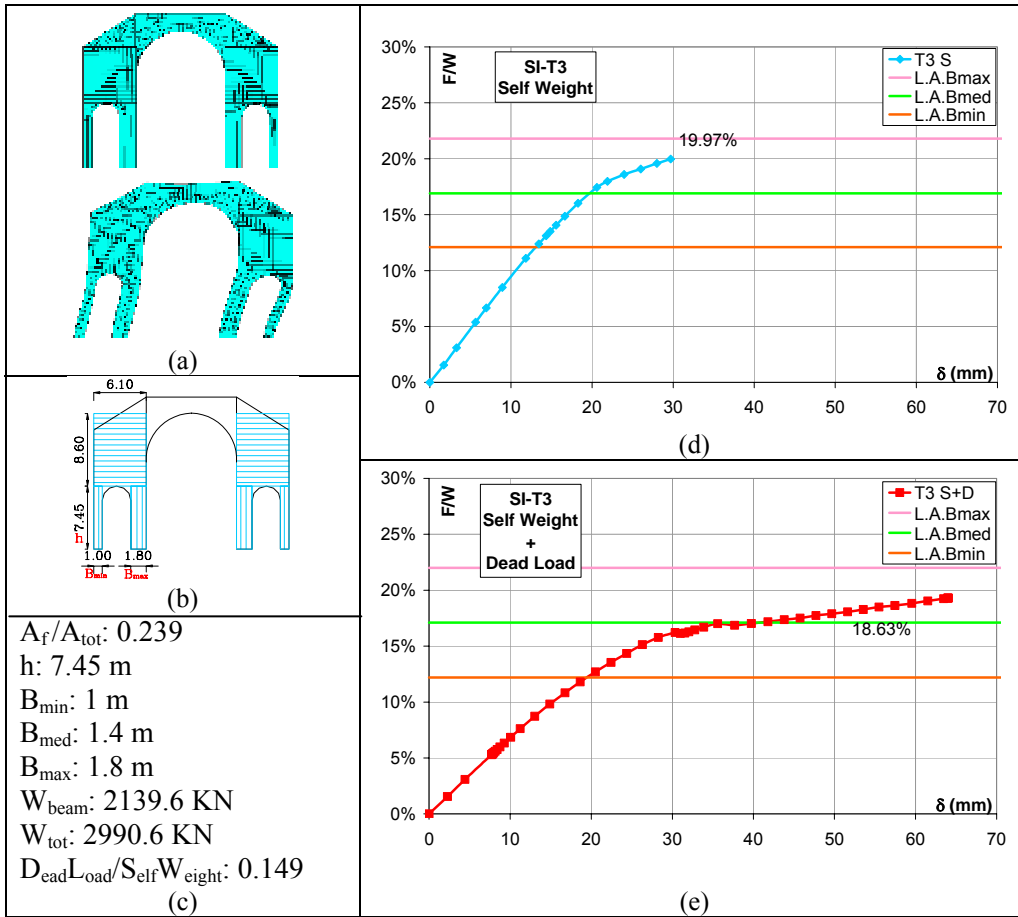


Figure 17. T3 macroelement – a) Mesh; b) Modelling; c) Simplified analysis data; d & e) Force/Displacement curves.

A good comparison between the two approaches has been verified in the second plot. In the first one, greater scatters are present.

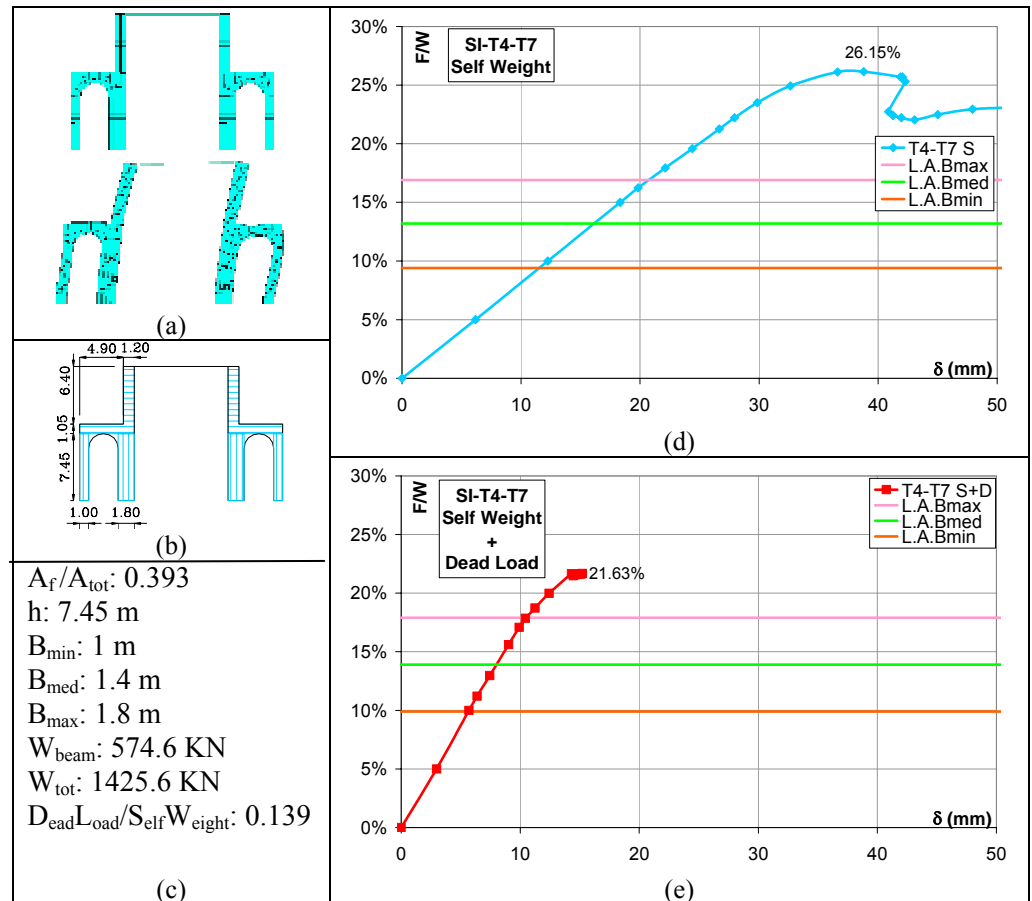


Figure 18. T4 - T5 - T6 - T7 macroelements – a) Mesh; b) Modelling; c) Simplified analysis data; d & e) Force/Displacement curves.

These inner elements are symmetrical around the Y axis so that only one curve is necessary per each load condition. The values reached through non linear analyses are larger than the values estimated by limit analyses in both the load conditions and, also in the hypothesis of different values of the base.

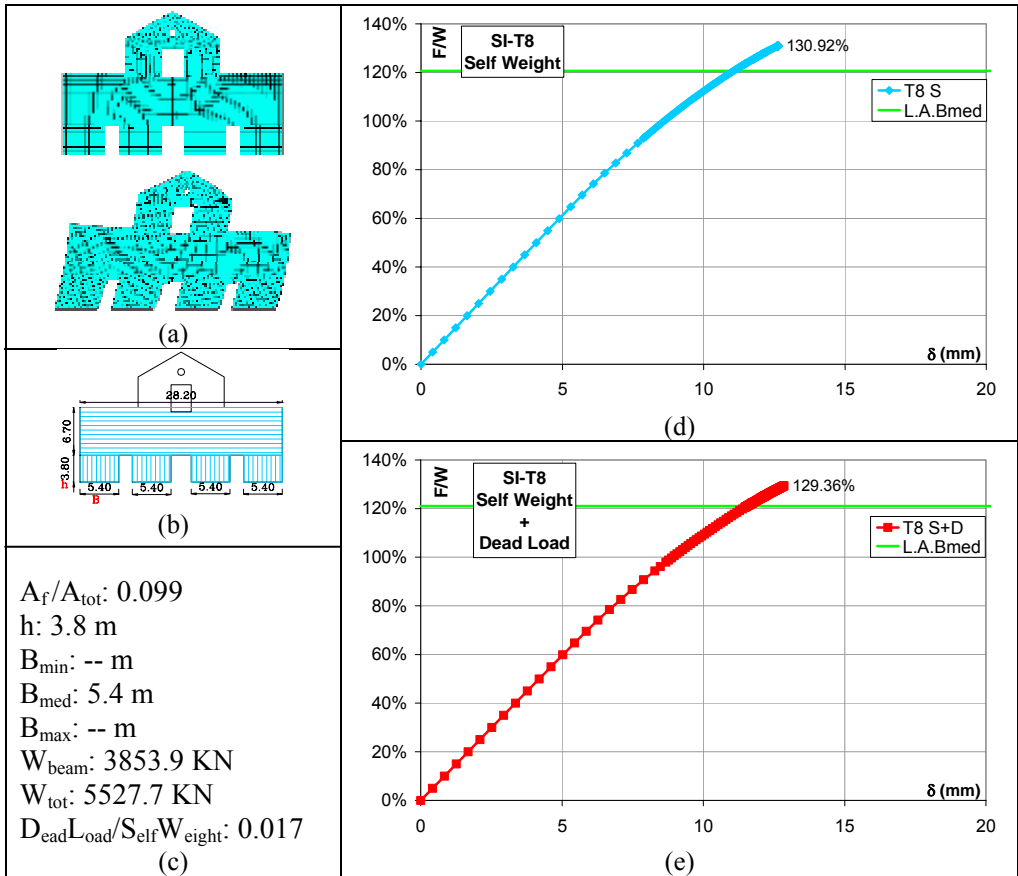
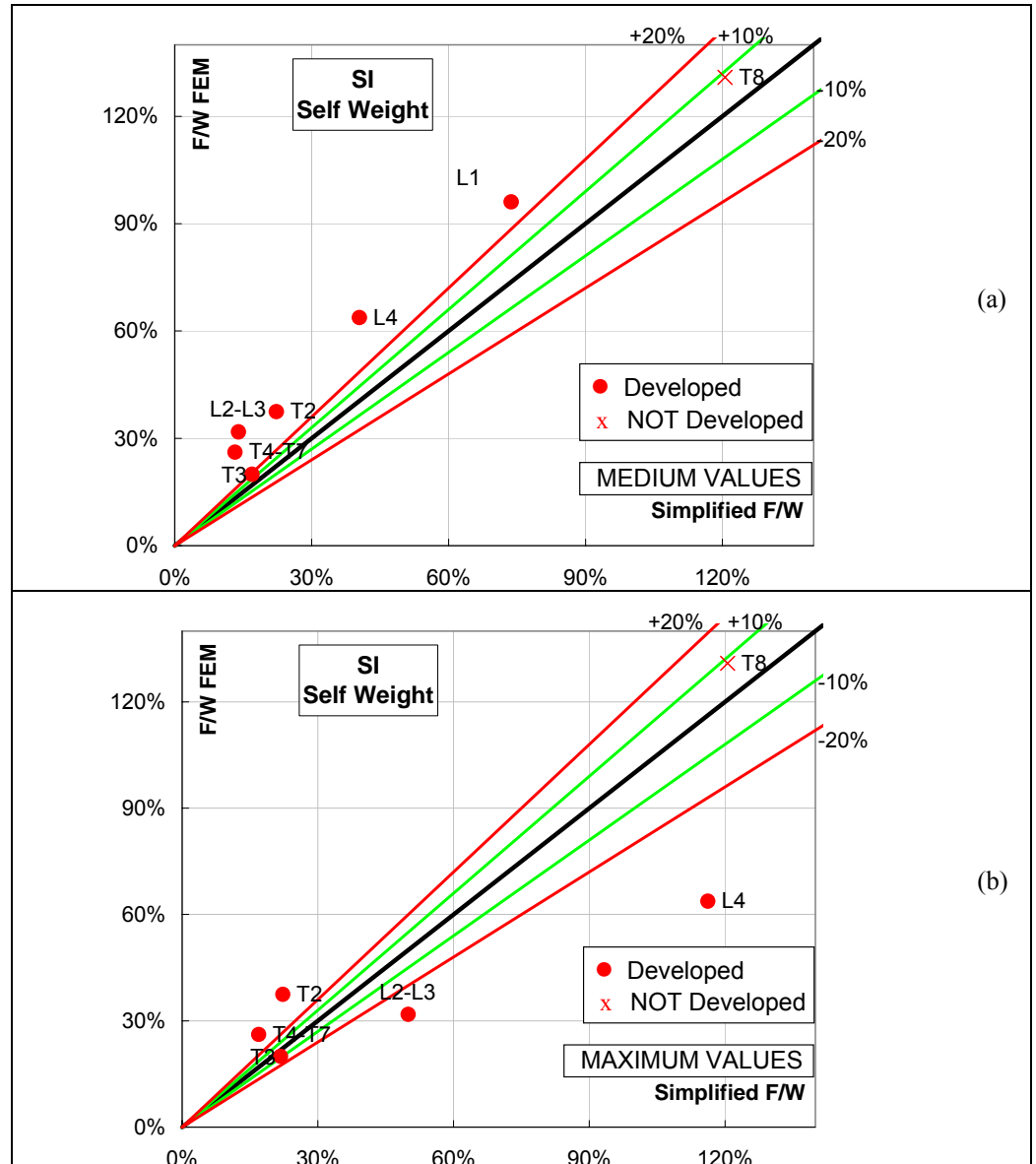


Figure 19. T8 macroelement – a) Mesh; b) Modelling; c) Simplified analysis data; d & e) Force/Displacement curves.

The façade of the SI church has a mass location on the top so that the storey mechanism has been considered. A good comparison in both the plots can be noticed.

### 3.2.1. SUMMARY OF THE SI RESULTS

The summary of the results in both the load conditions for the minimum and maximum size of the piers are reported in Fig. 20.



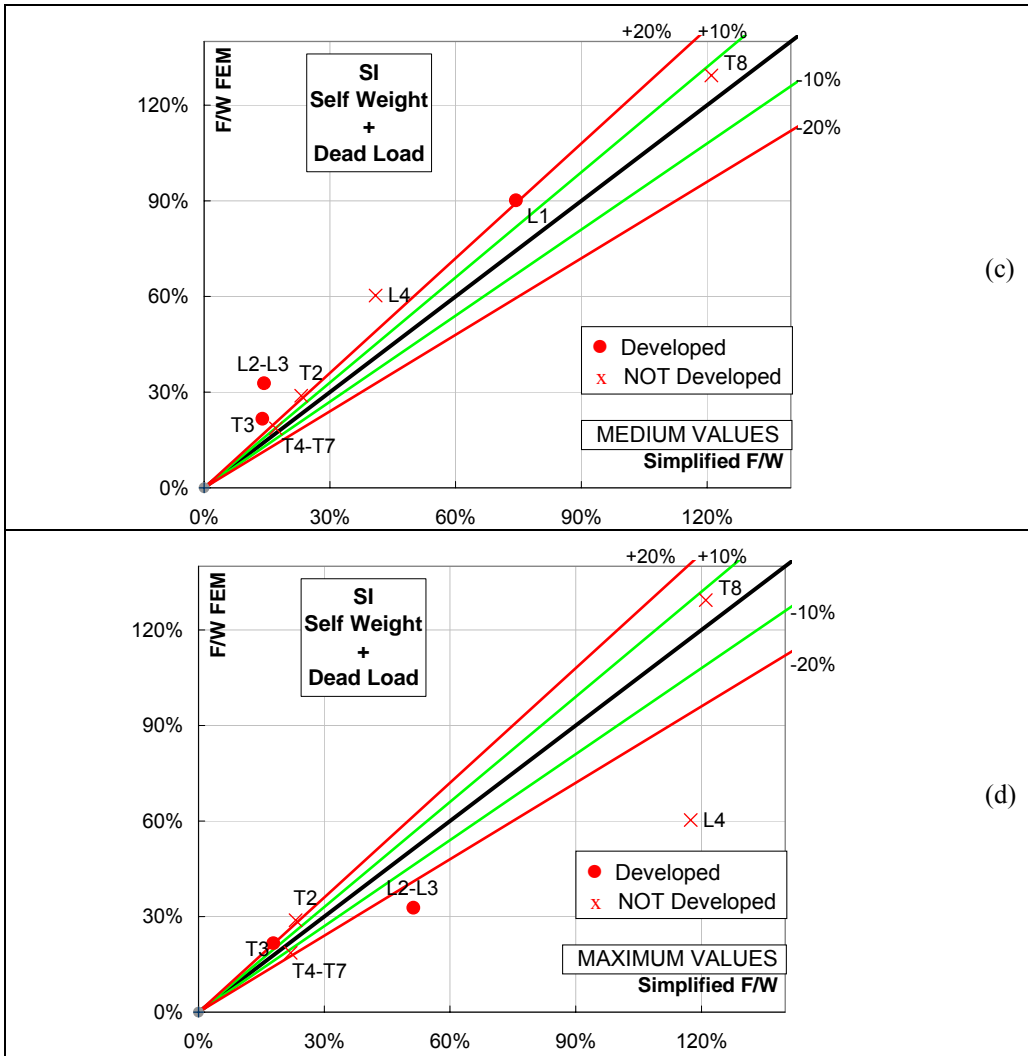


Figure 20. SI – Summary of the results.

Also in this case, the values of the collapse multiplier are generally safer according to the limit analysis than the non linear approach when the medium values are considered. And again, the case of self weight plus dead loads matches better than the other one.

### 3.3. S. GIOVANNI MAGGIORE

In Figure 21 the considered elements are enlightened.

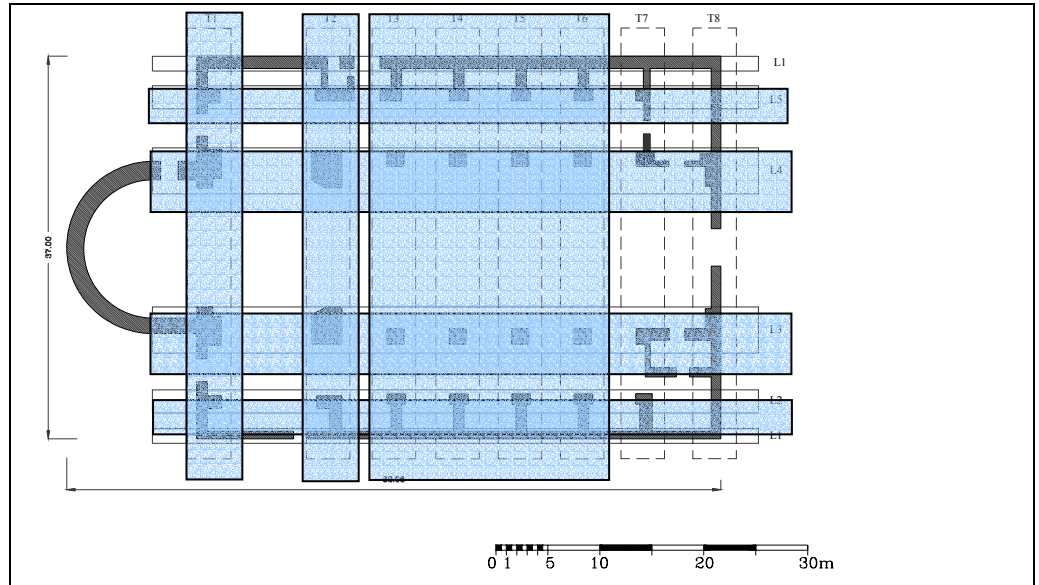


Figure 21. SGMG – Individuation of the macroelements in the plant.

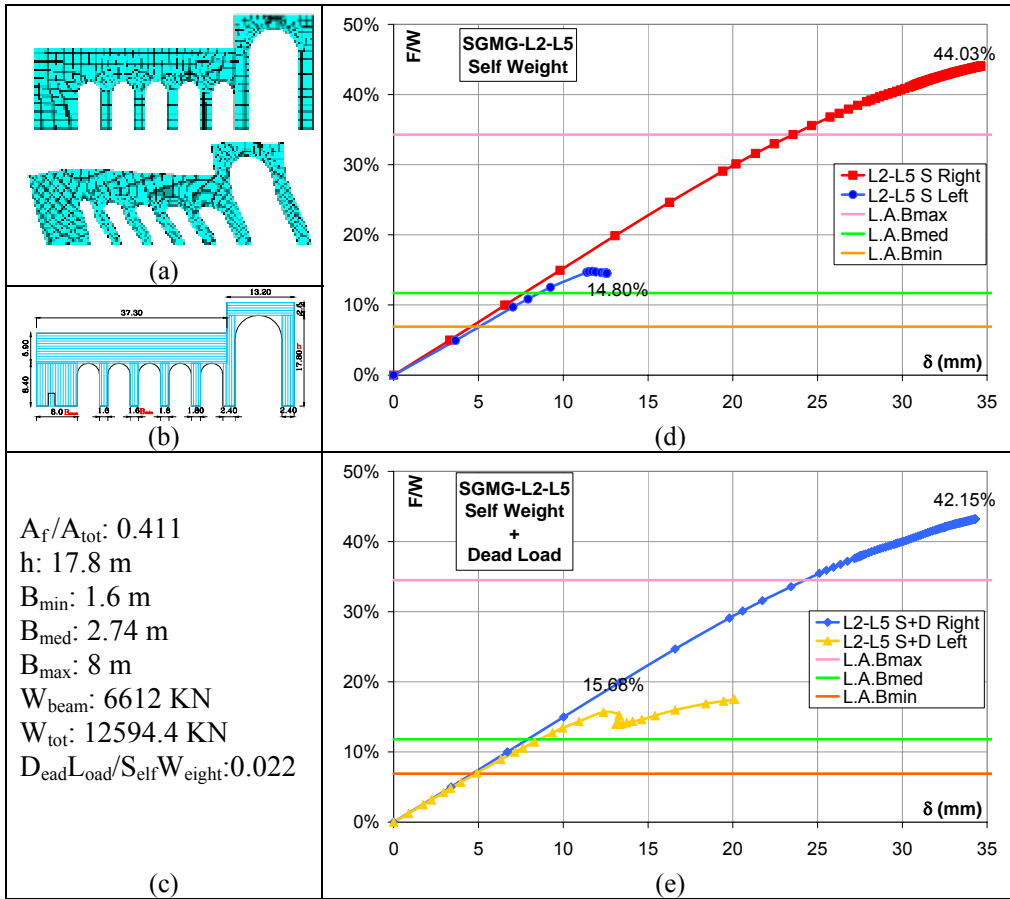


Figure 22. L2 & L5 macroelements – a) Mesh; b) Modelling; c) Simplified analysis data; d & e) Force/Displacement curves.

These longitudinal arcades inside the church show a storey mechanism. In both of the load condition the non linear analysis for horizontal actions coming from the left side are more penalizing. These values are close to the limit analysis value when the medium dimension of the piers is considered.



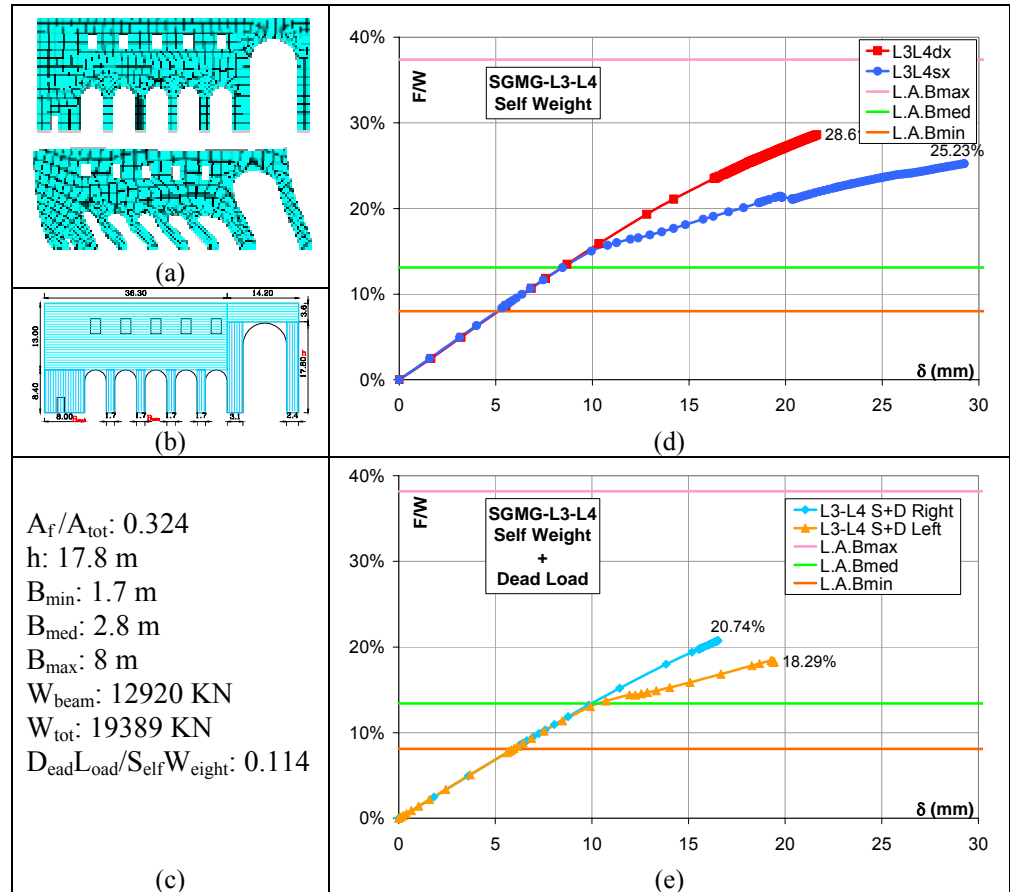


Figure 23. L3 & L4 macroelements – a) Mesh; b) Modelling; c) Simplified analysis data; d & e) Force/Displacement curves.

The analyses carried out with the non linear code show a consistent behaviour with close values for actions coming in the two directions. Unfortunately the scatter between these values and the limit state analyses are too large to consider the modelling a good result for the self weight load case. Fairly better the case in which the dead load is considered as well.

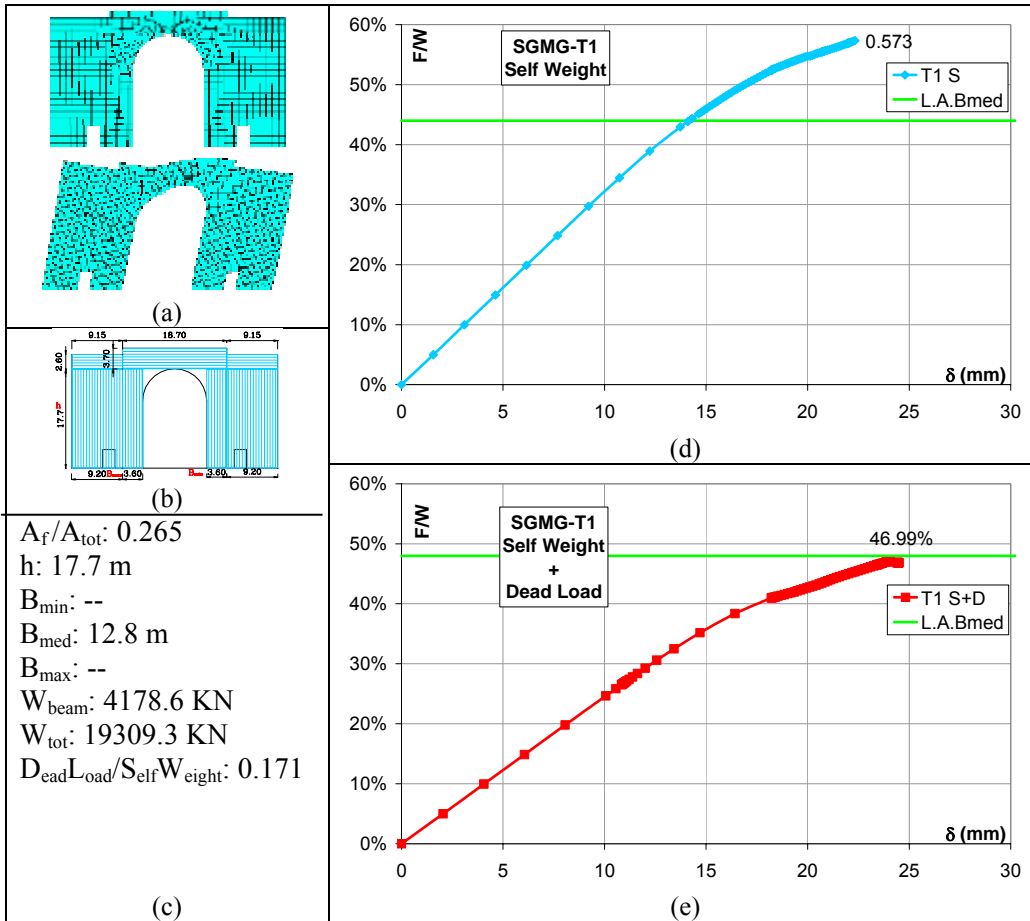


Figure 24. T1 macroelement – a) Mesh; b) Modelling; c) Simplified analysis data; d & e) Force/Displacement curves.

The first triumphal arch of this church is similar to a simple portal. Although this fact is clearly shown, the comparison between the two type if analyses is good only in the second case. In particular, in the first one the value of the non linear analysis overcomes the limit one and in the second it approaches it. The percentage of dead load over the self weight is around 17% but the results are quite different.

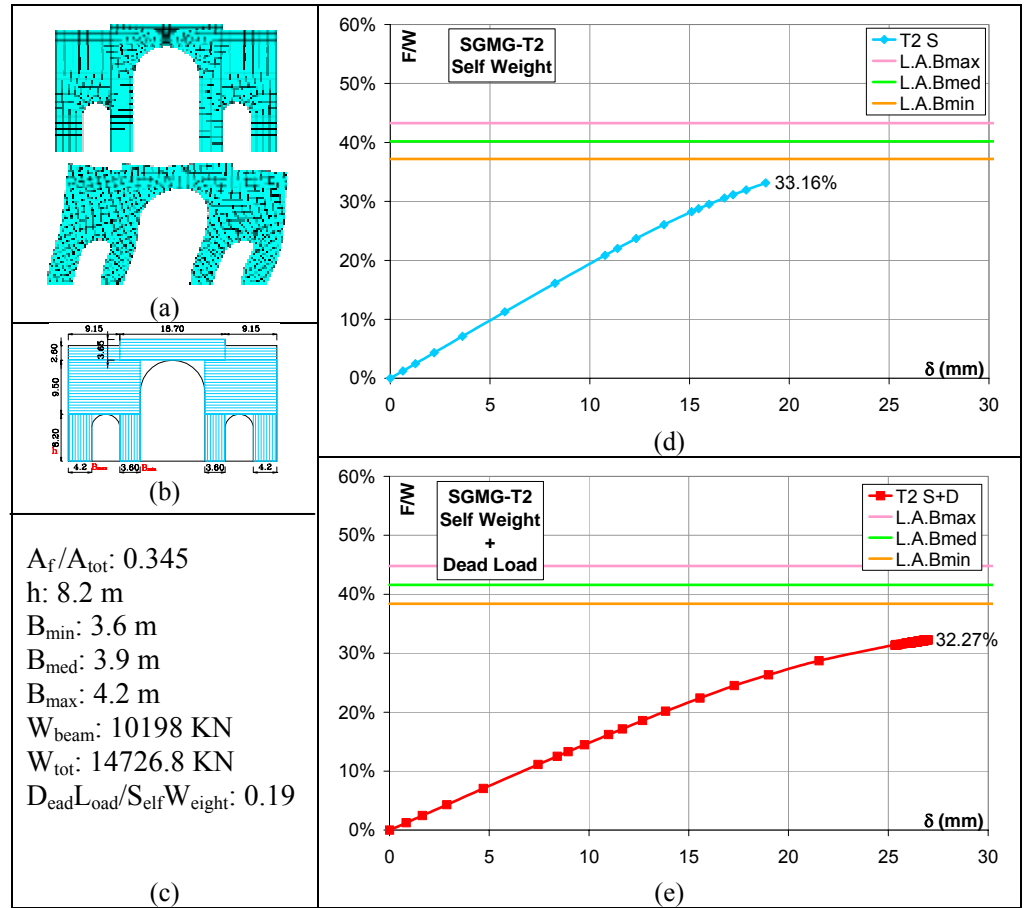


Figure 25. T2 macroelement – a) Mesh; b) Modelling; c) Simplified analysis data; d & e) Force/Displacement curves.

The second triumphal arch of SGMG presents again the classical behaviour of a portal frame. Indeed, the results of the non linear and limit analyses agree fairly well in both cases.

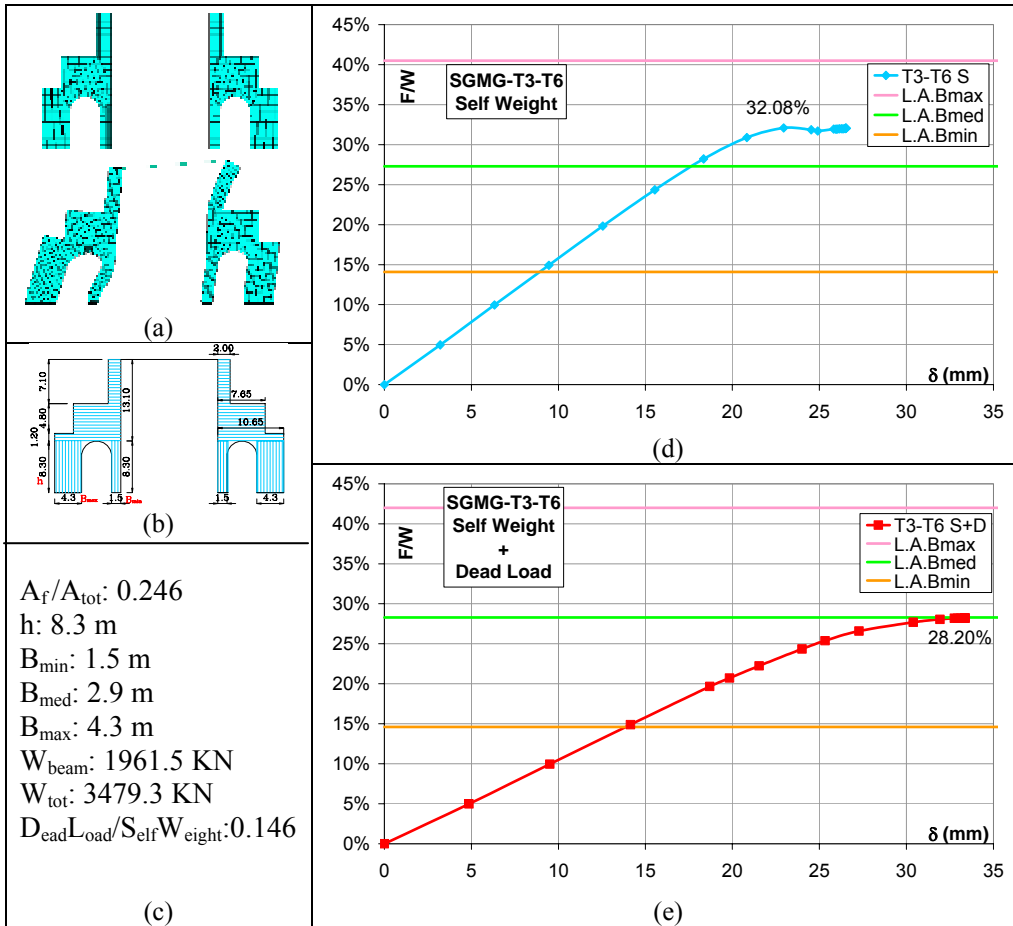
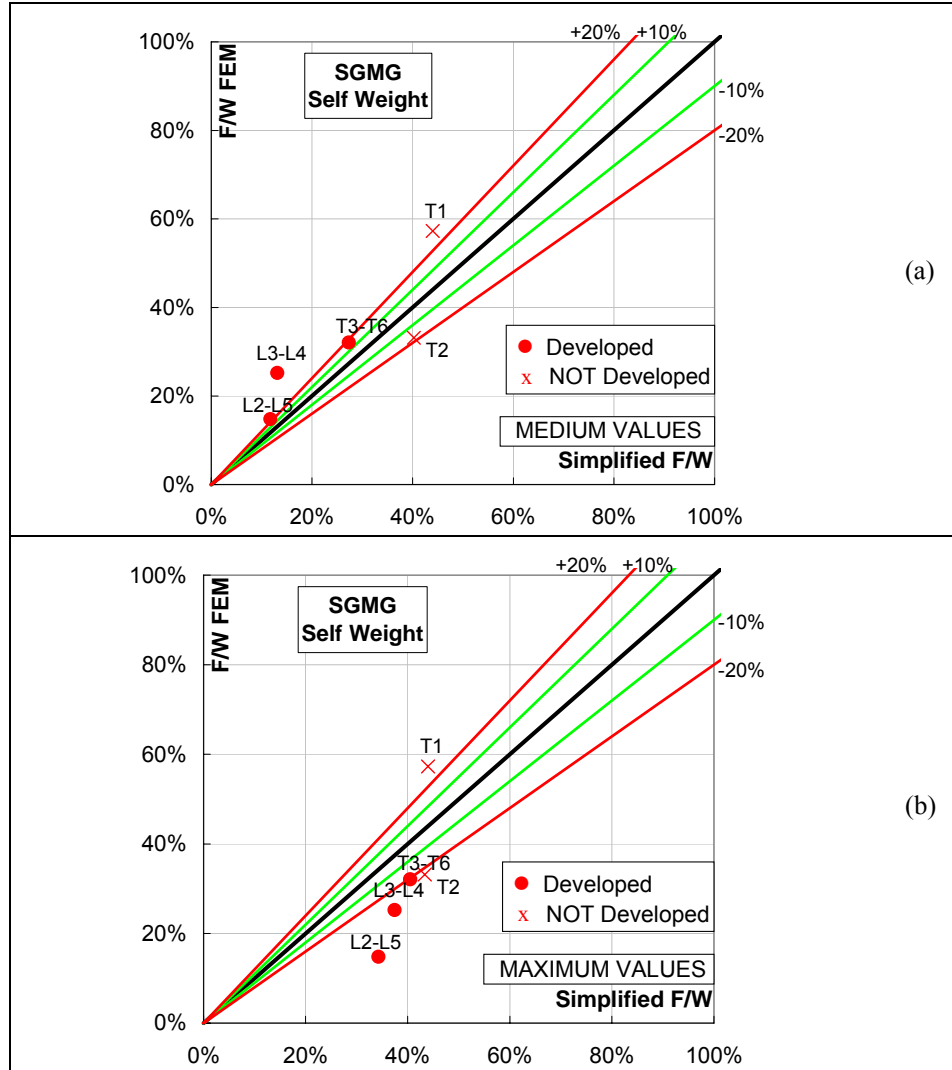


Figure 26. T3 – T4 – T5 – T6 macroelement – a) Mesh; b) Modelling; c) Simplified analysis data; d & e) Force/Displacement curves.

A good match can be noticed in these transversal elements of the church between the two adopted methodologies. Because of the difference between the dimensions of the piers, the simplified analysis gives distant results of the collapse multiplier value. About the non linear analyses, both of them reach a sub-horizontal branch, meaning that the maximum capacity has been reached.

**3.3.1. SUMMARY OF THE SGMG RESULTS**

In Figures 27, the summary of the conducted analyses are reported. In this case, the medium values considered in the simplified analysis match better than the ones with the maximum dimensions. The results are fairly inside the cone of the 20% scatters.



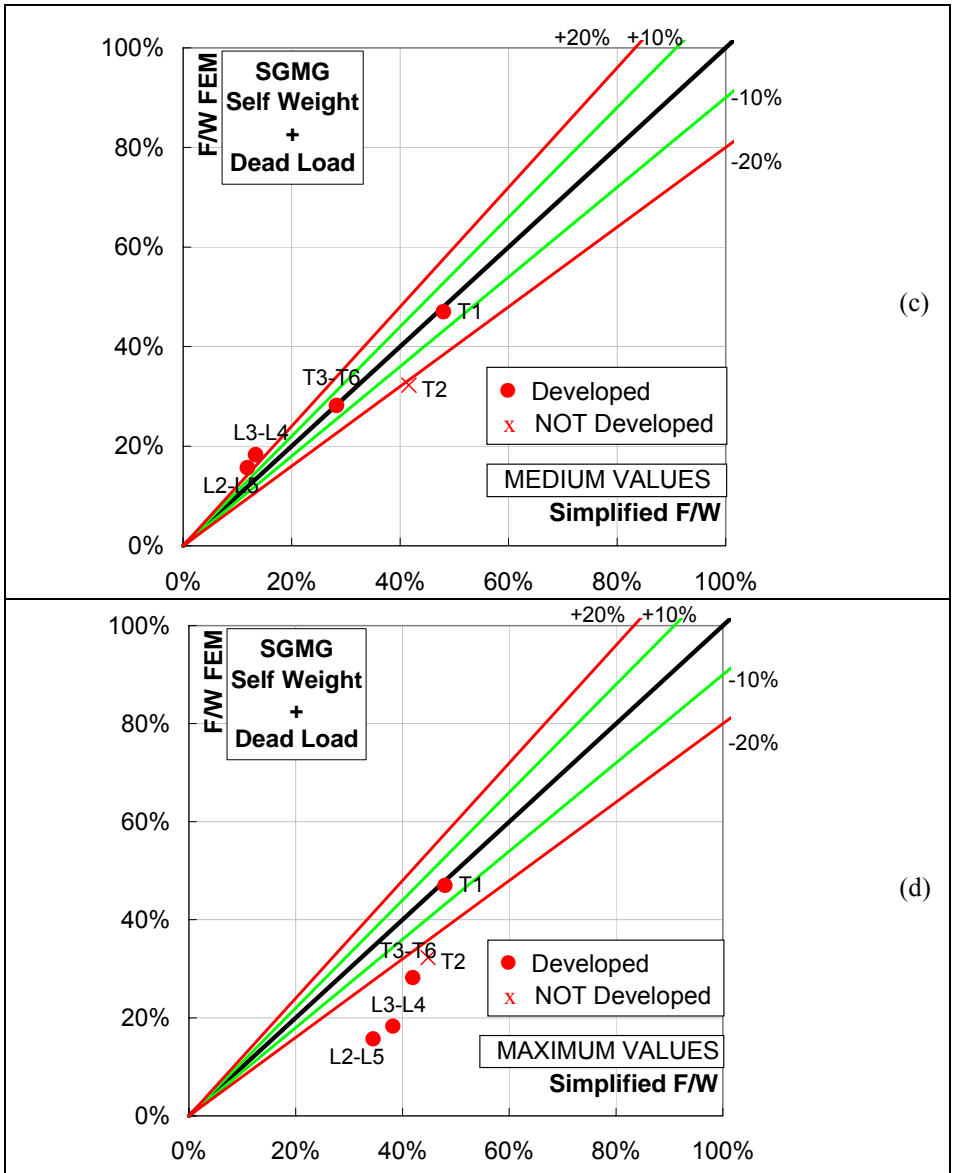


Figure 27. SGMG – Summary of the results.

### 3.4. S. PAOLO MAGGIORE

In Fig. 28 the considered macroelements are enlightened.

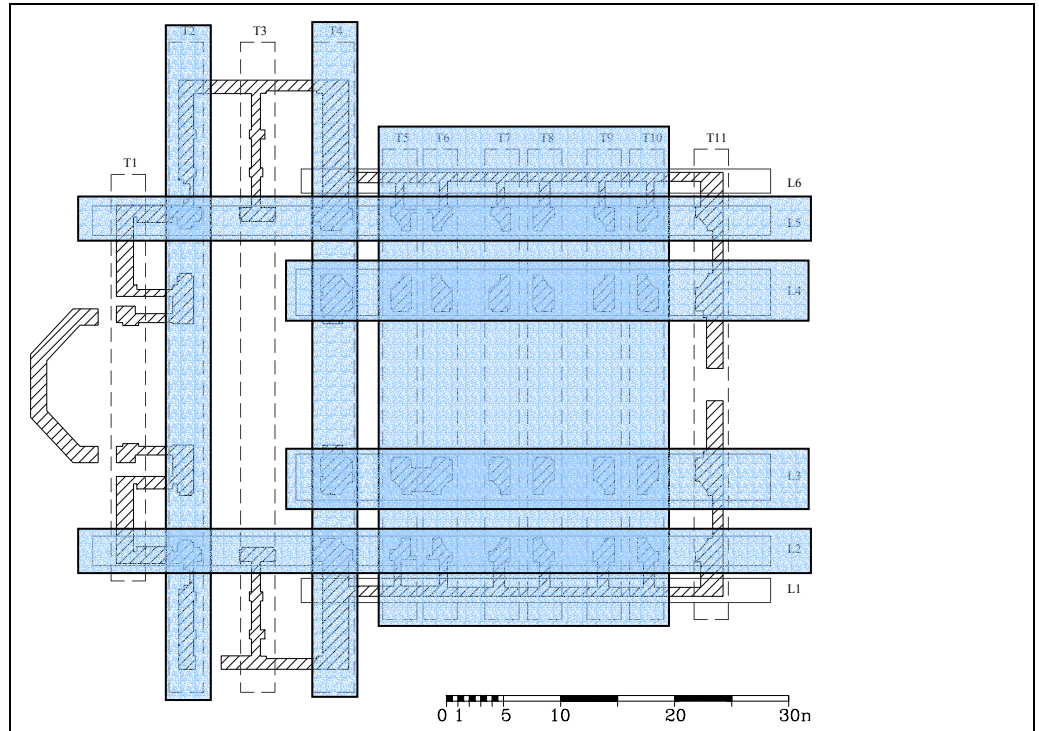


Figure 28. SP – Individuation of the macroelements in the plant.

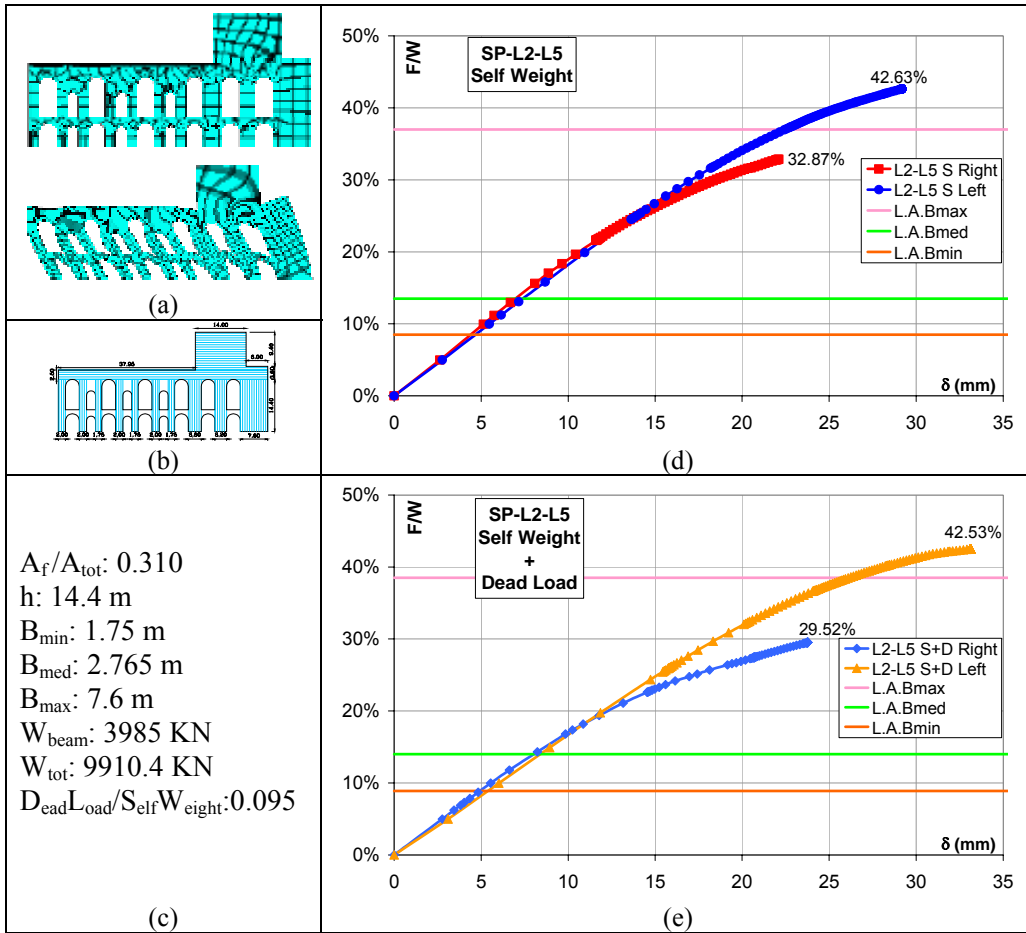


Figure 29. L2 – L5 macroelements – a) Mesh; b) Modelling; c) Simplified analysis data; d & e) Force/Displacement curves.

The non symmetry in the geometry and in the dead load has lead to four non different analyses. The small dimension of most of the piers has held to a fairly small collapse value. The non linear analyses are closer to the simplified approach if the maximum base is considered.



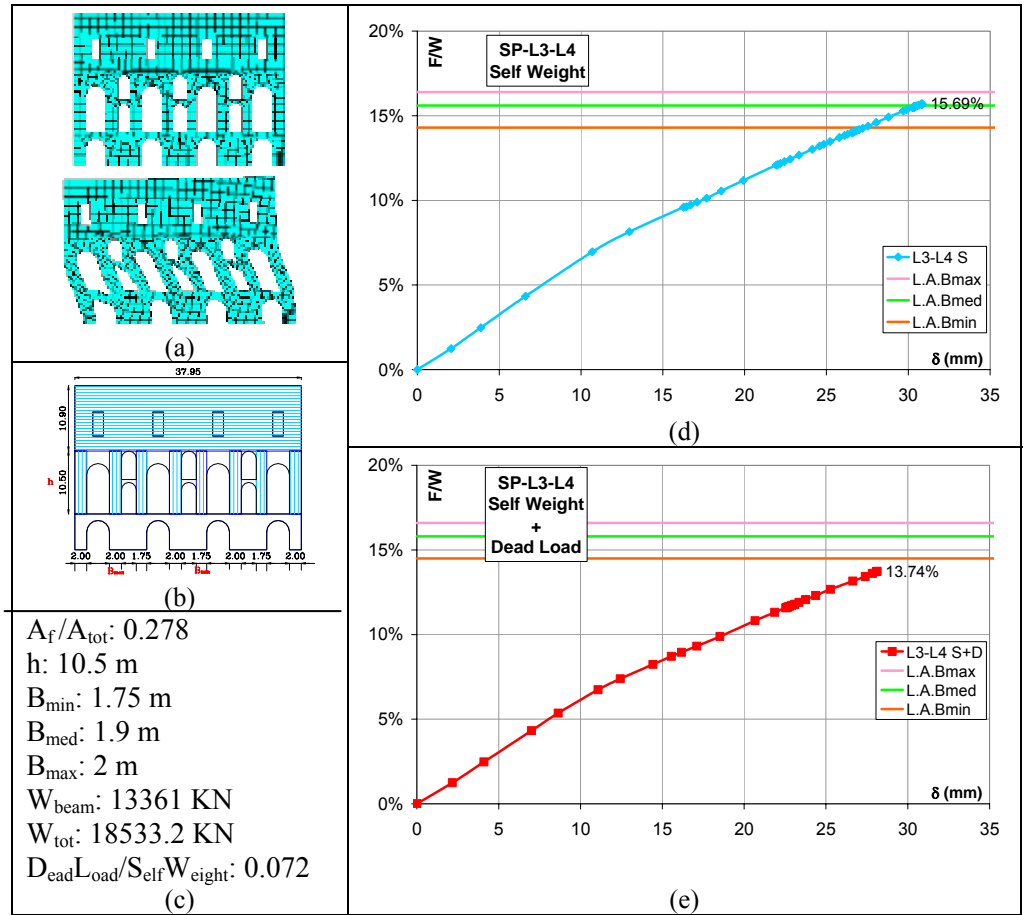


Figure 30. L3 – L4 macroelements – a) Mesh; b) Modelling; c) Simplified analysis data; d & e) Force/Displacement curves.

The inner arcade of SP shows a good match between the two methodologies although the non linear analyses do not develop completely in the plastic branch. It is worth noting that the simplified geometry has to consider the possible deformed shape under horizontal actions; in this case, because the base of the macroelement is stockier than the upper part, it has not been considered in the evaluation of the involved masses.

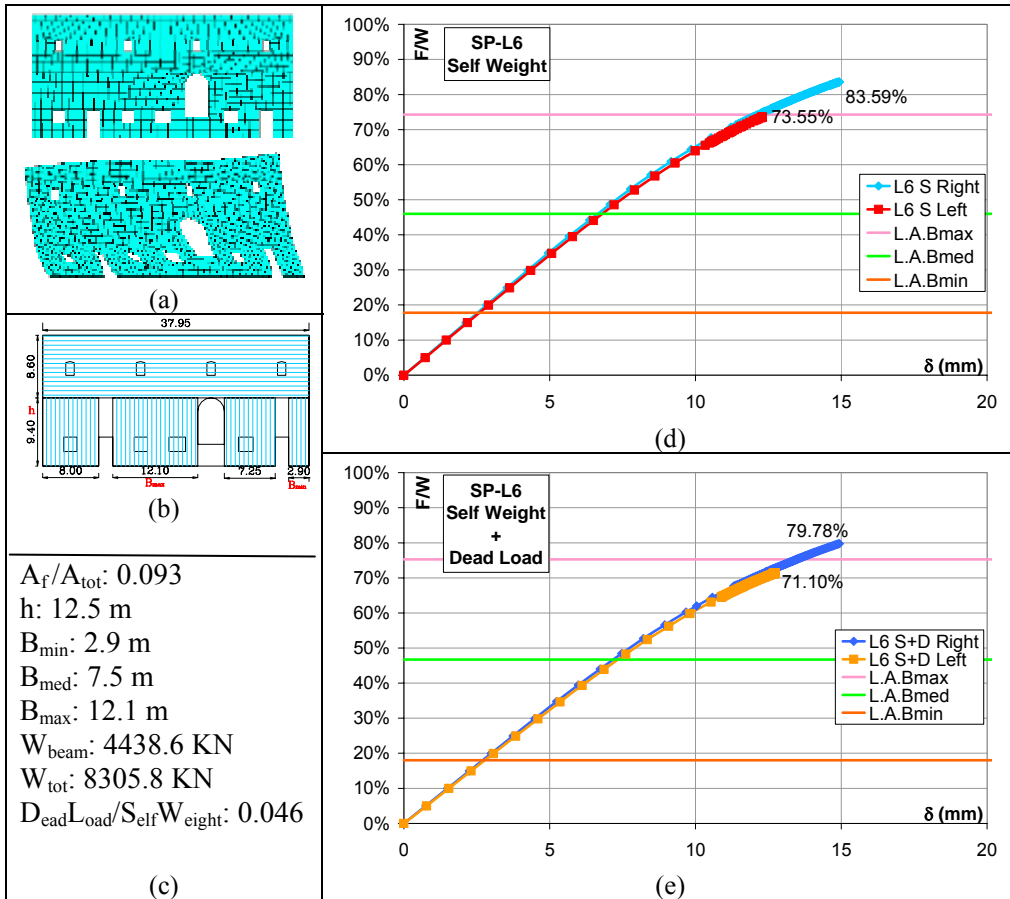


Figure 31. L6 macroelement – a) Mesh; b) Modelling; c) Simplified analysis data; d & e) Force/Displacement curves.

The ratio of the openings compared to the whole surface of this macroelement has been conducted to assimilate this macroelement to a portal frame panel. The values of the maximum base in the simplified analyses are fairly close to the non linear analyses results.

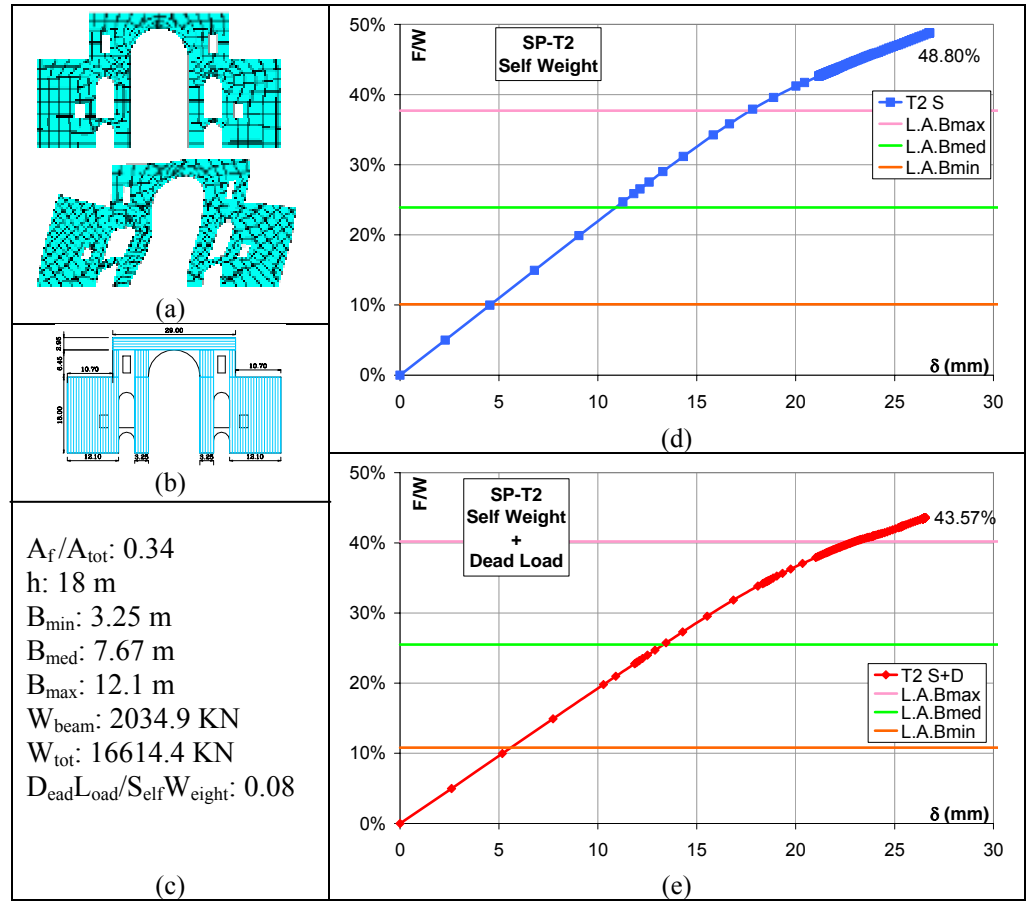


Figure 32. T2 macroelement – a) Mesh; b) Modelling; c) Simplified analysis data; d & e) Force/Displacement curves.

The storey mechanism individuated in the simplified geometry is not confirmed in the comparison with the non linear analysis whose values are fairly larger. In the models with and without the dead load, the values of the collapse multiplier are closer to the limit analysis when the maximum base of the piers is considered.

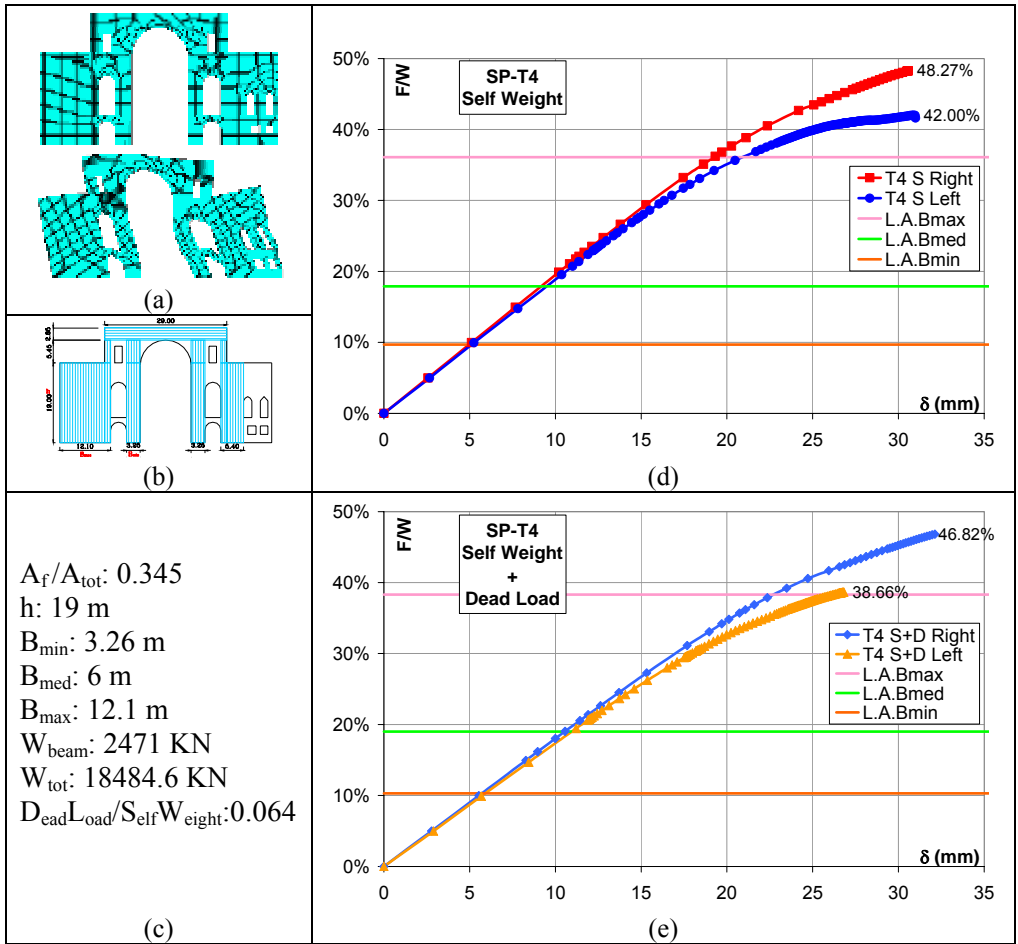


Figure 33. T4 macroelement – a) Mesh; b) Modelling; c) Simplified analysis data; d & e) Force/Displacement curves.

This transversal macroelement shows a fairly developed non linear branch. These values of the collapse multiplier are close to ones obtained using the maximum dimension of the pier instead of the medium one.

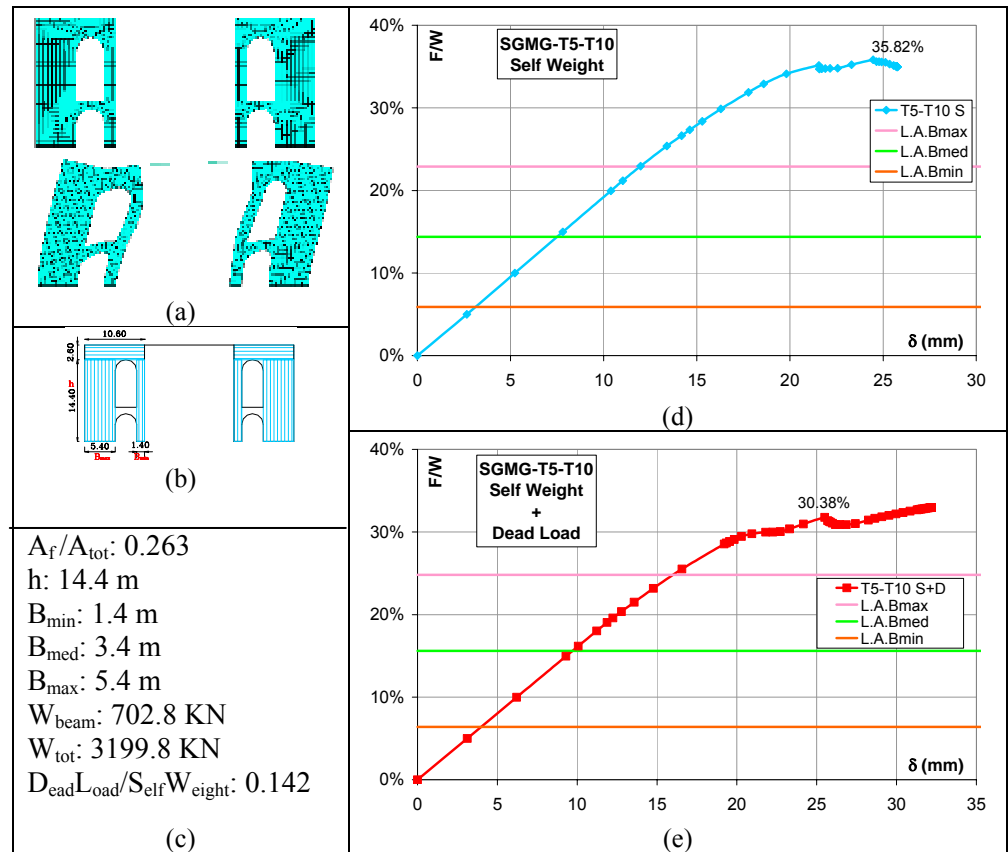
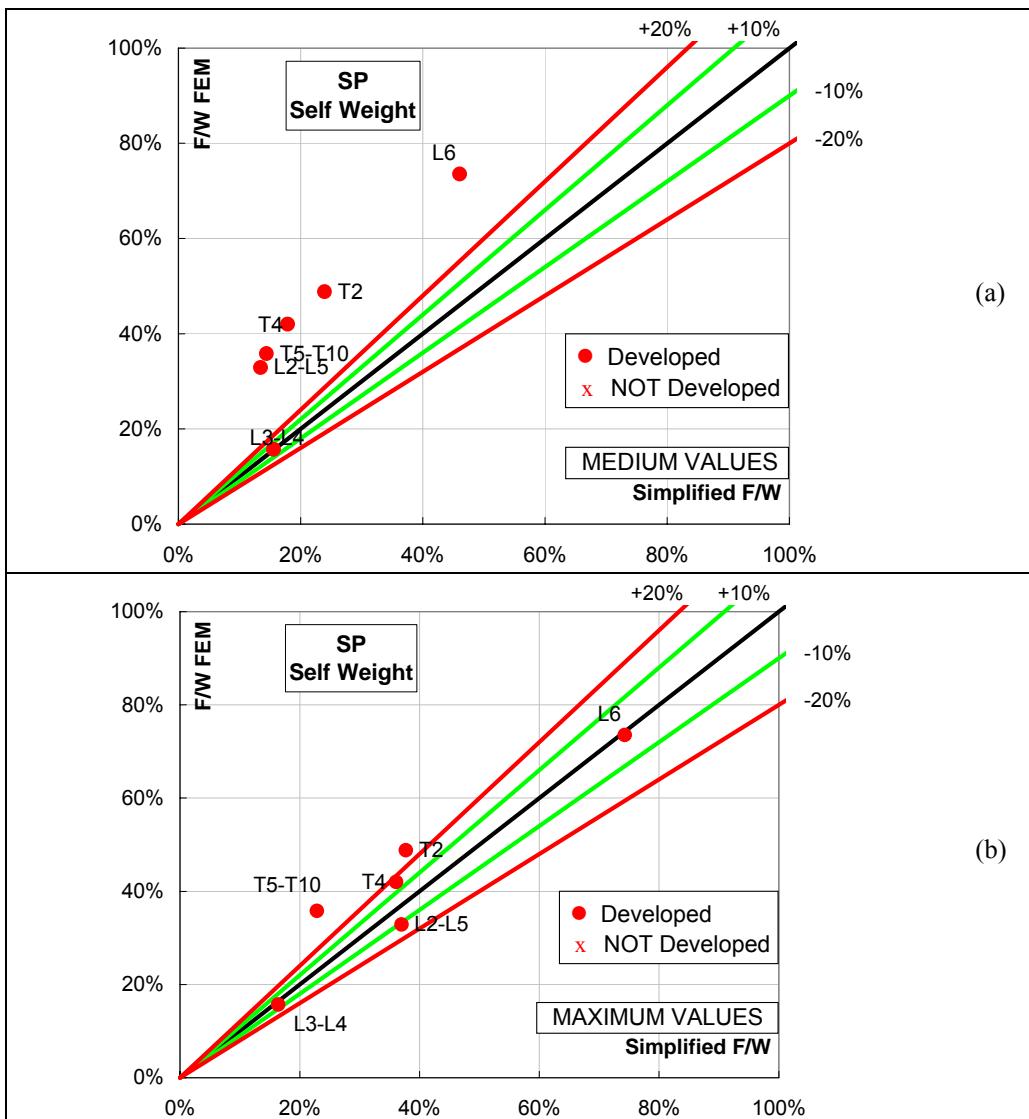


Figure 34. T5 – T6 – T7 – T8 – T9 – T10 macroelements – a) Mesh; b) Modelling; c) Simplified analysis data; d & e) Force/Displacement curves.

The internal arcades show a large difference of the non linear analysis compared to the limit analyses. The two ABAQUS curves even overcome the simplified evaluation with the maximum value of the base.

### 3.4.1. SUMMARY OF THE SP RESULTS

In Fig. 35 the last series of compared results are depicted.



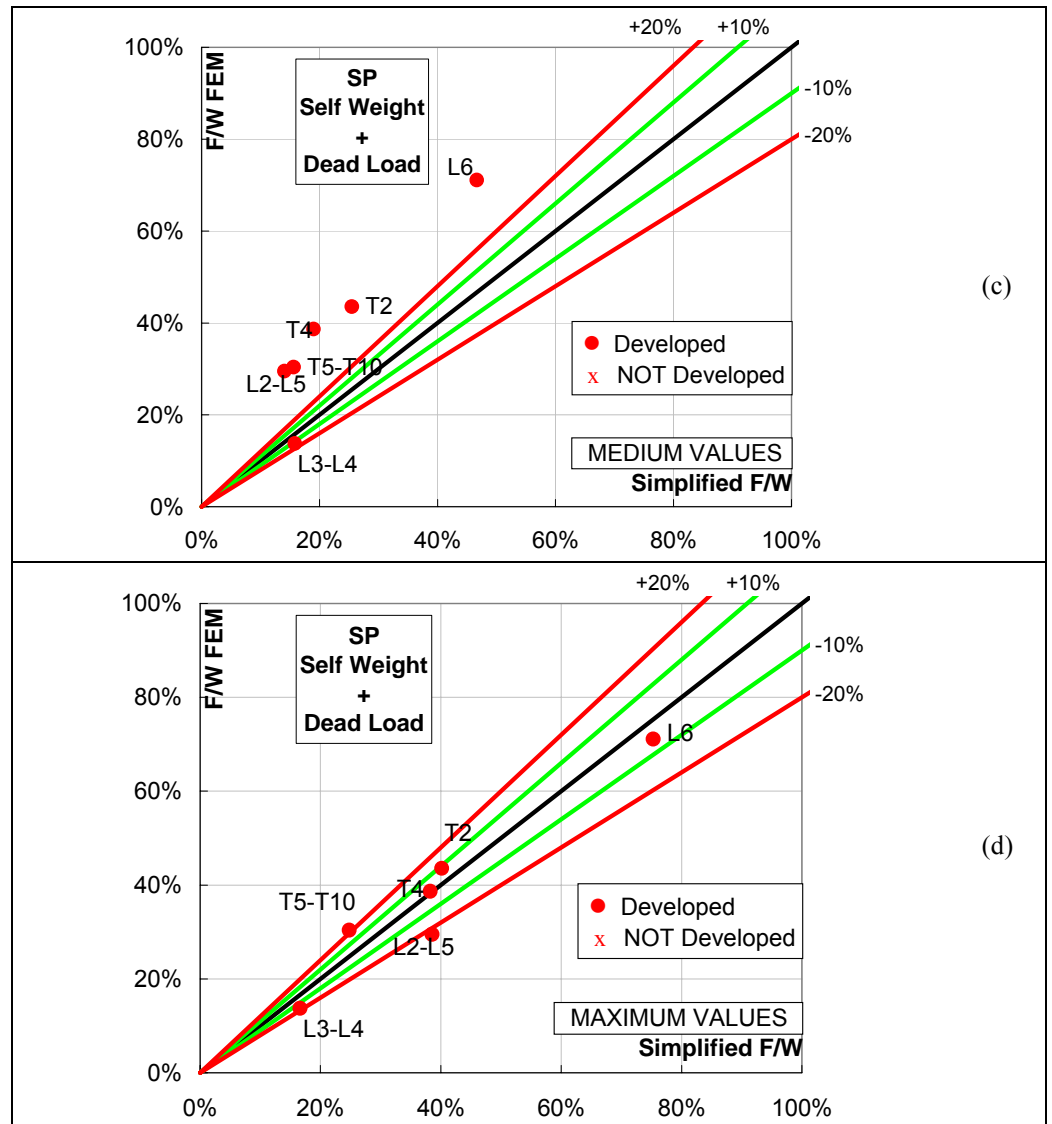
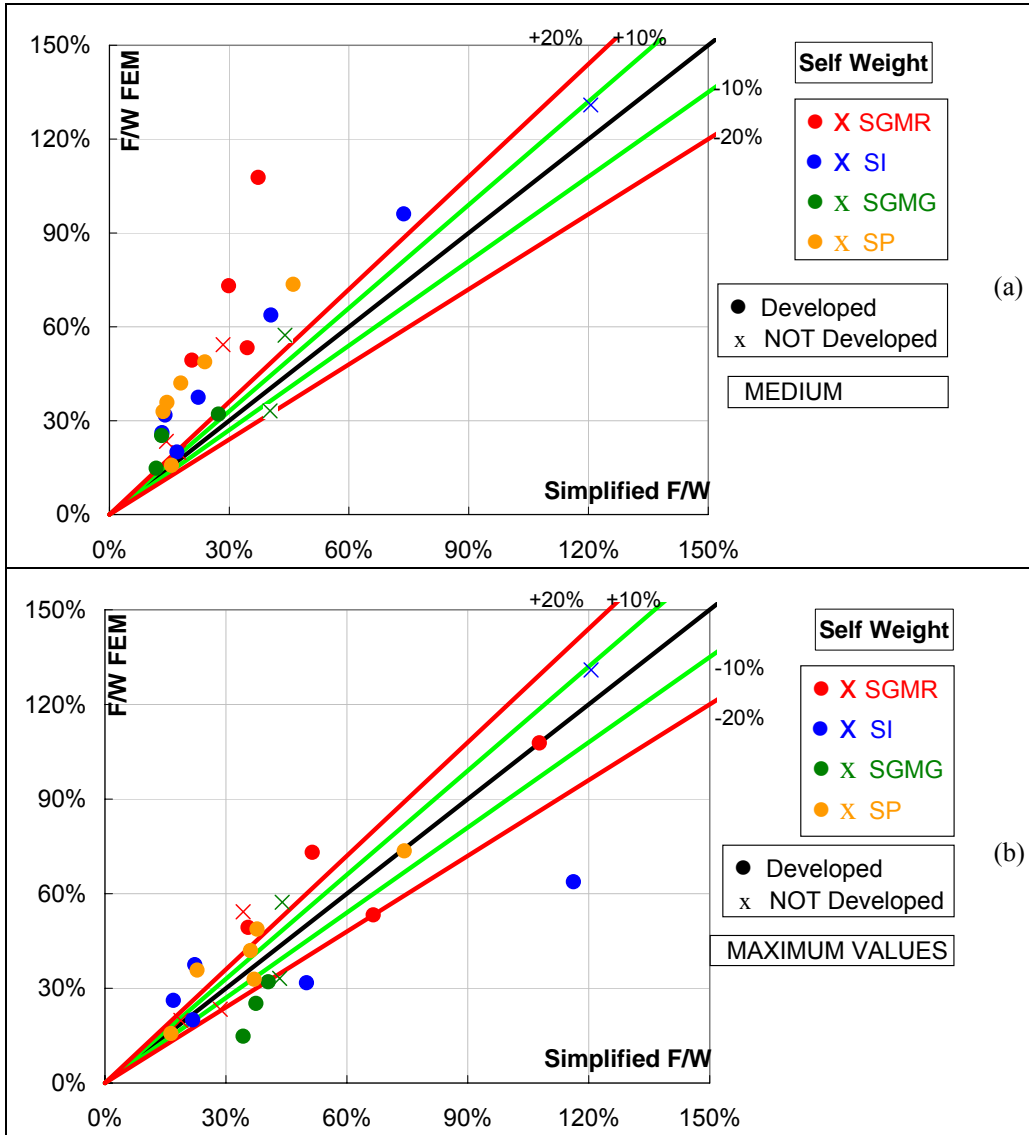


Figure 35. SP – Summary of the results.

Unfortunately, in both the load conditions, when the medium dimension is considered, the results do not match well being fairly higher in the non linear analyses. On the contrary, for maximum values of the piers, the results are fairly good when the self load or the self load plus the dead load is considered.

### 3.5. COLLECTION OF THE RESULTS

In Fig. 36 the evaluated collapse multipliers for all the case studies are plotted together.





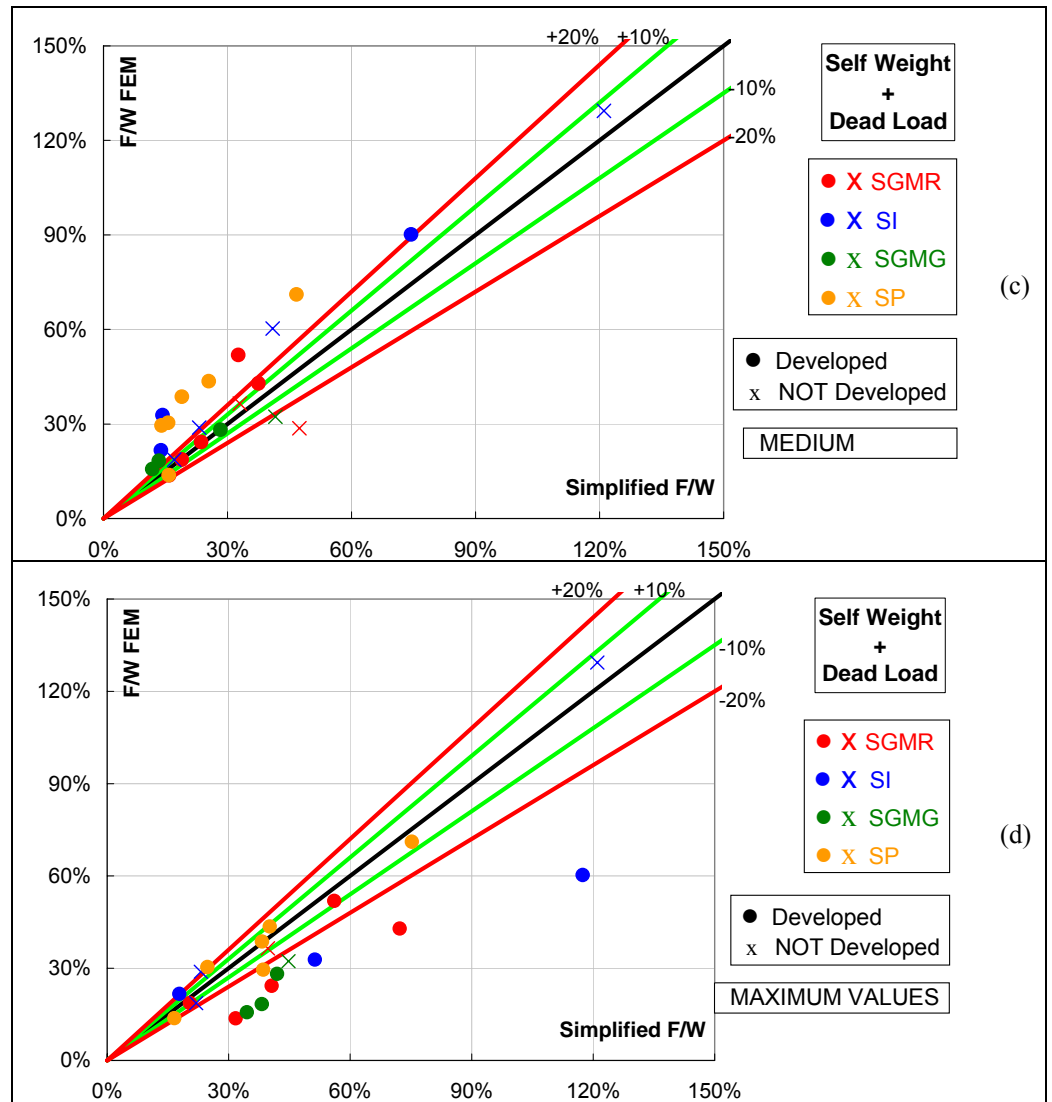


Figure 36. Summary of the results for all the churches.

As already stated in the single paragraphs, the adopted procedure provides values that are variable according to the selected values of the averaged pier width.

#### 4. CONCLUSIONS

In this chapter, the comparison between non linear analyses and simplified analyses with limit analysis has been conducted. In the simplified approach, different sizes of the pier dimensions have been selected. They correspond to the minimum, medium and maximum value of the column width. Furthermore, two load conditions, in presence or not of dead loads, have been considered.

When the medium value is taken into account, it has been noticed that, generally, greater error percentages are encountered in the model with the load condition considering the only self weight: in this case, the non linear analyses give high values; on the contrary the limit analysis gives small values of the collapse multiplier. In the load condition of self weight plus dead load, the scatters are smaller; this happens because of the presence of the dead load. It implies smaller collapse multiplier in the non linear analyses (the maximum values of the compression stresses are reached before) and greater values in the limit analysis (because the dead load, considered a stabilizing effect, is added into the weight of the beam). As a result, the two ranges become closer.

When the maximum pier is taken into account, the values of non linear analysis will be the same but limit analysis values will assume greater values, moving on the right side so that are inside the domain.

This evidence has been confirmed for the churches of SGMR, SI and SP. On the contrary, in the church of SGMG, medium values have shown a better comparison with non linear procedure.

From the above considerations, it can be derived that the use of simplified limit analysis approach, though approximated, is meaningfully able to provide indications on the collapse multiplier of the selected elements. Certainly, some issues arise about the validity of the calculated values since the adopted formulas are derived for a simple portal and require the choice of an average pier width. Nonetheless, it seems

to be an appealing path to follow in the study of the behaviour of structural elements at collapse.



## **CHAPTER 7**

### ***THE MASONRY POINTED ARCH***

#### **1. INTRODUCTION**

The masonry pointed arch, largely used in Gothic architecture, is known to generate lower horizontal thrust than the circular arch. While this fact is widely acknowledged and accepted, the structural behaviour of the pointed arch has not been investigated in detail. This chapter compares the circular and the pointed arch, evaluating the maximum and minimum thrust, and the collapse due to support displacement. Using limit analysis, a parametric study of such arches has been performed varying the angle of embrace, the thickness and the eccentricity of the centres. Graphical and numerical analyses have been carried out in order to predict failure as the supports are displaced. An extensive experimental campaign on model arches (illustrated in the following Chapter) is then used to verify the theoretical results allowing some new conclusions about the behaviour of the pointed arch.

### 1.1. THE ORIGIN OF THE POINTED ARCH

One of the most important contributors on Gothic cathedrals is Viollet-le-duc, whose *Dictionnaire raisonné de l'architecture française du XIe au XVIe siècle* [1875] is a milestone for the study of pointed arches. According to the author, some traces of them can be found in Egypt and Persia in the VI Century mainly for their aesthetic and stylistic value. However, until the end of the XI Century the unique type of arch used was the circular one and only during the XII Century, the arch formed by two parts of a circle was widely adopted in France and later in Europe. It disappeared with the end of the Middle Ages, around the XVI Century when, with the advent of the Renaissance, the circular arch was readopted.

There are a lot of controversies about the reason of the massive use of the pointed arch. According to [Viollet-le-duc E., 1875] the emergence of the pointed arch originated from the deformation in aging circular arches. When master builders of the time were restoring the leaning and the settlements of circular arches started to consider the old centre in the deformed position as a new centre of a new arch that had to be “broken”. As years went by, they built thinner circular arches and thicker pointed ones until the former were abandoned.

It is hard to believe [Abraham, 1934] that the master builders of the time knew the advantages of the pointed arch in terms of the smaller thrust they induced on the supports when it was first used. Rather the lack of space for the vaults' centrings or pure aesthetically reasons could have driven them to such marvellous constructions. At that time, experimentation with the basic structural elements to achieve a focusing of the forces in a skeleton structure of arch, pier and buttress and allowing the areas between to be opened up or glazed often led to structural failures. Gothic building failures were, therefore, a vital key to the structural progression of the cathedrals [Nelson B., 1971] and only with time, they could have acquired the sensibility to the reduction of thrust and used it more widely in their constructions.

For [Saunders, 1810] and [Frankl, 1962] the pointed arch was adopted in order to achieve the same height at crown for arches with different spans.

Regardless of the origin, according to [Viollet-le-duc E., 1875], starting from XIII century three main shapes of pointed arch were used (Fig. 1): 1) the arch generated from an equilateral triangle; 2) the arch with centres at one third of the span away from each of the supports (also called “arch for three points”); 3) the arch with centres at one fifth of the span away from each of the supports (also called “arch for five points”).

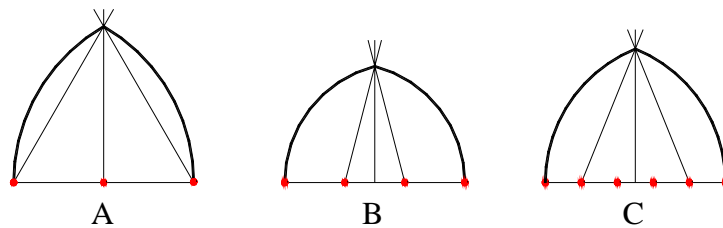


Figure 1. Common shapes of pointed arches. After Viollet-le-duc [1875] – *Dictionnaire raisonné de l'architecture française du XI<sup>e</sup> au XVI<sup>e</sup> siècle*. 6<sup>th</sup> Volume : p.440.

## 1.2. ANALYTICAL STUDIES ON MASONRY ARCHES

A quantitative static theory for arches was not defined until the end of XVII Century, even if there were some signs to understand the structural behaviour of constructions and to orient the building techniques. For example, Vitruvio in the sixth of the ten books on architecture mentions that vaults exercise a thrust on the adjacent walls or columns. In 1643 Derand and probably Martínez de Aranda in 1590 and Boccojani in 1546, proposed a geometric rule according to which the abutment for the circular arch is wider than that for the pointed arch (Fig. 2.a). It can be said that the proportions of the structural members was the most used criterion by master builders until the XVIII Century with almost no knowledge of static and strength. Among ancient scientists, Leonardo da Vinci is certainly an exception. In his notes and sketches there are ideas that were only developed three centuries later. In the Foster

Codex II fol. 82v there are sketches of an experimental measure of thrust and tension in the ties in arches including the pointed arch (Fig. 2.b).

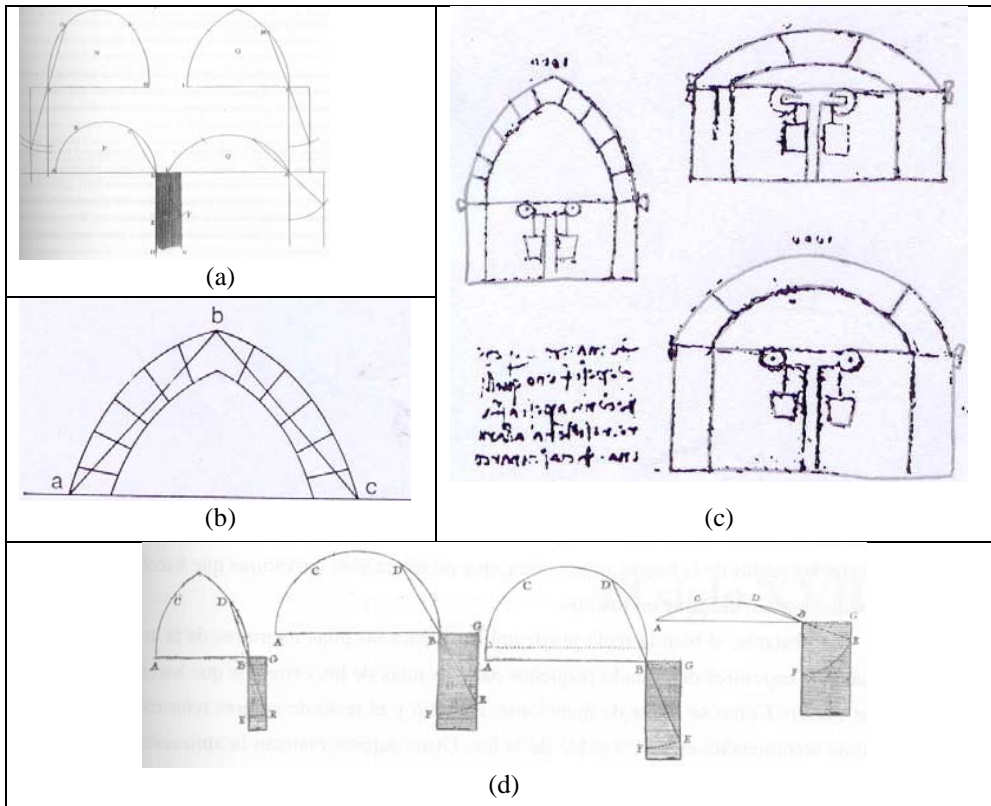


Figure 2. First steps in the analytical studies on masonry pointed arches.

- a) Source: Derand [1643] – *L'architecture des voutes ou l'art des trait et coupe des voutes* First Part, Chapter 6;
- b) Source: Leonardo da Vinci [1493-1505] – *Foster Codex* Vol. 2 fol. 82v ;
- c) After Couplet [1729] – *De la poussée des voutes*;
- d) Source: Blondel [1675] – *Cours d'architecture*. Paris: Lambert Roulland.

Besides, quoting da Vinci: “l’arco non si romperà, se la corda dell’archi di fori non toccherà l’arco di dentro” meaning that the arch will not fail if the chord on the extrados will not touch the intrados, the same proposed rule by Couplet only in the XVIII Century (Fig. 2.c). The first substantial steps in the static theory of arches and vaults were made by De la Hire in 1731 with “*Sur la construction des voutes dans les*



*edifices*” and Belidor in “*La science des Ingenieurs dans la condite des travaux de fortification et d’architecture civile*” who assumed rigid blocks provided of self-load and without friction. Another big step was made by Couplet with his two essays “*De la poussée des voutes*” in 1729 and “*Seconde partie de l’examen de la poussée des voutes*” in 1730. After 1770, an unexpected and extraordinary interest on the theory of arches and vaults developed so that it became topic of study for distinguished scientists like Bossut and Coulomb in France, Mascheroni and Salimbeni in Italy [Nascè V., Sabia D.; Giuffrè A., 1986; Benvenuto E., Corradi M. & Foce F., 1988; Foce F., Sinopoli A., 2001].

In 1737, in the light of Hooke’s principle of the inverted curve (*ut pendet continuum flexile, sic stabit continuum rigidum inversum*), Frezier considered the catenary curve as the ideal shape for an arch with a uniform thickness (Fig. 3.a). Although the idea was already well known among mathematicians, the French engineer contributed to its spreading comparing the catenary to a pointed arch.

One of the first researchers seeking an understanding of the failure modes of different types of arches is Méry in 1840. In his paper he analyzes the different position of the hinges for a circular, a basket handle and a pointed arch through the thrust line. He realized that in the pointed arch the key tends to rise and the lower parts tend to turn inside on the contrary of what happens in the circular arch (Fig.3.b). That theoretical line represents the path of the resultants of the compressive forces through the stone structures (this concept has been framed in the wider theory of limit analysis developed for masonry structures by Heyman since 1966).

In 1890, the German architect Ungewitter published a study conducted in 1794 by a Spanish mathematician, Padre Tosca, on the collapse of pointed arches (Fig. 3.c). They underlined the different role assumed by dead loads according to the shape of the arch. It’s fairly evident that a circular arch needs some mass on the haunches and that the pointed arch needs the load on the key stone.

In 1891 Baker, envisaging the possibility of an arch to fail for unequal settlement of the foundation, listed the three ways in which a masonry arch might yield: by the crushing of stone, by the sliding of one voussoir on another, or by the rotation about one edge of some joints. Neglecting the first mode, he focused on the last two mechanisms for a circular and a pointed arch (Fig. 3.d).

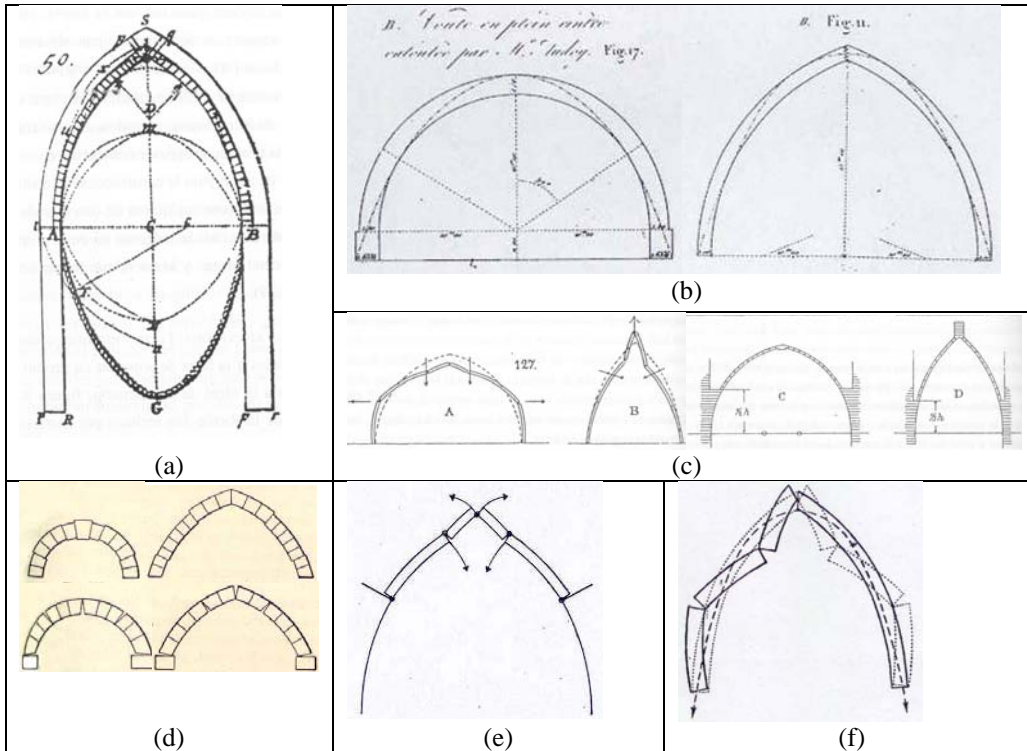


Figure 3. Upgradinds in the analytical studies in masonry pointed arches.

- a) Source: Frezier [1737] – *La théorie et la pratique de la coupe de pierres et des bois pour la construction des voutes et autres parties des batiments civils et militaires, ou traité de stéréotomie à l'usage de l'architecture.*
- b) Source: Méry [1840] – *Sur l'équilibre des voutes en berceau.* Plates CLXXXIII and CLXXXIV
- c) Source: Ungewitter [1859] – *Lehrbuch der gotischen constructionen.* p.447
- d) Source: Baker [1891] – *A treatise on masonry construction.* p.447
- e) Source: Abraham [1934] – *Viollet-le-duc et le ratioanlisme medieval.* p.16
- f) Source: Fitchen [1961] – *The construction of gothic cathedrals.* p. 81

Starting from Baker's work, Sondericker in 1907 considered only the failure due to rotation of the joints, noting that in a circular arch the centre of pressure moves upward at the crown and inward at the haunches, whilst in the case of a pointed arch or an arch very lightly loaded at the crown and heavily loaded at the haunches, the tendency may be for the crown to rise and the haunches to move inwards.

Later [Abraham, 1934] noticed that the failure mode in pointed arches is different from that in the circular ones finding that the former divides in six blocks with five rupture joints (Fig. 3.e).

Finally, [Fitchen, 1961] described the collapse of the pointed arch (Fig. 3.f) in four steps: the springs of the arch tend either to spread apart or to open their joints at the intrados, the arch tends to burst outward at the haunches, the joints of the intrados near the crown tend to open and the crown tends to rise.

## **2. PROBLEM STATEMENT**

This chapter intends to bring a new note on the study of masonry pointed arches. Although in the centuries the attention of researchers has been focused on arches, most of the times their shape was circular neglecting the pointed ones.

In particular, it has been noticed that in the relevant literature there are no expressions or indications of the values of maximum and minimum thrust. Besides, also the allowable displacements that can be tolerated by the structure in equilibrium have not been investigated.

Comparing step by step the behaviour of circular and pointed arches, this chapter seeks in detail these new topics. Varying the angle of embrace, the thickness and the eccentricity of the centres of the arches, the range of thrust values determined by the maximum and the minimum position of the thrust line and the range of possible support movements in the plane has been obtained. Numerical and graphical analyses have been performed and later compared with the results gained by experimental tests on model arches.

Finally, given a fixed span for an arch, the above parameters have been compared in the hypothesis that the thickness or the weight of the voussoirs is the same.

Purpose of this investigation is finding the best shape an arch can assume in terms of most displacements and height at the crown, less weight and thrust on the abutments.

### **3. METHODOLOGY**

On the base of Limit Analysis, the proposed methodology used to assess the behaviour of masonry arches is founded on a three step procedure. From the theoretical point of view, all the parameters have been evaluated firstly in a numerical way and then with graphical methods. Later, the results have been compared against each other with some experimental results explained in the following chapter.

Although in most masonry buildings arches and vaults are constructed with fill on top, providing an alternative force path, here it is assumed that the arch will act only under self weight neglecting the fill.

#### **3.1. NUMERICAL ALGORITHM**

In order to assess a variety of parameters through the application of equilibrium conditions from limit analysis, a rigorous numerical algorithm has been developed and then implemented in the commercially available software Matlab. Namely, the minimum possible thickness of arches, the range of thrust values, the allowable displacements in the plane of the arch and the change of internal forces as a result of the spreading supports have been obtained numerically through the construction of the thrust line in different states of the structure. These values can be found by examining the equilibrium of the central region of an arch. For example, to determine the minimum thrust, the correct hinge location is positioned where the thrust from the central region is maximized [Coulomb, 1773; Heyman J., 1972] or to calculate the

maximum allowable spreading of the support of an arch, the novel theory exposed by [Ochsendorf J., 2002] was followed. He determined the exact mode of failure and the maximum value of span increase as the supports move apart.

Because the intrados hinge location may change position and move toward the crown, various equilibrium states are possible and the arch can adopt different deformed shape per each as the span increases. Therefore, to solve the problem of spreading abutments, he realized that it is necessary to begin from a known equilibrium configuration and follow the equilibrium state of the structure as it deforms until the collapse.

### 3.2. GRAPHICAL STATICS

In the XIX Century graphical statics was discovered as a powerful method in structural engineering for equilibrium analysis. The shape of the thrust line in an arch can be found through graphical methods such as using the funicular polygon methods. Its position is indeterminate to the third degree such that for any arch there is a family of possible lines of thrust. The degeneracy can be extinguished once the magnitude of the horizontal force and the position of the line at two points are known. Master builders such as Maillart, Eiffel or Gaudì used it in the process design of their magnificent works. Because of the unwieldiness and tediousness of the method due to the complexity and uniqueness of the drawings, the charming graphical statics was abandoned in recent years in favor of numerical methods. More recently, the possibility of using computerized graphical methods for the analysis of structures was faced up by [Greenwold, Allen et Al., 2004] who introduced interactive static methods and later, deeply developed by [Block P., 2005] who presented new interactive computational analysis tools based on limit state analysis for the understanding of masonry structures.

The software Cabri was used in order to have a visual check of the results gained through the numerical code Matlab. The graphic static method is equally rigorous as

the numerical one based on the equilibrium of the voussoirs; in this case, however, it is the geometry of the structure being analyzed that controls the loads. Changes in the geometry will alter the volume and therefore the weight of the blocks. This influences the force polygon and hence the thrust line representing internal forces.

The possible thrust lines can be found using these graphical methods. One of the greatest advantages of this code is that it is possible to draw parametric models, so that every geometric characteristic can be changed. In this way, it can be avoided to draw a graphical static construction of every single structure being analyzed, and a quick tool to compare the relative influence of geometry on the range of possible stable conditions is provided.

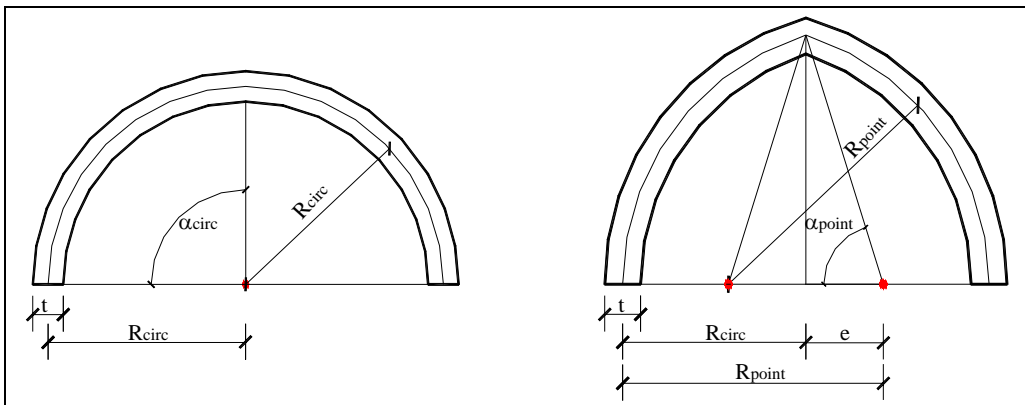


Figure 4. Symbols used in the parametric analysis.

In the case of arches, from the geometrical point of view, they can be roughly defined by their radius ( $R_{\text{circ}}$  for circular arches and  $R_{\text{point}}$  for pointed arches) and thickness ( $t$ ). But to characterize exactly their shape three fundamental values have to be fixed. They are the angle of embrace ( $\alpha_{\text{circ}}$  and  $\alpha_{\text{point}}$ ), the ratio of the thickness over the radius of the pointed arch ( $t/R_{\text{point}}$ ) and the eccentricity ( $e$ ) over the radius of the circular arch ( $e/R_{\text{circ}}$ ). If we define the eccentricity as the distance of the center of the arch from the vertical axis of symmetry, so that  $R_{\text{point}} = e + R_{\text{circ}}$ , a circular arch

has a ratio of  $e/R_{\text{circ}} = 0$  because its center coincides with the axis; on the other hand, pointed arches have two different centers and they are placed symmetrically with respect to the vertical axis (Fig. 4).

#### 4. MINIMUM THICKNESS

##### 4.1. THEORY

According to limit analysis, a real arch has a thickness sufficient to accommodate infinite possible thrust lines but there will only be one depth for which the arch is on the point of collapse without any movements of the supports, and that is the minimum thickness. A thinner arch cannot be constructed without the line of thrust passing outside the masonry, which would imply tension in the material in contradiction to the no-tension assumption. It also implies that for this thin arch the minimum and the maximum thrust will coincide.

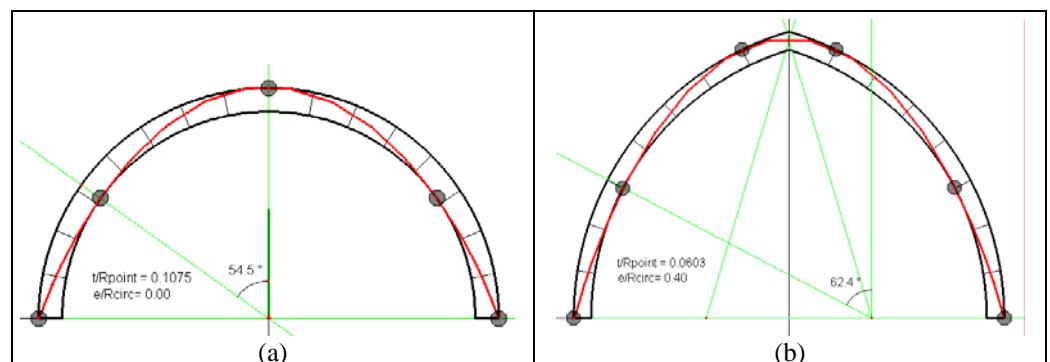


Figure 5. Thrust lines - a) in the circular arch; b) in the pointed arch.

As shown in Fig. 5 the circular arch is on the point of collapse by the theoretical formation of a five bar chain and the pointed arch will have one additional hinge (that is, a six-bar chain) that will disappear for any slight asymmetry. In both cases the mechanism will be reduced to the regular four-bar chain because of the suppression of one of the abutment hinges.

The problem consists into determining the value of the minimum thickness of the arch and the angle at which the hinges form. Already studied by [Couplet, 1729; Pétit, 1835; Milankovitch, 1907; Heyman, J., 1969; Sinopoli A., Corradi M. & Foce F., 1997] and recently systematically by [Ochsendorf J.A., 2002.] for the circular arch, this has never been analyzed for the pointed arch. [Méry M. E., 1840] points out the thrust lines position for the circular, the basket handle and the pointed arch in this particular case, finding that the minimum thickness is determined when seven collapse joints form because of an additional contact point at the intrados at the crown.

#### **4.2. NUMERICAL AND GRAPHICAL ANALYSES**

The numerical procedure follows the suggestion of [Heyman J., 1969], which basically uses the zero work condition due to the absence of dissipation at hinge level. With reference to Fig. 6, a starting value of  $t/R_{\text{point}}$  is chosen. Then several hinge configurations, chosen in user-controlled steps, are studied. For each of them the expression of total work is evaluated. If it is zero, the value of  $t/R_{\text{point}}$  is stored. Subsequently the ratio  $t/R_{\text{point}}$  is changed. The procedure, thus, gives a class of  $t/R_{\text{point}}$  ratio values for which the total work is zero. The maximum of them (according to the application of the “safe” theorem) represents the minimum thickness normalized to the radius.



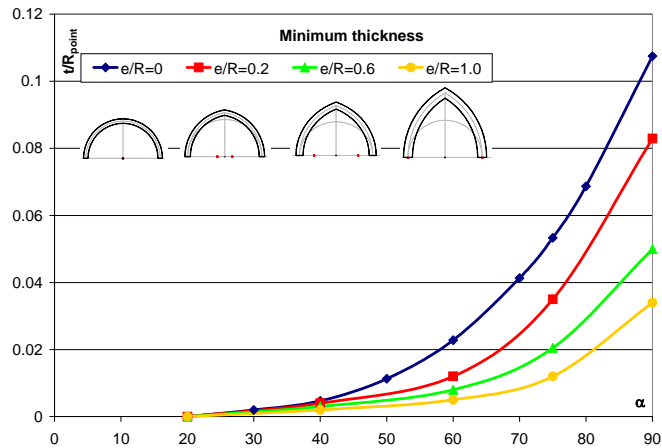


Figure 6. Minimum thickness for an arch.

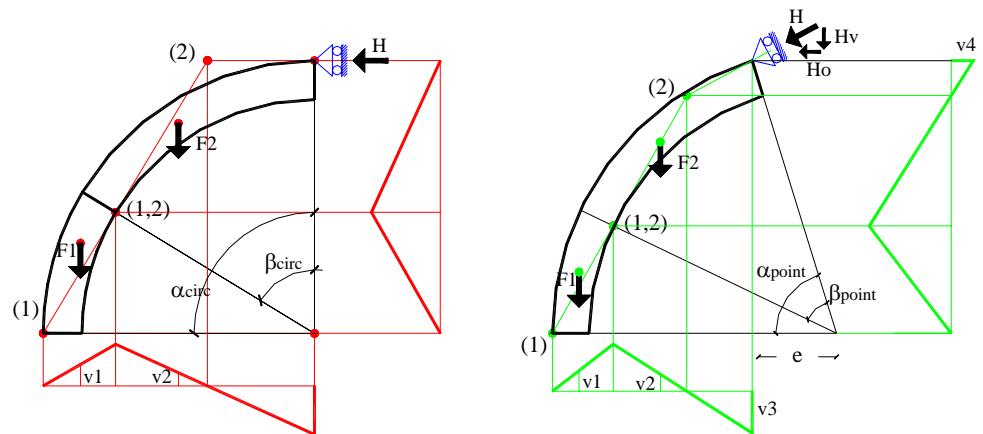


Figure 7. Kinematic chains determining of the minimum thickness of an arch.

Increasing the eccentricity, smaller thickness of the voussoirs is requested (Fig. 7) and hinge location to the crown is moved. The results gained through this script in Matlab have been verified against the results of graphical analysis in Cabri where a unique thrust line can be constructed.

## 5. THRUST VALUES

### 5.1. THEORY

According to the safe theorem, if it is possible to find at least one thrust line entirely contained in the shape of the arch, then the arch is “safe”. Generally, as soon as a thicker arch than the one for the minimum is considered, some thrust lines lie in the depth of the structure. Defining the minimum and the maximum thrust as the limits of the range of variability, a cracked arch will develop a minimum thrust when the supports are moved apart and a maximum one when the supports are moved together.

Figure 8 shows these lines in a circular and a pointed arch with a ratio  $e/R_{\text{circ}} = 0.6$ . While in the first one the thrust lines may touch the boundary in three points so that only three hinges need to form, in the latter one, for the minimum thrust, four hinges have to take place because the thrust line can not be pointed. But any slight asymmetry, whether of geometry of the arch or of loading, will ensure that only one of the hinges near to the crown will form, so that again a three hinges mechanism will form. Having the same span and thickness, it can be easily noticed that the pointed arch assumes lower values of maximum and minimum thrust compared to the circular arch.

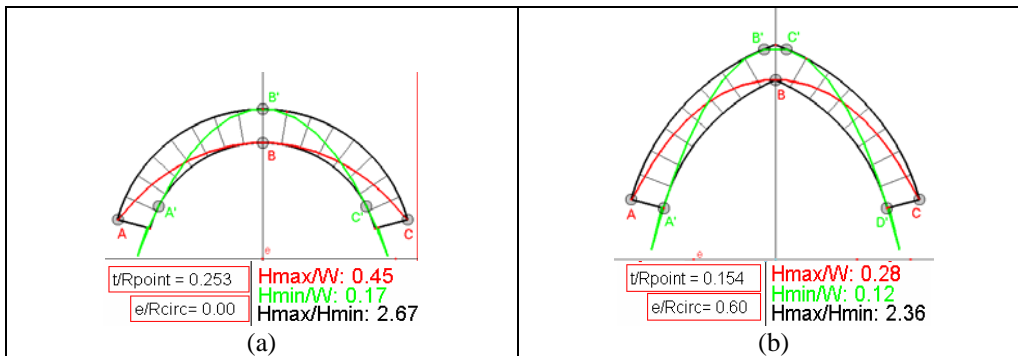


Figure 8. Maximum and minimum thrust lines – a) in the circular arch; b) in the pointed arch.

## 5.2. NUMERICAL AND GRAPHICAL ANALYSES

Using a similar algorithm as before, in which the  $t/R_{\text{point}}$  ratio is now parametrically introduced together to the value of the angle of embrace  $\alpha$  and the eccentricity  $e/R_{\text{circ}}$ , a more systematic analysis of pointed arches has been held varying the three parameters as shown in Fig. 9.

Three different values of the half embrace have been selected -  $90^\circ$ ,  $75^\circ$  and  $60^\circ$ - and four values for the ratio of  $e/R_{\text{circ}}$ : 0, 0.2, 0.6 and 1.0 varying the values of  $t/R_{\text{point}}$  from 0.04 to 0.24 with a step of 0.02.

Basically the script, varying the position of the hinges through the depth of the arch and applying the safe theorem, maximizes the value of the thrust writing the equilibrium conditions on each part of the structure. This happens for both the search of the minimum and the maximum values, simply inverting the position the hinges at the extrados or at the intrados of the structure.

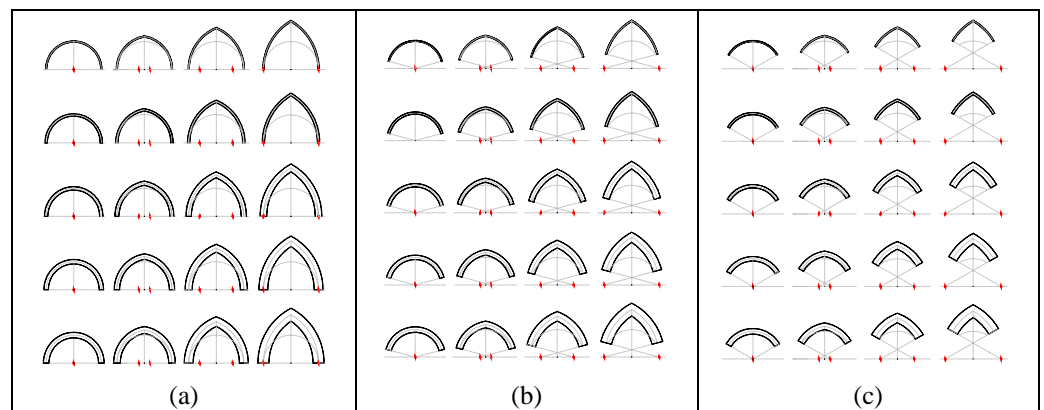


Figure 9. Study cases varying the embrace, the thickness and the eccentricity.  
a) embrace =  $90^\circ$ ; b) embrace =  $75^\circ$ ; c) embrace =  $60^\circ$ .

As already stated, because the geometry of the structure limits the range of possible thrust lines, the minimum and maximum thrust represent the smallest and the largest horizontal thrusts the structure transfers to its supports. In Fig. 10 the maximum and the minimum thrust normalized to the weight of the arch ( $H/W$ ) are

depicted as function of  $t/R_{point}$ . In particular, in each graph the value of  $e/R_{circ}$  is held constant and three different “scissors shape” curves are drawn. They represent the values of the minimum and maximum thrust varying the angle of embrace ( $90^\circ$ ,  $75^\circ$  and  $60^\circ$ ) for a fixed ratio of  $e/R_{circ}$ .

Obviously, there will be a unique value of this ratio for which the maximum and minimum thrust coincide and this is exactly the value of the minimum thickness of the arch. From the graphs it is clear that arches with embraces of  $90^\circ$  have to be thicker than those with embrace of  $75^\circ$  and  $60^\circ$  to stay up.

These analyses have highlighted that pointed arches assume lower values of thrust than the circular ones. More in detail, increasing the pointidness, smaller values are obtained.

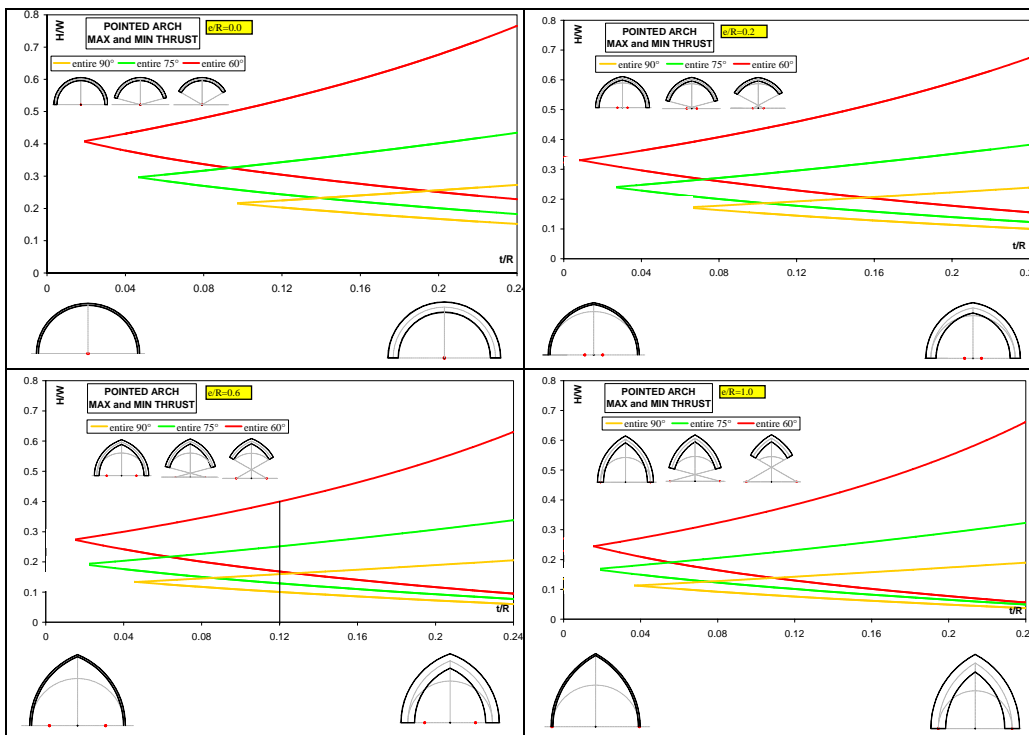


Figure 10. Maximum and minimum thrust in arches with constant  $e/R_{circ}$ .

Furthermore, the range of possible positions between the maximum and the minimum thrust decreases when the angle of embrace increases. For example, with reference to Fig. 10 (the third one), which represents pointed arches with values of  $e/R_{\text{circ}} = 0.6$ , for a value of  $t/R_{\text{point}} = 0.12$  the minimum and maximum values for the embrace of  $90^\circ$  are 0.10 and 0.16; they become 0.13 and 0.25 for the embrace of  $75^\circ$  and increase to 0.17 and 0.40 for the  $60^\circ$  embrace. It is evident that an arch with a given embrace has a bigger range of possible positions of the thrust line compared to an arch with a wider embrace, but that at the same time, larger values of thrust on the abutments are requested.

More significantly, similar results can be seen in Fig. 11.

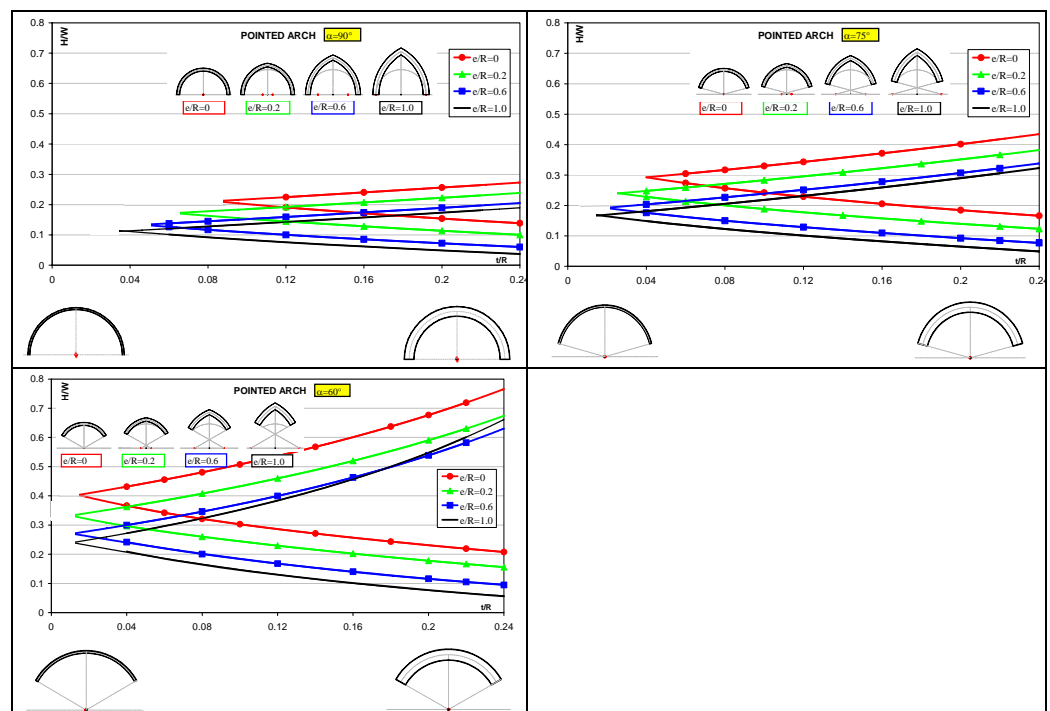


Figure 11. Maximum and minimum thrust in arches with constant embrace  $\alpha$ .

Holding fixed the variables on the two axes ( $H/W$  and  $t/R_{\text{point}}$ ) and the angle of embrace for each graph and varying the value of  $e/R_{\text{circ}}$  the arches' thrust is reported. It is easily recognized that increasing the eccentricity of the arch (or its "pointedness") the thrust values decrease and again, thinner arch can stand. Méry's statement "on remarquera qu'elle exige une épaisseur plus considerable: c'est le contraire de ce que nous avons observé pour les voutes en plein cintre et en anse de panier" (1840 – *Sur l'équilibre des voutes eu berceau* – p.66) that is "we'll notice that the pointed arch (with smaller embrace) will require a greater thickness: that is the contrary of what we have observed for the circular and the basket handle arches" is evidently false.

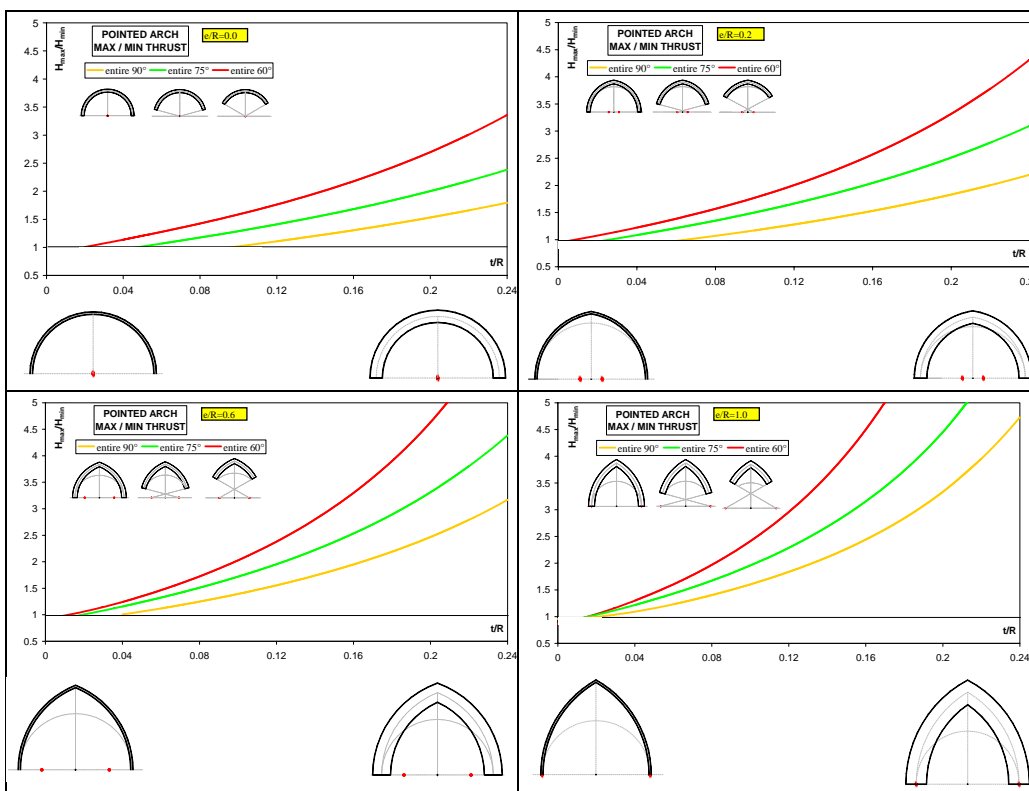


Figure 12. Ratio of the maximum over the minimum thrust.

A visualization of the ratio  $H_{\max}/H_{\min}$  can be seen in Fig. 12 where the minimum values are fixed to unity (i.e. the minimum thickness). It can be noticed that decreasing the embrace, higher values of  $H_{\max}/H_{\min}$  and thinner arches can be obtained. For the same value of embrace increasing  $e/R_{\text{circ}}$ , higher ratios  $H_{\max}/H_{\min}$  can be obtained.

In order to select the best shape for an arch, one may notice that highest and heaviest arches have smaller values of thrust but at the same time also smaller range of variability in terms of  $H_{\max}/H_{\min}$ . On the other hand, the shortest and the lightest arches have bigger values of  $H/W$  and  $H_{\max}/H_{\min}$ . From this point of view, therefore, the best solution is found in the  $e/R_{\text{circ}}$  range of 0.5-0.6 where the arches are not so high and heavy but have at the same time enough thrust variability.

## 6. HORIZONTAL SUPPORT DISPLACEMENT

### 6.1. THEORY

Historic masonry structures are commonly subjected to differential settlements in foundations, defects in constructions, consolidation of materials (creep in the mortar) and vibrations. The result of these actions is an increasing displacement over the life in the upper part of the constructions and the structure reacts by developing cracks, often showing large deformation capacity. Structures on spreading supports could collapse in one of two ways: a five-hinge mechanism (symmetrical in the circular arch and asymmetrical for the pointed one with the activation of only one of the two hinges close to the crown) or a three-hinge mechanism by snap-through if the thickness is sufficiently large. Generally, in the five-hinge collapse mechanism, the central portion of the arch is a three-hinged arch, which deforms to accommodate the span increase. Previous studies by [Ochsendorf J., 2002] show that this result is unsafe since the hinge locations are not fixed, but may move during the support displacements toward the crown of the arch.

Neglecting the cause of the displacements, the stability of the structure has been investigated, through kinematic and static analyses. Through the use of two codes, Matlab and Cabri, the analysis of the evolution of the thrust line in the arch as the supports are spreading has been performed. Although the procedures are different, the gained results agree with high accuracy. Following the method proposed and investigated by [Ochsendorf J., 2002] for the circular arch, a new script has been written in Matlab for the spreading of the support of the pointed arch.

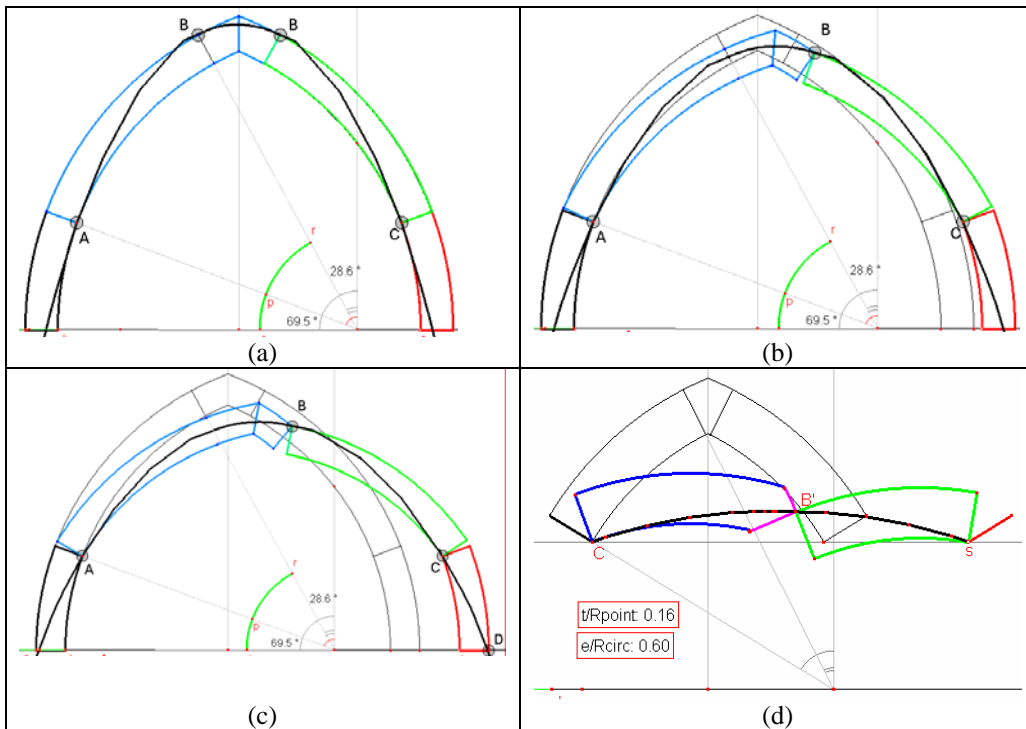


Figure 13. Procedure for the determination of maximum displacement for an arch.

a) minimum thrust; b) supports movement; c) first collapse condition; d) second collapse condition.

Mainly the steps are the following:

1. determination of the hinges' position imposing the minimum thrust's condition (Fig. 13.a);



2. imposition of the support's movement constantly updating the position of the thrust line (Fig. 13.b);
3. the first collapse condition is reached if the locus of pressure reaches one of the two supports (Fig. 13.c). This means that a fourth hinge will form and the structure becomes an instable collapse mechanism;
4. if the first collapse condition is not verified, the second one could occur if the snap through of the rigid blocks develops (Fig. 13.d);

If the last two conditions are not verified but the location of pressure goes inside the intrados, the hinge will move close to the support and all the procedure starts again from point 2 until the collapse (Fig. 14).

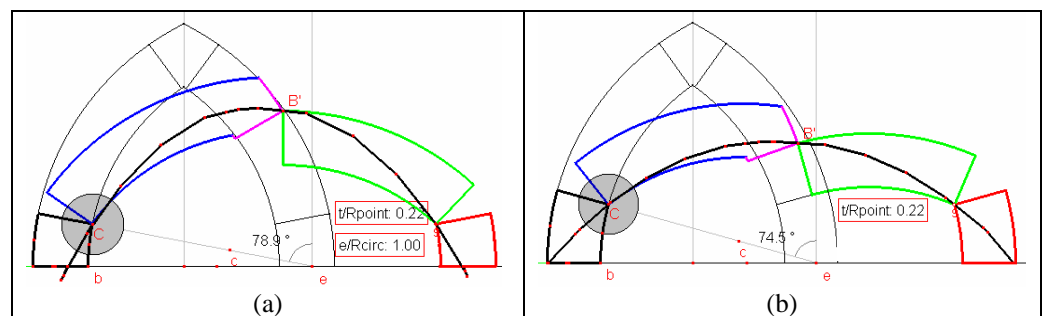


Figure 14. Movement of the hinge up to the crown in the sequence.

## 6.2. NUMERICAL AND GRAPHICAL ANALYSES

To get the solution for great displacements of the support, the rotation centres method was used. In Fig. 15 an example of the rigid bar mechanism is reported: moving the support on the right apart (the hinge A moves in A' and C is fixed), the initial position of point B (intersection of the circle in C and in A) is updated in B' as soon as A moves in A' (being again the intersection of the circle in C and in A').

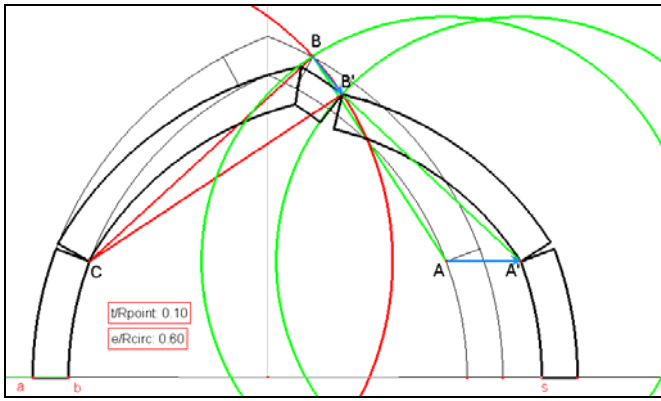


Figure 15. Rotation centres' method.

In Fig. 16 the values of the displacement due to the increasing of the span are presented. It is clear that pointed arches are able to deform much more than the circular arches before the collapse.

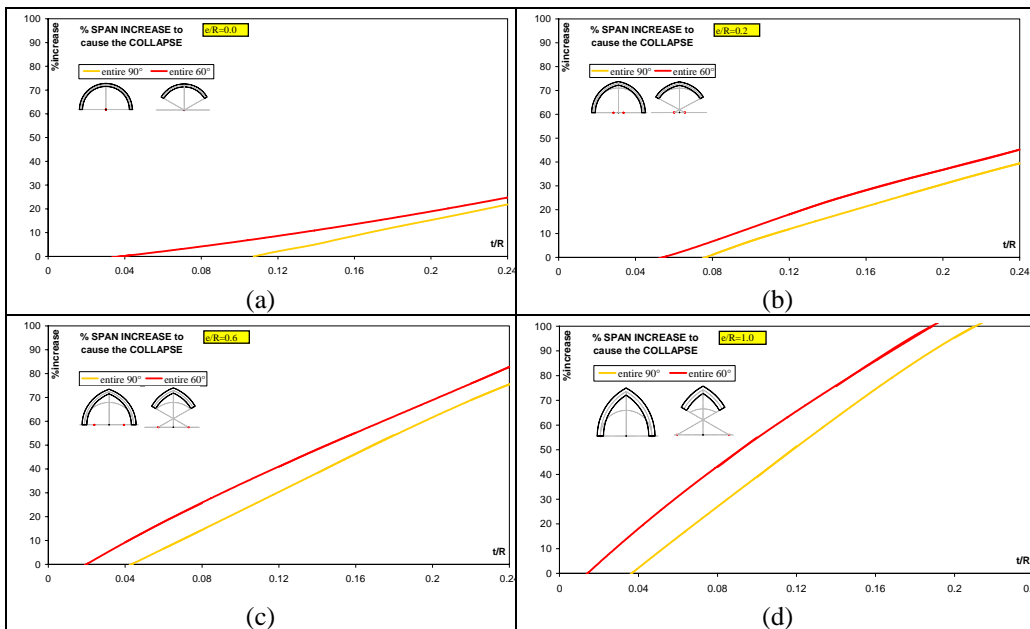


Figure 16. Span increase in arches.

Furthermore, on the same graph it is possible to see that arches with the same value of  $e/R_{\text{circ}}$  and  $t/R_{\text{point}}$  but with smaller embrace (from  $90^\circ$  to  $60^\circ$ ) have larger displacements before failure.

In Fig. 17 the values of the thrust increase in the arch after the displacement are shown. A higher percentage of the thrust increase is obtained either when the angle of embrace is reduced and when the eccentricity is increased.

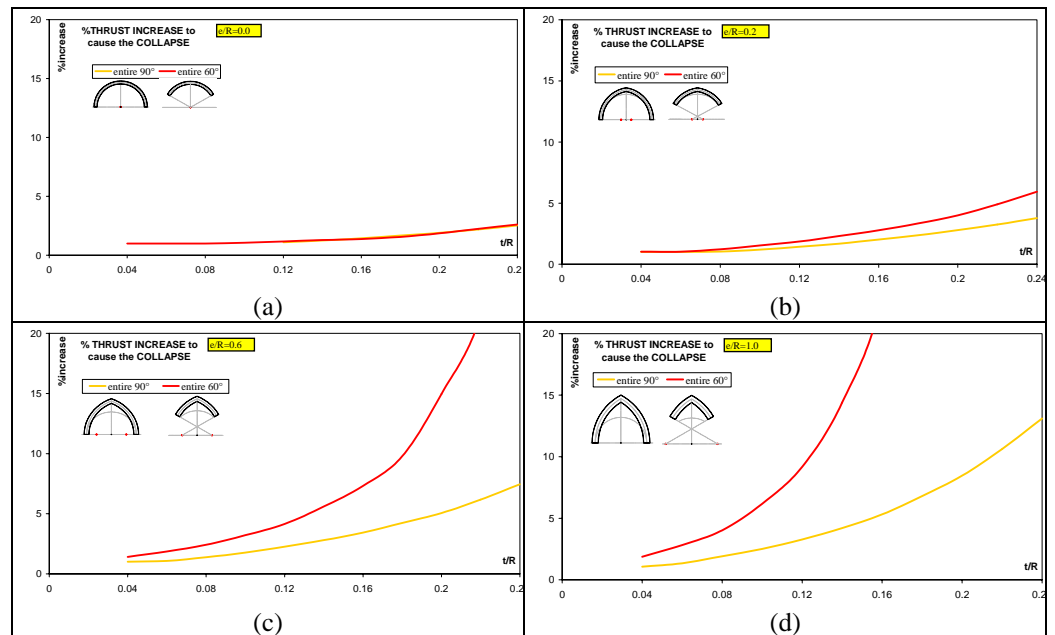


Figure 17. Thrust increase in the arch.

## 7. DOMAINS OF POSSIBLE DISPLACEMENTS

In 2000, Smars gave a very good representation of possible positions assumed by an arch keeping one support fixed and moving the other one. He defined a kinematically possible domain as the area representing all the positions spanned by the moving point assuming that blocks can not pervade and rotations are only in one verse. In the same way a statically possible domain is defined with the additional restriction that a thrust line has to be wholly contained inside the shape of the arch. In order to seek

how much a domain can change as the eccentricity of the centres is increased This powerful representation for arches under study has been used.. One of the comparisons is shown in Fig. 18 where the locus of all the statically admissible states of arches with same embrace ( $90^\circ$ ) and  $t/R_{\text{point}}$  ratio (0.12) are depicted with the hatched area.

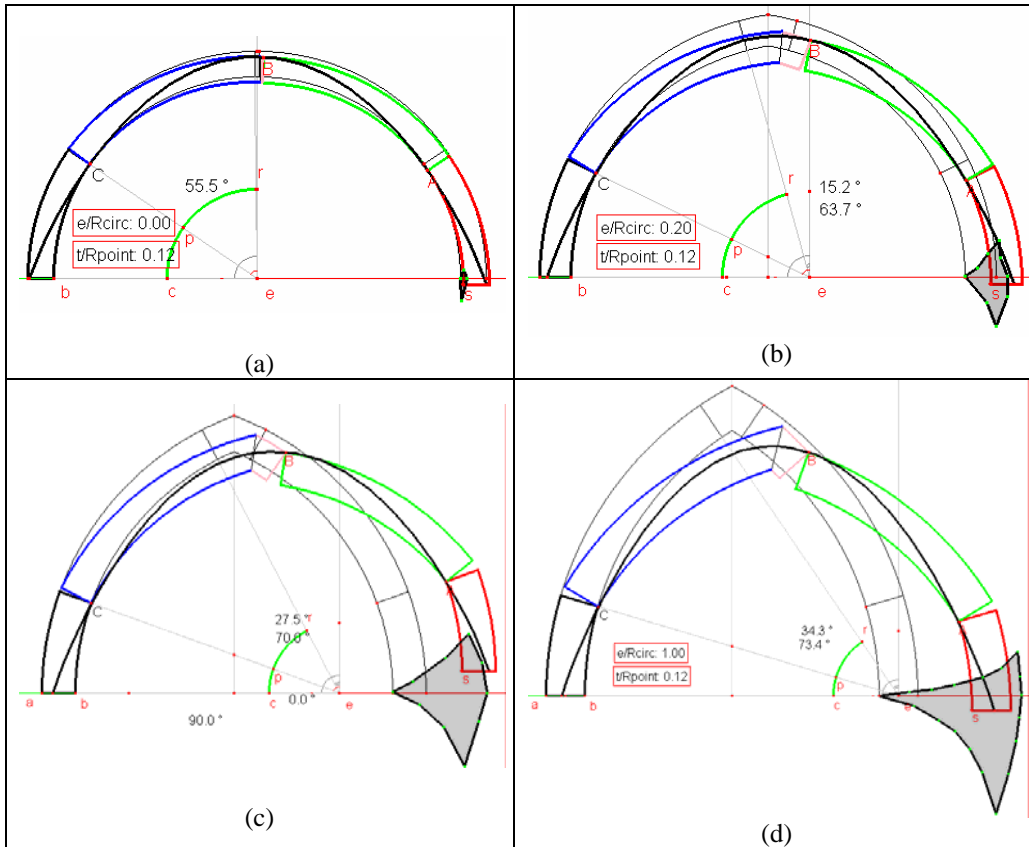


Figure 18. Statically and kinematically domains of possible displacements in the plane increasing the pointidness.

## 8. THE HALF ARCH

After having analyzed the behaviour of the whole arch, the half arch has also been considered because of its similarity to the flying buttress in the Gothic churches.

### 8.1. THRUST VALUES

In Fig. 19 the thrust lines for the entire and the half arches are compared varying the eccentricity of the centres (from 0 to 1.0). It has to be noticed that, in the case of the half arch, for the minimum thrust a different mechanism was pursued with the formation of the hinge exactly on the intrados at the crown.

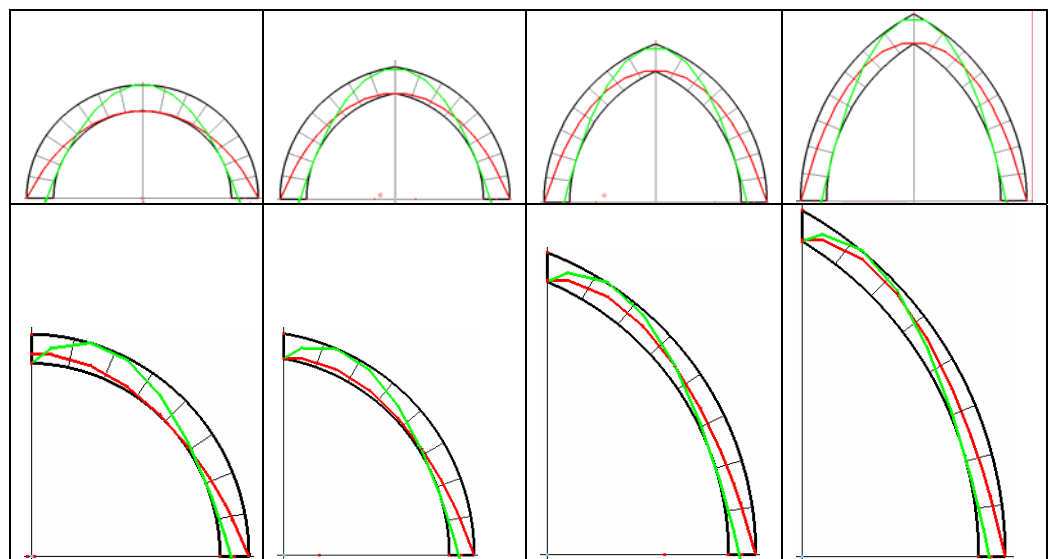


Figure 19. Minimum and maximum thrust lines for the entire and the half arch.

Similarly to Fig. 10, the values of the minimum and the maximum thrust, keeping constant the ratio  $e/R_{\text{circ}}$  for the half arch are reported in Fig. 20. Again for each eccentricity smaller values of the embrace have as a consequence possible thinner arches and bigger values of  $H_{\text{max}}/H_{\text{min}}$ . Surprisingly for a given angle the half circular

arch (Fig. 20.a) behaves better than any half pointed arch (Fig. 20.b,c,d) in terms of minimum thickness.

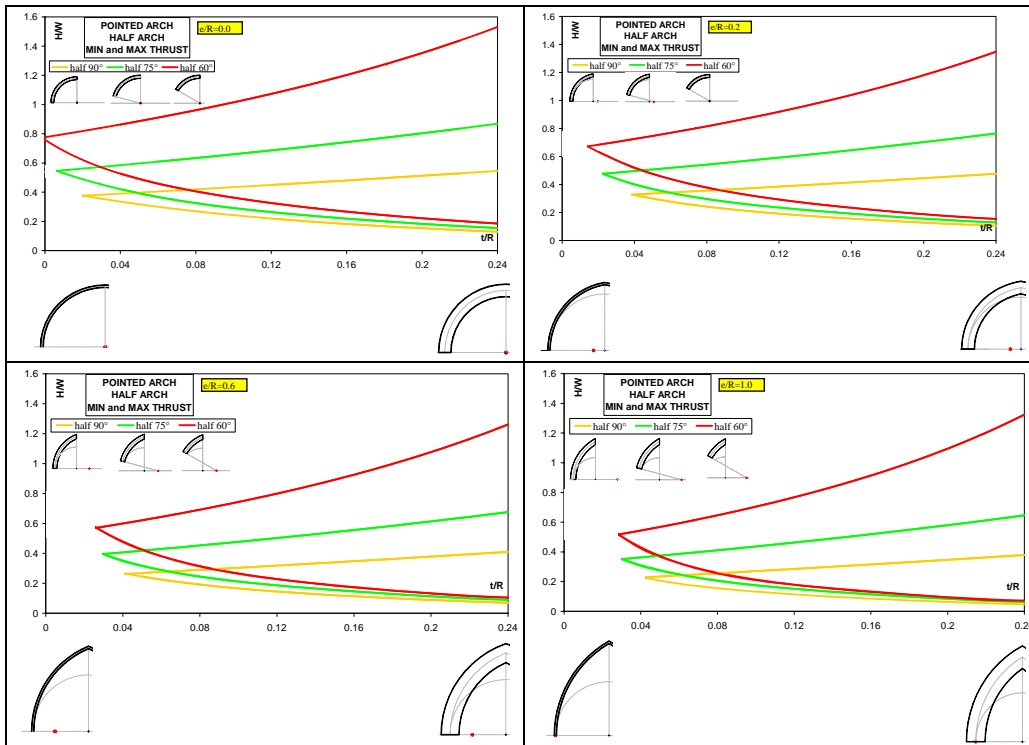


Figure 20. Maximum and minimum thrust in half arches with constant  $e/R_{circ}$ .

### 8.2. MAXIMUM DISPLACEMENTS

An application of the theoretical procedure developed and stated in §6 to get the maximum allowable displacement in an arch, was made on the study cases selected. In Fig. 21 for the half arch, the values of the displacement due to the increasing of the span are represented.

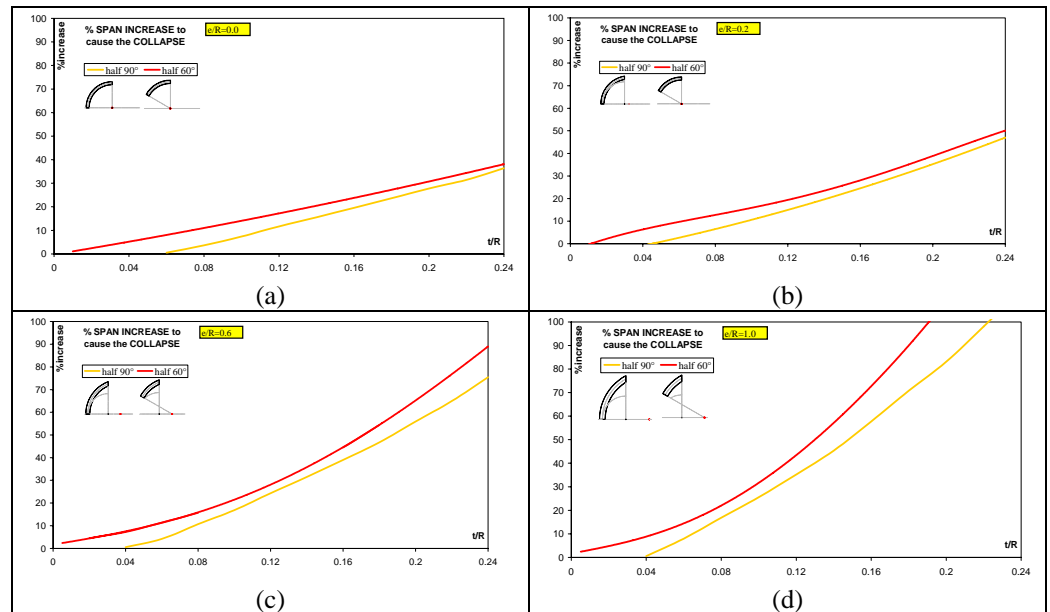


Figure 21. Span increase in half arches.

Again, it is clear that pointed arches are able to deform much more than the circular arches before the collapse. Furthermore, on the same graph it is possible to see that arches with the same value of  $e/R_{\text{circ}}$  and  $t/R_{\text{point}}$  but with smaller embrace (from  $90^\circ$  to  $60^\circ$ ) have larger displacements before failure.

### 9. ARCHES WITH THE SAME SPAN

In Fig. 22 the comparison of the circular arch with two pointed arches (with centres at the third and fifth point) in terms of horizontal thrust and overturning moment made by [Abraham, 1934] is shown. In the first set of arches, holding constant the span length, the material and the thickness of the blocks, the horizontal thrust and the overturning moment decrease when going from the circular arch (*case a*) to the first pointed arch with the centre at the third of the span (*case b*) to the second pointed arch with the centre at the fifth of the span (*case c*). The second set of compared arches has the same typology (one circular and two pointed ones), but holding

constant the span length and the material, the thickness of the blocks is varied so that the horizontal thrust is kept constant. As a result, the thickness increases when going from case a to case d and case e whilst the overturning moments decreases again.

In order to seek the best shape of an arch for a given span, similar analyses have been performed. In particular, the behaviour of arches with same span and thickness and later, same span and weight are compared.

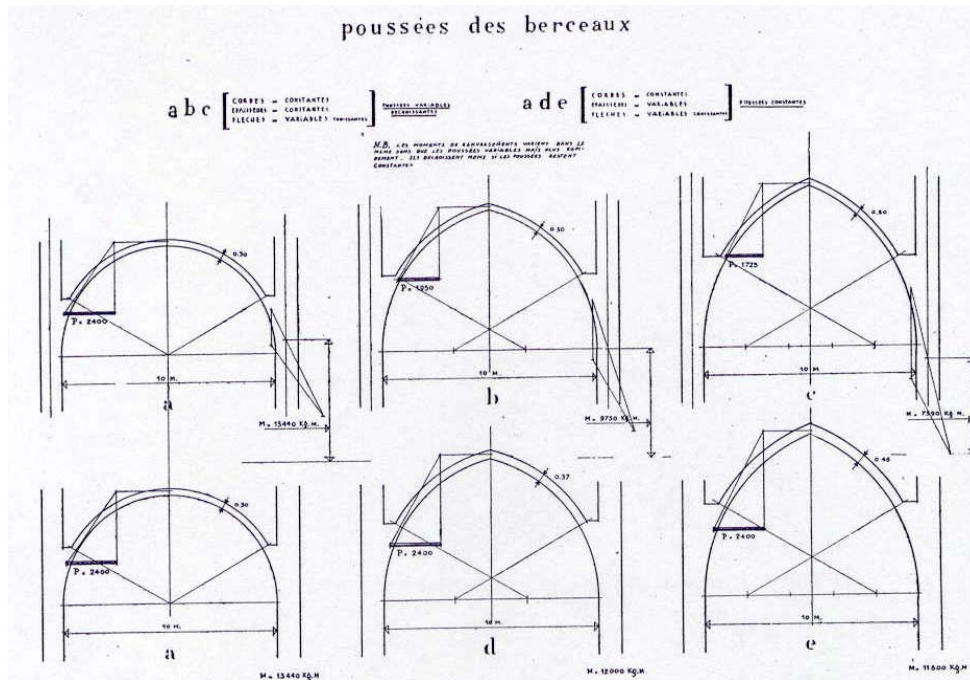


Figure 22. Arches with the same span. Source: Abraham [1934] – *Viollet-le-duc et le rationalisme medieval* – p.14.

### 9.1. SAME SPAN AND THICKNESS

Having chosen a span of 4 m and a thickness of 0.6 m, varying the  $e/R_{\text{circ}}$  ratio (from 0 to 1.0) and the angle of embrace (from  $90^\circ$  to  $60^\circ$ ), the height at the crown (Fig. 23.a), the weight (Fig. 23.b), the ratios  $H/W$  (Fig. 23.c) and  $H_{\text{max}}/H_{\text{min}}$  (Fig. 23.d) have been evaluated. In Fig. 23.a varying the values of  $e/R_{\text{circ}}$ , different heights



at the crown are drawn holding constant the value of the embrace. In numbers for  $e/R_{\text{circ}} = 0.2$ , the height at the crown will be 2.03 m for  $\alpha = 60^\circ$ , 2.47 m for  $\alpha = 75^\circ$  and 3.03 m for  $\alpha = 90^\circ$ .

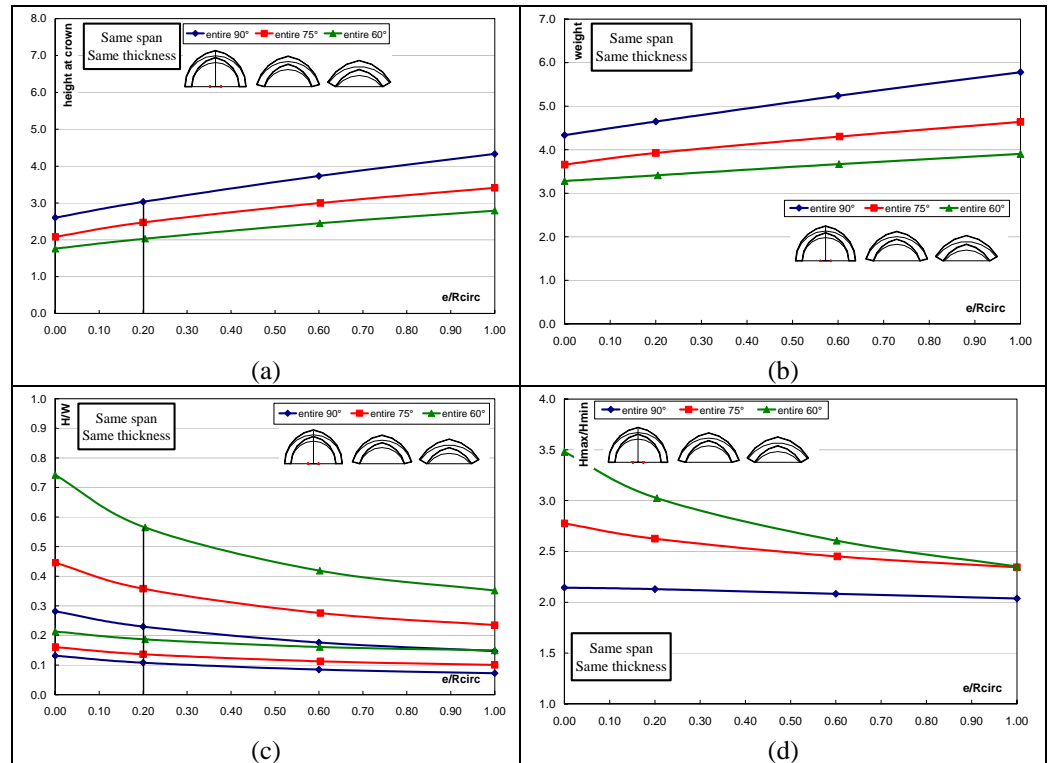


Figure 23. Main results for arches with same span and thickness.

a) height at the crown; b) weight; c) maximum and minimum thrust over weight ratio; d) maximum and minimum thrust ratio;

In Figure 23.b the weight of the arches, in terms of the area (neglecting the specific load and the depth of the arch in the other direction) are compared; for example for  $e/R_{\text{circ}} = 0.2$  smaller values of weight are obtained for smaller embraces. Graphing the values of the maximum and the minimum thrust (Fig. 23.c) it can be noticed that they generally decrease when the ratio  $e/R_{\text{circ}}$  is increased and, for a fixed value of  $e/R_{\text{circ}}$ , when the embrace is increased. In numbers, again for  $e/R_{\text{circ}} = 0.2$ ,

the maximum and the minimum thrust for  $\alpha = 60^\circ$  they are equal to 0.57 and 0.19, for  $\alpha = 75^\circ$  they are 0.36 and 0.14 and for  $\alpha = 90^\circ$  they are 0.23 and 0.11. In the last Figure (23.d) the values of  $H_{max}/H_{min}$  are reported: again they are decreasing as  $e/R_{circ}$  is increased.

**9.2. SAME SPAN AND WEIGHT**

A similar analysis has been conducted on arches with the same span - 4 m - and weight in terms of area - 4.33 m<sup>2</sup>.

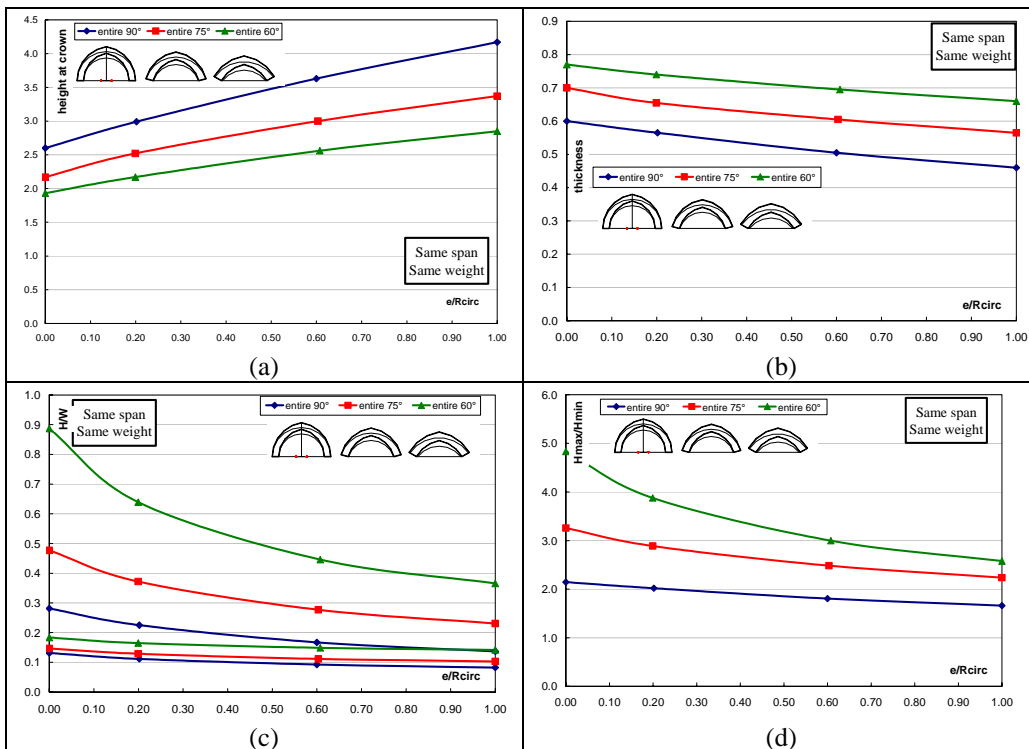


Figure 24. Main results for whole arches with same span and weight.  
 a) height at the crown; b) thickness; c) maximum and minimum thrust over weight ratio; d) maximum and minimum thrust ratio.

In this case, whilst the trend of the weight at the crown (Fig. 24.a), the ratios H/W (Fig. 24.c) and  $H_{max}/H_{min}$  (Fig. 24.d) are similar to the previous analyses, the

thickness of the arch will decrease when  $e/R_{\text{circ}}$  and the embrace are increased (Fig. 24.b). Again, best arch shapes are around  $e/R_{\text{circ}} = 0.6$ .

### 9.3. HALF AND WHOLE ARCHES WITH SAME SPAN AND THICKNESS

Adding the results gained in Fig. 23 to the values obtained for the half arch with same span and thickness, we obtain the graphs reported in Fig. 25.

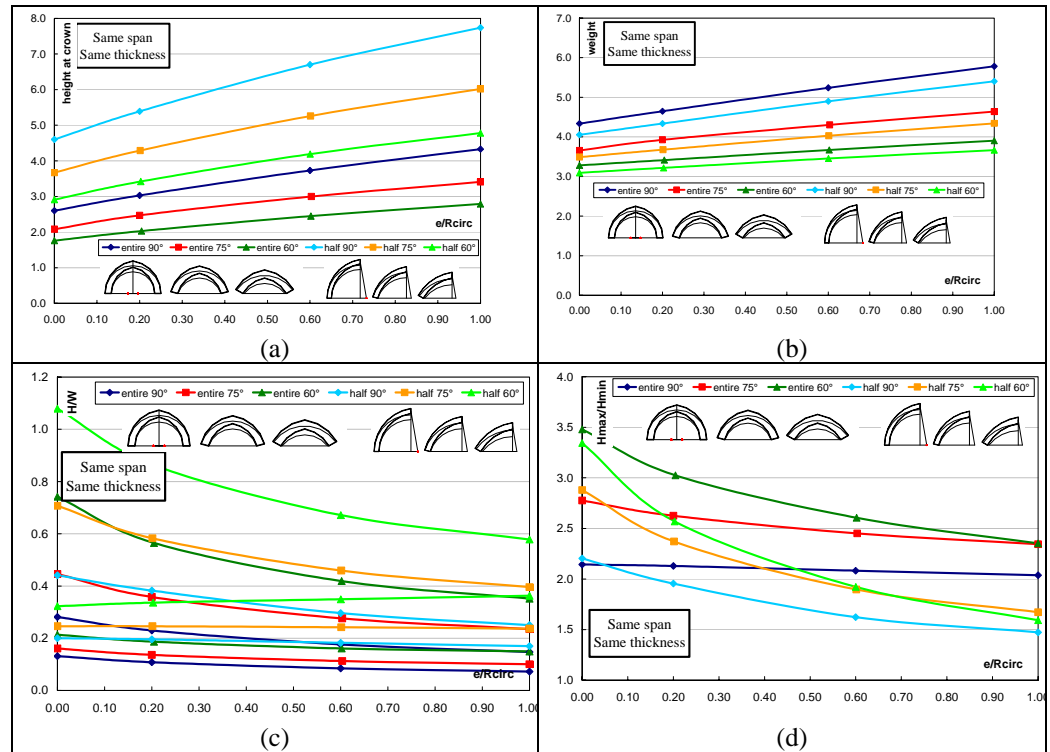


Figure 25. Main results for the whole and half arches with same span and thickness.  
 b) height at the crown; b) weight; c) maximum and minimum thrust over weight ratio; d) maximum and minimum thrust ratio.

For simplicity, one sample of circular arch and one sample of pointed arch ( $e/R_{\text{circ}} = 0.6$ ) were chosen. The results in terms of height, weight, minimum and maximum thrust and maximum displacements are visualized in Tab. 1.

Comparing the values, the tallest arch is the half pointed one and the shallowest is the whole circular one; the lightest one is the half circular arch and the heaviest is the whole pointed one.

About the thrust, the minimum values of the  $H_{max}$  and  $H_{min}$  are both those of the whole pointed arch but the greatest ratio of thrust is that of the half circular arch. In terms of displacements, again the whole pointed arch reaches the maximum value.

Compared to the other structures in Fig. 26 the visualization of the deformation for each type of arch at maximum displacements is depicted.

Span	4.0	4.0	4.0	4.0
Thickness	0.6	0.6	0.6	0.6
Height	2.6	3.73	4.6	6.7
Weight	4.32	5.24	4.05	4.89
Hmin	0.56	0.42	0.81	0.88
Hmax	1.21	0.89	1.82	1.47
$H_{max}/H_{min}$	2.16	2.12	2.25	1.67
Max displac	25%	48%	16%	12.5%

Table 1. Comparison of four arches with same span and thickness.

Therefore, it seems that the best behaviour of these arches is assumed by the whole pointed arch with  $e/R_{circ} = 0.6$  and that the worst is the half pointed arch with the highest value of  $H_{min}$ , a quite high value of  $H_{max}$  and the smallest possible displacement.

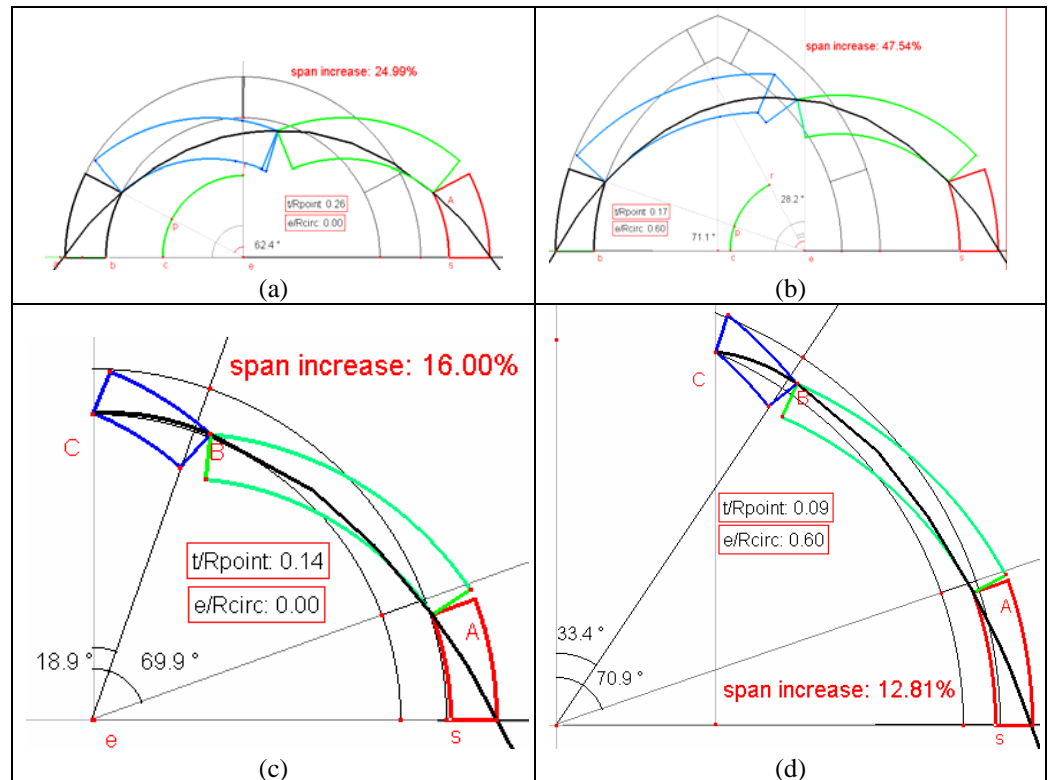


Figure 26. Collapse of the whole and the half arch with the same span.

## 10. CONCLUSIONS

This chapter analyzes the structural behaviour of whole and half masonry arches focusing on pointed arches. The following facts have been deduced:

The minimum and the maximum thrust lines of a whole pointed arch are slightly different from those of the circular arch. While in the latter three hinges are expected to form, the geometry of the pointed arch induces the formation of four hinges. Any slight asymmetry, however, whether in the geometry of the arch or in the loading, will ensure that only one of the hinges near the crown will form, so that again a three hinges mechanism will be activated.

In the thinnest circular arch there is the formation of five hinges whilst in the pointed arch there is an additional hinge. Determining the minimum thickness for

pointed arches, as the eccentricity is increased, smaller thickness of the voussoirs is requested and hinge location to the crown is moved. Keeping constant the value of the embrace, pointed arches can be thinner than circular arches. Increasing the value of the eccentricity allows even thinner arches to remain stable.

About the thrust values, the parametric analysis has allowed to note that for the whole arch:

- keeping constant the value of  $t/R_{\text{point}}$  and  $e/R_{\text{circ}}$ , the range of possible positions between the maximum and the minimum thrust (also quantifiable in terms of  $H_{\text{max}}/H_{\text{min}}$ ) decreases when the angle of embrace is increased from  $60^\circ$  to  $90^\circ$ ;
- keeping constant the value of  $e/R_{\text{circ}}$  and the angle of embrace, the value of  $H_{\text{max}}/H_{\text{min}}$  increases when the ratio  $t/R_{\text{point}}$  increases; keeping constant the angle of the embrace and the ratio  $t/R_{\text{point}}$ , the ratio  $H_{\text{max}}/H_{\text{min}}$  increases when the ratio  $e/R_{\text{circ}}$  is increased.

In the case of the half arch, a different location for the hinges has been considered; at the crown the hinge will only form at the intrados so that the half circular arch could be thinner than the half pointed one.

The theory developed by [Ochsendorf J., 2002] on circular arches for the displacement of the supports has been confirmed for pointed arches. The main result is that pointed arches can bear greater displacement than the circular arches. In particular:

- keeping constant the value of  $t/R_{\text{point}}$  and  $e/R_{\text{circ}}$ , the maximum displacement decreases when the angle of embrace is increased from  $60^\circ$  to  $90^\circ$ ;
- keeping constant the value of  $e/R_{\text{circ}}$  and the angle of embrace, the allowable displacement increases when the ratio  $t/R_{\text{point}}$  increases;
- keeping constant the angle of the embrace and the ratio  $t/R_{\text{point}}$ , the maximum value increases when the ratio  $e/R_{\text{circ}}$  is increased.

In case of arches with same span and thickness, highest and heaviest arches have smaller values of  $H/W$  and  $H_{\max}/H_{\min}$ ; the shallowest and the lightest ones have higher values of  $H/W$  and  $H_{\max}/H_{\min}$ .

In case of arches with the same span and weight, the thickness will decrease when  $e/R_{\text{circ}}$  and the angle of embrace are increased.

Comparing the behaviour of four arches (one whole circular, and pointed, one half circular and pointed) having same span and thickness, in terms of height, weight,  $H_{\min}$  and  $H_{\max}$ ,  $H_{\max}/H_{\min}$  and maximum displacement, it was found that the best shape of arch was the whole pointed one and that the worst was the half pointed one.

Moving one of the supports of the arch in any direction into the plane and tracing the domains of possible positions, pointed arches allow greater displacements in the plane. The domains increase when the eccentricity of the centres is increased and the angle of embrace decreased.

All the theoretical values have been checked each other with two different codes – Matlab (analytical code) and Cabri (visual graphic code) and the results agree.





## **CHAPTER 8:**

### **EXPERIMENTS ON POINTED ARCHES**

#### **1. INTRODUCTION**

Only few cases of experiments on arches (even in small scale) are reported in literature and none of them concerns pointed arches (with the exception of Leonardo's case). In 1732 Danisy, quoted by [Frezier, 1737](Fig.1.a), carried out a series of experiments on plaster arches investigating the collapse by the hinging of the voussoirs. [Méry, 1840] (Fig. 1.b) describes three experiments held by Boistard in 1810 on circular and hammer handle arches made by brick blocks jointed by thin layers of mortar with and without the load on the haunches. [Heyman J., 1999] reports a model of an arch built by Barlow in 1846 composed by six voussoirs and mortar made of small pieces of wood so that when three of the four pieces were removed the line of thrust became visible (Fig. 1.c). [Huerta S., 2001, 2004] made very simple models of a slightly pointed arch with cardboard (Fig. 1.d). Making four

different runs; in the first three he only moved one of the supports towards or away from the other one and up, in the fourth run he moved one support horizontally towards the second while moving the latter upwards. He has shown the capacity of the structure to respond to actions by cracking so that the position of the thrust line is unambiguously determined.

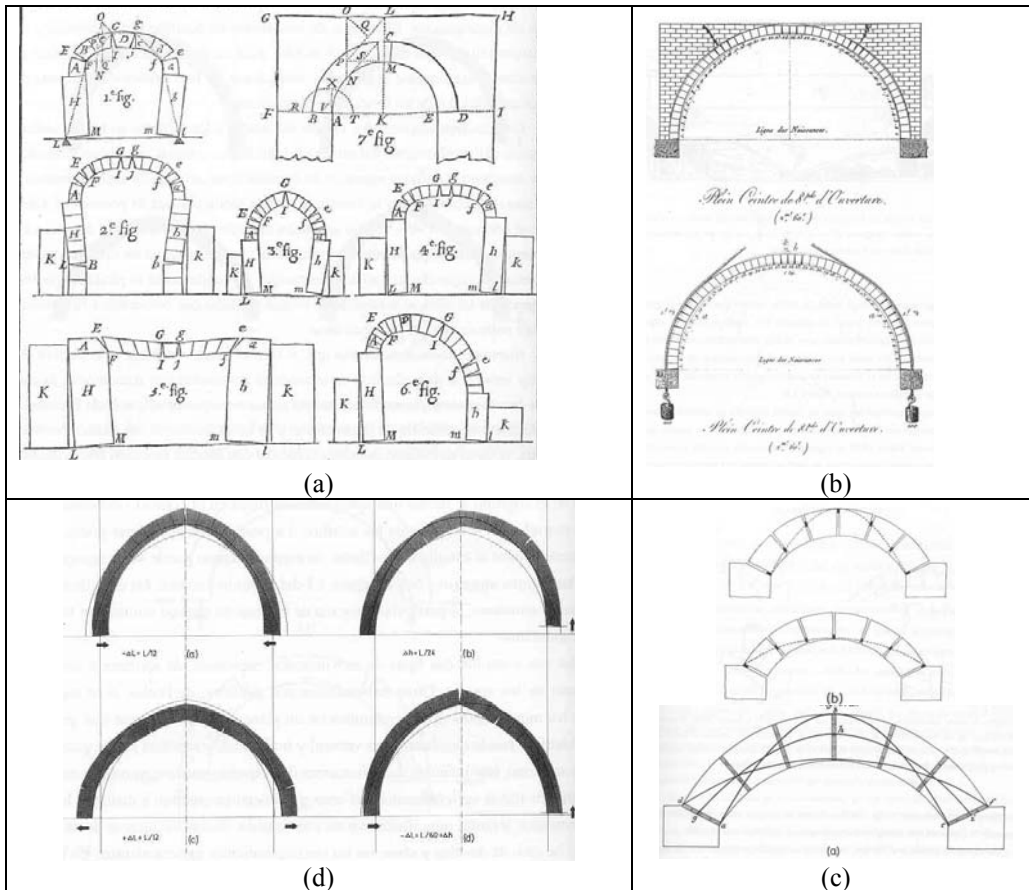


Figure 1. Experiments on arches in Literature.

- a) Source: Danyzy [1732] – *Méthode générale pour déterminer la résistance qu'il faut opposer à la poussée.*
- b) Source: Boistard [1810] – *Expériences sur la stabilité des voutes*
- c) Source: Barlow [1846] – *On the existence (pratically) of the line of equal horizontal thrust in aches, and the mode of determining it by geometrical construction.*

d) Source: Huerta [2001] – *Mechanics of masonry vaults: The equilibrium approach.*

## 2. THE EXPERIMENTAL CAMPAIGN

In order to verify the theory developed with the two computer codes (Matlab and Cabri) on arches collapse due to supports' displacements, an extensive experimental campaign on these elements, made with small concrete blocks, has been carried out. Having fixed the inner span to be 1 m and the angle of every single block equal to  $7.5^\circ$ , eight different types of arches were tested. In Fig. 2 the first four tests, characterized by the same value of  $t/R_{\text{point}} = 0.12$ , are shown.

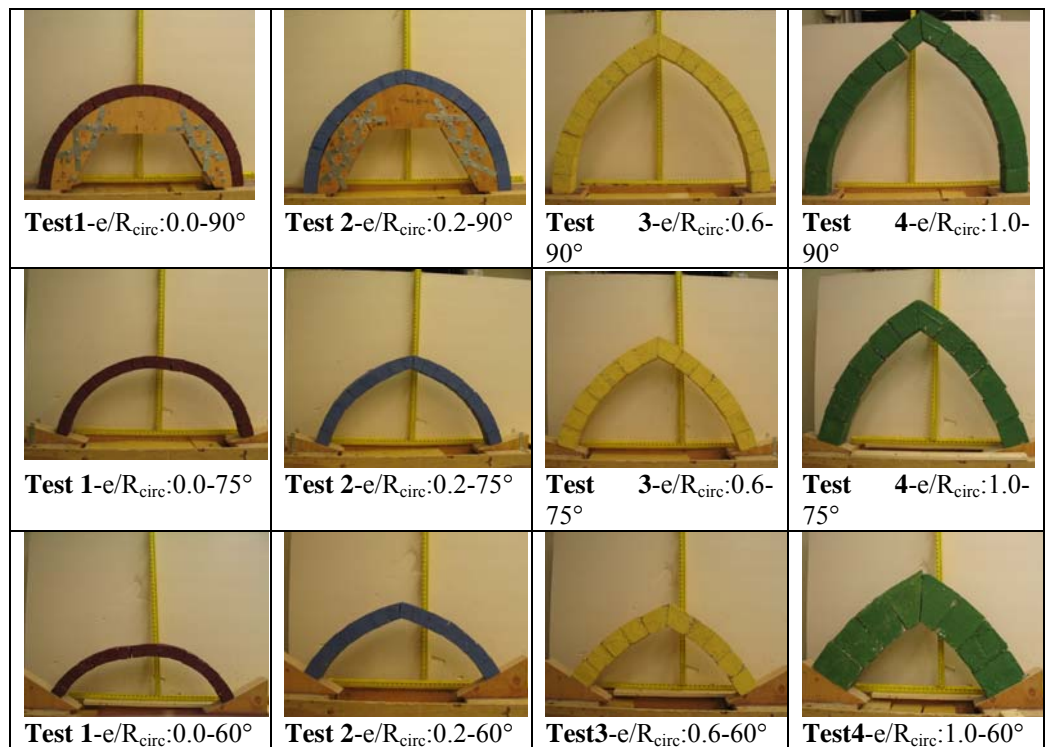


Figure 2. Tested arches with  $t/R_{\text{point}}=0.12$ .

Test 1 represents the arch with zero eccentricity or the circular arch, test 2 a slightly pointed arch ( $e/R_{\text{circ}} = 0.2$ ), test 3 a pointed arch ( $e/R_{\text{circ}} = 0.6$ ) and test 4 a

deeper pointed arch with  $e/R_{\text{circ}} = 1.0$ . Because of the choice of the size of the voussoirs, simply subtracting two blocks each time on both sides and placing two wedges at their place, it is possible to analyze the behaviour of the same arch in the three embraces of  $90^\circ$ ,  $75^\circ$  and  $60^\circ$ . The other four tests (not shown in Figure 2) have the same ratio of  $e/R_{\text{circ}}$  but values of  $t/R_{\text{point}} = 0.18$ , that is 1.5 time more the previous tests.

TEST	$e/R_{\text{circ}}$	$t/R_{\text{point}}$	angle	num.	Span	Height	Weight	Hmin	Hmax
			[deg]		[m]	[m]	[KN]	[KN]	[KN]
1	0	0.12	90	24	1.0	0.564	0.257	0.049	0.058
2	0.2	0.12	90	22	1.0	0.677	0.338	0.048	0.065
3	0.6	0.12	90	18	1.0	0.877	0.535	0.054	0.085
4	1.0	0.12	90	16	1.0	1.062	0.779	0.059	0.111
5	0	0.18	90	24	1.0	0.599	0.410	0.067	0.102
6	0.2	0.18	90	22	1.0	0.725	0.550	0.066	0.118
7	0.6	0.18	90	18	1.0	0.957	0.895	0.070	0.163
8	1.0	0.18	90	16	1.0	1.181	1.347	0.074	0.223
1	0	0.12	75	20	0.966	0.435	0.214	0.049	0.073
2	0.2	0.12	75	18	0.959	0.520	0.275	0.049	0.081
3	0.6	0.12	75	14	0.943	0.662	0.417	0.054	0.105
4	1.0	0.12	75	12	0.927	0.786	0.584	0.059	0.135
5	0	0.18	75	20	0.966	0.470	0.342	0.066	0.132
6	0.2	0.18	75	18	0.959	0.567	0.447	0.066	0.151
7	0.6	0.18	75	14	0.943	0.736	0.698	0.070	0.204
8	1.0	0.18	75	12	0.927	0.894	0.101	0.074	0.277
1	0	0.12	60	16	0.866	0.314	17.11	0.049	0.918
2	0.2	0.12	60	14	0.837	0.373	21.19	0.049	0.974
3	0.6	0.12	60	10	0.777	0.461	29.90	0.050	0.119
4	1.0	0.12	60	8	0.714	0.528	38.94	0.051	0.149
5	0	0.18	60	16	0.866	0.349	27.34	0.067	0.174
6	0.2	0.18	60	14	0.837	0.421	34.50	0.065	0.191
7	0.6	0.18	60	10	0.777	0.531	50.00	0.064	0.249
8	1.0	0.18	60	8	0.714	0.894	67.46	0.060	0.337

Table 1. Characteristic data of tested arches.

In Table 1 the test type, the value of  $e/R_{\text{circ}}$ ,  $t/R_{\text{point}}$  and the angle, the number of blocks, the span, the height, the weight (considering a specific load of  $24 \text{ kN/m}^3$ ) and the value of the minimum and maximum thrusts are presented.

It is noticeable that the shallowest arch is the circular arch (test 1) with an embrace of  $60^\circ$  with a height of 0.314 m and the tallest is the deepest pointed arch (test 8) with the embrace of  $90^\circ$ , 1.18 m high. Similarly, such arches are also respectively the lightest (test 1 with 0.171 KN of weight) and the heaviest (test 8 with 1.347 KN). About the minimum and the maximum thrust in absolute terms, the arches that express less thrust, 0.0486 KN is the smallest pointed one with an embrace of  $60^\circ$  and the arch with maximum thrust, 0.3372 KN, is test 8 with an embrace of  $60^\circ$ .

To be easily recognized, arches with the same value of eccentricity and varying thickness ( $t/R_{\text{point}} = 0.12$  and  $0.18$ ), were painted in different colours. Circular arches were painted in red, pointed arches with the ratio  $e/R_{\text{circ}} = 0.2$  in blue, with the value of  $e/R_{\text{circ}} = 0.6$  in yellow and with  $e/R_{\text{circ}} = 1.0$  in green.

Five different types of testes have been performed during the experimental campaign. The first one consisted in the evaluation of the friction coefficient; the other four ones consisted into moving one of the two supports of the arch away, towards, up and down from the other one. In order to have an average on the behaviour of each experiment, three trials have been done for each test so that around 200 trials were performed. A benchmark for slight inside and outside displacements (without any friction) of one of the two sides of the arch was built and a remotely controlled steel machine for the friction test and up and down movements was used. Two levels placed horizontally and vertically, measured the span and the height of the arches in the original position and at the failure. In order to avoid the sliding of the arch on the two supports, two pieces of wrinkled paper were placed on the surface of the bench-mark and on the two wedges when utilized.

### 3. FRICTION COEFFICIENT MEASURES

The failure of a masonry structure due to sliding has been detected by the researchers as often as the hinges mechanism. If the effect of the mortar is neglected, an arch is stable against sliding when the angle between the line of resistance and the normal is smaller than the angle of friction. The minimum angle of inclination with the normal at which sliding will occur is called the angle of repose and its tangent, or ratio of tangential to the normal component of the force, is called the coefficient of friction.

[Méry, 1840] states that the greatest danger of this type of failure threatens the spreading of arches and advises to use a value of 0.76. [Baker, 1891] points out that the value under the most unfavorable conditions – i.e. while mortar is wet – is about 0.50, which correspond to an angle of friction of about 25°. [Sondericker, 1907] says that in the case of masonry joints, the value of the friction coefficient is taken to be from 0.4 to 0.5. [Jorini, 1918] differentiates the coefficient of friction if the mortar is still wet or dried and indicates a range of variability between 0.5 and 0.75 (or a friction angle between 27° and 37°).

Authors	Year	Material	Friction Coeff.
Méry	1840	not specified	0.76
Baker	1891	not specified	0.5
Sondericker	1907	not specified	0.4 ÷ 0.5
Jorini	1918	not specified	0.5 ÷ 0.75
Meli	1972	brick	0.7 ÷ 1
Hegemier	1978	concrete blocks and mortar	0.7 ÷ 0.4
Hamid and Drysdale	1982	bricks and mortar	0.7 ÷ 1.5
Atkinson	1989	old and new concrete blocks	0.7 ÷ 1.15
Andreas and Maroder	1991	not specified	0.4
Calvi and Magenes	1991	bricks	0.59
Riddington and Jukes	1994	bricks and blocks	0.8 ÷ 0.92
Zorri	1994	bricks	0.5
Alpa, Gambarotta and Monetto	1996	not specified	0.5
Theodosius and Tassios	1996	not specified	0.3 ÷ 1.4

Table 2. Friction coefficient values indicated in literature.

Later, many researchers have done experimentations on stones, bricks or concrete blocks achieving the results shown in Tab. 2. The authors, the year of the publication of the results, the material with which the experiments were made with and the value of the friction coefficient are reported.

As it can be noticed, although in literature many values are cited, there is a certain discrepancy among them. For this reason, using a machine remotely controlled that allowed vertical displacements, the values of the angle for which the sliding failure occurs have been measured directly. For each group of blocks (each belonging to one of the eight tests) three pairs of blocks without paint and three painted ones have been randomly chosen; therefore, six samples of units per test for a total amount of 48 trials were tested.

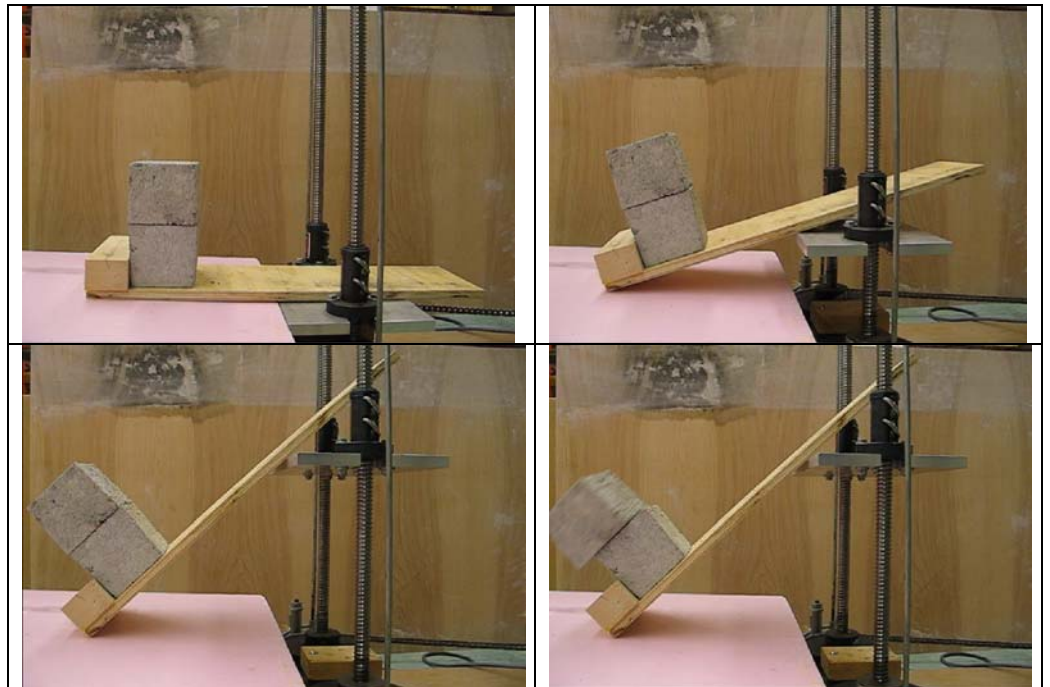


Figure 3. Friction test obtained moving up the steel plate remotely controlled.

In Fig. 3 four different moments in a general try of the test when the steel plate was moving up are captured, and in Tab. 3 the average values are reported.

TEST	Paint	Friction coefficient	Friction coeff. Average	Friction coeff. Total Average
1	YES	0.839	0.71	0.66
	NO	0.578		
2	YES	0.631	0.65	
	NO	0.674		
3	YES	0.864	0.77	
	NO	0.676		
4	YES	0.652	0.66	
	NO	0.667		
5	YES	0.601	0.59	
	NO	0.578		
6	YES	0.570	0.59	
	NO	0.609		
7	YES	0.528	0.53	
	NO	0.529		
8	YES	0.641	0.64	
	NO	0.650		

Table 3. Friction coefficient values from experimental testes.

The range of variability among the values is due to the fact that, although all the blocks have been built with the same amount of water (1 part), cement (2 part), sand (4 parts) and gravel (8 parts), they have not been made all together. Therefore, being a hand-made product, slight differences in the manufacturing are expected. First using the average of the painted blocks and the average of the unpainted ones, then using the average for each test and finally the average of all the tests, the friction coefficient that was found is 0.66, corresponding to a friction angle of 33.5°. This value has been very useful in the following tests to understand some collapse mechanisms not estimated in theory.



#### 4. MOVING THE SUPPORTS APART

This experiment, already done by [Ochsendorf J., 2002] on two small concrete circular arches ( $e/R_{\text{circ}} = 0$ ),  $t/R_{\text{point}} = 0.23$  and embrace of  $90^\circ$  in the first case and  $t/R_{\text{point}} = 0.13$  and embrace of  $80^\circ$  in the second one, showed that the collapse occurred in both cases by a four hinge mechanism when the locus of pressure points arrived at the extrados at the support (i.e. the arch exceeded the stability conditions for one of the supporting regions of the arch).

From Figure 4 to 7 the new experiments on pointed arches are visualized. Each of them represents a typical failure mechanism so that in Fig. 4 the circular arch ( $e/R_{\text{circ}} = 0$ ) is depicted, in Fig. 5 the first pointed arch with small eccentricity ( $e/R_{\text{circ}} = 0.2$ ), in Fig. 6 the arch with the eccentricity of 0.6 and at last, in Fig. 7 the arch with the ratio  $t/R_{\text{point}} = 1.0$ . For each picture, the Cabri model and three moments of the collapse have been chosen.

It is clearly visible that the failure mode and the hinge location with their movement up to the crown have been accurately predicted by the Matlab and Cabri models. As expected by theory the collapse occurred when the thrust line reached one of the two supports with a four hinges mechanism (or in some cases with a five hinges mechanism) in the thinnest arches with high value of the embrace (Fig. 4 - 5 - 6) and with the snap-through in the thickest ones with a small value of the embrace (Fig. 7); therefore, these collapse mechanisms depend fundamentally on the ratio  $t/R_{\text{point}}$  and on the angle of embrace.

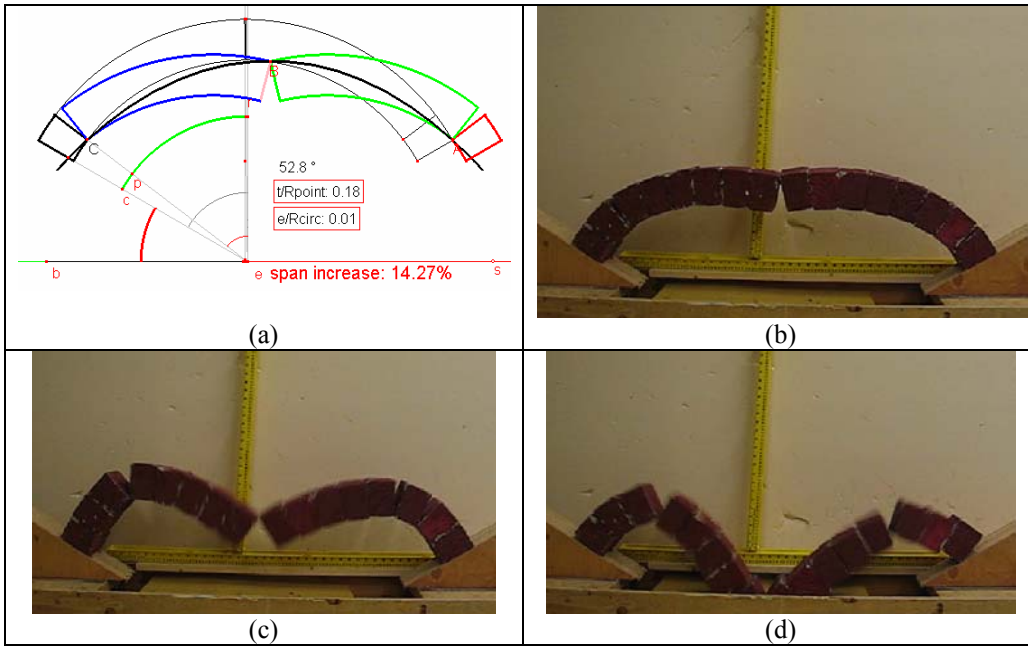


Figure 4. Test 5 -  $t/R_{point} : 0.18$  -  $e/R_{circ} : 0$  -  $\alpha : 60^\circ$  -- a) cabri model; b-c-d) test pictures.

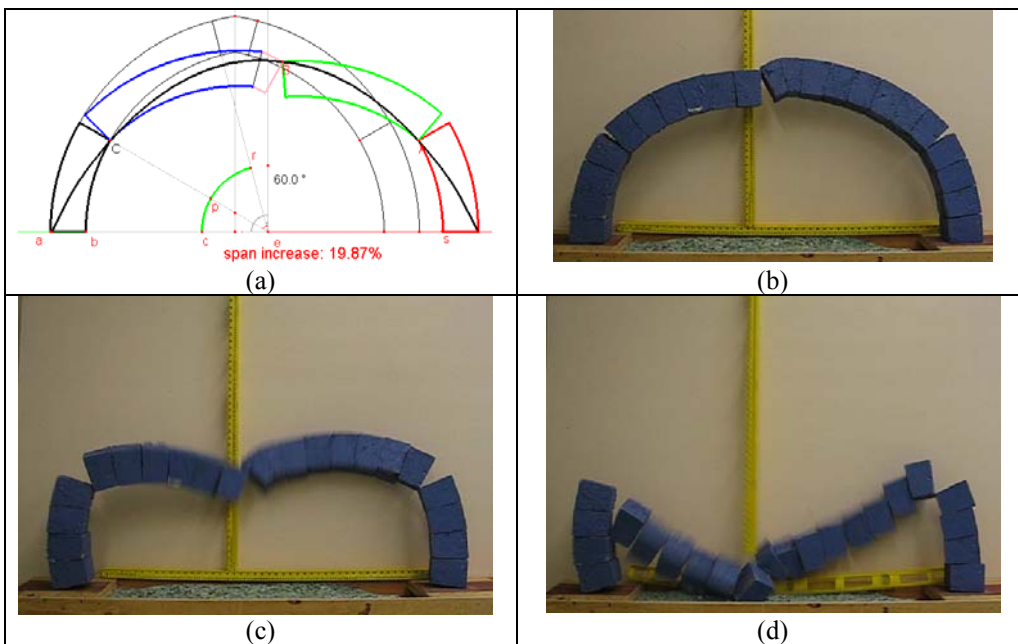


Figure 5. Test 6 -  $t/R_{point} : 0.18$  -  $e/R_{circ} = 0.2$  -  $\alpha : 90^\circ$  -- a) cabri model; b-c-d) test pictures.

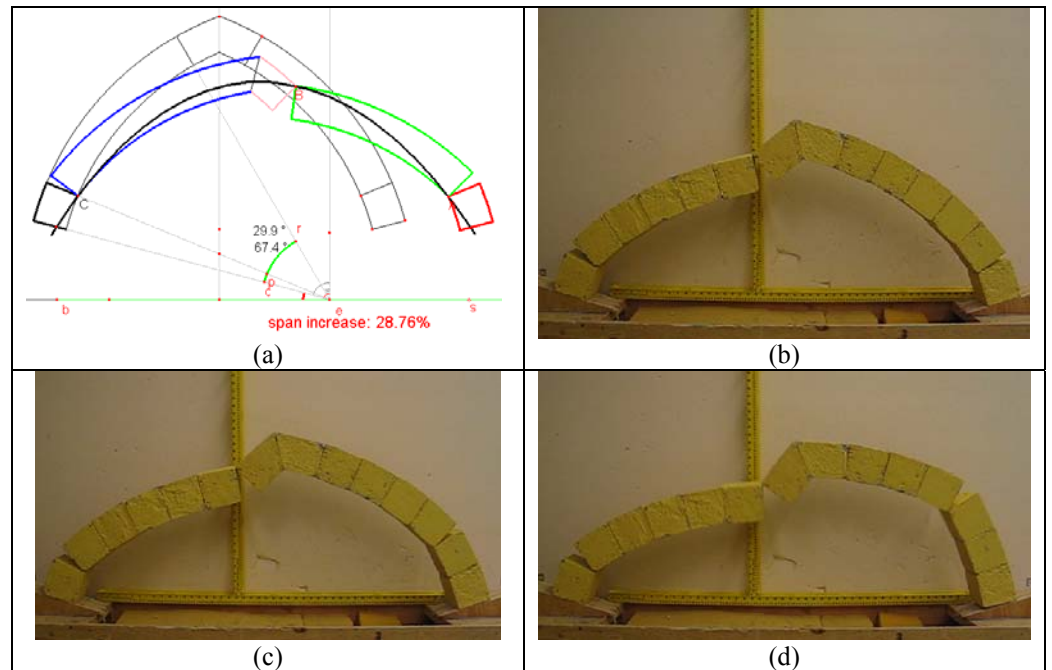


Figure 6. Test 3 -  $t/R_{point} : 0.12$  -  $e/R_{circ} = 0.6$  -  $\alpha : 75^\circ$  -- a) cabri model; b-c-d) test pictures.

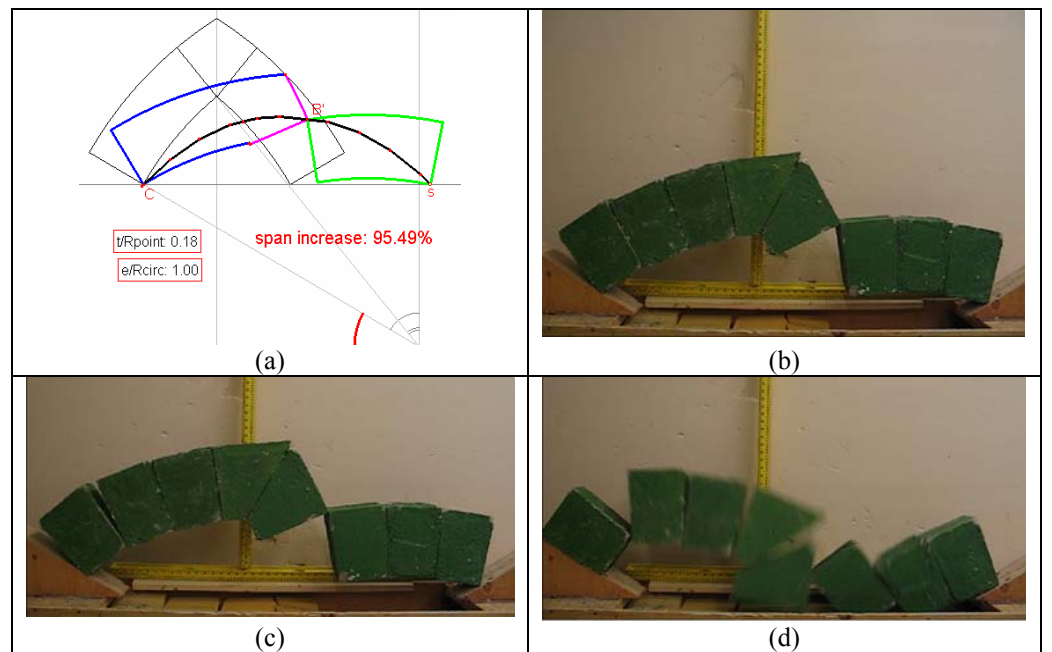


Figure 7. Test 8 -  $t/R_{point} : 0.18$  -  $e/R_{circ} = 1.0$  -  $\alpha : 60^\circ$  -- a) cabri model; b-c-d) test pictures.

MOVING THE SUPPORT APART							
TEST	$\alpha$	EXPERIMENTAL RESULTS			MATLAB/CABRI		
		HINGE	HINGE	Spread	HINGE	HINGE	Spread
	[deg]	[deg]	[deg]	[%]	[deg]	[deg]	[%]
<b>1</b>	90	--	--	--	0	55.5	2.13
<b>2</b>	90	--	--	--	17.1	62.1	11.04
<b>3</b>	90	30	67.5	18.27	29.5	67.02	24.61
<b>4</b>	90	37.5	75	29.35	37.5	75	51.42
<b>5</b>	90	0	52.5	7.00	0	59→52	11.26
<b>6</b>	90	15	60	16.33	17	69.5→62	27.50
<b>7</b>	90	30	75→60	33.00	29.5	74.5→59.5	48.77
<b>8</b>	90	37.5	75	39.00	37.5	75→67.5	70.12
<b>1</b>	75	0	52.5→45	7.61	0	55→48	9.91
<b>2</b>	75	15	52.5	12.28	17	62→39.6	17.14
<b>3</b>	75	30	67.5→45	25.26	29.5	67→37	30.49
<b>4</b>	75	37.5	75→52.5	29.67	37.5	75→37.5	31.00
<b>5</b>	75	0	52.5	12.50	0	59.5→44.5	17.91
<b>6</b>	75	15	67.5→52.5	23.16	17	69.6→9.6	18.72
<b>7</b>	75	30	67.5→45	29.79	29.5	74.5→29.5	33.79
<b>8</b>	75	--	--	--	37.5	75→52.5	70.91
<b>1</b>	60	0	37.5→30	8.43	0	55.5→10.5	8.91
<b>2</b>	60	22.5	60→37.5	17.28	17	54.6→32.1	17.70
<b>3</b>	60	30	60→45	25.32	29.5	59.6→44.5	35.94
<b>4</b>	60	37.5	60	38.03	37.5	60→52.5	50.945
<b>5</b>	60	0	52.5→37.5	14.12	0	59.5→14.5	14.90
<b>6</b>	60	15	60→45	27.50	17	54.6→39.6	27.49
<b>7</b>	60	30	60	37.50	29.5	59.5→52	52.19
<b>8</b>	60	37.5	60→52.5	66.20	37.5	60→52.5	75.00

Table 4. Comparison between experimental results and modelling moving the support apart.

In Table 4, the comparison between all the experimental results and the corresponding modelling moving the support apart is depicted. For the 24 test types (8 arches for 3 values of the embrace), the location of the hinges and the value of the spread normalized to the span are reported. In particular, if the hinge movement occurs, the initial and the final value are specified. For the experimental results, the average of the values on the three trials is reported. It is clearly visible that both the

values of the hinge location and of the spread agree very well with the value predicted by theory.

### 5. MOVING THE SUPPORTS TOGETHER

This time the experiments revealed failure mechanisms that had been neglected when the theoretical model has been developed. As can be seen from Fig. 8 to 11 the collapse now depends on the ratio  $e/R_{\text{circ}}$  and the angle of embrace, as opposed to  $t/R_{\text{point}}$  and the angle of embrace in the case discussed in § 4.

Mainly three different mechanisms have been identified: the first one (also called of “type I”), visible only in the circular arch, is almost similar to the mechanism activated when the supports are moved apart with the hinges forming on the same side (Fig. 8.a); the second type (type II) is activated for any kind of arch (Fig. 8.e, 9.e, 10.e, 11.e) and the third one (type III) only for pointed arches (Fig. 9.a, 10.a, 11.a).

The type II mechanism mainly consists in the formation of the hinges at the intrados up to the crown and at the extrados at the base. Two facts can influence the collapse: the thrust line reaching the physical boundary of the arch somewhere so that the fourth hinge can form (collapse for lack of stability) or the thrust line being is out of the friction cone (collapse for sliding). This aspect, initially neglected in the theory, was added after being observed in the experiments. Because nothing similar was cited in the literature, the only considered collapse was by instability with unsafe values of maximum displacements. For the circular and the first pointed arch ( $t/R_{\text{point}} = 0.2$ ) the collapse induced by sliding has preceded the collapse by instability that occurred in the last two arches ( $t/R_{\text{point}} = 0.6$  and  $t/R_{\text{point}} = 1.0$ ). Drawing for each sketch the thrust line and the friction cone for an angle of  $33.5^\circ$  (corresponding to the average friction value of 0.66 found through the experiments stated in §9), this phenomenon is clearly shown in the Cabri models depicted in the Fig. 8.e, 9.e, 10.e and 11.e. In the first two arches the thrust line goes out of the friction cone in the

hinge at the crown (point B') and is fully inside in the arch; in the last two arches, on the other hand, the thrust line is inside the cone of friction at the crown but reaches the boundary at least in an other point to form the fourth hinge.

The type III collapse only regards to the pointed arches (it substitutes the type I in the circular arch) and it is exactly the failure mode described by [Baker, 1891], [Abraham, 1934] and [Fitchen, 1961]. Although according to the cited references it occurs for angles of  $90^\circ$ , the experiments have shown that this collapse takes place only with embrace of  $60^\circ$  (Fig. 9.a, Fig. 10.a and Fig. 11.a) being the type II collapse effective with wider embraces.

Comparing the final value of the span decrease between theory and practice (Table 5), it can be noticed that they match very well within the average error percentage of 18.22% for the embrace of  $90^\circ$ , 16.46% for the embrace of  $75^\circ$  and 9.76% for the embrace of  $60^\circ$ .

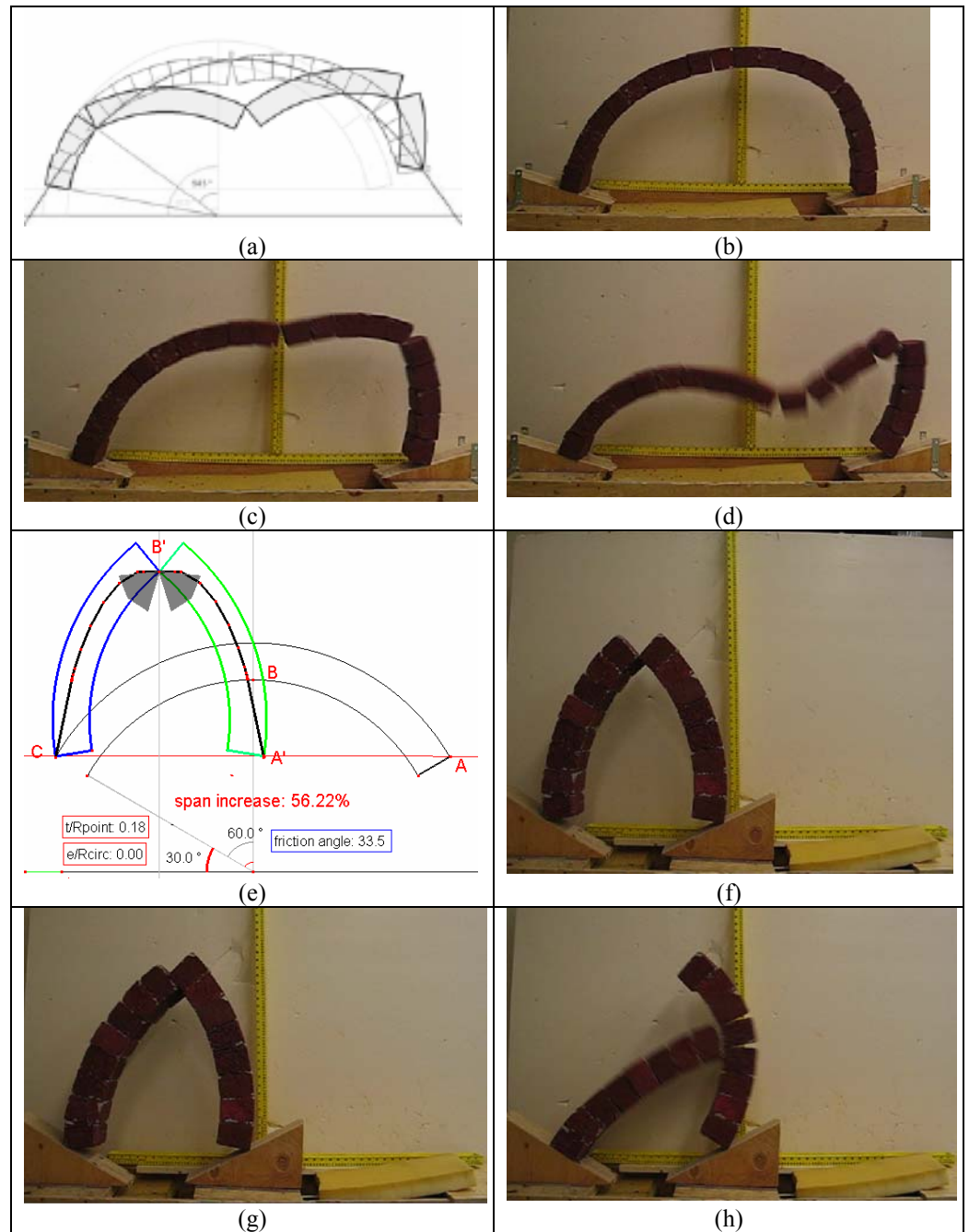


Figure 8. a-b-c-d) Test 5 -  $t/R_{\text{point}} : 0.18$  -  $e/R_{\text{circ}} = 0$  -  $\alpha : 75^\circ$  - type I of failure.

e-f-g-h) Test 5 -  $t/R_{\text{point}} : 0.18$  -  $e/R_{\text{circ}} = 0$  -  $\alpha : 60^\circ$  - type II of failure.

a) Source: Philippe Block Master of Science in Architecture Studies dissertation.

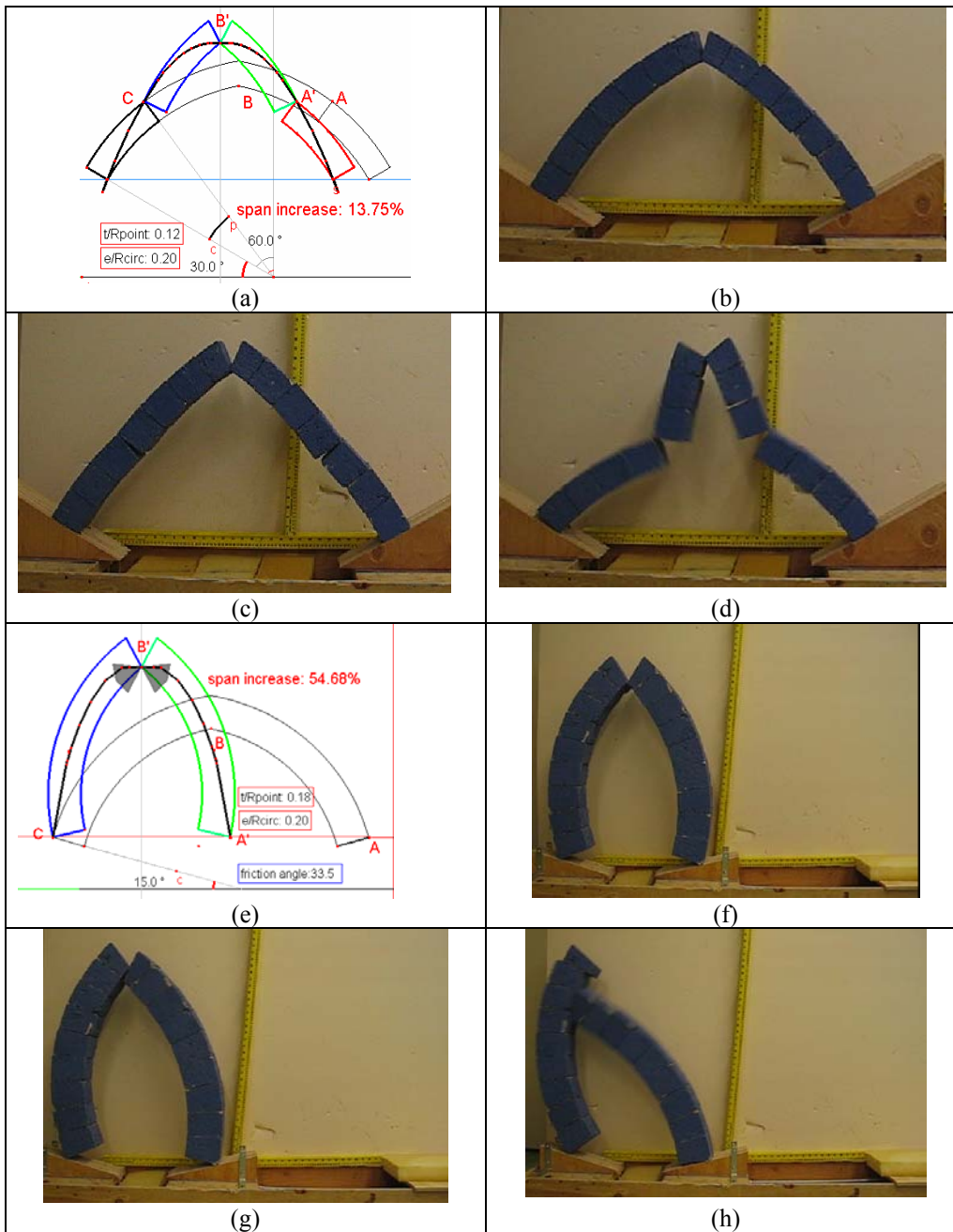


Figure 9. a-b-c-d) Test 2 -  $t/R_{point} : 0.12$  -  $e/R_{circ} = 0.2$  -  $\alpha : 60^\circ$  - type III of failure.  
 e-f-g-h) Test 6 -  $t/R_{point} : 0.18$  -  $e/R_{circ} = 0.2$  -  $\alpha : 75^\circ$  - type II of failure.



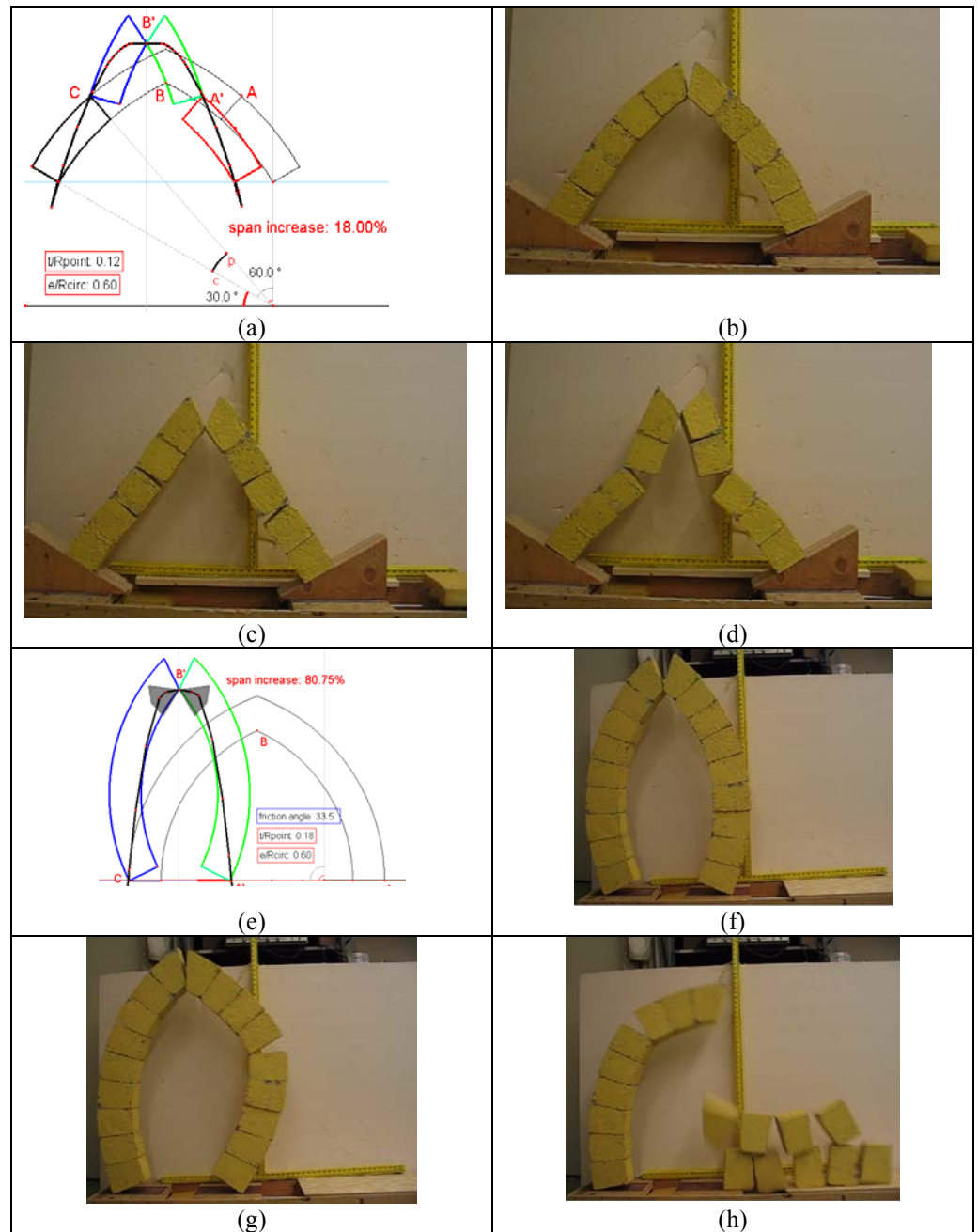


Figure 10. a-b-c-d) Test 3 -  $t/R_{point} : 0.12$  -  $e/R_{circ} = 0.6$  -  $\alpha : 60^\circ$  - type III of failure.  
 e-f-g-h) Test 7 -  $t/R_{point} : 0.18$  -  $e/R_{circ} = 0.6$  -  $\alpha : 90^\circ$  - type II of failure.

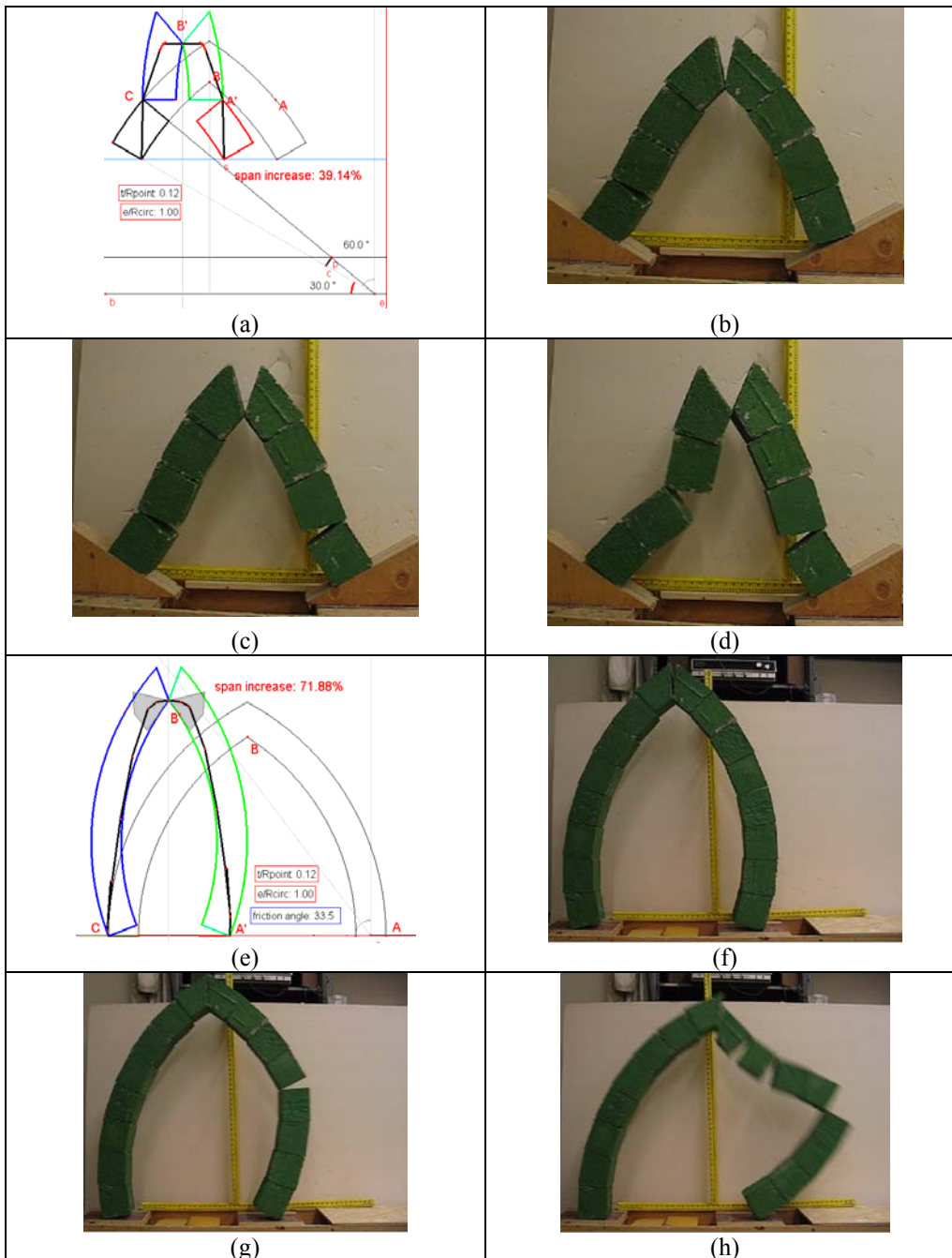


Figure 11. a-b-c-d) Test 4 -  $t/R_{point} : 0.12$  -  $e/R_{circ} = 1.0$  -  $\alpha : 60^\circ$  - type III of failure.  
 e-f-g-h) Test 4 -  $t/R_{point} : 0.12$  -  $e/R_{circ} = 1.0$  -  $\alpha : 90^\circ$  - type II of failure.

MOVING THE SUPPORT TOGETHER							
Test	$\alpha$	EXPERIMENTAL RESULTS					CABRI
		1 <sup>st</sup> hinge	2 <sup>nd</sup> -3 <sup>rd</sup> hinge	4 <sup>th</sup> hinge	Failure type	spread	spread
	[deg]	[deg]	[deg]	[deg]		[%]	[%]
1	90	--	--	--	--	--	--
2	90	--	--	--	--	--	10.42
3	90	0	90	52.5→60	II	49.54	49.08
4	90	0	90	60	II	45.00	71.88
5	90	7.5	90	52.5	II	3.83	3.92
6	90	0	90	52.5→37	II	31.83	51.05
7	90	0	90	52.5	II	73.68	80.75
8	90	--	--	--	Sliding	43.00	71.88
1	75	0→7.5	75	45→37.5	I	6.13	--
2	75	0	75	67.5 - 30	II and III	14.39	19.36
3	75	0	75	45	II,III and No coll.	58.60	Nocoll.
4	75	0	75	--	III and No coll.	75.82	Nocoll.
5	75	7.5	75	30→15	II	9.38	12.00
6	75	0	75	--	III – Sliding	53.68	54.68
7	75	0	75	--	Out of plane	48.57	Nocoll.
8	75	--	--	--	--	--	Nocoll.
1	60	22.5	60		I	15.75	--
2	60	0	37.5→30	--	III	11.25	13.75
3	60	0	60→37.5	--	III	17.30	18.00
4	60	0	60→45	--	III	32.86	39.14
5	60	0	60	--	III	55.69	56.22
6	60	0	60	--	Sliding	44.58	Nocoll.
7	60	0	60	--	II and No coll.	72.15	Nocoll.
8	60	--	--	--	--	--	Nocoll.

Table 5. Comparison between experimental results and modelling moving the support together.

## 6. MOVING THE SUPPORT VERTICALLY

The tests type was realized using a machine remotely controlled which allowed moving one of the two supports in vertical. Although the sharp corner of the blocks started damaging, as a consequence of the high number of testes previously done, the failures mode, the hinges location and the maximum displacement match very well with the ones predicted by theory.

Two different mechanisms are activated moving the support vertically as function of the pointidness of the arch. However, in both the cases, a four hinge mechanisms is activated: the difference is notable in the location of the hinges. For small values of the eccentricity, the collapse occurs along the development of the arch whilst for a great pointidness a hinge at the crown at the intrados will always develop.

From Figure 12 to 15, eight samples of arches have been chosen to represent the consistency of the results between theory and practice. Furthermore, it is enlightened that moving one support up produces the same results than moving the other support down, being the mechanism mirrored. As in the previous pictures, in the first one the Cabri model and the last three ones some captured frames during the experiments are shown.

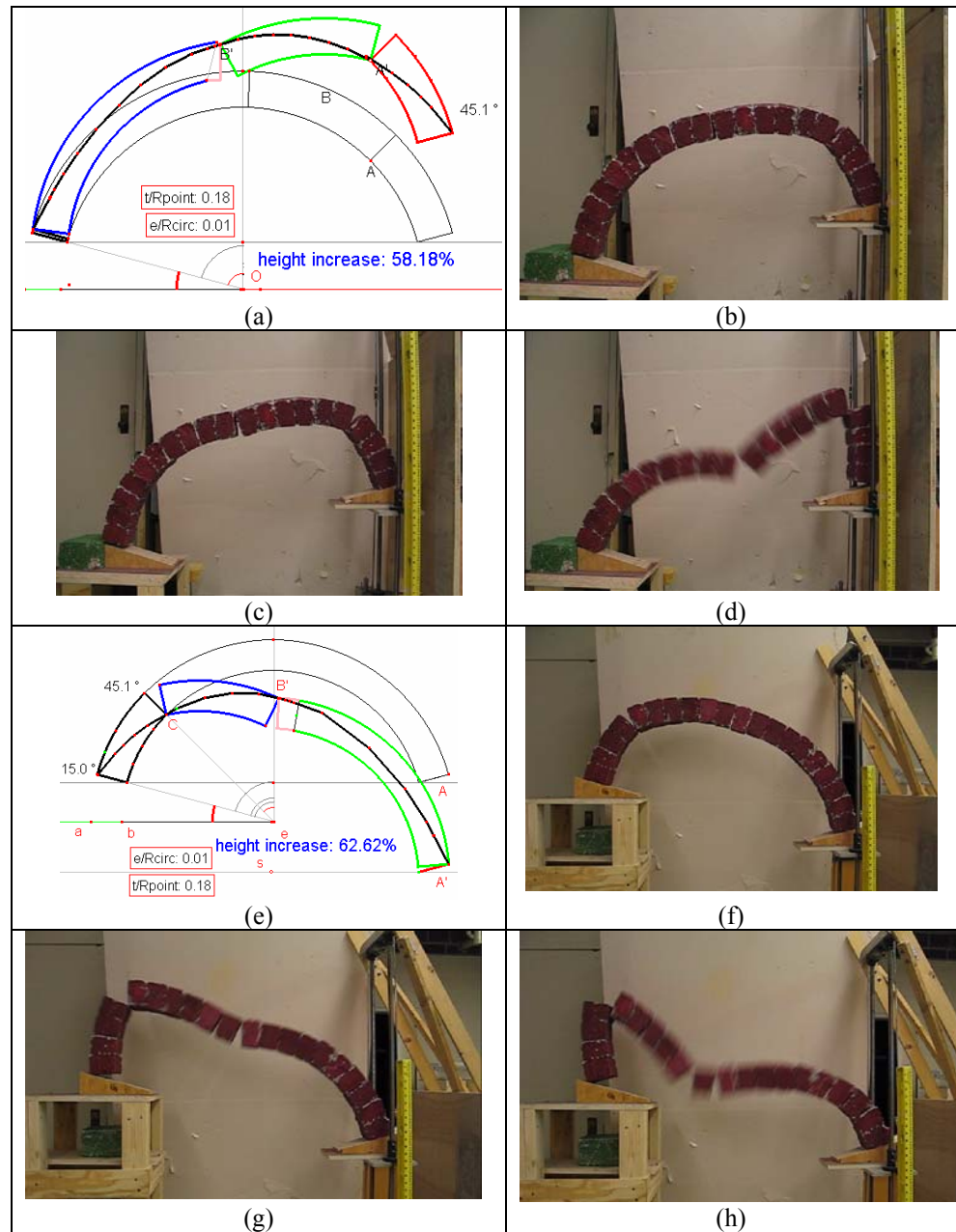


Figure 12. Test 5 -  $t/R_{point} :0.18$  -  $e/R_{circ}=0$  -  $\alpha:75^\circ$  - a/e) cabri model; b/f-c/g-d/h) test pictures.

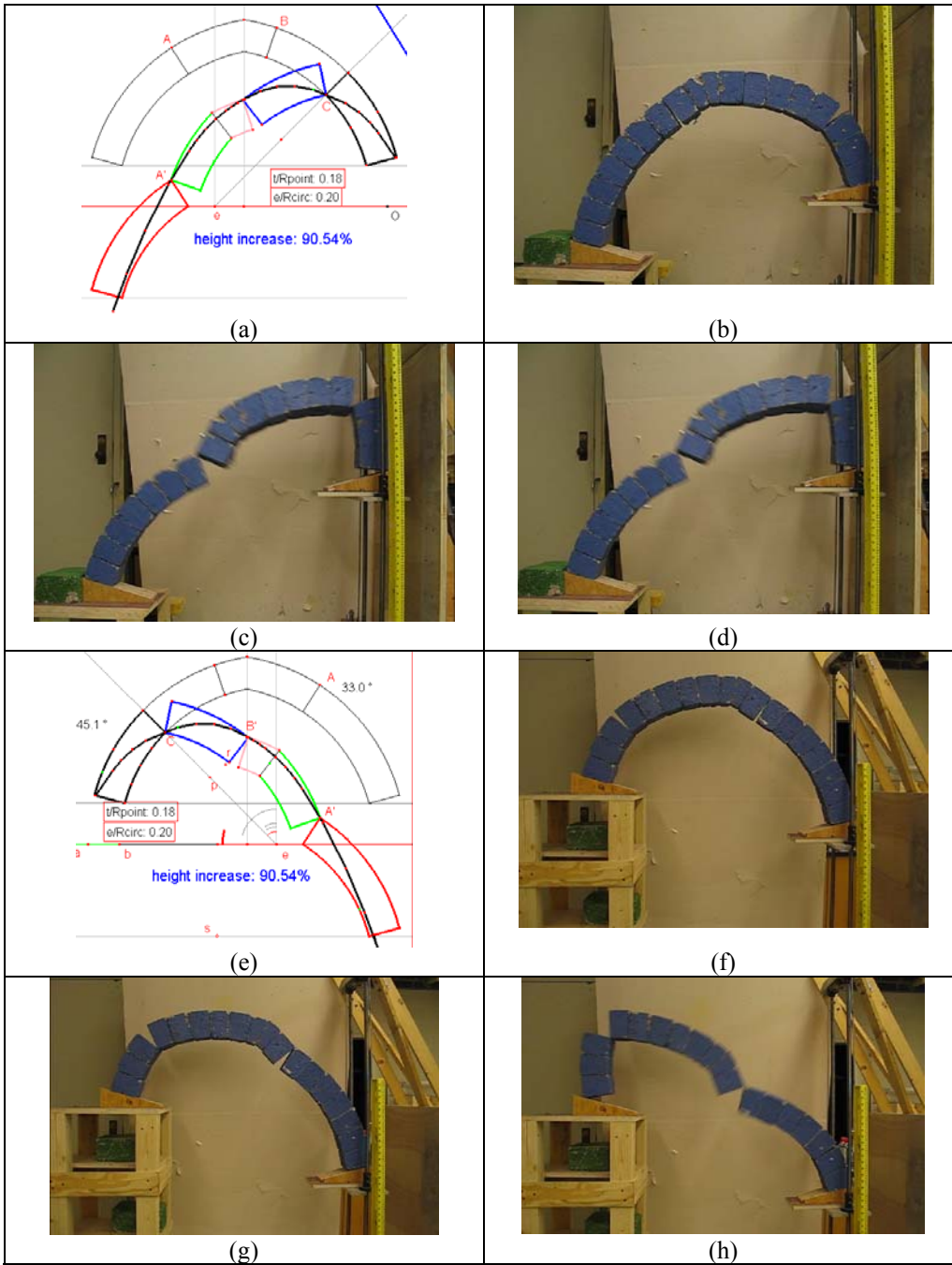


Figure 13. Test 6 -  $t/R_{point} :0.18$  - $e/R_{circ}=0.6$  - $\alpha:75^\circ$  -a/e) cabri model; b/f-c/g-d/h) test pictures.

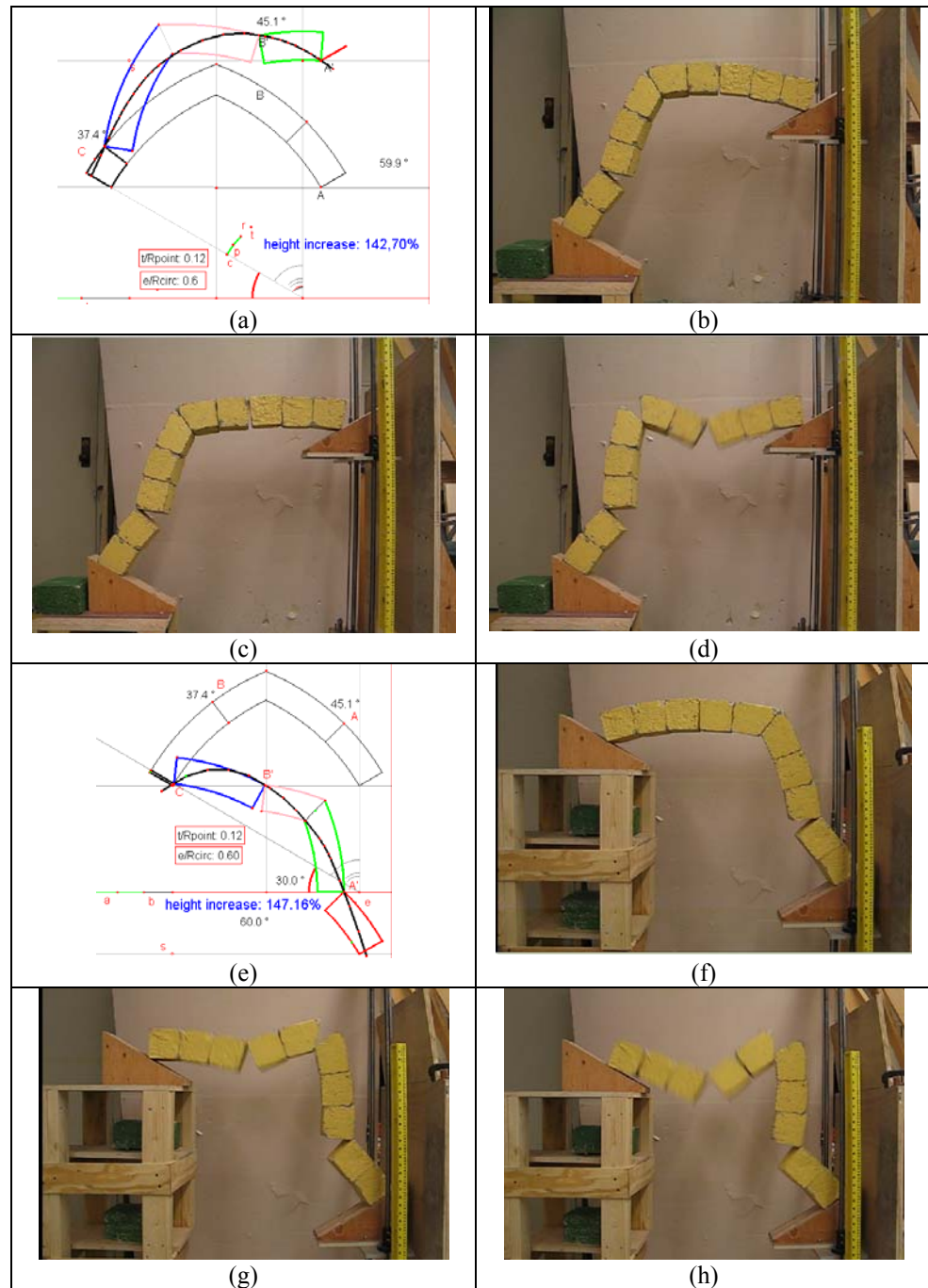


Figure 14. Test 3 - $t/R_{point} : 0.12$  - $e/R_{circ}=0.6$  -  $\alpha:60^\circ$  -a/e) cabri model; b/f-c/g-d/h) test pictures.

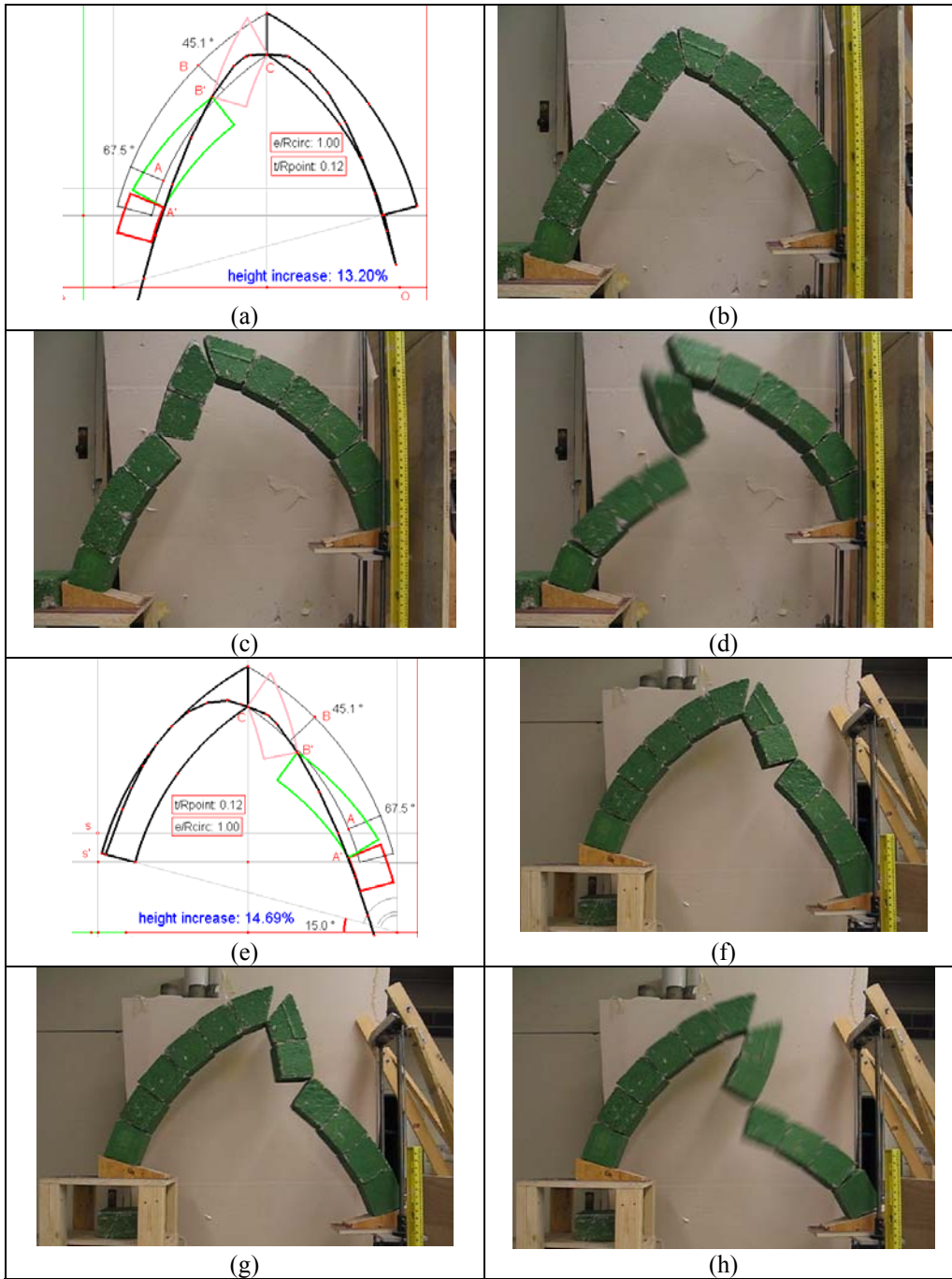


Figure 15. Test 4 - $t/R_{point} : 0.12$  - $e/R_{circ}=1.0$  -  $\alpha:75^\circ$  -a/e) cabri model; b/f-c/g-d/h) test pictures.



## 7. EXPERIMENTS VS MODELLING

The series of experiments held on different arches has delivered a better understanding of the real behaviour of these structures made by rigid blocks without any sort of mortar among the joints. Many of the results obtained through the theory developed with the Matlab and Cabri codes have been confirmed and, at the same time some matters otherwise neglected have been highlighted. Quoting [Huerta S., 2001] “Ars sine scientia nihil est – practice is nothing without theory, but theory without practice is simply dangerous”. In this spirit the experiments have been held and the comparison of theory and practice has resulted in very interesting discoveries.

First of all, the differences between theoretical and real arches have to be highlighted. In the model developed with Cabri and Matlab, the voussoirs are perfect rigid blocks with very sharp corners so that the hinge locations could occur exactly at the edge. To reproduce this situation in the lab only machined steel voussoirs would be suitable. Since this is not a common masonry structure, which is usually inexact in its construction, blocks made by concrete with naturally not perfectly defined edges were chosen. As a consequence, the hinges formations were expected to be slightly offset with respect to the theoretical model. The imperfect modelling of the blocks causes also slightly asymmetry in the whole arch so that the collapse could occur prematurely (for example in the circular arch the failure happens with a four hinge mechanism rather than a perfectly symmetrical five-hinge mechanism). Finally, when the arch approaches the collapse state, the thrust from the central region is nearly equal to the resistance of the supporting region of the arch. Any small movement will lead to changes in the stability of the system and to a premature collapse of the arch. In particular, small vibrations (due for example to the friction of the removable support when it is moving) will lead to the collapse of the arch and therefore it is highly difficult to reach the theoretical limit for the spreading of the supports.

The consequence of all these observations is that the theoretical approach predicts larger support separations measured just before collapse because of the perfect modelling of the blocks, the complete symmetry, the absolute absence of friction in the displacements and all the variables present in the lab that could lead to a premature collapse of the arches. What is more important is that the presented methods correctly predicted the final collapse mechanism in all the directions for the circular and especially for the pointed arches.

The first proof of the difference between theory and practice concerns the stability of test 1 ( $e/R_{\text{circ}} = 0$  and  $t/R_{\text{point}} = 0.12$ ) and test 2 ( $e/R_{\text{circ}} = 0.2$  and  $t/R_{\text{point}} = 0.12$ ) with the embrace of  $90^\circ$  before moving the support. In theory these two arches should stay because the minimum thickness for the circular arch is  $t/R_{\text{point}} = 0.1075$  and  $0.0829$  for the pointed arch; actually the blocks have a ratio of  $t/R_{\text{point}}$  of  $0.12$  which is larger than the minimum values. The two structures collapse as soon as the centring or the constraints at the supports are removed. This means that the values of  $t/R_{\text{point}}$  found analytically are theoretical.

Another consideration can be done for the heaviest arches (as in test 8 with the angle of embrace of  $90^\circ$  and  $75^\circ$ ). Although they should be able to deform more than the other tested arches, the expected mechanism never formed and the collapse occurred always prematurely in an out-of-the plane failure. However it has to be pointed out that such high values of  $t/R_{\text{point}}$  are almost never encountered in real cases (these arches have got a ratio  $t/R_{\text{point}} = 0.18$  that means for a span of  $1$  m a thickness of the voussoirs of  $0.22$  m that is almost  $1/5$  of the span). These results are therefore not so relevant.

All the other arches are within these two extremes and were therefore the main focus of the research. In order to compare the results gained by the experiments with those obtained by theory, the Matlab script was customized with the real size of the blocks (with an embrace of  $7.5^\circ$ ). It has to be pointed out that all the results presented in the previous chapter were obtained without considering specific dimension of the

blocks and the hinges could occur therefore at any point along the arch. In practice, instead, hinges are constrained to form only at the end of the real blocks so that the theoretical values will be slightly different from the experimental ones had the script been left unchanged. Then the collapse would happen sooner or later compared to the predicted results.

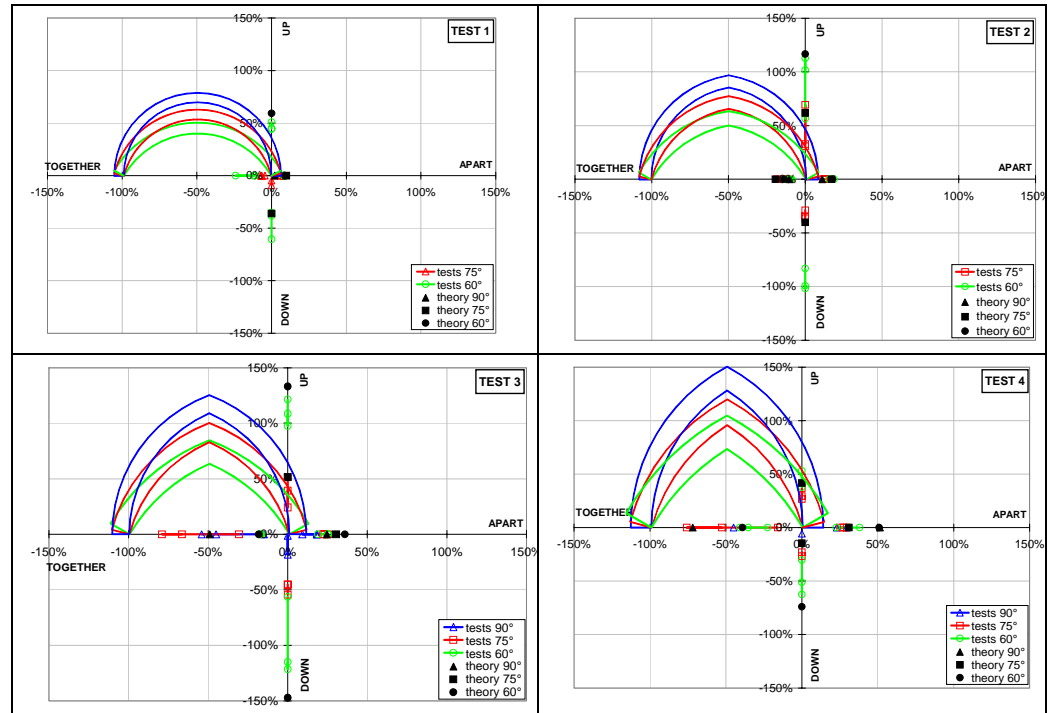


Figure 20. Comparison of the theoretical and experimental displacements in the plane -- test 1 to 4.

In Figure 20 the comparison between theoretical and experimental displacements in the plane is reported. On the vertical axis, the values of the up and down movements and on the horizontal axis, the values of the apart and together displacements are shown. Considering the initial length of the arch equal to the unity and supposing of moving the point at the support at the intrados of the arch, the possible displacements of this point until the collapse of the structure, in percentage

terms can be seen. It can be seen how the domain of possible states enlarges once the eccentricity is increased.

## 8. CONCLUSIONS

In order to check the theoretical results on pointed arches (illustrated in the previous Chapter), an extensive experimental campaign was held on rigid concrete blocks in small scale representing eight different pointed arches varying the eccentricity of the centres, the thickness of the blocks and the angle of embrace.

Five test types were made on the built arches: firstly, friction coefficient measures were taken on the blocks; then moving the supports horizontally apart and together and vertically up and down, the span variation was recorded.

The comparison of theoretical and experimental results has allowed to emphasize the limits of both of them. Perfect hinges, sharp blocks, exactly symmetric structures, absence of friction, all accepted hypotheses in the theory, can never exist in reality; as a consequence the theoretical numerical results are greater than those measured in the experiments. At the same time the presented methods correctly predicted the final collapse mechanisms for the circular and specially the pointed arches.

Moving the supports apart, two collapse mechanisms occurred: by a four hinge mechanism in the thinner arches with high value of the embrace and by the snap-through in the thicker ones with a small value of the embrace. These mechanisms depend fundamentally on the ratio  $t/R_{\text{point}}$  and on the angle of embrace.

Moving the support together, the collapse depends on the ratio  $e/R_{\text{circ}}$  and the angle of embrace and three different mechanisms have been identified:

- the type I occurs only in circular arches and is almost similar to the mechanism activated when the support is moved apart with the same hinges formation.
- the type II mainly consists in the formation of hinges at the intrados up to the crown and at the extrados at the base and two types of collapse can happen: four hinge mechanism and sliding.

- the type III, substituting the type I in the pointed arches which is described in literature, is activated only with small embraces.

Two different mechanisms are activated moving the support vertically as function of the pointidness of the arch. However, in both the cases, a four hinge mechanisms is activated: the difference is notable in the location of the hinges. For small values of the eccentricity, the collapse occurs along the development of the arch whilst for a great pointidness a hinge at the crown at the intrados will always develop.

Finally, the comparison between theoretical and experimental displacements along the axis in the plane is reported.



## CONCLUSIONS

In this thesis, masonry churches under horizontal actions have been studied. Such structures feature strong seismic vulnerability, both because of the mechanical properties of the material and the particular configuration. Besides, uncertainty of the conventional seismic action is detected. Different codes provide different spectra and, subsequently, different total seismic actions.

In order to assess such difficulties, the four basilicas of SGMR, SI, SGMG and SP have been selected. These study cases are analysed with a two step procedure in which the whole structure is analyzed in the linear field through a complete 3D model, and then the single structural elements are assessed in non linear field through FEA and limit analyses.

The following remarks can be stated:

Certain uniformity in the global plan-altimetric apparatus can be recognised so that the four churches can be regarded as deriving from a sort of three-dimensional

global model that changes only for a scale factor. Similarly, a common structural behaviour is expected and in the analyses confirmed.

The modal shapes for the analyzed constructions have shown low torsional and transversal stiffness and great out of the plane deformation. When rigid diaphragms are inserted to model retrofit interventions, greater global stiffness (especially in terms of torsion) and a more monolithic behaviour is detected. It has been noticed, furthermore, a stress concentration in the stiffer elements of the constructions (façade elements and in the transept zone) which absorb a larger amount of the total shear.

Given the already stated uncertainty in the characterisation of seismic actions, assessment of the behaviour at collapse through spectrum-independent analyses is preferable. In this aim, advanced nonlinear analyses using the code ABAQUS are carried out on the single macro-elements constituting the structural complex. This approach is apparently the most accurate methodology for structural analyses. The results, in fact, are reliable only providing that very precise material characterisation is made. This can be very tricky for historical existing structures. Additional difficulties also derive from the complex geometrical configuration of the studied non-conventional structures. Load-displacement curves providing the collapse multiplier, the horizontal stiffness and the maximum displacement of some control points are obtained for all the macro-elements. These curves are compared with the elastic demands derived through global analyses. It has been shown that generally the bearing capacity of these elements is smaller than the strength demand. Therefore, these constructions are prone to damage and retrofit techniques are necessary. The presence of a rigid slab at the height of the roof has not improved at all the seismic behaviour of the study cases. On the contrary, the effective use of such retrofit technique has to be carefully evaluated specially when adopted in ancient constructions.

In the light of the analyses conducted on these complex constructions it is derived that is quite hard following a unique procedure able to define with consistency the



most influencing quantities. Therefore, the necessity of defining a handy and suitable methodology for designers is strongly felt. In order to seek a simplified procedure on churches macroelements, a basic structural element in historical buildings, such as the portal frame, has been studied in detail. An analytical exact expression, derived using the kinematic theorem, and an approximate formula have been used for performing a parametric analysis varying geometrical proportions.

The extension of the single portal frame to the multi-bay frame has been applied in order to perform the comparison between non linear analyses and simplified analyses. The use of approximate expressions derived for the portal frame implies an averaging of the pier widths. When the medium value is taken into account, generally, greater error percentages are encountered in the model with the load condition considering the only self weight: in this case, the non linear analyses give higher values; on the contrary the limit analysis gives small values of the collapse multiplier. In the load condition of self weight plus dead load, the scatters are smaller. When the maximum pier is taken into account, the values of non linear analysis will be the same but limit analysis values will assume greater values, moving on the right side so that are inside the domain. This evidence has been confirmed for the churches of SGMR, SI and SP. On the contrary, in the church of SGMG, medium values have shown a better comparison with non linear procedure.

In the last part of the thesis, the structural behaviour of another typical element in ancient structures has been sought: it is the masonry arch. In order to determine the thrust ranges and the minimum thickness, a parametric analysis has been carried out on whole and half arches. A theory for the displacement of the supports has been developed: pointed arches can bear greater displacement than circular arches. This result is confirmed moving one of the supports in any direction into the plane and tracing the domains of possible positions. All the theoretical values have been checked with two different codes and the results agree well. Later, in order to verify these values, an extensive experimental campaign has been held on rigid concrete

blocks in small scale representing eight different pointed arches varying eccentricity, the thickness and the angle of embrace. Five types of test were made on the arches: first, friction coefficient measures were taken on the blocks; then moving the supports horizontally apart and together, and vertically up and down. The comparison of theoretical and experimental results has allowed to emphasize the limits of both of them. Perfect hinges, sharp blocks, exactly symmetric structures, absence of friction, all accepted hypothesis in the theory, can never exist in reality; as a consequence the theoretical numerical results are greater than those measured in the experiments. At the same time the presented methods correctly predicted the final collapse mechanisms for the circular and specially the pointed arches.

In the light of the conducted experiences in this study, in terms of modelling, analysis and testing, it is believed that masonry structures deserve great attention in the design and assessment process. Many mistakes can be made regarding the basic assumptions on the constitutive model of the material, the suitable structural modelling, the choice of the seismic action and an effective retrofit technique. Furthermore, churches are more sensitive to damages than other “conventional” structures for their characteristic typology.

The main features of these structures have been drawn throughout this work so that whatever similar construction will fairly show the same topics here presented.

About the material properties, only experimental campaigns on the structural constituents of the building under study could provide a good characterization.

Regarding the suitable analysis types, undoubtedly, a global three-dimensional analysis is necessary to get the general idea of the construction and understand its behaviour. On the other side, a useful quantitative result is the evaluation of the ultimate condition at collapse on bi-dimensional elements. This consideration is also made since the definition of the seismic forces for masonry structures according to different code provisions is not unique.

Simplified approaches do prove their appeal. Though some approximations are unavoidably to be made, in the aim of assessing the structural behaviour of ultimate capacity, such techniques seem to provide a very interesting path to follow in the future.



---

## References

- Abraham, P. 1934. *Viollet-le-duc et le rationalisme medieval*. Paris. Vincent Freal & C.
- Abrams D.P., 2000, Seismic response patterns for URM buildings. *TMS Journal*: pp. 71-78 July.
- Abrams D.P., 1997, Response of unreinforced masonry buildings. *Journal of Earthquake Engineering*: 1 n.1 pp. 257-273.
- Abrams D.P., 2001, Performance-based engineering concepts for URM structures *Prog. Struct. Engng. Mater.*: 3 n.1 pp. 48-56. John Wiley & Sons.
- Abruzzese D. Como M. & Grimaldi A., 1985, *Analisi limite di edifici in muratura soggetti a forze orizzontali*. Stato dell'arte in Italia sulla mecc. dell mur. Roma.
- Abruzzese D. Como M., 1990, *On the Horizontal Strength of the Masonry Cathedrals*. European Conference Earthquake Engineering. (9<sup>th</sup> ECEE). Moscow. Elsevier Science.
- Abruzzese D., Como M. & Lanni G., 1993, *Reinforcement Analysis in the restoration of masonry monuments*. IABSE SYMPOSIUM – Rome.
- Abruzzese D. & Lanni G., 1994, *The seismic behaviour of the historical masonry building with openings and horizontal reinforcing connections*. II International Conference on Earthquake Resistant Construction and Design. Berlin, June 15<sup>th</sup>-17<sup>th</sup>. Savidis Eds.
- Abruzzese D. Como M. & Lanni G. 1995. *Some results on the strength evaluation of vaulted masonry structures*. Structures in Architectural Studies, Materials and Analysis (STREMA 1995). Boston. Computational Mechanics Publications.

- Abruzzese D., Como M. & Lanni G., 1996, *The effects of steel reinforcing in the static analysis of masonry buildings under horizontal actions*. 11° WCEE – Acapulco.
- Alexandris A., Protopapa E. & Psycharis I., 2004, *Collapse mechanisms of masonry buildings derived by the distinct element method*. 13<sup>th</sup> World Conference of Earthquake Engineering (13<sup>th</sup>WCEE) – Vancouver.
- Alpa G., Gambarotta L. & Monetto I. 1996. *Equazioni costitutive per murature a blocchi squadrate*. La meccanica delle murature tra teoria e progetto. Messina. 18 - 20 settembre 1996.
- Anselmi C. De Rosa E. 2004Limit analysis of masonry structures SAHC IV - Padova
- Anthoine A., 1995, Derivation of the in-plane elastic Characteristics of masonry through homogenization theory. *International Journal of Solids and Structures*: 32 n. 2 pp. 137-163. Pergamon Press.
- Augenti N., 2004, *Il calcolo sismico degli edifici in muratura*. Torino. Utet Libreria.
- Augusti G. Ciampoli M. 2004Probability of collapse of monumental buildings under seismic loads SAHC IV - Padova
- Augusti G. Ciampoli M. & Giovenale P., 2001, Seismic vulnerability of monumental buildings. *Structural Safety*: 23 pp.253-274. Elsevier Science.
- Augusti G. Ciampoli M. & Zanobi S., 2002, Bounds to the probability of collapse of monumental buildings. *Structural Safety*: 24 pp.89-105. Elsevier Science.
- Azevedo J. Eeri M., Sincaian G. & Lemos J.V., 2000, Seismic behaviour of blocky masonry structures. *Earthquake spectra*: 16 – n.2 pp. 337-365.
- Baker, I.O. 1891. *A treatise on masonry construction*. New York. John Wiley & Sons.
- Bati S.B., Paradiso M. & Tempesta G., 1997, Archi in muratura soggetti a carichi e cedimenti delle imposte. *Costruire in laterizio*: 60.
- Benvenuto E., Corradi M. & Foce F., 1988, Sintesi storica sulla statica di archi, volte e cupole nel XIX secolo. *Palladio*: 1 n. 2 - Dicembre pp. 51- 68 Istituto Poligrafico e Zecca dello Stato Libreria dello Stato.
- Blasi C., & Foraboschi P., 1994, Analytical approach to collapse mechanisms of circular masonry arch. *Journal of Structural Engineering*: 120 n. 8 - August pp. 2288-2309.
- Block, P. 2005. *Equilibrium systems. Studies in Masonry Structure*. Master of Science in Architecture Studies dissertation. Massachusetts Institute of Technology, June 2005.
- Boothby T.E., 2001, Analysis of masonry arches and vaults. *Prog. Struct. Engng Mater.*: 3 pp. 246-256. John Wiley and Sons.
- Bosco D. Limongelli M.P., 1992, Sui meccanismi di collasso di pareti murarie sottoposte a spinta orizzontale. *Ingegneria Sismica*. Anno IX No.1 gennaio-aprile
- Briccoli Bati S. Paradiso M. & Tempesta G. 1997. Archi in muratura soggetti a carichi e cedimenti delle imposte. *Costruire in laterizio*: 60 pp. 436-443.

- Casolo S., Neumair S., Parisi M.A. & Petrini V., 2000, Analysis of seismic damage patterns in old masonry church facades: *Earthquake Spectra*: 16 n.4 pp.757-773.
- CEN, 2002. *Eurocode 8*. Design of structures for earthquake resistance. Part 1: General rules, seismic actions and rules for buildings. Draft n. 6.
- Como M., Grimaldi A., 1983, *Analisi limite di pareti murarie sotto spinta* in Quaderni di teoria e tecnica delle strutture, n. 546, Università di Napoli: Istituto di Tecnica delle Costruzioni. Lithorapid, Napoli.
- Como M. Lanni G. Sacco E., 1991, *Sul calcolo delle catene di rinforzo negli edifici in muratura soggetti ad azione sismica*. 5<sup>th</sup> Convegno Nazionale L'Ingegneria Sismica in Italia – Palermo 2001. 29th Sept. – 2nd Oct.
- Coulomb, C. 1773. *Essai sur une Application des Règles de Maximis et Minimis a Queleques Problèmes de Statique Relatifs a l'Architecture*. Trans. and ed. J. Heyman. 1972, reprinted 1997. *Coulmb's memoir on statics: An essay in the history of civil engineering*. Cambridge. University Press.
- CSI, 2000. *SAP 2000*: Users Manual. Berkley, California.
- D'Ayala D. Speranza E., 2003, Definition of collapse mechanism and seismic vulnerability of historic masonry buildings. *Earthquake Spectra*: 19 n.3 pp.749-509. EERI.
- Decanini L.D. Tocci C., 2004, *Sul comportamento sismico di pareti murarie sollecitate nel piano: riflessioni sui criteri di intervento*. XI Congresso Nazionale l'Ingegneria Sismica in Italia (XI ANIDIS). January, 25<sup>th</sup>-29<sup>th</sup> Genova.
- De Luca A., Giordano & A. Mele E., 2004, A simplified procedure for assessing the seismic capacity of masonry arches. *Engineering Structures*: 26 n.13 pp.1915-1929. Elsevier Science.
- De Luca, A., Mele, E., Romano, A., Patierno, C. & Giordano, A. 2004. *Valutazione approssimata della capacità portante di elementi murari tipici di chiese a pianta basilicale*. XI Congresso Nazionale "L'ingegneria Sismica in Italia", Genova, January 25-29.
- De Luca, A., Mele, E., Romano, A. & Giordano, A. 2004. *Capacità sotto azioni orizzontali di 4 edifici a pianta basilicale*. XI Congresso Nazionale "L'ingegneria Sismica in Italia", Genova, January 25-29.
- Dogliani F., Moretti, A., e Petrini, V. 1994, *Le chiese e il terremoto*, LINT, Trieste.
- Fitchen, J. 1961. *The construction of gothic cathedrals*. Oxford, Clarendon Press.
- Foraboschi P., 2001, Strength Assessment of masonry arch retrofitted using composite reinforcements. *Masonry International*: 15 n.1 pp.17-25.
- Foce F. & Sinopoli A., 2001. Rilettura meccanica di regole costruttive per strutture ad arco tra XVI e XVII secolo. *XV AIMETA* di Meccanica Teorica e Applicata.
- Frankl, P. 1962. *Gothic architecture*. Great Britain, Penguin Books.

- Genna F., Di Pasqua M. & Veroli M., 1998, Numerical analysis of old masonry buildings: a comparison among constitutive models. *Engineering structures*: 20 n. 1-2 pp. 37-53. Elsevier Science.
- Giordano A. 2000. *Numerical Modelling of Masonry Structures Using the Abaqus "Concrete"*. Model ABAQUS Users' Conference. Newport, Rhode Island.
- Giordano, A., Mele, E., e De Luca, A. 2002. Modelling of historical masonry structures: comparison of different approaches through a case study. *Engineering Structures*: 24 pp. 1057 - 1069. Elsevier Science.
- Giuffrè, A. 1986. *La stabilità delle strutture: I muri di sostegno, gli archi, le volte*. Roma, Edizione NIS.
- Heyman J., 1966, *The stone skeleton* in International Journal of Solids and Structures, vol. 2, pp. 249 to 279, Pergamon Press, Great Britain.
- Heyman, J. 1968. On the rubble vaults of the middle ages and other matters. *Gazette des Beaux-Arts*. 71: 177-188.
- Heyman, J. 1969. The safety of masonry arches. *International Journal of Solids and Structures* 11: 363-385. Great Britain: Pergamon Press.
- Heyman, J. 1995. *The Stone Skeleton*. Cambridge - Cambridge University Press.
- Heyman J., 1998, *Mechanical behaviour of arches and vaults*. II Structural Analysis of Historical Constructions. (SAHC II). Barcelona.
- Heyman, J. 1999. *The science of Structural Engineering*. London: Imperial College Press.
- HKS. 2004. ABAQUS Theory Manual. USA.
- Huerta, S. 2001. *Mechanics of masonry vaults: The equilibrium approach*. III Structural Analysis of Historical Constructions. (SAHC III) Guimares. P.B. Lourenco, P. Roca eds.
- Huerta, S. 2004. *Arcos bóvedas y cúpulas. Geometría y equilibrio en el cálculo tradicional de estructuras de fábrica*. Madrid, Instituto Juan de Herrera.
- International textbook company. 1910. *International library of technology*. United States. International textbook company.
- Lagomarsino S., 1998, *A new methodology for the post earth-quake investigation of ancient churches*. 11<sup>th</sup> European Conference on Earthquake Engineering (11<sup>th</sup> ECEE), Rotterdam. Balkema.
- Lagomarsino S. et Al., 1999, *Modelli di calcolo per il miglioramento sismico delle chiese*. IX ANIDIS. Palermo.
- Lee. J.S. Pande G.N. et Al., 1996, Numerical modelling of brick masonry panels subject to lateral loadings. *Computers & Structures*: 61 n.4 pp.735-745. Pergamon Press.
- Lemos J.V., 2004, *Modelling stone masonry dynamics with 3DEC*. I° UDEC/3DEC Symposium.



- Lo Bianco M. Mazzarella C., 1985, *Sulla sicurezza sismica delle strutture in muratura a blocchi*. Stato dell'arte in Italia sulla mecc. delle mur. Roma.
- Lourenco P.B., 1997, *Two aspects related to the analysis of masonry structures: size effect and parameter sensitivity*. TU-DELFT report n. 03.21.1.31.25; TNO-BOUW report n. 97-NM-R1533.
- Lourenco P.B., 1998, *Experimental and numerical issues in the modelling of the mechanical behaviour of masonry*. II Structural Analysis of Historical Constructions (IISAHC) – Barcelona.
- Lourenco P.B., 2001, *Analysis of historical constructions: from trust-lines to advanced simulations*. III Structural Analysis of Historical Constructions (III SAHC) – Guimares.
- Lourenco P.B., 2002, Computations on historic masonry structures. *Prog. Struct. Engng Mater.*: 4 pp. 301-319. John Wiley and Sons.
- Luciano R. & Sacco E., 1997, Homogenization technique and damage model for old masonry material. *Int. J. Solids Struct.*: 34 n. 24 pp. 3191-3208.
- Luciano R. & Sacco E., 1998, A damage model for masonry structures. *Eur. J. Mech. A/Solids*: 17 n.2 pp. 285-303.
- Manzouri T., Schuller P., Shing P.B. 1996, Repair and retrofit of unreinforced masonry structures. *Earthquake Spectra*: 12 n.4 pp.903-922.
- Manzouri T., Shing B. Amadei B. et Al.. 1995. *Repair and retrofit of unreinforced masonry walls: experimental evaluation and finite element analysis*. Buffalo. Department of Civil, Environmental & Architectural Engineering – University of Colorado.
- Mark, R. 1972. The structural analysis of Gothic cathedrals. *Scientific American*. 90-99.
- Massonet C., Save M., 1980, *Calcolo plastico a rottura delle costruzioni*, CLUP, Milano.
- Mele E., De Luca A. & Giordano G. 2003, Modelling and analysis of basilica under earthquake loading. *Journal of Cultural Heritage*: 4 n.4 pp.355-367. Elsevier Science.
- Mele E., De Luca A., and Giagnuolo C., 1999. *L'effetto di alcuni interventi di adeguamento sismico sul comportamento di edifici in muratura*. IX Congresso Nazionale "L'ingegneria Sismica in Italia", Torino, September 20-23.
- Mele E., De Luca A. 1999, *Behaviour and modelling of masonry church buildings in seismic regions*. II International Symposium Earthquake Resistant Engineering Structures, Catania, September.
- Mele E., Gatto D., & De Luca A., 2001, *Structural analysis of basilica churches: a case study*. X Congresso Nazionale "L'ingegneria Sismica in Italia", Potenza - Matera, September 9-13.
- Meli R. & Sanchez-Ramirez R., 1996, *Considerations on the seismic safety of historical monuments*. 11° WCEE - Acapulco

- Méry M. E. 1840. Sur l'équilibre des voutes en berceau. *Annales des ponts et chaussées*. 2° semester: 50-70. Paris.
- Ministero dei Lavori Pubblici, 1996. *Decreto Ministeriale 16 gennaio 1996*. Norme tecniche relative ai criteri generali per la verifica di sicurezza delle costruzioni e dei carichi e sovraccarichi.
- Molins Borrell C., 1995, *Characterization of the mechanical behaviour of masonry*. I Structural Analysis of Historical Constructions (I SAHC) - Barcelona
- Nascè V. Sabia D. *Teoria e pratica nella costruzione dei ponti in muratura tra XVIII e XIX secolo*. Dipartimento di Ingegneria dei Sistemi Edilizi e Territoriali – Politecnico di Torino. Report on Carlo Bernardo Mosca: un ingegnere architetto tra Illuminismo e Restaurazione.
- Nelson, B. 1971. *Structural principles behind the failure of gothic churches*. Thesis dissertation. Massachusetts Institute of Technology, June 1971.
- Ochsendorf, J.A. 2002. Collapse of masonry structures. Ph.D. dissertation, Department of Engineering, Cambridge University, June 2002.
- Ochsendorf, J.A. 2005. The masonry arch on spreading support. *Structural Engineer*. London. (Submitted for review January 2005).
- Ordinanza del Presidente del Consiglio dei Ministri n. 3274. 20.03.2003. Primi elementi in materia di criteri generali per la classificazione sismica del territorio nazionale e di normative tecniche per le costruzioni in zona sismica.
- Ordinanza del Presidente del Consiglio dei Ministri n. 3431. 03.05.2005. Ulteriori modifiche ed integrazioni all'Ordinanza del Presidente del Consiglio dei Ministri n° 3274 del 20 Marzo 2003 recante "Primi elementi in materia di criteri generali per la classificazione sismica del territorio nazionale e di normative tecniche per le costruzioni in zona sismica".
- Orduna A. & Lourenco P.B., 2001, *Limit analysis as a tool for the simplified assessment of ancient masonry structures*. III Structural Analysis of Historical Constructions (III SAHC) - Guimares.
- Pegon P. & Anthoine A., 1997, Numerical Strategies for solving continuum damage problems with softening: application to the homogenization of masonry. *Computers & Structures*: 64 n. 1-4 pp.623-642. Pergamon Press.
- Pegon P., Pinto A.V. & Geradin M., 2001, Numerical modelling of stone-block monumental structures. *Computer & Structures*: 79 pp.2165-2181. Pergamon Press.
- Penna A., Lagomarsino S., 2004, *Seismic assessment of masonry structures by non linear macro-element analysis*. SAHC IV – Padova.
- Pistone G., 1994, *Computer modelling of the behaviour of S. Giovanni church in Farigliano* X International Brick and Block Masonry Conference (X IBMAC) – Calgary.

- Presidenza del Consiglio superiore dei LL. PP. – Servizio Tecnico Generale. dicembre 1998. *Linee Guida per la progettazione, esecuzione e collaudo di strutture isolate dal sisma.*
- Ramasco R., 1993, *Dinamica delle strutture*, CUEN, Napoli.
- Roca P. Pellegrini L. & Onate E., 1998, Analysis of the structure of gothic cathedrals application to Barcelona cathedral. *II Structural Analysis of Historical Constructions (IISAHC)* – Barcelona.
- Roca P. Gonzalez JL., 1996. *A summary of the opinions put forward during the discussions.* I Structural Analysis of Historical Constructons (I SAHC) – Barcelona.
- Roeder-Carbo G.M. & Ayala A.G., 2001, *An evaluation of methods for the determination of the structural stability of historic masonry arches.* III Structural Analysis of Historical Constructions (III SAHC) – Guimares.
- Sacchi Landriani G. Riccioni R. 1982. *Comportamento statico e sismico delle strutture murarie.* CLUP. Milano.
- Salonikios T., Karakostas C., Lekidis V. & Anthoine A., 2003, Comparative inelastic pushover analysis of masonry frames. *Engineering structures*: 25 pp.1515-1523. Elsevier Science.
- Schlegel R. & Rautenstrauch K., 2004, *Comparative computations of masonry arch bridges using continuum and discontinuum mechanics.* I° UDEC/3DEC Symposium.
- Schlegel R. & Rautenstrauch K., 2004, *Failure analysis of masonry shear walls.* I° UDEC/3DEC Symposium.
- Sinopoli A., Corradi M. & Foce F., 1997, Modern formulation for preelastic theories of masonry arches. *Journal of Engineering Mechanics*: March - pp. 204-213.
- Sinopoli A., 1985, *Le strutture monumentali come sistemi a vincoli unilateri. Qualità dell'equilibrio, dinamica e fenomeni impulsivi.* Stato dell'arte in Italia sulla mecc. dell mur. Rome.
- Smars, P. 2000. *Etudes sur la stabilité des arcs et voûtes.* Ph.D. dissertation, Catholic University in Leuven, Belgium, March 2000.
- Sondericker, J. 1907. *Graphic Statics with applications to trusses, beams and arches.* New York. John Wiley & Sons.
- Swain G. 1927. *Structural Engineering – stresses, graphical statics and masonry.* New-York. McGraw-Hill.
- Tzamtzis A.D. & Asteris P.G., 2004, FE Analysis of complex discontinuous and jointed structural systems parte 1 (state of art). *Electronic Journal of Structural Engineering*: 1 – pp. 75-92.
- Tzamtzis A.D. & Asteris P.G., 2004, FE Analysis of complex discontinuous and jointed structural systems parte 2 (masonry walls). *Electronic Journal of Structural Engineering*: 1 – pp. 93-107.

- 
- Valluzzi MR, Cardani G, Binda L., 2004, *Seismic vulnerability methods for masonry buildings in historical centres: validation and application for prediction analyses*. XIII World Conference on Engineering Structures (XIII WCEE) – August 1<sup>st</sup>-6<sup>th</sup> Vancouver.
- Viollet-le-duc, E.E. 1875. Arc, Construction, Ogive. *Dictionnaire raisonné de l'architecture française du XIe au XVIe siècle*. Paris. A. Morel 1: 45-87. 3: 17-40. 6: 421-447.
- Zucchini A. & Lourenco P.B., 2002, A micro-mechanical model for the homogenisation of masonry. *International Journal of Solids and Structures*: 39 pp. 3233-3255. Pergamon Press.
- Zucchini A. & Lourenco P.B., 2004, A coupled homogenisation-damage model for masonry cracking. *Computers & Structures*: 82 pp.917-929. Elsevier Science.

```

clear all
%MINIMUM THICKNESS in MASONRY ARCHES
%geometry and variables
out=[ ];
test=[ ];
%geometry
Rcirc=[-];
e_over_Rcirc=[-];
e=Rcirc*e_over_Rcirc;
compldeg=[-];
compl=compldeg*pi/180;
teta=asin((e*sin(compl))/Rcirc);
omega=pi-compl-teta;
Rpoint=(e^2+Rcirc^2-2*e*Rcirc*cos(omega))^0.5;
stepangledeg=0.01;
fiapointmin=asin (e/Rpoint);
fiapoint=pi/2-compl-fiapointmin;
fibpoint=(20:stepangledeg:70)*(pi/180);
stepratio=0.0001;
t_over_Rpoint=(0.01:stepratio:0.12);
%cicles
for j=1:length(fibpoint)
k=1;
t=Rpoint*t_over_Rpoint(k);
h=t/2;
r1=Rpoint-h;
r2=Rpoint+h;
rad=(r1^3-r2^3)/(r1^2-r2^2);
%voussoir areas
A1=((fiapoint-fibpoint(j))*(r2^2))/2;
a1=((fiapoint- fibpoint(j))*(r1^2))/2;
A2=( fibpoint(j)*(r2^2))/2;
a2=( fibpoint(j)*(r1^2))/2;
%vertical loads
F1=(A1-a1);
F2=(A2-a2);
%distance of centroids from the arch centre
G1point=4*rad*sin((fiapoint-fibpoint(j))/2)/(3*(fiapoint-fibpoint(j)));
G2point=4*rad*sin(fibpoint(j)/2)/(3* fibpoint(j));
%coordinates of centroids, fixed and relative centres
XG1point=G1point*sin((fiapoint+fibpoint(j))/2+fiapointmin);
YG1point=G1point*cos((fiapoint+fibpoint(j))/2+fiapointmin);
XG2point=G2point*sin(fibpoint(j)/2+fiapointmin);
YG2point=G2point*cos(fibpoint(j)/2+fiapointmin);
X1point=(h+Rpoint)*sin(fiapoint+fiapointmin);
Y1point=(h+Rpoint)*cos(fiapoint+fiapointmin);

```

```

X12point=(Rpoint-t/2)*sin(fibpoint(j)+fiapointmin);
Y12point=(Rpoint-t/2)*cos(fibpoint(j)+fiapointmin);
lpoint=(Y12point-Y1point)/(X12point-X1point);
X2point=(X1point*lpoint-Y1point+(Rpoint+h)*cos(fiapointmin))/lpoint;
Y2point=(Rpoint+h)*cos(fiapointmin);
%rotation angle
alfa= atan((X1point-X12point)/(X12point-X2point));
alfadeg=alfa*180/pi;
%vertical displacements
VG1=(X1point-XG1point);
VG2=(XG2point-X2point)*tan(alfa);
%principle of virtual works
PVW=F1*VG1+F2*VG2;

while (round(10*PVW) ~= 0) & (k < length(t_over_Rpoint))
k=k+1;
t=Rpoint*t_over_Rpoint(k);
h=t/2;
r1=Rpoint-h;
r2=Rpoint+h;
rad=(r1^3-r2^3)/(r1^2-r2^2);
%voussoir areas
A1=((fiapoint-fibpoint(j))*(r2^2))/2;
a1=((fiapoint- fibpoint(j))*(r1^2))/2;
A2=( fibpoint(j)*(r2^2))/2;
a2=( fibpoint(j)*(r1^2))/2;
%vertical loads
F1=(A1-a1);
F2=(A2-a2);
%distance of centroids from the arch centre
G1point=4*rad*sin((fiapoint-fibpoint(j))/2)/(3*(fiapoint-fibpoint(j)));
G2point=4*rad*sin(fibpoint(j)/2)/(3* fibpoint(j));
%coordinates of centroids, fixed and relative centres
XG1point=G1point*sin((fiapoint+fibpoint(j))/2+fiapointmin);
YG1point=G1point*cos((fiapoint+fibpoint(j))/2+fiapointmin);
XG2point=G2point*sin(fibpoint(j)/2+fiapointmin);
YG2point=G2point*cos(fibpoint(j)/2+fiapointmin);
X1point=(t/2+Rpoint)*sin(fiapoint+fiapointmin);
Y1point=(t/2+Rpoint)*cos(fiapoint+fiapointmin);
X12point=(Rpoint-t/2)*sin(fibpoint(j)+fiapointmin);
Y12point=(Rpoint-t/2)*cos(fibpoint(j)+fiapointmin);
lpoint=(Y12point-Y1point)/(X12point-X1point);
X2point=(X1point*lpoint-Y1point+(Rpoint+h)*cos(fiapointmin))/lpoint;
Y2point=(Rpoint+h)*cos(fiapointmin);
%rotation angle
alfa= atan((X1point-X12point)/(X12point-X2point));

```

---

```
alfadeg=alfa*180/pi;
%vertical displacements
VG1=(X1point-XG1point);
VG2=(XG2point-X2point)*tan(alfa);
%principle of virtual works
PVW=F1*VG1+F2*VG2;
end
test(j)=PVW;
out(j) = t/Rpoint;
end
max(out)
[Y,I] = max(out);
(fibpoint(I)+fiapointmin)*180/pi
figure
subplot(2,1,1)
plot(fibpoint*180/pi,out)
subplot(2,1,2)
plot(fibpoint*180/pi,test)
```

```

clear all
% MAXIMUM SPREAD in MASONRY ARCHES
% geometry and variables
Rcirc=[-];
e_over_Rcirc=[-];
e=Rcirc*e_over_Rcirc;
t_over_Rpoint = [-];
compledeg=[-];
compl=compledeg*pi/180;
Rpoint=e+Rcirc;
alphapointmin=asin (e/Rpoint);
alphapoint=pi/2-compl-alphapointmin;
t = Rpoint*t_over_Rpoint;
h = t/2;
r1 = Rpoint-h;
r2 = Rpoint+h;
rad = (r1^3 - r2^3)/(r1^2 - r2^2);
riga=0;
stepangle=0.5;
amin = alphapointmin*180/pi;
amax = amin+alphapoint*180/pi;
lux=2*((Rpoint-h)*sin(alphapointmin+alphapoint)-e);
height=((Rpoint+h)*cos(alphapointmin)-(Rpoint-h)*cos(alphapointmin+alphapoint));
% Coordinate system is XY with origin at the centre of circle
X_O=[0];
Y_O=[0];
% Find coordinates of point C and D
XC = (Rpoint+h)*sin(alphapointmin);
YC = (Rpoint+h)*cos(alphapointmin);
XD = (Rpoint+h)*sin(alphapointmin+alphapoint);
YD = (Rpoint+h)*cos(alphapointmin+alphapoint);
for a=(amin+stepangle):stepangle:(amax-stepangle);
    arads = (pi/180)*a;
    XB = (Rpoint+h)*sin(arads);
    YB = (Rpoint+h)*cos(arads);
    % Find x-coordinate of centre of gravity of arch segment BC
    C1 = (4/3)*rad*(sin((arads-alphapointmin)/2))/(arads-alphapointmin);
    XM1 = C1*sin((arads+alphapointmin)/2);
    YM1= C1*cos((arads+alphapointmin)/2);
    M1 = (arads-alphapointmin)*(r2^2-r1^2)/2;
    for b=(a+stepangle):stepangle:amax;
        brads= (pi/180)*b;
        riga=riga+1;
        XA = (Rpoint-h)*sin(brads);
        YA = (Rpoint-h)*cos(brads);
    end
end

```



---

```

% Find x-coordinate of centre of gravity of arch segment BA
C2 = 4/3*rad*sin((brads-arads)/2)/(brads-arads);
XM2 = C2*sin((arads+brads)/2);
YM2 = C2*cos((arads+brads)/2);
M2 = (brads-arads)*(r2^2-r1^2)/2;
% Compute value of thrust
thrustin=(M1*(XA-XB)+M2*(XA-XM2))/(YB-YA);
% Find mass of the last arch segment
M3 = (alphapoint+alphapointmin-brads)*(r2^2-r1^2)/2;
% Find weight of the arch
Wtot=2*(M1+M2+M3);
%matrix datas
L(riga,1)=alphapointmin;
L(riga,2)=arads;
L(riga,3)=brads;
L(riga,4)=(alphapoint+alphapointmin);
L(riga,5)=Wtot;
L(riga,6)=thrustin;
L(riga,7)=M1;
L(riga,8)=M2;
L(riga,9)=M3;
L(riga,10)=XA;
L(riga,11)=YA;
L(riga,12)=XB;
L(riga,13)=YB;
L(riga,14)=XM1;
L(riga,15)=YM1;
L(riga,16)=XM2;
L(riga,17)=YM2;
L(riga,18)=alphapointmin*180/pi;
L(riga,19)=arads*180/pi;
L(riga,20)=brads*180/pi;
L(riga,21)=(alphapoint+alphapointmin)*180/pi;
end
end
% thrust
[Hmin,ind] = max(L(:,6));
%print results
L(ind,(5));
L(ind,(18:21))
Hmin/Wtot
arads=L(ind,2);
brads=L(ind,3);
thrustin=L(ind,6);
M1=L(ind,7);
M2=L(ind,8);

```

```

M3=L(ind,9);
XA=L(ind,10);
YA=L(ind,11);
XB=L(ind,12);
YB=L(ind,13);
XM1=L(ind,14);
YM1=L(ind,15);
XM2=L(ind,16);
YM2=L(ind,17);
% Find x-coordinate of hinge E
XE=-(XA-2*e);
YE=YA;
LBE = (((XB-XE)^2+(YE-YB)^2)^.5);
LBA = (((XA-XB)^2+(YB-YA)^2)^.5);
% step variation
step=-;
stepvh=-;
XA1=0;
thrustfinh=[-100];
XBh=0;
YBh=0;
for XA1=(XA+step):step:50
    a12=(-YE+YA)^2/(-XE+XA1)^2+1;
    b12=(XE^2+YE^2-LBE^2-XA1^2-YA^2+LBA^2)*(-YE+YA)/(-XE+XA1)^2+...
        2*XE*(-YE+YA)/(-XE+XA1)-2*YE;
    c12=(XE^2+YE^2-LBE^2-XA1^2-YA^2+LBA^2)^2/(4*(-XE+XA1)^2)+...
        XE*(XE^2+YE^2-LBE^2-XA1^2-YA^2+LBA^2)/(-XE+XA1)+XE^2+YE^2-LBE^2;
    YB1=(-b12+(b12^2-4*a12*c12)^0.5)/(2*a12);
    XB1=(-XE^2-YE^2+LBE^2+XA1^2+YA^2-LBA^2-2*YB1*(YA-YE))/(2*(XA1-XE));
    YA1=YA;
    % verify snap-through is not occurred
    if ((imag(XB1)<0) | (imag(XB1)>0))
        spreadsnap= (XA1-XA)/lux*100
        dipspread=((YC-YC1)/height*100)
        dipOCH=(YC-YC1)/t
        thrustincrease=thrust/thrustin
    break
end
if((imag(YB1)<0) | (imag(YB1)>0))
    spreadsnap= (XA1-XA)/lux*100
    dipspread=((YC-YC1)/height*100)
    dipOCH=(YC-YC1)/t
    thrustincrease=thrust/thrustin
break
end
LCB=(((XC-XB)^2+(YC-YB)^2)^.5);

```

```

LCE=(((XC-XE)^2+(YC-YE)^2)^.5);
a34=(-YB1+YE)^2/(-XB1+XE)^2+1;
b34=(XB1^2+YB1^2-LCB^2-XE^2-YE^2+LCE^2)*(-YB1+YE)/(-XB1+XE)^2+...
2*XB1*(-YB1+YE)/(-XB1+XE)-2*YB1;
c34=(XB1^2+YB1^2-LCB^2-XE^2-YE^2+LCE^2)^2/(4*(-XB1+XE)^2)+...
XB1*(XB1^2+YB1^2-LCB^2-XE^2-YE^2+LCE^2)/(-XB1+XE)+XB1^2+YB1^2-
LCB^2;
YC1=(-b34+(b34^2-4*a34*c34)^0.5)/(2*a34);
XC1=(-XB1^2-YB1^2+LCB^2+XE^2+YE^2-LCE^2-2*YC1*(YE-YB1))/(2*(XE-XB1));
XD1=XD+(XA1-XA);
YD1=YD;
LXM1E = (((XM1-XE)^2+(YM1-YE)^2)^.5);
LXM1B = (((XM1-XB)^2+(YM1-YB)^2)^.5);
a56=(-YB1+YE)^2/(-XB1+XE)^2+1;
b56=(XB1^2+YB1^2-LXM1B^2-XE^2-YE^2+LXM1E^2)*(-YB1+YE)/(-XB1+XE)^2+...
2*XB1*(-YB1+YE)/(-XB1+XE)-2*YB1;
c56=(XB1^2+YB1^2-LXM1B^2-XE^2-YE^2+LXM1E^2)^2/(4*(-XB1+XE)^2)+...
XB1*(XB1^2+YB1^2-LXM1B^2-XE^2-YE^2+LXM1E^2)/(-
XB1+XE)+XB1^2+YB1^2-LXM1B^2;
YM11=(-b56+(b56^2-4*a56*c56)^0.5)/(2*a56);
XM11=(-XB1^2-YB1^2+LXM1B^2+XE^2+YE^2-LXM1E^2-2*YM11*(YE-
YB1))/(2*(XE-XB1));
M11=M1;
LXM2B = (((XM2-XB)^2+(YM2-YB)^2)^.5);
LXM2A = (((XM2-XA)^2+(YM2-YA)^2)^.5);
a78=(-YB1+YA)^2/(-XB1+XA1)^2+1;
b78=(XB1^2+YB1^2-LXM2B^2-XA1^2-YA^2+LXM2A^2)*(-YB1+YA)/(-
XB1+XA1)^2+...
2*XB1*(-YB1+YA)/(-XB1+XA1)-2*YB1;
c78=(XB1^2+YB1^2-LXM2B^2-XA1^2-YA^2+LXM2A^2)^2/(4*(-XB1+XA1)^2)+...
XB1*(XB1^2+YB1^2-LXM2B^2-XA1^2-YA^2+LXM2A^2)/(-
XB1+XA1)+XB1^2+YB1^2-LXM2B^2;
YM21=(-b78+(b78^2-4*a78*c78)^0.5)/(2*a78);
XM21=(-XB1^2-YB1^2+LXM2B^2+XA1^2+YA^2-LXM2A^2-2*YM21*(YA-
YB1))/(2*(XA1-XB1));
M21=M2;
C3 = 4/3*rad*sin((alphapoint+alphapointmin-brads)/2)/(alphapoint+alphapointmin-brads);
XM3 = C3*sin ((alphapoint+alphapointmin+brads)/2);
XM31=XM3+(XA1-XA);
M31=M3;
M4=M2;
XM4=-(XM2-2*e);
YM4=YM2;
LXM4E = (((XM4-XE)^2+(YM4-YE)^2)^.5);
LXM4B = (((XB-XM4)^2+(YB-YM4)^2)^.5);
a910=(-YB1+YE)^2/(-XB1+XE)^2+1;

```

```

b910=(XB1^2+YB1^2-LXM4B^2-XE^2-YE^2+LXM4E^2)*(-YB1+YE)/(-
XB1+XE)^2+...
    2*XB1*(-YB1+YE)/(-XB1+XE)-2*YB1;
c910=(XB1^2+YB1^2-LXM4B^2-XE^2-YE^2+LXM4E^2)^2/(4*(-XB1+XE)^2)+...
    XB1*(XB1^2+YB1^2-LXM4B^2-XE^2-YE^2+LXM4E^2)/(-
XB1+XE)+XB1^2+YB1^2-LXM4B^2;
YM41=(-b910+(b910^2-4*a910*c910)^0.5)/(2*a910);
XM41=(-XB1^2-YB1^2+LXM4B^2+XE^2+YE^2-LXM4E^2-2*YM41*(YE-
YB1))/(2*(XE-XB1));
M5=M1;
XM5=-(XM1-2*e);
YM5=YM1;
LXM5E = (((XM5-XE)^2+(YM5-YE)^2)^.5);
LXM5B = (((XB-XM5)^2+(YB-YM5)^2)^.5);
a1112=(-(-YB1+YE)^2/(-XB1+XE)^2)+1;
b1112=(XB1^2+YB1^2-LXM5B^2-XE^2-YE^2+LXM5E^2)*(-YB1+YE)/(-
XB1+XE)^2+...
    2*XB1*(-YB1+YE)/(-XB1+XE)-2*YB1;
c1112=(XB1^2+YB1^2-LXM5B^2-XE^2-YE^2+LXM5E^2)^2/(4*(-XB1+XE)^2)+...
    XB1*(XB1^2+YB1^2-LXM5B^2-XE^2-YE^2+LXM5E^2)/(-
XB1+XE)+XB1^2+YB1^2-LXM5B^2;
YM51=(-b1112+(b1112^2-4*a1112*c1112)^0.5)/(2*a1112);
XM51=(-XB1^2-YB1^2+LXM5B^2+XE^2+YE^2-LXM5E^2-2*YM51*(YE-
YB1))/(2*(XE-XB1));
% Find distances
L1=XA-XM2;
L11=abs((XE-XM41));
L2=XA-XM1;
L21=abs((XE-XM51));
L3=XM1-XE;
L31=XM11-XE;
L4=XB-XE;
L41=XB1-XE;
thrustfin=(((M4*L11+M5*L21+M1*L31)/L41)+M2)*(XD1-XA1)+M3*(XD1-
XM31)/((YA1-YD1)+(YB1-YE)*(XD1-XA1)/L41); % -mobile
%thrustfin=(((M4*L1+M5*L2+M1*L3)/L4)+M2)*(XD-XA)+M3*(XD-XM3)/((YA-
YD)+(YB-YE)*(XD-XA)/L4) % -fisso
thrust=(((M4*L11+M5*L21+M1*L31)/L41)*(XA1-XB1)+M2*(XA1-XM21))/((YB1-
YA1)+(YB1-YE)*(XA1-XB1)/L41);
if thrustfin>0
    if thrust > thrustfin
        spreadthrust= ((XA1-XA)/lux*100)
        dipthrust=((YC-YC1)/height*100)
        dipOCH=(YC-YC1)/t
        thrustincrease=thrust/thrustin
    break

```

```

end
end
v=1;
vrads=v*pi/180;
CV=(4/3)*rad*sin(vrads/2)/(vrads);
XV=CV*sin(brads-vrads/2);
YV=CV*cos(brads-vrads/2);
m=vrads*(r2^2-r1^2)/2;
LXVB = (((XV-XB)^2+(YV-YB)^2)^.5);
LXVA = (((XV-XA)^2+(YV-YA)^2)^.5);
a1314=((-YB1+YA)^2/(-XB1+XA1)^2)+1;
b1314=(XB1^2+YB1^2-LXVB^2-XA1^2-YA^2+LXVA^2)*(-YB1+YA)/(-
XB1+XA1)^2+...
2*XB1*(-YB1+YA)/(-XB1+XA1)-2*YB1;
c1314=(XB1^2+YB1^2-LXVB^2-XA1^2-YA^2+LXVA^2)^2/(4*(-XB1+XA1)^2)+...
XB1*(XB1^2+YB1^2-LXVB^2-XA1^2-YA^2+LXVA^2)/(-
XB1+XA1)+XB1^2+YB1^2-LXVB^2;
YV1=(-b1314+(b1314^2-4*a1314*c1314)^0.5)/(2*a1314);
XV1=(-XB1^2-YB1^2+LXVB^2+XA1^2+YA^2-LXVA^2-2*YV1*(YA-
YB1))/(2*(XA1-XB1));
phiBA=atan((YB-YA)/(XA-XB));
phiB1A1=atan((YB1-YA1)/(XA1-XB1));
phi=phiBA-phiB1A1;
X_01=XA1-r1*sin(brads-phi);
Y_01=YA1-r1*cos(brads-phi);
sum=pi/2-brads+vrads+phi;
Rf= (((M4*L11+M5*L21+M1*L31-thrust*(YB1-YE))/L41+M2)*(XA1-X_01)+...
thrust*(YA1-Y_01)-m*(XV1-X_01))/(((M4*L11+M5*L21+M1*L31-thrust*...
(YB1-YE))/L41+M2-m)*cos(sum)+thrust*sin(sum));
%one voussoir before hinge E
phiBE=atan(abs(YB-YE)/abs(XE-XB));
phiB1E=atan(abs(YB1-YE)/abs(XE-XB1));
phi2=phiBE-phiB1E;
X_02=XE+r1*sin(brads-phi2);
Y_02=YE-r1*cos(brads-phi2);
sum2=pi/2-brads+vrads+phi2;
XV2=-(XV-2*e);
YV2=YV;
LXV2B = (((XV2-XB)^2+(YV2-YB)^2)^.5);
LXV2E = (((XV2-XE)^2+(YV2-YE)^2)^.5);
a1516=((-YB1+YE)^2/(-XB1+XE)^2)+1;
b1516=(XB1^2+YB1^2-LXV2B^2-XE^2-YE^2+LXV2E^2)*(-YB1+YE)/(-
XB1+XE)^2+...
2*XB1*(-YB1+YE)/(-XB1+XE)-2*YB1;
c1516=(XB1^2+YB1^2-LXV2B^2-XE^2-YE^2+LXV2E^2)^2/(4*(-XB1+XE)^2)+...

```

```

XB1*(XB1^2+YB1^2-LXV2B^2-XE^2-YE^2+LXV2E^2)/(-
XB1+XE)+XB1^2+YB1^2-LXV2B^2;
YV21=(-b1516+(b1516^2-4*a1516*c1516)^0.5)/(2*a1516);
XV21=(-XB1^2-YB1^2+LXV2B^2+XE^2+YE^2-LXV2E^2-2*YV21*(YE-
YB1))/(2*(XE-XB1));
Rf2= ((-(M4*L11+M5*L21+M1*L31-thrust*(YB1-YE))/L41+M1+M5+M4)*...
(-XE+X_02)+thrust*(YE-Y_02)-m*(-XV21+X_02))/(-(M4*L11+M5*L21+...
M1*L31-thrust*(YB1-YE))/L41+M1+M5+M4-m)*cos(sum2)+thrust*sin(sum2));
vh=0;

while (Rf2<r1) & (vh<(b-stepvh))
  bradsh= brads-vh*(pi/180);
  %Find new x-coordinate of hinge E
  XEh=-(Rpoint-h)*sin(bradsh)-2*e);
  YEh=(Rpoint-h)*cos(bradsh);
  LBEh = (((XB-XEh)^2+(YEh-YB)^2)^.5);
  for XAh=(XA1+step):step:50
    a1718=((-YEh+YA)^2/(-XEh+XAh)^2)+1;
    b1718=(XEh^2+YEh^2-LBEh^2-XAh^2-YA^2+LBA^2)*(-YEh+YA)/(-
XEh+XAh)^2+...
    2*XEh*(-YEh+YA)/(-XEh+XAh)-2*YEh;
    c1718=(XEh^2+YEh^2-LBEh^2-XAh^2-YA^2+LBA^2)^2/(4*(-XEh+XAh)^2)+...
    XEh*(XEh^2+YEh^2-LBEh^2-XAh^2-YA^2+LBA^2)/(-
XEh+XAh)+XEh^2+YEh^2-LBEh^2;
    YBh=(-b1718+(b1718^2-4*a1718*c1718)^0.5)/(2*a1718);
    XBh=(-XEh^2-YEh^2+LBEh^2+XAh^2+YA^2-LBA^2-2*YBh*(YA-
YEh))/(2*(XAh-XEh));
    YAh=YA;
    %verify snap-through is not occurred
    if ((imag(XBh)<0) | (imag(XBh)>0))
      spreadsnap= (XAh-XA)/lux*100
      thrustincrease=thrust/thrustin
      dipspread=((YC-YCh)/height*100)
      dipOCH=(YC-YCh)/t

    break
  end
  if((imag(YBh)<0) | (imag(YBh)>0))
    spreadsnap= (XAh-XA)/lux*100
    thrustincrease=thrust/thrustin
    dipspread=((YC-YCh)/height*100)
    dipOCH=(YC-YCh)/t

  break
end
LCB=(((XC-XB)^2+(YC-YB)^2)^.5);

```

```

LCEh = (((XC-XEh)^2+(YC-YEh)^2)^.5);
a2728=(-YBh+YEh)^2/(-XBh+XEh)^2+1;
b2728=(XBh^2+YBh^2-LCB^2-XEh^2-YEh^2+LCEh^2)*(-YBh+YEh)/(-
XBh+XEh)^2+...
      2*XBh*(-YBh+YEh)/(-XBh+XEh)-2*YBh;
c2728=(XBh^2+YBh^2-LCB^2-XEh^2-YEh^2+LCEh^2)^2/(4*(-
XBh+XEh)^2)+...
      XBh*(XBh^2+YBh^2-LCB^2-XEh^2-YEh^2+LCEh^2)/(-
XBh+XEh)+XBh^2+YBh^2-LCB^2;
YCh=(-b2728+(b2728^2-4*a2728*c2728)^0.5)/(2*a2728);
XCh=(-XBh^2-YBh^2+LCB^2+XEh^2+YEh^2-LCEh^2-2*YCh*(YEh-
YBh))/(2*(XEh-XBh));
XDh=XD+(XAh-XA);
YDh=YD;
LXM1Eh = (((XM1-XEh)^2+(YM1-YEh)^2)^.5);
a1920=(-YBh+YEh)^2/(-XBh+XEh)^2+1;
b1920=(XBh^2+YBh^2-LXM1B^2-XEh^2-YEh^2+LXM1Eh^2)*(-YBh+YEh)/(-
XBh+XEh)^2+...
      2*XBh*(-YBh+YEh)/(-XBh+XEh)-2*YBh;
c1920=(XBh^2+YBh^2-LXM1B^2-XEh^2-YEh^2+LXM1Eh^2)^2/(4*(-
XBh+XEh)^2)+...
      XBh*(XBh^2+YBh^2-LXM1B^2-XEh^2-YEh^2+LXM1Eh^2)/(-
XBh+XEh)+XBh^2+YEh^2-LXM1B^2;
YM1h=(-b1920+(b1920^2-4*a1920*c1920)^0.5)/(2*a1920);
XM1h=(-XBh^2-YBh^2+LXM1B^2+XEh^2+YEh^2-LXM1Eh^2-2*YM1h*(YEh-
YBh))/(2*(XEh-XBh));
a2122=(-YBh+YA)^2/(-XBh+XAh)^2+1;
b2122=(XBh^2+YBh^2-LXM2B^2-XAh^2-YA^2+LXM2A^2)*(-YBh+YA)/(-
XBh+XAh)^2+...
      2*XBh*(-YBh+YA)/(-XBh+XAh)-2*YBh;
c2122=(XBh^2+YBh^2-LXM2B^2-XAh^2-YA^2+LXM2A^2)^2/(4*(-
XBh+XAh)^2)+...
      XBh*(XBh^2+YBh^2-LXM2B^2-XAh^2-YA^2+LXM2A^2)/(-
XBh+XAh)+XBh^2+YBh^2-LXM2B^2;
YM2h=(-b2122+(b2122^2-4*a2122*c2122)^0.5)/(2*a2122);
XM2h=(-XBh^2-YBh^2+LXM2B^2+XAh^2+YA^2-LXM2A^2-2*YM2h*(YA-
YBh))/(2*(XAh-XBh));
XM3h=XM3+(XAh-XA);
% Find x-coordinate of centre of gravity of new arch segment BEh
C4h = 4/3*rad*sin((bradsh-arads)/2)/(bradsh-arads);
M4h = (bradsh-arads)*(r2^2-r1^2)/2;
XM4h=-(C4h*sin((arads+bradsh)/2)-2*e);
YM4h = C4h*cos((arads+bradsh)/2);
LXM4hEh = (((XM4h-XEh)^2+(YM4h-YEh)^2)^.5);
LXM4hB = (((XB-XM4h)^2+(YB-YM4h)^2)^.5);
a2324=(-YBh+YEh)^2/(-XBh+XEh)^2+1;

```

```

b2324=(XBh^2+YBh^2-LXM4hB^2-XEh^2-YEh^2+LXM4hEh^2)*(-
YBh+YEh)/(-XBh+XEh)^2+...
2*XBh*(-YBh+YEh)/(-XBh+XEh)-2*YBh;
c2324=(XBh^2+YBh^2-LXM4hB^2-XEh^2-YEh^2+LXM4hEh^2)^2/(4*(-
XBh+XEh)^2)+...
XBh*(XBh^2+YBh^2-LXM4hB^2-XEh^2-YEh^2+LXM4hEh^2)/(-
XBh+XEh)+XBh^2+YBh^2-LXM4hB^2;
YM4h1=(-b2324+(b2324^2-4*a2324*c2324)^0.5)/(2*a2324);
XM4h1=(-XBh^2-YBh^2+LXM4hB^2+XEh^2+YEh^2-LXM4hEh^2-
2*YM4h1*(YEh-YBh))/(2*(XEh-XBh));
LXM5Eh = (((XM5-XEh)^2+(YM5-YEh)^2)^.5);
a2526=(-YBh+YEh)^2/(-XBh+XEh)^2+1;
b2526=(XBh^2+YBh^2-LXM5B^2-XEh^2-YEh^2+LXM5Eh^2)*(-YBh+YEh)/(-
XBh+XEh)^2+...
2*XBh*(-YBh+YEh)/(-XBh+XEh)-2*YBh;
c2526=(XBh^2+YBh^2-LXM5B^2-XEh^2-YEh^2+LXM5Eh^2)^2/(4*(-
XBh+XEh)^2)+...
XBh*(XBh^2+YBh^2-LXM5B^2-XEh^2-YEh^2+LXM5Eh^2)/(-
XBh+XEh)+XBh^2+YBh^2-LXM5B^2;
YM5h=(-b2526+(b2526^2-4*a2526*c2526)^0.5)/(2*a2526);
XM5h=(-XBh^2-YBh^2+LXM5B^2+XEh^2+YEh^2-LXM5Eh^2-2*YM5h*(YEh-
YBh))/(2*(XEh-XBh));
% Find distances
L1h=abs((XEh-XM4h1));
L2h=abs((XEh-XM5h));
L3h=XM1h-XEh;
L4h=XBh-XEh;
L1hn=abs((XEh-XM4h));
L2hn=abs((XEh-XM5));
L3hn=XM1-XEh;
L4hn=XB-XEh;
thrustfinh=(((M4h*L1h+M5*L2h+M1*L3h)/L4h)+M2)*(XDh-XAh)+M3*(XDh-
XM3h)/...
((YAh-YDh)+(YBh-YEh)*(XDh-XAh)/L4h);% mobile
% thrustfinh=(((M4h*L1hn+M5*L2hn+M1*L3hn)/L4hn)+M2)*(XD-
XA)+M3*(XD-XM3)/...
((YA-YD)+(YB-YE)*(XD-XA)/L4hn)% fisso
thrusth=(((M4h*L1h+M5*L2h+M1*L3h)/L4h)*(XAh-XBh)+M2*(XAh-
XM2h))/((YBh-YAh)+...
(YBh-YEh)*(XAh-XBh)/L4h);

if thrustfinh>0
if thrusth > thrustfinh
spreadthrust= ((XAh-XA)/lux*100)
dipthrust=((YC-YCh)/height*100)
dipOCH=(YC-YCh)/t

```



```

        thrustincrease=thrusth/thrustin
        break
    end
end
%one voussoir before hinge Eh
phiBEh=atan(abs(YB-YEh)/abs(XEh-XB));
phiBhEh=atan(abs(YBh-YEh)/abs(XEh-XBh));
phi2h=phiBEh-phiBhEh;
X_02h=XEh+r1*sin(bradsh-phi2h);
Y_02h=YEh-r1*cos(bradsh-phi2h);
sum2h=pi/2-bradsh+vrads+phi2h;
XV2h=-(CV*sin(bradsh-vrads/2)-2*e);
YV2h=CV*cos(bradsh-vrads/2);
LXV2hB = (((XV2h-XB)^2+(YV2h-YB)^2)^.5);
LXV2hEh = (((XV2h-XEh)^2+(YV2h-YEh)^2)^.5);
a2930=(-YBh+YEh)^2/(-XBh+XEh)^2+1;
b2930=(XBh^2+YBh^2-LXV2hB^2-XEh^2-YEh^2+LXV2hEh^2)*(-YBh+YEh)/(-
XBh+XEh)^2+...
2*XBh*(-YBh+YEh)/(-XBh+XEh)-2*YBh;
c2930=(XBh^2+YBh^2-LXV2hB^2-XEh^2-YEh^2+LXV2hEh^2)^2/(4*(-
XBh+XEh)^2)+...
XBh*(XBh^2+YBh^2-LXV2hB^2-XEh^2-YEh^2+LXV2hEh^2)/(-
XBh+XEh)+XBh^2+YBh^2-LXV2hB^2;
YV2h=(-b2930+(b2930^2-4*a2930*c2930)^0.5)/(2*a2930);
XV2h=(-XBh^2-YBh^2+LXV2hB^2+XEh^2+YEh^2-LXV2hEh^2-
2*YV2h*(YEh-YBh))/(2*(XEh-XBh));
Rf2h=(-(M4h*L1h+M5*L2h+M1*L3h-thrusth*(YBh-
YEh))/L4h+M1+M5+M4h)*(-XEh+X_02h)+...
thrusth*(YEh-Y_02h)-m*(-XV2h+X_02h)/((-M4h*L1h+M5*L2h+M1*L3h-
thrusth*(YBh-YEh))...
/L4h+M1+M5+M4h-m)*cos(sum2h)+thrusth*sin(sum2h));
if (Rf2h<r1)
    vh=vh+stepvh;
    break
end
end

if thrustfinh>0
    if thrusth > thrustfinh
        break
    end
end
if ((imag(XBh)<0) | (imag(XBh)>0))
    break
end
if((imag(YBh)<0) | (imag(YBh)>0))

```

```
        break
    end
end
if thrustfinh>0
    if thrusth > thrustfinh
        break
    end
end
if ((imag(XBh)<0) | (imag(XBh)>0))
    break
end
if((imag(YBh)<0) | (imag(YBh)>0))
    break
end
end
initialhinge=brads*180/pi
finalhinge=brads*180/pi-vh
```